Addressing delivery and synthesis challenges for peptide-based cancer vaccines

By

Rebecca Lynn Holden

B.S. Chemistry
Baylor University, 2015

Submitted to the Department of Chemistry
in Partial Fulfillment of the Requirements for the Degree of

Doctor of Philosophy
in Chemistry

at the

Massachusetts Institute of Technology

September 2020

Signature of Author: _____
Department of Chemistry
July 20, 2020

Certified by: _____
Bradley L. Pentelute
Associate Professor of Chemistry
Thesis Supervisor

Accepted by: _____
Adam Willard
Associate Professor
Graduate Officer

This doctoral thesis has been examined by a committee of the
Department of Chemistry as follows:

Professor Elizabeth M. Nolan …….

Thesis Committee Chair

Ivan R. Cottrell Professor of Immunology

Professor Bradley L. Pentelute……..

Thesis Supervisor

Associate Professor of Chemistry

Catherine L. Drennan……

Thesis Committee Member

Professor of Biology and Chemistry, HHMI Investigator

Addressing delivery and synthesis challenges for peptide-based cancer vaccines

By

Rebecca Lynn Holden

Submitted to the Department of Chemistry on July 20, 2020
in Partial Fulfillment of the Requirements for
the Degree of Doctor of Philosophy in Chemistry

Abstract

Therapeutic peptide vaccines have the potential to elicit and direct an anti-cancer T cell response, but their clinical efficacy has been limited in part by poor delivery to the lymphatic system, inefficient cell uptake, and scalable synthesis in the case of personalized vaccines. The work presented in this thesis explores several approaches to address these challenges.

First, we use our fast-flow automated synthesis technology to confront the synthesis bottleneck for patient-specific 'neoantigen' vaccines, which have shown early promise but are hindered by slow production. We synthesize a particularly challenging set of peptides from a previous clinical trial as a test case, demonstrating that our technology can produce the majority of sequences in sufficient quantities with comparable or higher purity than a commercial vendor in a fraction of the time.

Turning towards vaccine design, we explore several approaches to address the lymphatic and intracellular delivery of peptide antigens. We demonstrate the generality and anti-tumor efficacy of vaccines containing cell-penetrating peptides (CPPs), sequences shown to enhance the cell uptake of various cargo. We characterize their mechanism and identify several unanticipated contributors, namely trafficking to the lymph nodes, serum stability, and extended presentation *in vivo*. We then expand on an existing approach to mediate lymphatic trafficking via binding serum albumin by exploring additional albumin binding moieties. Next, we develop a straightforward and general approach to directly quantify antigen presentation and implement this technique to explore two strategies to design more effective vaccines, including CPPs.

Finally, we build on previous work using CPPs to deliver antisense oligonucleotides (ASOs), another application that we pursued in tandem with cancer vaccines. We combine amphipathic and cationic CPPs to create chimeric sequences that synergistically enhance activity of an ASO and access new routes of uptake not utilized by either parent CPP.

Drawing from our experience using CPPs to deliver ASOs as well as our expertise in peptide synthesis and design, we provide insight into the rapid production of personalized vaccines and efficient delivery of vaccine antigens. This thesis represents a new area of research for our lab, one in which we will hopefully continue to apply our unique skillset and perspective.

Thesis Supervisor: Bradley L. Pentelute
Associate Professor of Chemistry

Acknowledgements

The past five years have been some of the greatest years of my life but also the hardest, challenging me in ways that I could not predict. Earning a PhD is a difficult journey; and earning a PhD while coming out is a real trip. I have learned so much, grown stronger as a person, and become a better and more confident scientist. I owe a great deal of gratitude to everyone who has helped me make it through.

I want to start by thanking my thesis advisor, Prof. Brad Pentelute. His enthusiasm from the moment I joined the lab set the tone for my entire grad school career. I am grateful for his guidance and mentorship, which always seemed to be exactly what I needed. He encouraged me to propose my own ideas early on and his confidence in me allowed me to grow as an independent scientist. At the same time, he provided direction and encouragement whenever I needed it. His support extended beyond scientific guidance, helping me improve my communication and presentation skills and providing invaluable professional advice. Finally, of course, I would like to thank Brad for cultivating a supportive and collaborative lab culture that has significantly shaped both my research and my entire experience at MIT.

I could not have asked for a more invested and supportive thesis committee chair than Prof. Liz Nolan. I want to thank her for being an amazing mentor. It was always evident during our meetings that she genuinely cared about my research and my growth as a scientist. I appreciate her many insightful questions and thoughtful suggestions over the years. I am especially grateful more recently for her postdoc application and general career advice.

Than you to Prof. Cathy Drennan, who has been another incredible mentor. I appreciated her encouragement throughout grad school, particularly during my second- and third-year exams. Her advice for my postdoc search and her support with fellowship applications has been invaluable, and I am extremely grateful.

I am thankful to my collaborators in the Irvine lab, beginning with Prof. Darrell Irvine, who has provided a great deal of advice and scientific guidance for many of the projects described in this thesis. I am also grateful to Coralie, whose insight and advice over the last few years helped me to be a better scientist and whose sincerity, thoughtfulness, and humor made her a great colleague and friend. Thank you to Kelly, who was both a collaborator and a mentor during my first couple of years in grad school. I am grateful for her organization and positivity getting several of these projects up and running. I would also like to thank Dan, Josetta, and Naveen for their contributions to our work.

I would like to express my gratitude to Prof. Cathy Wu and Prof. Nir Hacohen for a productive and exciting collaboration on their neoantigen vaccines. I have learned a lot working with them and look forward to learning more in the future. I would also like to thank Keerthi, Sisi, Matt, Zhuting, and the whole Neovax subgroup.

I cannot imagine what my experience in grad school would have been without my amazing colleagues and friends in the Pentelute lab. Thank you to my best friend Azin, whose compassion, vivacity, and sarcasm always brightened my day. I am grateful to have worked with someone so supportive, who was always willing to listen and help with anything going on in my research or personal life. Thank you to Nina, whose cheerfulness and style brightened our space. I am grateful for her thoughtfulness, generosity, and mentorship. I know I can turn to her any time in the future. I would like to thank Colin for being my first person in the lab and teaching me so much. He was a delight to work with and helped me through some of the hardest moments of grad school. Thank you to Justin for being an easygoing, practical, and encouraging friend and collaborator. I am grateful to Alex M. for being a willing teacher, a caring friend, and a fun roommate. He truly is the definition of precious. I would also like to thank Ethan for his commiseration and for the scientific input he happily provided anytime I asked. Thank you to Charlotte for being dependably upbeat and always willing to help. I owe a great deal of

gratitude to Anthony Q. for his tireless efforts to keep the Orbitrap running, as well as his down-to-earth kindness and his many, many, many jokes. I am thankful to Carly for being amazing to work with and a brilliant sand volleyball team captain. Thank you to Alex L. and Tuang for being my comrades throughout the grad school process, especially second- and third-year exams. I would like to thank Nick for being an enthusiastic collaborator and for organizing our immunotherapy super-group meetings. And finally, I would like to thank all of my other friends and colleagues who have made the past five years so enlightening and enjoyable: Katie, Jessie, Rachael, Zak, Mette, Diómedes, Joe, Aaron, Deborah, Surin, and everyone else in the Pentelute lab. I am also grateful to Christine, Katherine, and Alex (and Eli) from the Kiessling lab for their scientific input and friendship.

I want to extend a huge thank you to all of the friends that I made outside of lab. In particular, I would like to thank Lindsey, who became an immediate friend and who has been a source of endless support, commiseration, and sangria. I also want to thank Marty, who was one of the first friends I made in Cambridge and whose kindness and originality have been welcome constants throughout grad school. I enjoyed our trips together almost as much as I enjoyed being roommates. Thank you to Sheena, the gentlest spirit I know; Dmitro, one of my favorites; Zach, who will be relieved to know that he is also one of my favorites; and Brendan, who is a treasure. Thank you to Alex, Aubrey, Ashley, and Chad—Candace's amazing friends who not only gave me their stamp of approval but became my friends, too. I am thankful to Erin for their care and wisdom. I also want to thank my comrades from Boston Feminists for Liberation, who have taught me so much. It has been a pleasure to organize with and befriend such incredible people.

I would like to thank Regina Spektor, Noname, Chance the Rapper, and Freddie Mercury. Their work has provided joy, comfort, and inspiration and seen me through the last five years. I am also grateful for the craft brewing and abundant greenery in the lovely cities of Cambridge and Somerville for bringing indispensable moments of peace, stress relief, and creativity.

Thank you to all of my friends from before I moved to Cambridge who helped me get through the last few years: Caitlin, Stefan, ChicAnya, Rae, Vincent, Chelsea, Ian, Niki, and Martin. Even being apart, they were there for me when I needed it and I am deeply grateful for their love and support. I am especially thankful to Caitlin, who is the kind of friend who hops on a ten-hour overnight bus when you need her without a second thought. She is my person and I am glad to have her.

And, of course, I want to thank my family. Thank you to my sister, Kelly, who brought the party—and her cat—with her when she visited and who can practically read my mind. Her determination and compassion continue to inspire me. Thank you to my parents for helping me through grad school and my whole education in more ways than I can count. I am so grateful to them for always listening, for their constant support and encouragement, and for their generosity. I want to thank my Dad for looking out for me and my mom for always checking in to make sure I was all right—and for her patience when I took a day or two (or more) to respond. Finally and most of all, I want to thank my partner, Candace. She has been the best part of my experience at MIT and I have a hard time imaging grad school without her. I am grateful to have someone so supportive, brilliant, and effortlessly funny in my life; someone who challenges me to be the best version of myself.

Table of Contents

List of Figures

List of Tables

Chapter 1: Background and Overview

1.1 Cancer immunotherapy and T cells

Cancer immunotherapy has revolutionized the field of oncology in recent years, with several FDA-approved therapies becoming mainstays of treatment and an explosion of preclinical research providing promising new approaches.[1–4] It incorporates a broad range of therapies designed to act in some capacity on the patient's immune system, rather than on the tumor itself, in order to elicit an anti-tumor immune response.[5] In doing so, these therapies take advantage of several key hallmarks of the immune system: precise targeting of distinct cell subsets; self-amplification of responses; and the formation immunological memory that provides a rapid response in the case of disease recurrence.[5,6] While various approaches have targeted different aspects of the immune system, most focus consistently on T cells.[1–5]

T cells are part of the adaptive immune response, meaning that they respond to specific antigens.[6,7] Once naïve antigen-specific T cells are activated, they differentiate into effector cells and exert their disease-controlling function. Eventually, this response diminishes and some of these effector cells differentiate into long-lived memory T cells which can be readily re-activated as needed.[6] Two subtypes of T cells exist, distinguished by expression of two surface markers: $CD4^+$ and $CD8^+$. Upon activation, $CD8^+$ T cells become 'cytotoxic T lymphocytes' (CTLs), which can selectively kill target cells, while $CD4^+$ T cells become 'helper' T cells, which exert a range of functions that mediate and coordinate different elements of the immune response.[6,7] While there is a growing interest in the $CD4^+$ T cell response, $CD8^+$ T cells have been the focus of most immunotherapies to date due to their ability to directly kill tumor cells.[7,8]

Checkpoint blockade, which 'takes the brakes off' the CTL response, is the hallmark cancer immunotherapy.[3,7] It comprises a series of monoclonal antibodies that block different 'immune checkpoints' by binding inhibitory signaling receptors on T cells, antigen presenting cells, or tumor cells in order to block signals that either diminish CTL cell activation or dampen an ongoing CTL cell response. A handful of different checkpoint therapies have demonstrated remarkable clinical success, transforming the standard of care in melanoma and other highly mutagenic cancers.[3–5] Ongoing work seeks to characterize additional immune checkpoints and identify candidate antagonists for these inhibitory receptors.[9] Checkpoint therapies are limited by incomplete responses and off-target toxicity. While efficacy is often dramatic in patients who respond to checkpoint, a substantial fraction of patients exhibit little to no response.[3,10] This discrepancy is attributed to an inconsistency in the level of pre-existing anti-tumor responses; when no response is present initially, there is little gain from a therapy that enhances the magnitude or quality of the T cell response.[3,7] Additionally, significant autoimmune side

effects have been observed in some patients.[3,7] There is a need for therapies that can stimulate an anti-tumor T cell response and provide greater selectivity towards tumor cells.

Another key class of immunotherapy that has recently entered the clinic is chimeric antigen receptor T cells (CAR-Ts). In this approach, patient T cells are removed and the native T cell receptor is replaced by a chimeric antigen receptor *ex vivo*, which combines a binding domain against a previously-identified tumor antigen with native T cell receptor transmembrane and signaling domains.[2,7] This approach has proved promising for several hematologic malignancies, most notably B cell leukemias and lymphomas, but there are significant toxicity concerns associated with excessive activation and cytokine release.[11,12] Additionally, the process of identifying tumor-specific antigens and constructing and validating CARs is labor-intensive, further complicated by the heterogeneous nature of solid tumors which makes identification of broadly-applicable antigens highly challenging. Ongoing work is currently seeking to refine this approach and provide more nuanced control over the CAR-T response, but there is a need for immunotherapies that are more safe, cost-effective and scalable.[2,13,14]

A third class of cancer immunotherapy that has seen growing interest in the last decade is vaccination. Cancer vaccines supply tumor antigens to antigen-presenting cells in order to activate a tumor-specific T cell response.[1,7,15–17] They differ from conventional vaccines in that the approach is therapeutic, rather than prophylactic; i.e., designed to engage the immune system against an ongoing disease rather than simply guard against future encounters. Cancer vaccines have the potential to elicit anti-tumor immunity in patients without an existing response and to increase the magnitude of existing responses.[18–22] However, these responses can be limited in magnitude and their therapeutic efficacy is untested. They exhibit minimal side effects and indeed are designed to minimize off-target effects by guiding the immune response against tumor antigens. There is evidence that combining these vaccines with checkpoint blockade and possibly other immunotherapies can achieve greater anti-tumor efficacy.[18,23–25] A range of different vaccine platforms and designs have been developed, which will be explored in greater detail in section 1.4. While promising, cancer vaccine technologies require significant improvement to reach their full potential.

1.2 T cell activation and vaccine components

Cancer vaccines prime a T cell response against tumor antigens. Understanding their mechanism of action and designing improved vaccines requires insight into the process of T cell activation. Naïve T cells are activated upon interacting with antigen presenting cells (APCs), in particular dendritic cells (DCs), in the presence of several necessary stimuli: a cognate interaction between the T cell receptor, which varies between individual T cells, and an antigen peptide presented by the DC; and the interaction of co-stimulatory molecules at the surface of the T cell and DC.[6,26,27] The DC co-stimulatory signaling molecules are upregulated in the presence of inflammatory stimuli, e.g. upon innate immune activation.[6,26,27] Successful vaccines must therefore engage innate immunity in addition to providing relevant antigens. For vaccine which contain isolated antigen(s) rather than a whole pathogen, this is done by also including a component called an adjuvant designed to engage innate immune receptors and trigger an inflammatory response.[15,32] Optimal adjuvant design is a critical element of vaccine development, and indeed most of the approved cancer vaccines consist only of an adjuvant designed to activate innate immunity. However, this work focuses on the TCR/cognate antigen signal and the antigen component of these vaccines.

Antigens presented to T cells are short, linear peptides that generally range in length from 8-11 amino acids for $CD8^+$ T cells and ~13-20 amino acids for $CD4^+$ T cells.[6,26] They are bound non-covalently to a surface protein called the major histocompatibility complex (MHC), also referred to as human leukocyte antigen (HLA) in humans. MHC class I, or MHC-I (HLA-I), binds $CD8^+$ T cell antigens and facilitates interaction with the TCR in a process known as antigen presentation, while MHC-II (HLA-II) presents antigen to CD4+ T cells.[6,26] Vaccines designed to elicit a T cell response must include one or more antigens, either within native proteins in whole pathogens in the case of conventional vaccines, or as isolated peptides, proteins, or antigen-encoding nucleic acids.[6,15–17]

Presentation of extracellular antigens by DCs, including vaccine antigens, involves uptake, proteolytic processing into short peptide epitopes, loading onto MHC, and display at the cell surface. This first requires trafficking to the lymph node, where these interactions occur, either as a result of passive antigen transport through the lymphatics or uptake by activated DCs which then home to the lymph nodes.[6,26,28] The predominant pathway for processing $CD8^+$ T cell antigens occurs in the cytosol. In all other nucleated cells, healthy or tumor cells, peptide fragments resulting from proteasomal degradation of cytosolic peptides are transported to the endoplasmic reticulum for further proteolytic processing, loaded onto newly synthesized MHC-

I, and displayed at the cell surface in order to allow CD8+ T cell surveillance for infection or transformation.[6,26] In addition to this pathway, DCs present extracellular antigen in a process known as 'cross-presentation' in which antigens are endocytosed, gain cytosolic access, and then follow the canonical MHC-I loading route.[6,26,29] While other pathways exist, this is the predominant pathway by which DCs present extracellular antigen to CD8+ T cells.[29] It is worth noting that endosomal escape into the cytosol is poorly characterized and may be a bottleneck in the presentation of vaccine antigens.

1.3 Vaccine antigen classes

The antigens included in cancer vaccines belong to two major classes, tumor associated antigens and tumor-specific antigens. Tumor associated antigens (TAAs) are present in healthy tissue but overexpressed or differentially expressed in tumor cells.[30,31] TAAs for a given cancer are present in many patients with little variability, simplifying their identification and production. However, vaccinating against TAAs can have predictable side effects, as stimulating an immune response against TAAs can damage healthy tissue as well.[30,31] Over 70 clinical trials have used TAAs in therapeutic vaccines.[17] The other general class of tumor antigens used in cancer vaccines are tumor specific antigens (TSAs), which are present in tumor cells but absent in healthy tissue. This includes cancer-germline (also called cancer-testis) antigens, which are derived from proteins that are typically expressed in germline cells, but not presented due to a lack of MHC-I expression.[30,31] TSAs also include antigens that arise from mutations occurring within tumor cells that, if expressed, can yield antigen peptides that do not exist in healthy tissue, termed 'neoantigens.'[30,31]

Neoantigens are attractive vaccine candidates that have elicited significant interest in recent years due to their high specificity, lower inherent risk, and their generally higher immunogenicity, as they represent new antigen sequences that have not been subject to immune tolerance.[1,16] Several clinical trials have demonstrated that personalized vaccines are indeed able to stimulate and strengthen T cell responses to neoantigens, although the magnitude and efficacy of these responses remains limited.[18–21] As neoantigens arise from mutations, they are tumor-specific and therefore patient-specific. While a handful of frequently-occurring mutations, often in cancer-driver genes, have been identified as 'shared neoantigens,' the majority of neoantigens will need to be addressed in personalized vaccines.[1,7,16] Next-generation sequencing and recent computational tools to predict candidate antigen peptides have brought this process closer to a feasible reality.[32] However, production of patient-specific

vaccines remains a significant challenge. The handful of clinical trials conducted to date, especially those using peptide vaccines, were hindered by technical challenges associated with vaccine synthesis and purification and generally limited to small patient cohorts.[18–21] While a range of challenges exist for these vaccines and for cancer vaccines broadly, addressing the production bottleneck for personalized neoantigen vaccines is a major concern. Developing a more rapid and practical approach to synthesize neoantigen vaccines could enable future clinical trials and, ultimately, make this potentially powerful therapy broadly accessible.

1.4 Vaccine formats

As described in section 1.1, vaccines consisting of defined tumor antigens have gained significant interest in the field of cancer immunotherapy. They offer control over antigen selection and design, have a generally high safety profile, and are more practical than many cell-based approaches, offering the possibility of off-the-shelf vaccines produced for shared tumor antigens.[1,7] These antigens, which are ultimately presented to T cells as short, linear peptides, are supplied in a number of different formats including whole DCs, viral or bacterial vectors, peptides, proteins, or by DNA or RNA encoding the appropriate antigen sequences.

Some approaches involve treating DCs or precursor cells with antigen *ex vivo* then administering these antigen-loaded cells to patients.[33] Clinical trials using this approach saw good safety profiles and some efficacy, with one system using tumor lysate to treat DCs *ex vivo*, Sipleucel-T, receiving FDA approval.[34] Ongoing work seeks to more efficiently mature DCs with a desired phenotype and introduce defined antigens.[33,35] While promising, *ex vivo* approaches can more be time-intensive and costly than other vaccination strategies. Approaches using bacterial or viral vectors have also been explored and while promising for their ability to self-amplify and generate high immune responses, associated safety concerns continue to cast doubt on their broad utility.[36,37]

Nucleic acid-based vaccines have been developed for shared tumor antigens as well as personalized neoantigens. Due to their biological role upstream of translation and, in some cases, their ability to self-amplify, they could be more efficient than peptide- or protein-based vaccines.[38,39] Vaccines comprised of plasmid DNA are highly stable and have been shown to elicit immune responses in animal models.[49,51] However, their immunogenicity is limited by poor intracellular and nuclear delivery.[39–42] Moreover, they carry the potential risk of integration into host DNA, which could cause transformation.[43] RNA-based vaccines have shown promise as a safer alternative and have been implemented in dozens of clinical trials

including a personalized neoantigen vaccine trial.[20,38] Their decreased stability relative to DNA is a concern and they face similar challenges regarding intracellular delivery. Substantial ongoing work seeks to address these challenges, for example: enhancing stability with non-natural bases or other chemical modifications, formulating RNA as liposomes or lipid nanoparticles to improve their stability and enhance trafficking to the spleen, and constructing self-replicating RNAs to amplify the level of antigen presentation.[38,44–46]

Peptide- and protein-based vaccines, which contain the actual peptide sequences presented to T cells, have been used extensively in preclinical and clinical research. Several clinical trials have indicated that proteins and peptides containing shared tumor antigens are safe and capable of eliciting a T cell response.[15,47–50] While proteins offer a higher stability to proteolysis than shorter peptides, peptide vaccines carry several practical advantages: they are straightforward to handle and benchtop stable and, similarly to DNA and RNA, they are readily accessible by chemical synthesis.[51,52] They are also readily amenable to chemical modification via incorporation of non-natural monomers. However, like other large biomolecules, they are hampered by poor delivery across biological membranes and cytosolic access is likely a bottleneck limiting their efficacy.[15–17,51,53] In addition to dozens of clinical studies employing shared tumor antigens, peptide vaccines have been used in a handful of clinical trials testing patient-specific neoantigen vaccines.[15–19,22] While promising, further development is required to enhance the magnitude and quality of vaccine-induced T cell responses and, in the case of neoantigen vaccines, expand peptide production capabilities. Peptide vaccines are of considerable interest in vaccine development and extensive, ongoing work seeks to address their associated limitations, namely: production (for neoantigen vaccines), intracellular and cytosolic delivery, proteolytic stability, and biodistribution.[1,21–24] Taking these considerations along with our expertise in peptide synthesis, we elected to focus on synthetic peptides as the antigen format in our efforts to improve cancer vaccines.

1.5 Delivery of peptide vaccines

Effective delivery to the appropriate tissues, cells, and subcellular compartments is a significant challenge hindering the efficacy of cancer vaccines, including peptide antigens. Substantial effort has been dedicated to addressing the various levels to this problem, including stability to proteolysis, trafficking to the lymph nodes or spleen, delivery to specific cell types, and intracellular—particularly cytosolic—delivery.[7,15,51] A range of strategies have been

developed to address these challenges include various classes of nanoparticles, antibodies and other targeting moieties, albumin binding lipids, and cell-penetrating peptides.

Nanoparticle vaccine delivery systems potentially address several aspects of the peptide vaccine delivery challenge: increasing stability to proteolysis by encapsulating or occluding antigen peptides and allowing multivalent incorporation of targeting and/or membrane crossing moieties.[53] They can offer several additional benefits to vaccine efficacy, including controlled release of antigen or adjuvant molecules and co-delivery of antigen and adjuvant stimuli to the same antigen-presenting cells.[54] However, biocompatibility remains a critical concern as the immunogenicity of some nanoparticles, while providing intrinsic adjuvant activity, can cause severe or allergic reactions.[55] The complex synthesis and assembly of many nanoparticles further complicates their practical utility. Ultimately, reports of nanoparticle systems for cancer vaccine delivery focus largely on design and *in vitro* validation with some testing in animal models and clinical implementation is likely farther on the horizon than other approaches.[53]

Another approach aims to improve delivery of vaccine antigens to cell types of interest, namely various DC subsets, by covalent attachment to a targeting moiety. This has been primarily achieved by conjugating peptide or protein antigens to monoclonal antibodies (mAbs) targeting cell surface receptors such as DEC205 or Clec9A on cross-presenting DCs.[56] Other targeting moieties have also been explored, including a range of antibody derivatives such as scFvs and nanobodies, as well as other classes of ligands like synthetic polymers that bind DC receptors.[57,58] In addition to directing vaccine antigens to the appropriate cell types, careful selection of the target receptor might also promote favorable intracellular processing by guiding antigen to late v. early endocytic compartments.[59] While promising, this work largely remains limited to *in vitro* and animal studies.

Another recently-identified strategy to promote vaccine antigen trafficking to lymph nodes involves binding to serum albumin. It has been demonstrated that size is a major contributing factor in determining whether a molecule injected subcutaneously traffics to the blood stream or the lymphatics, with increasing size favoring partitioning to the lymphatics.[60] This effect is likely a factor contributing to the success of nanoparticle and antibody-based approaches, as these alterations increase the overall size of the vaccine construct. Recently, Liu et al. determined that conjugation to lipid moieties that bind serum albumin could similarly facilitate lymph node trafficking, presumably by increasing the effective size of the vaccine molecule by associating with the 66 kDa protein.[61] This strategy, deemed 'albumin hitchhiking,' is similar to the dye-targeting to lymph nodes done during sentinel lymph node trafficking and demonstrated impressive increases in vaccine efficacy in animal models.[61–63]

Developing creative ways to enhance lymph node trafficking could yield more effective cancer vaccines.

Enhancing intracellular delivery is another key strategy to improve the efficacy of peptide vaccines.[17] In particular, cytosolic delivery is an important goal for vaccines designed to elicit a $CD8^+$ T cell response. The most salient approach to address intracellular delivery uses cell-penetrating peptides, which are discussed in detail in the following section (1.6).

1.6 Cell-penetrating peptides

Cell-penetrating peptides (CPPs) are a broad class of peptides demonstrated to enhance the intracellular and, in some cases, cytosolic delivery of a variety of cargo. Since the first CPPs were discovered thirty years ago, over 1,000 sequences have been identified including sequences derived from natural proteins, novel sequences that are rationally designed or randomly generated, and chimeras combining one or more known CPPs.[64–66] They range in length from approximately 5 to 40 amino acids and vary in their biophysical characteristics, with many sequences containing a large proportion of cationic residues while others are negatively charged or neutral. Most sequences are hydrophilic or amphiphilic, while some are more hydrophobic in nature.[65]

The mechanisms of CPP-mediated cell entry have been debated at length, and consist of two main classes: endocytosis and direct translocation across the cell membrane.[64–67] Virtually all CPPs appear to promote endocytosis to some extent, but the endocytic mechanism for different sequences as well as the efficiency of internalization vary.[64–69] Early studies supporting direct translocation as the primary route for some sequences were later called into question, but it appears that some degree of direct translocation across the cell and/or endosomal membrane occurs under some conditions by a variety of proposed mechanisms.[70–75] CPPs have been demonstrated to promote the intracellular delivery of a variety of cargo, including fluorophores and other small molecules, other peptide sequences, proteins, and nucleic acids as well as nucleic acid analogs.[64,75–78] Notably, the efficiency and often the mechanism of cell uptake depend in part on the cargo, as well as on the CPP sequence, cell type, and treatment concentration.[64–66,79–82] All of these factors must be considered in selecting a CPP for a given application.

CPPs have been applied to enhance vaccine efficacy, likely by boosting intracellular delivery.[83,84] A handful of CPP sequences have been demonstrated to increase antigen delivery *in vitro*, including several highly cationic sequences as well as CPPs that are amphiphilic in

nature.[83–90] Characterization of the mechanism of uptake for two of these sequences indicated that uptake is largely energy-dependent, that is, via endocytosis; further, analysis of one sequence demonstrated that antigen presentation proceeds primarily via the canonical MHC-I loading pathway, requiring cytosolic delivery.[91,92] Several CPPs have been demonstrated to enhance endogenous T cell priming against vaccine antigens in animal models, including non-human primates, and have shown efficacy in several murine tumor models.[93–96] One sequence designed by Derouazi and colleagues has entered a Phase I clinical trial.[97] While highly promising due to their ease of synthesis and versatility, only a handful of CPP sequences have been explored. Additionally, studies have been limited to a small number of model tumor antigens or, in many cases, an epitope from ovalbumin which is notoriously immunogenic relative to the majority of tumor antigens.[85–87,93–96] Further, the mechanism by which CPPs enhance peptide vaccine efficacy is incompletely characterized, especially *in vivo* with regards to the actual level of uptake into different antigen presenting cells, stability, and lymph node trafficking. Addressing these outstanding mechanistic questions, expanding the range of CPPs tested, and demonstrating their generalizability to different antigens could confirm CPPs as a viable strategy to enhance the therapeutic efficacy of peptide cancer vaccines.

1.7 Overview of thesis

This thesis will address challenges related to peptide cancer vaccines, with an aim to increase their effectiveness and generalizability by improving their synthesis and delivery. This work builds off our lab's expertise in CPP optimization and design to aid in the delivery of synthetic nucleotide analogs for exon skipping as well as our automated fast-flow synthesis technology. Chapter 2 details the application of our synthesis technology to the production of a personalized neoantigen vaccine. Chapter 3 explores the generalizability and mechanism of CPPs for peptide vaccine delivery, implicating lymph node trafficking as well as intracellular delivery as critical factors in their success. Chapter 4 further expands on lymph node trafficking as a key strategy to enhance vaccine efficacy using two albumin binding moieties, including an albumin binding peptide. Chapter 5 details the development of a new technique to directly measure antigen presentation and applies this approach to evaluate two approaches to designing more effective peptide vaccines. The sixth and final chapter, which covers work towards our lab's original CPP project, uses chimeric CPPs to deliver an antisense oligonucleotide that facilitates exon skipping.

Chapter 2 addresses the production bottleneck in personalized cancer vaccines. As described above, high-throughput genome sequencing and computation have enabled rapid identification of mutation-derived, patient-specific neoantigens which can be synthesized and formulated as a vaccine, but generating the vaccine peptides for each patient in a rapid and affordable fashion remains difficult. High-throughput peptide synthesis technology is therefore urgently needed for personalized cancer vaccines to succeed in the clinic. Previously, we developed automated flow peptide synthesis technology that greatly accelerates the production of synthetic peptides. We show that this technology permits the synthesis of high-quality peptides for personalized medicine. Automated flow synthesis produces 30-mer peptides in less than 35 minutes and 15- to 16-mer peptides in less than 20 minutes. The purity of these peptides is comparable with or higher than the purity of peptides produced by other methods. This work illustrates how automated flow synthesis technology can enable personalized therapy by accelerating peptide synthesis and increasing purity. We envision that implementing this technology in clinical settings will greatly increase capacity to generate clinical-grade peptides on demand, which is a key step in reaching the full potential of personalized vaccines for the treatment of cancer and other diseases.

Chapter 3 confronts the delivery challenges associated with peptide vaccines using cell-penetrating peptides (CPPs). As highlighted previously, CPPs are a straightforward approach to enhance the anti-tumor efficacy of peptide vaccines by improving uptake by antigen presenting cells. However, their impact on antigen behavior *in vivo* remains largely uncharacterized and reports to date concern only a limited number of CPPs and model antigens. Here, we screen a set of CPPs to compare their impact on T cell priming as well their mechanism of action at the cellular and systems levels. All CPPs increased antigen uptake and T cell activation *in vitro* and the majority also enhanced endogenous T cell priming *in vivo*, by up to 20-fold. A top CPP, penetratin, similarly enhanced vaccine immunogenicity for other tumor antigens and provided significantly greater tumor protection compared to a vaccine with the unmodified antigen. After confirming that CPPs increase uptake by antigen presenting cells, according to their expected mechanism, we then explored their impact on antigen delivery and presentation *in vivo*. We determined that CPPs promote delivery to the lymph nodes and suggest passive trafficking mediated by serum protein binding as a likely mechanism. We demonstrate that CPPs prolong antigen serum stability and extend the duration of presentation in the draining lymph node, suggesting a temporal component to CPP-mediated vaccine immunogenicity. These findings support CPPs as a general strategy to boost the immunogenicity and efficacy of

therapeutic peptide vaccines and indicate several additional factors beyond intracellular delivery that contribute to their activity.

Chapter 4 further expands on the use strategies that promote lymphatic trafficking to address the delivery challenge for peptide vaccines. As described above, one previously reported strategy involves binding of endogenous albumin upon injection via a diacyl lipid, which allows peptide antigens to "hitchhike" to the draining lymph node in a similar manner to the mechanism of action of sentinel lymph node mapping dyes used clinically. Here, we explore the scope of potential albumin binding moieties by testing whether an albumin-binding peptide and a small molecule, a-tocopherol, can successfully boost vaccine immunogenicity *in vivo*. We demonstrate that multiple albumin-binding moieties conjugated to peptide antigens enhanced lymph node accumulation and subsequent T cell priming.

Chapter 5 describes the development of a new technique to measure presentation of an antigen of interest and its implementation screening two potential strategies for improving peptide vaccines. The ability to directly measure presentation of specific MHC-associated antigens could facilitate new avenues of investigation, including screening strategies to boost the presentation of vaccine antigens. We aimed to develop a new technique that is straightforward, quantitative, and higher throughput than existing techniques by combining direct elution of antigens from the surface of intact cells followed by targeted, high-sensitivity LC-MS/MS analysis. We validated the ability of this approach to quantify MHC-presented antigens in a generalizable manner, then applied it to characterize the dynamics of vaccine antigen presentation. With this technique in hand, we then began to explore the impact of D-amino acid substitution as well as the impact of CPP conjugation on the magnitude and kinetics of vaccine antigen presentation. While instrumentation limits its sensitivity to the level of other MS-based techniques, we anticipate that the simplicity of our approach could enable design of vaccine antigens with optimal presentation and characterization of this fundamental process.

Chapter 6 does not concern cancer vaccines and instead focuses on the design of chimeric CPPs for our lab's original CPP application, improving the delivery of phosphorodiamidate morpholino oligonucleotides (PMOs). PMOs are a promising class of therapeutics for genetic disease. PMOs designed for "exon skipping" must be internalized into cells, reach the nucleus, and act on pre-mRNA to mediate their effects. One tactic for improving PMO delivery and exon skipping is to covalently conjugate PMOs to CPPs. Here we report the synthesis of PMOs conjugated to CPP chimeras, constructed by combining multiple CPPs into one sequence. The chimeric CPPs synergistically improve PMO activity up to 70-fold over the PMO alone, beyond the expected effects of each component peptide. By investigating the

design space of CPP chimeras, we demonstrate that all components must be covalently attached, that the order of the two sequences matters, and that peptide identity can tune activity. We identified one chimera (pVEC-Bpep) to investigate in more detail and found that it engages different mechanisms of endocytosis than its parent peptides. We also examined the extent to which the beneficial effect comes from improved cellular uptake as opposed to the downstream steps required for exon skipping. Given the complexity of intracellular delivery, we anticipate this work will lead researchers to consider combining molecules with different physicochemical properties in order to aid in the delivery of biologic cargoes. Earlier projects using CPPs to deliver PMOs informed both this project as well as the application of CPPs to cancer vaccines, which we explored in parallel.

This thesis tackles the synthesis bottleneck in producing personalized neoantigen vaccines using our in-house automated technology. It then applies our expertise in delivering large biomolecules gained with PMOs to the delivery of peptide vaccine antigens. After surveying a set of CPPs to demonstrate that they can deliver a range of vaccine antigens and enhance anti-tumor efficacy, we dissect their mechanism of action and determine that in addition to mediating intracellular delivery, they also promote lymph node trafficking via serum protein binding. We then assess several other albumin binding moieties for their ability to promote lymph node trafficking and vaccine efficacy. I also present a new technique to measure antigen presentation, facilitating vaccine optimization. The work described in this thesis represents a new direction for our lab that applies our existing synthesis and delivery capabilities to the challenge of therapeutic cancer vaccines.

1.8 References

(1) Sahin, U.; Türeci, Ö. Personalized Vaccines for Cancer Immunotherapy. *Science* **2018**, *359* (6382), 1355–1360. https://doi.org/10.1126/science.aar7112.

(2) June, C. H.; O'Connor, R. S.; Kawalekar, O. U.; Ghassemi, S.; Milone, M. C. CAR T Cell Immunotherapy for Human Cancer. *Science* **2018**, *359* (6382), 1361–1365. https://doi.org/10.1126/science.aar6711.

(3) Ribas, A.; Wolchok, J. D. Cancer Immunotherapy Using Checkpoint Blockade. *Science* **2018**, *359* (6382), 1350–1355. https://doi.org/10.1126/science.aar4060.

(4) Jenkins, R. W.; Fisher, D. E. Treatment of Advanced Melanoma in 2020 and Beyond. *Journal of Investigative Dermatology* **2020**. https://doi.org/10.1016/j.jid.2020.03.943.

(5) Waldman, A. D.; Fritz, J. M.; Lenardo, M. J. A Guide to Cancer Immunotherapy: From T Cell Basic Science to Clinical Practice. *Nature Reviews Immunology* **2020**, 1–18. https://doi.org/10.1038/s41577-020-0306-5.

(6) Abbas, A.; Lichtman, A.; Pillai, S. *Cellular and Molecular Immunology*, 9th ed.; Elsevier, 2017.

(7) Waldman, A. D.; Fritz, J. M.; Lenardo, M. J. A Guide to Cancer Immunotherapy: From T Cell Basic Science to Clinical Practice. *Nature Reviews Immunology* **2020**, 1–18. https://doi.org/10.1038/s41577-020-0306-5.
(8) Borst, J.; Ahrends, T.; Bąbała, N.; Melief, C. J. M.; Kastenmüller, W. CD4 + T Cell Help in Cancer Immunology and Immunotherapy. *Nature Reviews Immunology* **2018**, *18* (10), 635–647. https://doi.org/10.1038/s41577-018-0044-0.
(9) Qin, S.; Xu, L.; Yi, M.; Yu, S.; Wu, K.; Luo, S. Novel Immune Checkpoint Targets: Moving beyond PD-1 and CTLA-4. *Mol. Cancer* **2019**, *18* (1), 155. https://doi.org/10.1186/s12943-019-1091-2.
(10) Hamid, O.; Robert, C.; Daud, A.; Hodi, F. S.; Hwu, W. J.; Kefford, R.; Wolchok, J. D.; Hersey, P.; Joseph, R.; Weber, J. S.; Dronca, R.; Mitchell, T. C.; Patnaik, A.; Zarour, H. M.; Joshua, A. M.; Zhao, Q.; Jensen, E.; Ahsan, S.; Ibrahim, N.; Ribas, A. Five-Year Survival Outcomes for Patients with Advanced Melanoma Treated with Pembrolizumab in KEYNOTE-001. *Ann. Oncol.* **2019**, *30* (4), 582–588. https://doi.org/10.1093/annonc/mdz011.
(11) Schuster, S. J.; Svoboda, J.; Chong, E. A.; Nasta, S. D.; Mato, A. R.; Anak, Ö.; Brogdon, J. L.; Pruteanu-Malinici, I.; Bhoj, V.; Landsburg, D.; Wasik, M.; Levine, B. L.; Lacey, S. F.; Melenhorst, J. J.; Porter, D. L.; June, C. H. Chimeric Antigen Receptor T Cells in Refractory B-Cell Lymphomas. *N. Engl. J. Med.* **2017**, *377* (26), 2545–2554. https://doi.org/10.1056/NEJMoa1708566.
(12) Laetsch, T. W.; Myers, G. D.; Baruchel, A.; Dietz, A. C.; Pulsipher, M. A.; Bittencourt, H.; Buechner, J.; De Moerloose, B.; Davis, K. L.; Nemecek, E.; Driscoll, T.; Mechinaud, F.; Boissel, N.; Rives, S.; Bader, P.; Peters, C.; Sabnis, H. S.; Grupp, S. A.; Yanik, G. A.; Hiramatsu, H.; Stefanski, H. E.; Rasouliyan, L.; Yi, L.; Shah, S.; Zhang, J.; Harris, A. C. Patient-Reported Quality of Life after Tisagenlecleucel Infusion in Children and Young Adults with Relapsed or Refractory B-Cell Acute Lymphoblastic Leukaemia: A Global, Single-Arm, Phase 2 Trial. *The Lancet Oncology* **2019**, *20* (12), 1710–1718. https://doi.org/10.1016/S1470-2045(19)30493-0.
(13) Fiorenza, S.; Ritchie, D. S.; Ramsey, S. D.; Turtle, C. J.; Roth, J. A. Value and Affordability of CAR T-Cell Therapy in the United States. *Bone Marrow Transplant.* **2020**. https://doi.org/10.1038/s41409-020-0956-8.
(14) Lim, F. L. W. I.; Ang, S. O. Emerging CAR Landscape for Cancer Immunotherapy. *Biochem. Pharmacol.* **2020**, 114051. https://doi.org/10.1016/j.bcp.2020.114051.
(15) Hollingsworth, R. E.; Jansen, K. Turning the Corner on Therapeutic Cancer Vaccines. *npj Vaccines* **2019**, *4* (1), 1–10. https://doi.org/10.1038/s41541-019-0103-y.
(16) Hu, Z.; Ott, P. A.; Wu, C. J. Towards Personalized, Tumour-Specific, Therapeutic Vaccines for Cancer. *Nature Reviews Immunology* **2018**, *18* (3), 168–182. https://doi.org/10.1038/nri.2017.131.
(17) Ma, M.; Liu, J.; Jin, S.; Wang, L. Development of Tumour Peptide Vaccines: From Universalization to Personalization. *Scandinavian Journal of Immunology n/a* (n/a), e12875. https://doi.org/10.1111/sji.12875.
(18) Ott, P. A.; Hu, Z.; Keskin, D. B.; Shukla, S. A.; Sun, J.; Bozym, D. J.; Zhang, W.; Luoma, A.; Giobbie-Hurder, A.; Peter, L.; Chen, C.; Olive, O.; Carter, T. A.; Li, S.; Lieb, D. J.; Eisenhaure, T.; Gjini, E.; Stevens, J.; Lane, W. J.; Javeri, I.; Nellaiappan, K.; Salazar, A.; Daley, H.; Seaman, M.; Buchbinder, E. I.; Yoon, C. H.; Harden, M.; Lennon, N.; Gabriel, S.; Rodig, S. J.; Barouch, D. H.; Aster, J. C.; Getz, G.; Wucherpfennig, K.; Neuberg, D.; Ritz, J.; Lander, E. S.; Fritsch, E. F.; Hacohen, N.; Wu, C. J. An Immunogenic Personal Neoantigen Vaccine for Melanoma Patients. *Nature* **2017**, *547* (7662), 217–221. https://doi.org/10.1038/nature22991.

(19) Keskin, D. B.; Anandappa, A. J.; Sun, J.; Tirosh, I.; Mathewson, N. D.; Li, S.; Oliveira, G.; Giobbie-Hurder, A.; Felt, K.; Gjini, E.; Shukla, S. A.; Hu, Z.; Li, L.; Le, P. M.; Allesøe, R. L.; Richman, A. R.; Kowalczyk, M. S.; Abdelrahman, S.; Geduldig, J. E.; Charbonneau, S.; Pelton, K.; Iorgulescu, J. B.; Elagina, L.; Zhang, W.; Olive, O.; McCluskey, C.; Olsen, L. R.; Stevens, J.; Lane, W. J.; Salazar, A. M.; Daley, H.; Wen, P. Y.; Chiocca, E. A.; Harden, M.; Lennon, N. J.; Gabriel, S.; Getz, G.; Lander, E. S.; Regev, A.; Ritz, J.; Neuberg, D.; Rodig, S. J.; Ligon, K. L.; Suvà, M. L.; Wucherpfennig, K. W.; Hacohen, N.; Fritsch, E. F.; Livak, K. J.; Ott, P. A.; Wu, C. J.; Reardon, D. A. Neoantigen Vaccine Generates Intratumoral T Cell Responses in Phase Ib Glioblastoma Trial. *Nature* **2019**, *565* (7738), 234–239. https://doi.org/10.1038/s41586-018-0792-9.

(20) Sahin, U.; Derhovanessian, E.; Miller, M.; Kloke, B.-P.; Simon, P.; Löwer, M.; Bukur, V.; Tadmor, A. D.; Luxemburger, U.; Schrörs, B.; Omokoko, T.; Vormehr, M.; Albrecht, C.; Paruzynski, A.; Kuhn, A. N.; Buck, J.; Heesch, S.; Schreeb, K. H.; Müller, F.; Ortseifer, I.; Vogler, I.; Godehardt, E.; Attig, S.; Rae, R.; Breitkreuz, A.; Tolliver, C.; Suchan, M.; Martic, G.; Hohberger, A.; Sorn, P.; Diekmann, J.; Ciesla, J.; Waksmann, O.; Brück, A.-K.; Witt, M.; Zillgen, M.; Rothermel, A.; Kasemann, B.; Langer, D.; Bolte, S.; Diken, M.; Kreiter, S.; Nemecek, R.; Gebhardt, C.; Grabbe, S.; Höller, C.; Utikal, J.; Huber, C.; Loquai, C.; Türeci, Ö. Personalized RNA Mutanome Vaccines Mobilize Poly-Specific Therapeutic Immunity against Cancer. *Nature* **2017**, *547* (7662), 222–226. https://doi.org/10.1038/nature23003.

(21) Dillman, R. O.; Cornforth, A. N.; Nistor, G. I.; McClay, E. F.; Amatruda, T. T.; Depriest, C. Randomized Phase II Trial of Autologous Dendritic Cell Vaccines versus Autologous Tumor Cell Vaccines in Metastatic Melanoma: 5-Year Follow up and Additional Analyses. *J Immunother Cancer* **2018**, *6* (1), 19. https://doi.org/10.1186/s40425-018-0330-1.

(22) Chamani, R.; Ranji, P.; Hadji, M.; Nahvijou, A.; Esmati, E.; Alizadeh, A. M. Application of E75 Peptide Vaccine in Breast Cancer Patients: A Systematic Review and Meta-Analysis. *European Journal of Pharmacology* **2018**, *831*, 87–93. https://doi.org/10.1016/j.ejphar.2018.05.010.

(23) Moynihan, K. D.; Opel, C. F.; Szeto, G. L.; Tzeng, A.; Zhu, E. F.; Engreitz, J. M.; Williams, R. T.; Rakhra, K.; Zhang, M. H.; Rothschilds, A. M.; Kumari, S.; Kelly, R. L.; Kwan, B. H.; Abraham, W.; Hu, K.; Mehta, N. K.; Kauke, M. J.; Suh, H.; Cochran, J. R.; Lauffenburger, D. A.; Wittrup, K. D.; Irvine, D. J. Eradication of Large Established Tumors in Mice by Combination Immunotherapy That Engages Innate and Adaptive Immune Responses. *Nat Med* **2016**, *22* (12), 1402–1410. https://doi.org/10.1038/nm.4200.

(24) Collins, J. M.; Redman, J. M.; Gulley, J. L. Combining Vaccines and Immune Checkpoint Inhibitors to Prime, Expand, and Facilitate Effective Tumor Immunotherapy. *Expert Rev Vaccines* **2018**, *17* (8), 697–705. https://doi.org/10.1080/14760584.2018.1506332.

(25) Grenier, J. M.; Yeung, S. T.; Khanna, K. M. Combination Immunotherapy: Taking Cancer Vaccines to the Next Level. *Front Immunol* **2018**, *9*, 610. https://doi.org/10.3389/fimmu.2018.00610.

(26) Janeway, C. A.; Travers, P.; Walport, M.; Shlomchik, M. J. *Immunobiology: The Immune System in Health and Disease*, 5th ed.; Garland Science: New York, 2001.

(27) Tai, Y.; Wang, Q.; Korner, H.; Zhang, L.; Wei, W. Molecular Mechanisms of T Cells Activation by Dendritic Cells in Autoimmune Diseases. *Front Pharmacol* **2018**, *9*. https://doi.org/10.3389/fphar.2018.00642.

(28) Liu, H.; Moynihan, K. D.; Zheng, Y.; Szeto, G. L.; Li, A. V.; Huang, B.; Van Egeren, D. S.; Park, C.; Irvine, D. J. Structure-Based Programming of Lymph-Node Targeting in Molecular Vaccines. *Nature* **2014**, *507* (7493), 519–522. https://doi.org/10.1038/nature12978.
(29) Joffre, O. P.; Segura, E.; Savina, A.; Amigorena, S. Cross-Presentation by Dendritic Cells. *Nat Rev Immunol* **2012**, *12* (8), 557–569. https://doi.org/10.1038/nri3254.
(30) Vigneron, N. Human Tumor Antigens and Cancer Immunotherapy. *Biomed Res Int* **2015**, *2015*. https://doi.org/10.1155/2015/948501.
(31) Ilyas, S.; Yang, J. C. Landscape of Tumor Antigens in T-Cell Immunotherapy. *J Immunol* **2015**, *195* (11), 5117–5122. https://doi.org/10.4049/jimmunol.1501657.
(32) Jurtz, V.; Paul, S.; Andreatta, M.; Marcatili, P.; Peters, B.; Nielsen, M. NetMHCpan-4.0: Improved Peptide-MHC Class I Interaction Predictions Integrating Eluted Ligand and Peptide Binding Affinity Data. *J. Immunol.* **2017**, *199* (9), 3360–3368. https://doi.org/10.4049/jimmunol.1700893.
(33) Wculek, S. K.; Cueto, F. J.; Mujal, A. M.; Melero, I.; Krummel, M. F.; Sancho, D. Dendritic Cells in Cancer Immunology and Immunotherapy. *Nature Reviews Immunology* **2020**, *20* (1), 7–24. https://doi.org/10.1038/s41577-019-0210-z.
(34) Kantoff, P. W.; Higano, C. S.; Shore, N. D.; Berger, E. R.; Small, E. J.; Penson, D. F.; Redfern, C. H.; Ferrari, A. C.; Dreicer, R.; Sims, R. B.; Xu, Y.; Frohlich, M. W.; Schellhammer, P. F.; IMPACT Study Investigators. Sipuleucel-T Immunotherapy for Castration-Resistant Prostate Cancer. *N. Engl. J. Med.* **2010**, *363* (5), 411–422. https://doi.org/10.1056/NEJMoa1001294.
(35) Tanyi, J. L.; Bobisse, S.; Ophir, E.; Tuyaerts, S.; Roberti, A.; Genolet, R.; Baumgartner, P.; Stevenson, B. J.; Iseli, C.; Dangaj, D.; Czerniecki, B.; Semilietof, A.; Racle, J.; Michel, A.; Xenarios, I.; Chiang, C.; Monos, D. S.; Torigian, D. A.; Nisenbaum, H. L.; Michielin, O.; June, C. H.; Levine, B. L.; Powell, D. J.; Gfeller, D.; Mick, R.; Dafni, U.; Zoete, V.; Harari, A.; Coukos, G.; Kandalaft, L. E. Personalized Cancer Vaccine Effectively Mobilizes Antitumor T Cell Immunity in Ovarian Cancer. *Sci Transl Med* **2018**, *10* (436). https://doi.org/10.1126/scitranslmed.aao5931.
(36) Sato-Dahlman, M.; LaRocca, C. J.; Yanagiba, C.; Yamamoto, M. Adenovirus and Immunotherapy: Advancing Cancer Treatment by Combination. *Cancers (Basel)* **2020**, *12* (5). https://doi.org/10.3390/cancers12051295.
(37) Flickinger, J. C.; Rodeck, U.; Snook, A. E. Listeria Monocytogenes as a Vector for Cancer Immunotherapy: Current Understanding and Progress. *Vaccines (Basel)* **2018**, *6* (3). https://doi.org/10.3390/vaccines6030048.
(38) Wadhwa, A.; Aljabbari, A.; Lokras, A.; Foged, C.; Thakur, A. Opportunities and Challenges in the Delivery of MRNA-Based Vaccines. *Pharmaceutics* **2020**, *12* (2). https://doi.org/10.3390/pharmaceutics12020102.
(39) Hobernik, D.; Bros, M. DNA Vaccines-How Far From Clinical Use? *Int J Mol Sci* **2018**, *19* (11). https://doi.org/10.3390/ijms19113605.
(40) Kutzler, M. A.; Weiner, D. B. DNA Vaccines: Ready for Prime Time? *Nat. Rev. Genet.* **2008**, *9* (10), 776–788. https://doi.org/10.1038/nrg2432.
(41) Tejeda-Mansir, A.; García-Rendón, A.; Guerrero-Germán, P. Plasmid-DNA Lipid and Polymeric Nanovaccines: A New Strategic in Vaccines Development. *Biotechnology and Genetic Engineering Reviews* **2019**, *35* (1), 46–68. https://doi.org/10.1080/02648725.2018.1560552.
(42) Lim, M.; Badruddoza, A. Z. M.; Firdous, J.; Azad, M.; Mannan, A.; Al-Hilal, T. A.; Cho, C.-S.; Islam, M. A. Engineered Nanodelivery Systems to Improve DNA Vaccine Technologies. *Pharmaceutics* **2020**, *12* (1), 30. https://doi.org/10.3390/pharmaceutics12010030.

(43) Wang, Z.; Troilo, P. J.; Wang, X.; Griffiths, T. G.; Pacchione, S. J.; Barnum, A. B.; Harper, L. B.; Pauley, C. J.; Niu, Z.; Denisova, L.; Follmer, T. T.; Rizzuto, G.; Ciliberto, G.; Fattori, E.; Monica, N. L.; Manam, S.; Ledwith, B. J. Detection of Integration of Plasmid DNA into Host Genomic DNA Following Intramuscular Injection and Electroporation. *Gene Ther.* **2004**, *11* (8), 711–721. https://doi.org/10.1038/sj.gt.3302213.

(44) Pardi, N.; Hogan, M. J.; Porter, F. W.; Weissman, D. MRNA Vaccines - a New Era in Vaccinology. *Nat Rev Drug Discov* **2018**, *17* (4), 261–279. https://doi.org/10.1038/nrd.2017.243.

(45) Pastor, F.; Berraondo, P.; Etxeberria, I.; Frederick, J.; Sahin, U.; Gilboa, E.; Melero, I. An RNA Toolbox for Cancer Immunotherapy. *Nat Rev Drug Discov* **2018**, *17* (10), 751–767. https://doi.org/10.1038/nrd.2018.132.

(46) Sayour, E. J.; Grippin, A.; De Leon, G.; Stover, B.; Rahman, M.; Karachi, A.; Wummer, B.; Moore, G.; Castillo-Caro, P.; Fredenburg, K.; Sarkisian, M. R.; Huang, J.; Deleyrolle, L. P.; Sahay, B.; Carrera-Justiz, S.; Mendez-Gomez, H. R.; Mitchell, D. A. Personalized Tumor RNA Loaded Lipid-Nanoparticles Prime the Systemic and Intratumoral Milieu for Response to Cancer Immunotherapy. *Nano Lett.* **2018**, *18* (10), 6195–6206. https://doi.org/10.1021/acs.nanolett.8b02179.

(47) Takeoka, T.; Nagase, H.; Kurose, K.; Ohue, Y.; Yamasaki, M.; Takiguchi, S.; Sato, E.; Isobe, M.; Kanazawa, T.; Matsumoto, M.; Iwahori, K.; Kawashima, A.; Morimoto-Okazawa, A.; Nishikawa, H.; Oka, M.; Pan, L.; Venhaus, R.; Nakayama, E.; Mori, M.; Doki, Y.; Wada, H. NY-ESO-1 Protein Cancer Vaccine With Poly-ICLC and OK-432: Rapid and Strong Induction of NY-ESO-1-Specific Immune Responses by Poly-ICLC. *J. Immunother.* **2017**. https://doi.org/10.1097/CJI.0000000000000162.

(48) Ishihara, M.; Tono, Y.; Miyahara, Y.; Muraoka, D.; Harada, N.; Kageyama, S.; Sasaki, T.; Hori, Y.; Soga, N.; Uchida, K.; Shiraishi, T.; Sato, E.; Kanda, H.; Mizuno, T.; Webster, G. A.; Ikeda, H.; Katayama, N.; Sugimura, Y.; Shiku, H. First-in-Human Phase I Clinical Trial of the NY-ESO-1 Protein Cancer Vaccine with NOD2 and TLR9 Stimulants in Patients with NY-ESO-1-Expressing Refractory Solid Tumors. *Cancer Immunol. Immunother.* **2020**, *69* (4), 663–675. https://doi.org/10.1007/s00262-020-02483-1.

(49) Slingluff, C. L.; Petroni, G. R.; Olson, W. C.; Smolkin, M. E.; Chianese-Bullock, K. A.; Mauldin, I. S.; Smith, K. T.; Deacon, D. H.; Varhegyi, N. E.; Donnelly, S. B.; Reed, C. M.; Scott, K.; Galeassi, N. V.; Grosh, W. W. A Randomized Pilot Trial Testing the Safety and Immunologic Effects of a MAGE-A3 Protein plus AS15 Immunostimulant Administered into Muscle or into Dermal/Subcutaneous Sites. *Cancer Immunol. Immunother.* **2016**, *65* (1), 25–36. https://doi.org/10.1007/s00262-015-1770-9.

(50) Sabbatini, P.; Tsuji, T.; Ferran, L.; Ritter, E.; Sedrak, C.; Tuballes, K.; Jungbluth, A. A.; Ritter, G.; Aghajanian, C.; Bell-McGuinn, K.; Hensley, M. L.; Konner, J.; Tew, W.; Spriggs, D. R.; Hoffman, E. W.; Venhaus, R.; Pan, L.; Salazar, A. M.; Diefenbach, C. M.; Old, L. J.; Gnjatic, S. Phase I Trial of Overlapping Long Peptides from a Tumor Self-Antigen and Poly-ICLC Shows Rapid Induction of Integrated Immune Response in Ovarian Cancer Patients. *Clin. Cancer Res.* **2012**, *18* (23), 6497–6508. https://doi.org/10.1158/1078-0432.CCR-12-2189.

(51) Hos, B. J.; Tondini, E.; van Kasteren, S. I.; Ossendorp, F. Approaches to Improve Chemically Defined Synthetic Peptide Vaccines. *Front. Immunol.* **2018**, *9*. https://doi.org/10.3389/fimmu.2018.00884.

(52) Mijalis, A. J.; Thomas, D. A.; Simon, M. D.; Adamo, A.; Beaumont, R.; Jensen, K. F.; Pentelute, B. L. A Fully Automated Flow-Based Approach for Accelerated Peptide

Synthesis. *Nat. Chem. Biol.* **2017**, *13* (5), 464–466. https://doi.org/10.1038/nchembio.2318.
(53) Wang, J.; Hu, X.; Xiang, D. Nanoparticle Drug Delivery Systems: An Excellent Carrier for Tumor Peptide Vaccines. *Drug Delivery* **2018**, *25* (1), 1319–1327. https://doi.org/10.1080/10717544.2018.1477857.
(54) Wang, C.; Li, P.; Liu, L.; Pan, H.; Li, H.; Cai, L.; Ma, Y. Self-Adjuvanted Nanovaccine for Cancer Immunotherapy: Role of Lysosomal Rupture-Induced ROS in MHC Class I Antigen Presentation. *Biomaterials* **2016**, *79*, 88–100. https://doi.org/10.1016/j.biomaterials.2015.11.040.
(55) Sun, B.; Xia, T. Nanomaterial-Based Vaccine Adjuvants. *J Mater Chem B* **2016**, *4* (33), 5496–5509. https://doi.org/10.1039/C6TB01131D.
(56) Keler, T.; He, L.; Ramakrishna, V.; Champion, B. Antibody-Targeted Vaccines. *Oncogene* **2007**, *26* (25), 3758–3767. https://doi.org/10.1038/sj.onc.1210375.
(57) Duarte, J. N.; Cragnolini, J. J.; Swee, L. K.; Bilate, A. M.; Bader, J.; Ingram, J. R.; Rashidfarrokhi, A.; Fang, T.; Schiepers, A.; Hanke, L.; Ploegh, H. L. Generation of Immunity against Pathogens via Single-Domain Antibody-Antigen Constructs. *J. Immunol.* **2016**, *197* (12), 4838–4847. https://doi.org/10.4049/jimmunol.1600692.
(58) Jarvis, C. M.; Zwick, D. B.; Grim, J. C.; Alam, M. M.; Prost, L. R.; Gardiner, J. C.; Park, S.; Zimdars, L. L.; Sherer, N. M.; Kiessling, L. L. Antigen Structure Affects Cellular Routing through DC-SIGN. *Proc. Natl. Acad. Sci. U.S.A.* **2019**, *116* (30), 14862–14867. https://doi.org/10.1073/pnas.1820165116.
(59) Chatterjee, B.; Smed-Sörensen, A.; Cohn, L.; Chalouni, C.; Vandlen, R.; Lee, B.-C.; Widger, J.; Keler, T.; Delamarre, L.; Mellman, I. Internalization and Endosomal Degradation of Receptor-Bound Antigens Regulate the Efficiency of Cross Presentation by Human Dendritic Cells. *Blood* **2012**, *120* (10), 2011–2020. https://doi.org/10.1182/blood-2012-01-402370.
(60) McLennan, D. N.; Porter, C. J. H.; Charman, S. A. Subcutaneous Drug Delivery and the Role of the Lymphatics. *Drug Discov Today Technol* **2005**, *2* (1), 89–96. https://doi.org/10.1016/j.ddtec.2005.05.006.
(61) Liu, H.; Moynihan, K. D.; Zheng, Y.; Szeto, G. L.; Li, A. V.; Huang, B.; Van Egeren, D. S.; Park, C.; Irvine, D. J. Structure-Based Programming of Lymph-Node Targeting in Molecular Vaccines. *Nature* **2014**, *507* (7493), 519–522. https://doi.org/10.1038/nature12978.
(62) Tsopelas, C.; Sutton, R. Why Certain Dyes Are Useful for Localizing the Sentinel Lymph Node. *J. Nucl. Med.* **2002**, *43* (10), 1377–1382.
(63) Lindner, V.; Heinle, H. Binding Properties of Circulating Evans Blue in Rabbits as Determined by Disc Electrophoresis. *Atherosclerosis* **1982**, *43* (2–3), 417–422. https://doi.org/10.1016/0021-9150(82)90040-5.
(64) Milletti, F. Cell-Penetrating Peptides: Classes, Origin, and Current Landscape. *Drug Discov. Today* **2012**, *17* (15–16), 850–860. https://doi.org/10.1016/j.drudis.2012.03.002.
(65) Kauffman, W. B.; Fuselier, T.; He, J.; Wimley, W. C. Mechanism Matters: A Taxonomy of Cell Penetrating Peptides. *Trends Biochem. Sci.* **2015**, *40* (12), 749–764. https://doi.org/10.1016/j.tibs.2015.10.004.
(66) Copolovici, D. M.; Langel, K.; Eriste, E.; Langel, Ü. Cell-Penetrating Peptides: Design, Synthesis, and Applications. *ACS Nano* **2014**, *8* (3), 1972–1994. https://doi.org/10.1021/nn4057269.
(67) LeCher, J. C.; Nowak, S. J.; McMurry, J. L. Breaking in and Busting out: Cell-Penetrating Peptides and the Endosomal Escape Problem. *Biomol Concepts* **2017**, *8* (3–4), 131–141. https://doi.org/10.1515/bmc-2017-0023.

(68) Richard, J. P.; Melikov, K.; Vives, E.; Ramos, C.; Verbeure, B.; Gait, M. J.; Chernomordik, L. V.; Lebleu, B. Cell-Penetrating Peptides: A Reevaluation of the Mechanism of Cellular Uptake. *Journal of Biological Chemistry* **2003**, *278* (1), 585–590. https://doi.org/10.1074/jbc.M209548200.
(69) Deprey, K.; Becker, L.; Kritzer, J.; Plückthun, A. Trapped! A Critical Evaluation of Methods for Measuring Total Cellular Uptake versus Cytosolic Localization. *Bioconjug. Chem.* **2019**, *30* (4), 1006–1027. https://doi.org/10.1021/acs.bioconjchem.9b00112.
(70) He, J.; Kauffman, W. B.; Fuselier, T.; Naveen, S. K.; Voss, T. G.; Hristova, K.; Wimley, W. C. Direct Cytosolic Delivery of Polar Cargo to Cells by Spontaneous Membrane-Translocating Peptides. *Journal of Biological Chemistry* **2013**, *288* (41), 29974–29986. https://doi.org/10.1074/jbc.M113.488312.
(71) Alves, I. D.; Bechara, C.; Walrant, A.; Zaltsman, Y.; Jiao, C.-Y.; Sagan, S. Relationships between Membrane Binding, Affinity and Cell Internalization Efficacy of a Cell-Penetrating Peptide: Penetratin as a Case Study. *PLOS ONE* **2011**, *6* (9), e24096. https://doi.org/10.1371/journal.pone.0024096.
(72) Sani, M.-A.; Separovic, F. How Membrane-Active Peptides Get into Lipid Membranes. *Acc. Chem. Res.* **2016**, *49* (6), 1130–1138. https://doi.org/10.1021/acs.accounts.6b00074.
(73) Qian, Z.; Dougherty, P. G.; Pei, D. Monitoring the Cytosolic Entry of Cell-Penetrating Peptides Using a PH-Sensitive Fluorophore. *Chem Commun (Camb)* **2015**, *51* (11), 2162–2165. https://doi.org/10.1039/c4cc09441g.
(74) LaRochelle, J. R.; Cobb, G. B.; Steinauer, A.; Rhoades, E.; Schepartz, A. Fluorescence Correlation Spectroscopy Reveals Highly Efficient Cytosolic Delivery of Certain Penta-Arg Proteins and Stapled Peptides. *J. Am. Chem. Soc.* **2015**, *137* (7), 2536–2541. https://doi.org/10.1021/ja510391n.
(75) Maiolo, J. R.; Ferrer, M.; Ottinger, E. A. Effects of Cargo Molecules on the Cellular Uptake of Arginine-Rich Cell-Penetrating Peptides. *Biochim. Biophys. Acta* **2005**, *1712* (2), 161–172. https://doi.org/10.1016/j.bbamem.2005.04.010.
(76) Lundin, P.; Johansson, H.; Guterstam, P.; Holm, T.; Hansen, M.; Langel, U.; EL Andaloussi, S. Distinct Uptake Routes of Cell-Penetrating Peptide Conjugates. *Bioconjug. Chem.* **2008**, *19* (12), 2535–2542. https://doi.org/10.1021/bc800212j.
(77) Wu, R. P.; Youngblood, D. S.; Hassinger, J. N.; Lovejoy, C. E.; Nelson, M. H.; Iversen, P. L.; Moulton, H. M. Cell-Penetrating Peptides as Transporters for Morpholino Oligomers: Effects of Amino Acid Composition on Intracellular Delivery and Cytotoxicity. *Nucleic Acids Res.* **2007**, *35* (15), 5182–5191. https://doi.org/10.1093/nar/gkm478.
(78) Kardani, K.; Milani, A.; H Shabani, S.; Bolhassani, A. Cell Penetrating Peptides: The Potent Multi-Cargo Intracellular Carriers. *Expert Opin Drug Deliv* **2019**, *16* (11), 1227–1258. https://doi.org/10.1080/17425247.2019.1676720.
(79) El-Andaloussi, S.; Järver, P.; Johansson, H. J.; Langel, U. Cargo-Dependent Cytotoxicity and Delivery Efficacy of Cell-Penetrating Peptides: A Comparative Study. *Biochem. J.* **2007**, *407* (2), 285–292. https://doi.org/10.1042/BJ20070507.
(80) Wolfe, J. M.; Fadzen, C. M.; Choo, Z.-N.; Holden, R. L.; Yao, M.; Hanson, G. J.; Pentelute, B. L. Machine Learning To Predict Cell-Penetrating Peptides for Antisense Delivery. *ACS Cent Sci* **2018**, *4* (4), 512–520. https://doi.org/10.1021/acscentsci.8b00098.
(81) Tünnemann, G.; Martin, R. M.; Haupt, S.; Patsch, C.; Edenhofer, F.; Cardoso, M. C. Cargo-Dependent Mode of Uptake and Bioavailability of TAT-Containing Proteins and Peptides in Living Cells. *FASEB J.* **2006**, *20* (11), 1775–1784. https://doi.org/10.1096/fj.05-5523com.

(82) Fischer, R.; Waizenegger, T.; Köhler, K.; Brock, R. A Quantitative Validation of Fluorophore-Labelled Cell-Permeable Peptide Conjugates: Fluorophore and Cargo Dependence of Import. *Biochim. Biophys. Acta* **2002**, *1564* (2), 365–374. https://doi.org/10.1016/s0005-2736(02)00471-6.
(83) Yang, J.; Luo, Y.; Shibu, M. A.; Toth, I.; Skwarczynskia, M. Cell-Penetrating Peptides: Efficient Vectors for Vaccine Delivery. *Curr Drug Deliv* **2019**, *16* (5), 430–443. https://doi.org/10.2174/1567201816666190123120915.
(84) Skwarczynski, M.; Toth, I. Cell-Penetrating Peptides in Vaccine Delivery: Facts, Challenges and Perspectives. *Ther Deliv* **2019**, *10* (8), 465–467. https://doi.org/10.4155/tde-2019-0042.
(85) Brooks, N.; Esparon, S.; Pouniotis, D.; Pietersz, G. A. Comparative Immunogenicity of a Cytotoxic T Cell Epitope Delivered by Penetratin and TAT Cell Penetrating Peptides. *Molecules* **2015**, *20* (8), 14033–14050. https://doi.org/10.3390/molecules200814033.
(86) Derouazi, M.; Di Berardino-Besson, W.; Belnoue, E.; Hoepner, S.; Walther, R.; Benkhoucha, M.; Teta, P.; Dufour, Y.; Yacoub Maroun, C.; Salazar, A. M.; Martinvalet, D.; Dietrich, P.-Y.; Walker, P. R. Novel Cell-Penetrating Peptide-Based Vaccine Induces Robust CD4+ and CD8+ T Cell-Mediated Antitumor Immunity. *Cancer Res.* **2015**, *75* (15), 3020–3031. https://doi.org/10.1158/0008-5472.CAN-14-3017.
(87) Batchu, R. B.; Gruzdyn, O.; Potti, R. B.; Weaver, D. W.; Gruber, S. A. MAGE-A3 with Cell-Penetrating Domain as an Efficient Therapeutic Cancer Vaccine. *JAMA Surg* **2014**, *149* (5), 451–457. https://doi.org/10.1001/jamasurg.2013.4113.
(88) Wu, H.; Zhuang, Q.; Xu, J.; Xu, L.; Zhao, Y.; Wang, C.; Yang, Z.; Shen, F.; Liu, Z.; Peng, R. Cell-Penetrating Peptide Enhanced Antigen Presentation for Cancer Immunotherapy. *Bioconjug. Chem.* **2019**, *30* (8), 2115–2126. https://doi.org/10.1021/acs.bioconjchem.9b00245.
(89) Giannouli, C.; Brulet, J.-M.; Gesché, F.; Rappaport, J.; Burny, A.; Leo, O.; Hallez, S. Fusion of a Tumour-Associated Antigen to HIV-1 Tat Improves Protein-Based Immunotherapy of Cancer. *Anticancer Res.* **2003**, *23* (4), 3523–3531.
(90) Shahbazi, S.; Bolhassani, A. Comparison of Six Cell Penetrating Peptides with Different Properties for in Vitro and in Vivo Delivery of HPV16 E7 Antigen in Therapeutic Vaccines. *Int. Immunopharmacol.* **2018**, *62*, 170–180. https://doi.org/10.1016/j.intimp.2018.07.006.
(91) Pouniotis, D.; Tang, C.-K.; Apostolopoulos, V.; Pietersz, G. Vaccine Delivery by Penetratin: Mechanism of Antigen Presentation by Dendritic Cells. *Immunol. Res.* **2016**, *64* (4), 887–900. https://doi.org/10.1007/s12026-016-8799-5.
(92) Buhl, T.; Braun, A.; Forkel, S.; Möbius, W.; van Werven, L.; Jahn, O.; Rezaei-Ghaleh, N.; Zweckstetter, M.; Mempel, M.; Schön, M. P.; Haenssle, H. A. Internalization Routes of Cell-Penetrating Melanoma Antigen Peptides into Human Dendritic Cells. *Exp. Dermatol.* **2014**, *23* (1), 20–26. https://doi.org/10.1111/exd.12285.
(93) Pouniotis, D. S.; Esparon, S.; Apostolopoulos, V.; Pietersz, G. A. Whole Protein and Defined CD8(+) and CD4(+) Peptides Linked to Penetratin Targets Both MHC Class I and II Antigen Presentation Pathways. *Immunol. Cell Biol.* **2011**, *89* (8), 904–913. https://doi.org/10.1038/icb.2011.13.
(94) Belnoue, E.; Di Berardino-Besson, W.; Gaertner, H.; Carboni, S.; Dunand-Sauthier, I.; Cerini, F.; Suso-Inderberg, E.-M.; Wälchli, S.; König, S.; Salazar, A. M.; Hartley, O.; Dietrich, P.-Y.; Walker, P. R.; Derouazi, M. Enhancing Antitumor Immune Responses by Optimized Combinations of Cell-Penetrating Peptide-Based Vaccines and Adjuvants. *Mol. Ther.* **2016**, *24* (9), 1675–1685. https://doi.org/10.1038/mt.2016.134.

(95) Grau, M.; Walker, P. R.; Derouazi, M. Mechanistic Insights into the Efficacy of Cell Penetrating Peptide-Based Cancer Vaccines. *Cell. Mol. Life Sci.* **2018**, *75* (16), 2887–2896. https://doi.org/10.1007/s00018-018-2785-0.
(96) Belnoue, E.; Mayol, J.-F.; Carboni, S.; Di Berardino Besson, W.; Dupuychaffray, E.; Nelde, A.; Stevanovic, S.; Santiago-Raber, M.-L.; Walker, P. R.; Derouazi, M. Targeting Self and Neo-Epitopes with a Modular Self-Adjuvanting Cancer Vaccine. *JCI Insight* **2019**, *5*. https://doi.org/10.1172/jci.insight.127305.
(97) Phase 1b Study to Evaluate ATP128, With or Without BI 754091, in Patients With Stage IV Colorectal Cancer - Full Text View - ClinicalTrials.gov https://clinicaltrials.gov/ct2/show/NCT04046445 (accessed Jun 15, 2020).

Chapter 2: Automated Flow Synthesis of Tumor Neoantigen Peptides for Personalized Immunotherapy

The work presented in this chapter has been reproduced from the following publication:

Truex, N. L.,* Holden, R. L.,* Wang, B.-Y., Chen, P.-G., Hanna, S., Hu, Z., Shetty, K., Olive, O., Neuberg, D., Hacohen, N., Keskin, D. B., Ott, P. A., Wu, C. J. & Pentelute, B. L. Automated Flow Synthesis of Tumor Neoantigen Peptides for Personalized Immunotherapy. *Sci. Rep.* **10,** 723 (2020).

**These authors contributed equally to this work.*

Author contributions:

R.L.H., N.L.T., C.J.W. and B.L.P. designed the study. N.L.T, B.-Y.W., P.-G.C. and S.H., collected, analyzed, and interpreted the peptide synthesis and purification data for the immunizing peptides. R.L.H. collected, analyzed, and interpreted the peptide synthesis and purification data for the assay peptides. B.L.P., K.S., O.O., D.B.K., N.H. and P.A.O. also analyzed and interpreted data. Z.H. performed the IFN-γ ELISPOT assays. D.N., R.L.H., and N.L.T. performed statistical analyses. R.L.H., N.L.T., C.J.W. and B.L.P. wrote the manuscript that was validated by all the authors.

2.1 Introduction

Personalized medicine guided by genome-sequencing technology represents a new paradigm for disease treatment and prevention.[1] These therapies offer the promise of precision, but also present a formidable challenge—administering custom-made treatments on demand.[2-4] Providing these treatments in a rapid and affordable fashion remains a barrier that currently limits their potential.[5,6]

A salient example for personalized medicine is that of personalized neoantigen vaccines for cancer, in which on-demand manufacturing for individual patients is a challenge.[7-13] These vaccines are based on the array of somatic mutations that can form in a tumor, which encode novel, tumor-specific antigens, called 'neoantigens'. Immune targeting of multiple neoantigens in concert is expected to promote selective immune activation against cancer cells and prevent immunologic escape. Indeed, five clinical trials testing personalized neoantigen vaccines in patients with melanoma and glioblastoma multiforme have shown that these treatments can generate immune responses in humans.[12-16] Synthetic long peptides are a mainstay of the treatments, which have also been administered in conjunction with adjuvants.[17,18] Four of the five clinical trials with personalized cancer vaccines have used synthetic peptides in the immunizing formulation,[12-15] while the fifth study used synthetic RNA.[16] All five trials also used several dozen shorter peptides per patient to perform *ex vivo* immune monitoring studies.

Personalized neoantigen-targeting vaccine studies use hundreds of peptides that range in length from 8 to 30 amino acids. In designing the peptides, several studies have adopted the following workflow: After a tumor biopsy, mutated epitopes were identified using whole-exome sequencing (WES) of tumor and normal cells in parallel; Epitope peptides (EPTs) of 8 to 10 amino acids that can bind to personal human leukocyte antigen (HLA) alleles were then identified using class I binding predictive algorithms;[19] Up to 20 minimal class I epitope peptides were chosen as neoantigen vaccine targets, and were included within synthetic long immunizing peptides (IMPs) of 15 to 30 amino acids; The peptides were then synthesized by a commercial peptide vendor, cleaved and purified under good manufacturing practice (GMP) conditions, and then administered to the patient as immunizing peptides (see Fig. 2.1A). The long peptides, IMPs, were synthesized for vaccine administration, because similar peptides have been shown to effectively stimulate antigen-specific $CD4^+$ and $CD8^+$ T cells.[17,18] In addition, shorter overlapping assay peptides (ASPs) were synthesized to evaluate immune responses. Figure 2.1B illustrates the EPTs, ASPs, and IMPs, summarizing the quantity of each set designed per patient. In the earlier studies, the average lead time to generate 20 IMPs ranged

from 18 to 20 weeks, which was largely devoted to the time-consuming and expensive synthesis of clinical-grade peptides.[12,13] Minimizing this time and cost is vital to allow treatment of other cancer types, including metastatic cancers.

In 2017, we introduced an automated flow peptide synthesizer that accelerates the rate of peptide synthesis.[20] This synthesizer builds on our previous advances with flow chemistry of fluorenylmethyloxycarbonyl (Fmoc)-based solid-phase peptide synthesis.[20-24] The flow conditions can achieve quantitative amide-bond coupling in seconds, while standard microwave or batch peptide syntheses require minutes or even hours. Our automated flow synthesizer (see Fig. 2.1C) is composed of five main modules: (1) three solvent pumps, which continuously draw solutions of amino acids, activator base, deprotection agents, *N*,*N*-diisopropylethylamine (DIPEA), or *N*,*N*-dimethylformamide (DMF); (2) reagent storage bottles; (3) two heating loops, which preheat the solutions prior to flowing into the reaction vessel; (4) one heated reaction chamber, which stores the solid-support resin for synthesis; and (5) one UV-vis detector (not shown), which allows relative quantification of Fmoc removal during the deprotection step.

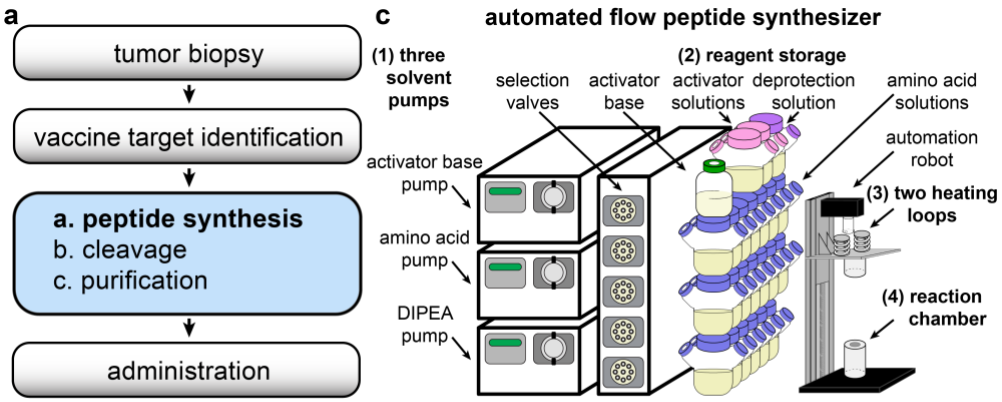

b

name	description	peptide sequence	length	quantity per vaccine
WT	wild type	THISISANEXAMPLESEQUENCE		
IMP	immunizing peptide	THISISANEXVMPLESEQUENCE	~ 30	~ 20
ASP	assay peptide	ISANEXVMPLESEQ	~ 15	~1 to 3 per IMP
EPT	epitope peptide	ANEXVMPLE	9 or 10	~1 to 3 per IMP

Figure 2.1. Peptide design and production for a personalized neoantigen vaccine. (a) Workflow for the design and production of neoantigen vaccines. (b) Example peptide sequences for a wild type (WT), immunizing (IMP), immune monitoring assay (ASP), and epitope (EPT) peptide. (c) Schematic illustration of an automated flow peptide synthesizer (without connective capillary tubing and UV-vis module).

Here we describe how automated flow peptide synthesis can facilitate the production of neoantigen peptides for personalized cancer vaccines. We show that automated flow peptide synthesis can produce high-quality 30-mer IMPs in less than 35 minutes, while other peptide

synthesis methods take several hours or days. We also show these peptides are equal or higher in quality when compared to peptides produced by microwave or batch synthesis, and that these peptides can be purified. Further, we demonstrate that automated flow synthesis technology enables high-throughput production of a set of 15- to 16-mer ASPs for immune-assessment assays. Our results illustrate how automated flow synthesis increases the rate and quality of peptide production. We envision that manufacturing neoantigen vaccines using this technology will greatly reduce turnaround time and increase availability, thereby enabling true on-demand administration of these personalized treatments.

2.2 Results and Discussion

Limitations of conventional peptide synthesis for personalized neoantigens. Generating the peptides needed for personalized neoantigen vaccines has been difficult using conventional peptide synthesis. Across two clinical studies, personalized neoantigen vaccines were designed, produced, and administered to 22 patients with either high-risk melanoma (NCT01970358) or newly diagnosed glioblastoma (NCT02287428).[12,13] The peptides varied in length from 13 to 34 amino acids, and averaged 23 amino acids. The peptides were synthesized by a commercial peptide vendor using conventional synthesis. The median turnaround time from design to synthesis was 18 to 20 weeks. Although 598 immunizing peptides were designed for these studies, only 400 peptides (67%) could be synthesized and purified (≥95% purity).

As a representative test case to evaluate the limits of neoantigen peptide production by our automated flow synthesis technology, we selected a set of 29 IMPs that were particularly difficult and time consuming to synthesize, called IMPs **1**–**29** (see Table 2.1). These peptides originated from 19 different genes and had previously been designed for inclusion in a vaccine.[12]

When the commercial vendor attempted to produce IMPs **1**–**29**, their efforts yielded successful syntheses for only 17 of the 29 peptides. Of these 17, only 10 passed purity analysis requirements after purification (>95% HPLC purity). The other 7 IMPs remained lower in purity (89–94% HPLC purity), even after two or three rounds of purification. Challenges encountered throughout the synthesis and purification led to substantial manufacturing delays, and ultimately resulted in only 10 of 29 IMPs returned, or a 66% failure rate (see Fig. 2.2.A).

The following describes our synthesis and purification of IMPs **1**–**29** using automated flow peptide synthesis (see Fig. 2.2B). We envisioned that producing this set of 30-mer peptides

would test the limits of this technology and establish whether flow synthesis can facilitate on-demand production of the immunizing peptides for personalized cancer vaccines.

Table 2.1. Sequences of IMPs **1**–**29** from a previous clinical trial.

	amino acid sequence	gene origin	IMP length	vendor purity	purified purity
IMP **1**	LTPLTLIQRMNLLMKISIHKLQKSEF	PTEN	26	94	95
IMP **2**	MNLLMKISIHKLQKSEFFFIKRDKT	PTEN	25	89	95
IMP **3**	DNEPDHYILTPLTLIQRMNLLMKISI	PTEN	26		95
IMP **4**	IQRMNLLMKISIHKLQKSEFFFIKRDKTP	PTEN	29		84
IMP **5**	RSSFIQHNMTHTRENPFYAKNVGKLFTTA	ZNF599	29	94	96
IMP **6**	THTRENPFYAKNVGKLFTTAPHLLNI	ZNF599	26	96	98
IMP **7**	KIKELLPDWGGQHHGLREVLAAALFAS	CPT1C	27	99	96
IMP **8**	DWGGQHHGLREVLAAALFASCLWGA	CPT1C	25		69
IMP **9**	SFKLENLEFPDMPLEEWQEIDEKINEMK	AXDND1	28	95	95
IMP **10**	FTLQIRGRERFEMYRELNEALELKD	TP53	25		56
IMP **11**	TLQIRGRERFEMYRELNEALELK	TP53	23		92
IMP **12**	RAELQASDHRPVMAIVEVEVQEVDVG	SYNJ2	26		47
IMP **13**	HRPVMAIVEVEVQEVDVGARERVF	SYNJ2	24		96
IMP **14**	YSLDSSGNQNLYAMYQLSHFQSISVL	PLEKHM3	26		53
IMP **15**	SSGNQNLYAMYQLSHFQSISVLG	PLEKHM3	23	92	83
IMP **16**	TMLVSSLRDHFPDLPLHIHTHDTS	PC	24	93	99
IMP **17**	HIRPLEKEKVIPLVTSFIEAL	UTP20	21	98	97
IMP **18**	KEKVIPLVTSFIEALFMTVDKGSFGK	UTP20	26		97
IMP **19**	DLNPLIKLSGAYLVDDYDPDTSL	IGF2R	23	96	97
IMP **20**	KLSGAYLVDDYDPDTSLFINVCR	IGF2R	23		98
IMP **21**	GDFSREWAEAQHMMRELRNRNFGKHL	LAMA3	26	90	95
IMP **22**	DPRWIRAWWGGFLLCGALLF	SLCO3A1	20		60
IMP **23**	SNLDITPDDPRWIRAWWGGFLLCGA	SLCO3A1	25		45
IMP **24**	MEKQDKWTRKNIKNTRLIHFGDIQA	PLBD1	25	99	75
IMP **25**	AHVIEDQHKFPNYFGKEIIGGMLDI	CWF19L2	25	93	87
IMP **26**	YLTTVELYRCLEARQQEKHFEVLIS	KIF18B	25	97	96
IMP **27**	YLTTVELYRCLEARQQEK	KIF18B	18	99	95
IMP **28**	RRSTECSIHLEVIVDRPLQVFHVD	PCDHAC2	24	98	88
IMP **29**	RLPGSSDCAASASKVVGITDDVFLPK	FAM193A	26	97	95

[a]Determined by analytical RP-HPLC by integrating the peptide and impurity peaks at 214 nm.

[b]Synthesized using batch peptide synthesis by the commercial vendor.

[c]Synthesized using automated flow peptide synthesis.

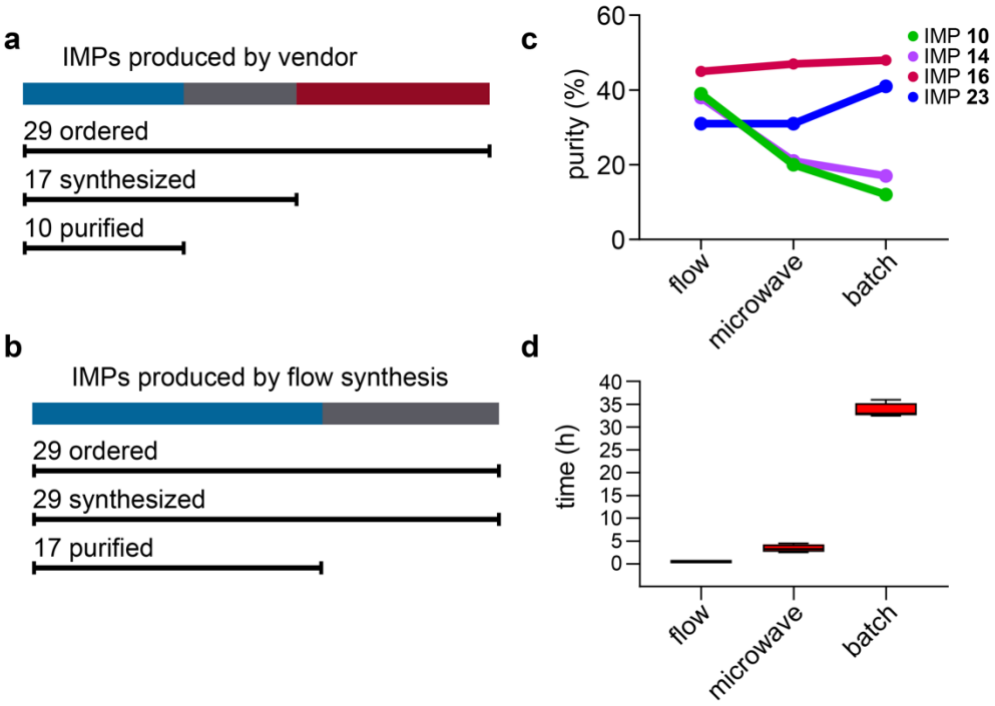

Figure 2.2. Comparison of peptide synthesis methods. (a) Summary of IMPs produced by a commercial peptide vendor. (b) Summary of IMPs produced by flow synthesis. (c) RP-HPLC purity of unpurified (crude) IMP **10**, IMP **14**, IMP **16**, and IMP **23** produced by flow, microwave, and batch synthesis. (d) Synthesis times of the four IMPs by flow, microwave, and batch methods. The upper, middle and lower hinges of the box plot indicate 75th, 50th and 25th quartiles, the whiskers extend to 1.5× the interquartile range below and above the lower and upper hinge, respectively. The Kruskal-Wallis test was used for comparing the synthesis times, which indicated the synthesis times are significantly different for each method (P = 0.0002).

Comparison of flow, microwave, and traditional batch synthesis. First, we compared automated flow peptide synthesis with other methods. We synthesized four IMPs by flow, microwave, and batch peptide synthesis, using homologous coupling reagents and conditions for each method (see Tables 2.4 and 2.5), then we compared the synthesis quality and time.

We selected IMP **10**, IMP **14**, IMP **16**, and IMP **23** to compare the flow, microwave, and batch peptide synthesis methods. We synthesized these IMPs on a 0.1 mmol scale by manually loading the C-terminal amino acid residue onto HMPB-ChemMatrix resin. We then coupled the subsequent amino acids with an excess of activated amino acid, according to previously published protocols for flow (10 equiv.),[20] microwave (5 equiv.),[25] and batch (12 equiv.)[26] peptide synthesis. After completion of the syntheses, the peptides were cleaved from the resin and the protecting groups were removed with a trifluoroacetic acid cleavage cocktail. The

peptides were then precipitated with diethyl ether (-80 ^{o}C), resuspended with CH_3CN in H_2O with 0.1% trifluoroacetic acid (TFA) and lyophilized. After lyophilization, we obtained the crude unpurified peptides as their TFA salts (white or yellow powder).

We then evaluated the quality of each synthesis by analyzing the unpurified IMPs using analytical RP-HPLC and LC/MS. The HPLC data were recorded using an Agilent Zorbax 5 µm 300SB-C3 column (2.1 x 150 mm) with a gradient of 5–65% CH_3CN with 0.08% TFA in H_2O with 0.1% TFA and a flow rate of 0.8 mL/min over 24 min (see Fig. 2.3). We determined the peptide purity from each chromatogram by measuring the relative integrals of the peaks at 214 nm (see Fig. 2.2C). The average purity of the IMPs produced by flow synthesis was 38%, while the average purity of the IMPs produced by microwave and batch peptide synthesis was 30%. Corroboratory HPLC data were also recorded using a Phenomenex Aeris 3.6 µm WIDEPORE C4 column (see Fig. 2.4). This analysis gave similar results: immunizing peptides produced by flow synthesis are comparable (IMPs **16** and **23**) or higher (IMPs **10** and **14**) in purity than those produced by microwave or batch synthesis. These results show that flow synthesis can generate peptides at a similar or higher purity compared to conventional synthesis methods (see Fig. 2.5).

In addition, the automated flow technology substantially reduced the synthesis time. The markedly shorter synthesis time for flow synthesis reflects the efficiency of the technology rather than the reaction conditions. Each flow synthesis was complete in less than 35 min, and all four peptides were complete in less than three hours. By comparison, each microwave synthesis was complete after 4 to 6 h and each batch synthesis was complete after 24 to 48 h (see Fig. 2.2D, Fig. 2.5).

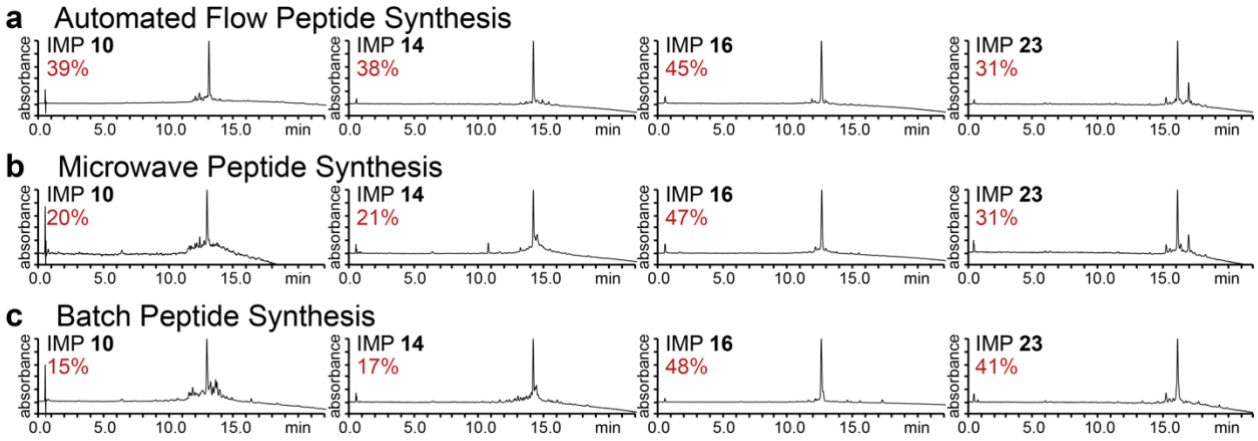

Figure 2.3. Analytical RP-HPLC traces of IMP 10, IMP 14, IMP 16, and IMP 23. Produced by (a) automated flow, (b) microwave, and (c) batch synthesis. Conditions: Agilent Zorbax 5 µm 300SB-C3 column (2.1 × 150 mm) with a gradient of 5–65% CH_3CN with 0.08% TFA in H_2O with 0.1% TFA and a flow rate of 0.8 mL/min over 24 min.

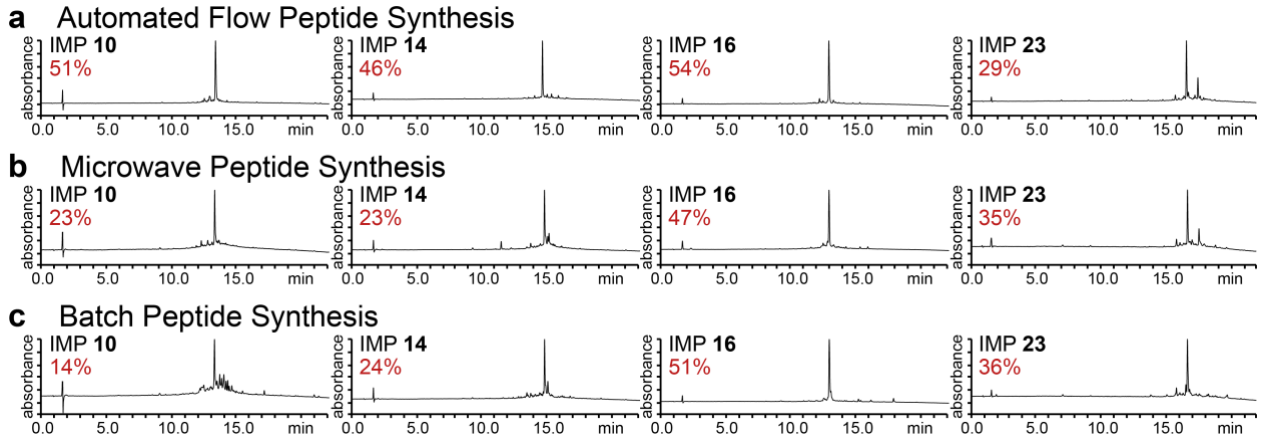

Figure 2.4. Analytical RP-HPLC traces of IMP 10, IMP 14, IMP 16, and IMP 23. Produced by (a) automated flow, (b) microwave, and (c) batch synthesis. Conditions: Phenomenex Aeris 3.6 µm WIDEPORE C4 column (4.6 × 150 mm) with a gradient of 5–65% CH_3CN with 0.08% TFA in H_2O with 0.1% TFA and a flow rate of 0.8 mL/min over 24 min.

IMP **10**

synthesis method	synthesis time (hh:mm)	mass (mg)	purity (%)	yield (%)
flow	00:31	107	39	22
microwave	04:30	55	20	6
batch	32:48	45	15	4

IMP **14**

synthesis method	synthesis time (hh:mm)	mass (mg)	purity (%)	yield (%)
flow	00:31	123.5	38	29
microwave	02:30	27	21	4
batch	36:18	124	17	13

IMP **16**

synthesis method	synthesis time (hh:mm)	mass (mg)	purity (%)	yield (%)
flow	00:30	93	45	24
microwave	03:06	82	47	22
batch	33:00	95	48	26

IMP **23**

synthesis method	synthesis time (hh:mm)	mass (mg)	purity (%)	yield (%)
flow	00:30	59	31	11
microwave	03:30	12	31	2
batch	32:54	59	41	15

Figure 2.5. Summary of synthesis data for unpurified IMPs 10, 14, 16, and 23 synthesized by flow, microwave, and batch peptide synthesis. Each graph shows synthesis time, isolated mass (mg), unpurified purity (%), and isolated yield (%). Purity (%) was determined with analytical RP-HPLC using an Agilent Zorbax 5 µm 300SB-C3 column (2.1 × 150 mm) by integrating the chromatogram peaks at 214 nm. Yield (%) was calculated based on the mass and purity of recovered peptide from a resin cleavage on a 0.05 mmol scale.

Automated flow peptide synthesis of a neoantigen vaccine. We set out to produce at least 20 of 29 IMPs, which was the target number of peptides per vaccine in previous clinical trials.[12,13] We performed these syntheses on a 0.1 mmol scale by manually loading the C-terminal amino acid residue onto HMPB-ChemMatrix resin, then coupling the subsequent amino acids in flow. After the syntheses were complete (<35 min), we cleaved and lyophilized the peptides to obtain the unpurified peptides as the TFA salt (white or yellow powder). Mass spectrometry (ESI) analysis of the unpurified peptides showed that the desired mass was the main product for all 29 IMPs. Analytical RP-HPLC was then used to quantify the purity, which further indicated that automated flow peptide synthesis successfully produced all 29 IMPs (Fig. 2.6). Table 2.2 summarizes the purity and yield of each unpurified IMP.

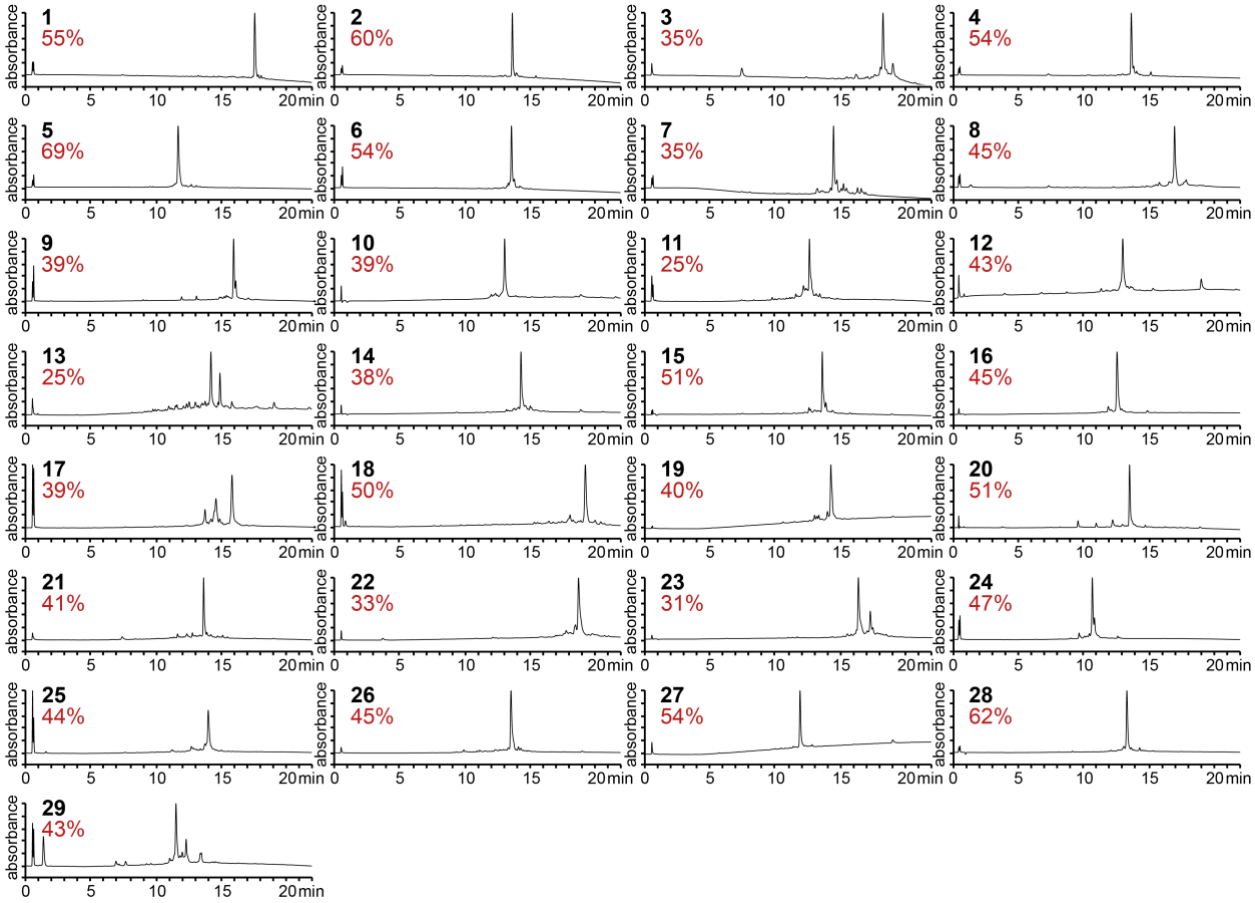

Figure 2.6. Unpurified neoantigen peptides produced by automated flow peptide synthesis. Analytical RP-HPLC traces of the unpurified IMPs **1**–**29**. The relative integration of each IMP is shown on its corresponding trace (red), and was determined by integrating the peptide and impurity peaks at 214 nm. Conditions: Agilent Zorbax 5 µm 300SB-C3 column (2.1 × 150 mm) with a gradient of 5–65% CH_3CN with 0.08% TFA in H_2O with 0.1% TFA and a flow rate of 0.8 mL/min over 24 min.

Purification of IMPs. We purified IMPs **1**–**29** to evaluate whether we could obtain these peptides in high purity for use in a vaccine (≥95%). The IMPs were purified by suspending them in a solution of CH_3CN in H_2O with 0.1% TFA, followed by preparative RP-HPLC and lyophilization of the clean fractions to obtain the IMPs as TFA salts (white powder). We then evaluated the purified IMPs by analytical RP-HPLC (see Fig. 2.7), and confirmed the results with corroboratory RP-HPLC analysis (see Fig. 2.8). Table 2.2 summarizes the final purity, HPLC retention time, and isolated yield for each IMP, based on the cleavage of 0.05 mmol (50% of resin from a 0.1 mmol scale synthesis). Before purification, 3 IMPs were obtained with a purity of ≥60%, 7 with a purity between 50 and 59%, 9 with a purity between 40 and 49%, and 10 with a purity of <40% (see Fig. 2.9). After purification, 17 IMPs were obtained with a

purity of ≥95%, 5 with a purity between 80 and 94%, and 7 with a purity of <80% (see Fig. 2.9). The yield based on the loading of the first amino acid varied from 2 to 27% (3 to 47 mg), and averaged 11% (19 mg).

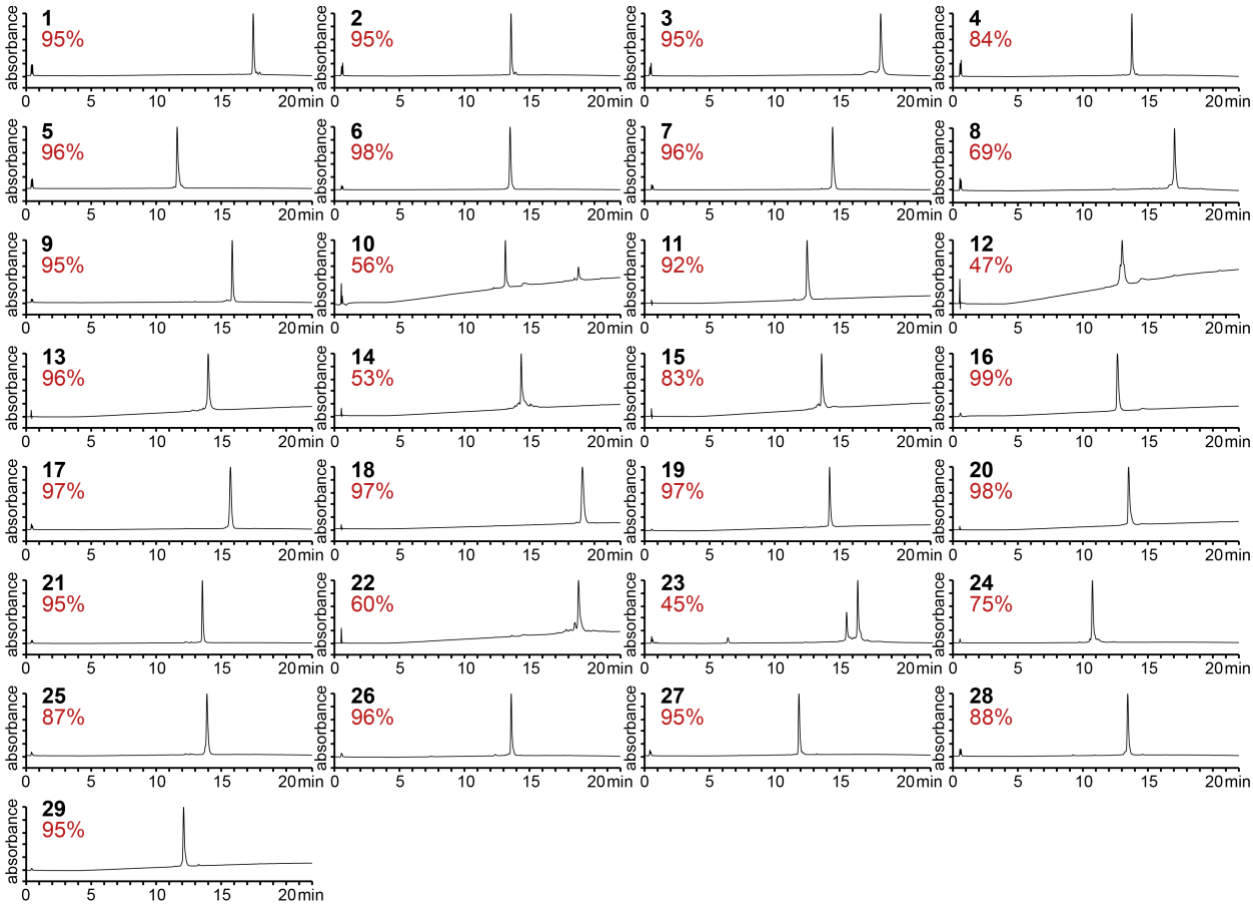

Figure 2.7. Purified neoantigen peptides produced by automated flow peptide synthesis. Analytical HPLC traces of the purified IMPs **1**–**29**. The relative integration of each IMP is shown on its corresponding trace (red), and was determined by integrating the peptide and impurity peaks at 214 nm. Conditions: Agilent Zorbax 5 µm 300SB-C3 column (2.1 × 150 mm) with a gradient of 5–65% CH_3CN with 0.08% TFA in H_2O with 0.1% TFA and a flow rate of 0.8 mL/min over 24 min.

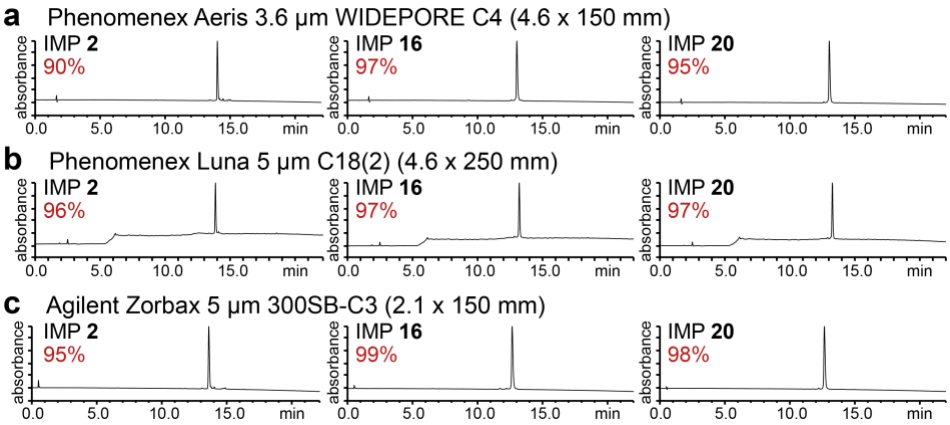

Figure 2.8. Analytical RP-HPLC traces of purified IMP 2, IMP 16, and IMP 20. Conditions: (a) Phenomenex Aeris 3.6 µm WIDEPORE C4 column (4.6 × 150 mm) with a gradient of 5–65% CH_3CN with 0.08% TFA in H_2O with 0.1% TFA and a flow rate of 0.8 mL/min over 24 min; (b) Phenomenex Luna 5 µm C18(2) column (4.6 × 250 mm) with a gradient of 0–70% CH_3CN in H_2O with 0.1% TFA and a flow rate of 1.5 mL/min over 20 min; and (c) Agilent Zorbax 5 µm 300SB-C3 column (2.1 × 150 mm) with a gradient of 5–65% CH_3CN with 0.08% TFA in H_2O with 0.1% TFA and a flow rate of 0.8 mL/min over 24 min.

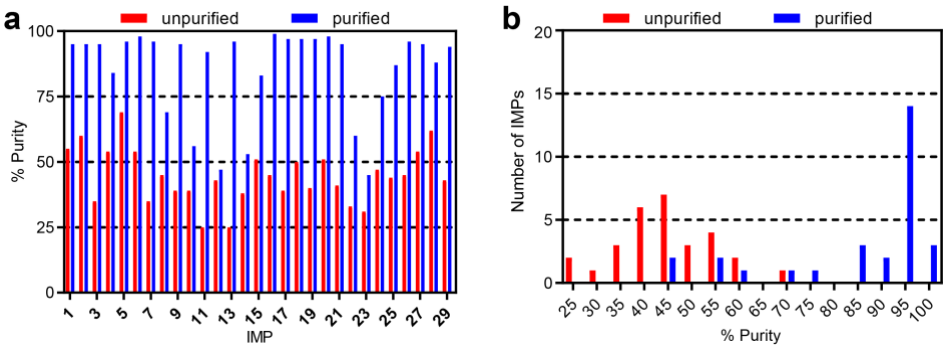

Figure 2.9. Characterization of IMPs produced by automated flow peptide synthesis. The graphs show (a) the individual purity and (b) the distribution of purity for IMPs **1**–**29**, before and after purification. The unpurified and purified purity is shown with red and blue bars, respectively.

Table 2.2. Summary of yield and purity data for unpurified and purified IMPs **1**–**29** synthesized by automated flow peptide synthesis**.**

	average M.W.	automated flow synthesis	unpurified yield	unpurified purity	purified yield	purified yield	ret. time by	purified purity	commercial vendor purity
IMP **1**	3096.82	31	101.1	55	18.1	10	17.5	95	94
IMP **2**	3096.76	30	95.9	60	31.5	16	13.5	95	89
IMP **3**	3082.67	31	93.5	35	26.3	15	18.2	95	
IMP **4**	3591.36	35	141.4	54	36.6	16	13.7	84	
IMP **5**	3396.78	35	100.5	69	50.8	24	11.7	96	94
IMP **6**	2983.37	33	109.6	54	30.4	17	13.5	98	96
IMP **7**	2957.41	32	77.8	35	7.3	4	14.4	96	99
IMP **8**	2666.00	30	26.6	45	8.0	5	17.0	69	
IMP **9**	3482.88	33	103.8	39	46.6	24	15.9	95	95
IMP **10**	3157.56	31	107.3	39	6.9	4	13.0	56	
IMP **11**	2895.30	34	100.2	25	25.7	14	12.5	92	
IMP **12**	2877.21	32	73.8	43	5.1	3	13.0	47	
IMP **13**	2765.16	30	86.9	25	3.3	2	14.2	96	
IMP **14**	2966.26	31	123.5	38	3.5	2	14.3	53	
IMP **15**	2544.81	27	47.7	51	16.1	12	13.6	83	92
IMP **16**	2770.12	30	93.1	45	47.2	27	12.6	99	93
IMP **17**	2432.91	25	59.9	39	9.3	6	15.8	97	98
IMP **18**	2885.41	31	51.6	50	9.7	6	19.0	97	
IMP **19**	2537.80	27	44.8	40	8.3	6	14.2	97	96
IMP **20**	2604.90	27	53.0	51	7.0	5	13.5	98	
IMP **21**	3216.59	33	108.1	41	30.6	15	13.6	95	90
IMP **22**	2377.83	24	35.1	33	12.4	9	18.7	60	
IMP **23**	2860.24	30	59.1	31	5.5	3	16.4	45	
IMP **24**	3071.52	31	82.3	47	6.2	3	10.7	75	99
IMP **25**	2872.26	30	80.7	44	32.1	19	14.0	87	93
IMP **26**	3069.48	34	65.9	45	18.8	10	13.5	96	97
IMP **27**	2243.53	22	78.2	54	21.5	16	11.9	95	99
IMP **28**	2849.25	30	91.3	62	13.3	8	13.4	88	98
IMP **29**	2634.00	31	34.7	43	11.3	7	12.2	95	97

[a]Calculated molecular weight.

[b]Determined gravimetrically by weighing the peptide on an analytical balance.

[c]Based on recovery from cleaving 50% of resin from a 0.1 mmol peptide synthesis.

[d]Determined by analytical RP-HPLC by integrating the peptide and impurity peaks at 214 nm.

[e]Zorbax 5 µm 300SB-C3 column (2.1 × 150 mm), 5–65% of CH_3CN (0.08% TFA) in H_2O (0.1% TFA) at 0.8 mL/min over 24 min.

[f]Phenomenex Luna 5 µm C18(2) column (4.6 × 250 mm), 0–70% of CH_3CN (0.1% TFA) in H_2O (0.1% TFA) at 1.5 mL/min over 20 min.

These results illustrate that high-fidelity peptide synthesis can facilitate purification. For the 17 purified IMPs obtained with ≥95% purity, the unpurified precursors averaged 46% purity. For the 9 that remained lower in purity, the unpurified precursors averaged 43% purity. This observation shows that a higher quality peptide synthesis can facilitate purification and, in turn, accelerate production overall.

High-throughput production of ASPs. Given the importance of shorter neoantigen peptides for immune monitoring, we determined whether we could rapidly produce ASPs and EPTs using our automated flow synthesis technology. In patients vaccinated with 20 IMPs, approximately 40–50 of these peptides, 14–15 amino acids in length, are required for immune monitoring.

Since these peptides are not used for immunizations, they can be produced with lower purity (>70%) and in lower amounts (1 mg). We selected a set of ASPs as a test case to synthesize by automated flow peptide synthesis, called ASPs **1**–**48**. Table 2.3 lists the sequences and lengths of the ASPs we produced by flow synthesis and also shows the final purity.

We synthesized the ASPs in a similar fashion as the IMPs, but also developed an efficient workflow for isolating these peptides from resin in parallel. This workflow, combined with flow synthesis, permitted the production of ASPs in a remarkably high-throughput fashion. Figure 2.10 summarizes the ASP purity after synthesis and purification.

We were able to successfully produce all 48 ASPs by automated flow peptide synthesis. The syntheses were complete in less than 20 min. We then cleaved multiple ASPs from resin in parallel. After the syntheses were complete, the resin was rinsed with CH_2Cl_2 and aspirated under vacuum until dry. We transferred an aliquot (~100 mg) of the dried resin into a 24-well filter plate. Within the plate, each well contained a filter at the bottom and, underneath the plate, a syringe-like dispenser. After covering the dispensers with luer-lock syringe caps, we added a TFA cleavage solution (2 mL) to each well for 2 h. We precipitated the peptides by adding chilled (-80 ^{o}C) diethyl ether (5 mL) to each well, removing the syringe caps, and allowing the solution to drain. We performed two additional washes with diethyl ether, then added a solution of H_2O/CH_3CN (90:10) with 6 M guanidine at pH 2 (1 mL) to re-suspend the peptides in solution. We then used a vacuum manifold to drain the solutions into separate glass screw-top vials (1 mL) for immediate purification. We found that this procedure worked well for isolating ASPs in a high-throughput fashion on a small scale (100 mg of resin).

Table 2.3. Sequences from a set of ASPs for a personalized neoantigen vaccine.

	amino acid sequence	length	purity (%)
ASP **1**	ISTSSTIANILAAAV	15	86[b]
ASP **2**	IANILAAAVASISNQ	15	99[b]
ASP **3**	NNISNFFAKILFEEA	15	88[a]
ASP **4**	FAKILFEEANGRLVAS	16	92[b]
ASP **5**	SYEAYVLNIVRFLKK	15	88[a]
ASP **6**	YVLNIVRFLKKYKDSA	16	94[a]
ASP **7**	VRFLKKYKDSAQRDD	15	93[a]
ASP **8**	MEQGDWLIEGDLQVL	15	91[b]
ASP **9**	DWLIEGDLQVLDRVY	15	92[a]
ASP **10**	EGDLQVLDRVYWNDG	15	83[a]
ASP **11**	EQLRPLLASSLPLAV	15	73[a]
ASP **12**	LRPLLASSLPLAVRY	15	52[a]
ASP **13**[c]	YFQIGYMISLIAFFT	15	
ASP **14**[c]	ISLIAFFTNFYIQTY	15	
ASP **15**	HPSTVLDHKLEWVLY	15	78[a]
ASP **16**	HNLATYVFLHTMKGT	15	82[a]
ASP **17**	STVLDHKLEWVLYNE	15	78[a]
ASP **18**	RVTSAIHLIDSNTLQ	15	82[a]
ASP **19**	AIHLIDSNTLQVADI	15	65[a]
ASP **20**	IDSNTLQVADIDGST	15	82[a]
ASP **21**	TSISVHRYLGICHSL	15	54[a]
ASP **22**	HRYLGICHSLRALRW	15	88[a]
ASP **23**	ICHSLRALRWGRPRL	15	82[a]
ASP **24**	NPLYWNVVARWKHKT	15	90[a]
ASP **25**	NVVARWKHKTRKLSRA	16	82[a]
ASP **26**	KHKTRKLSRAFGSPY	15	95[a]
ASP **27**	ATYVFLHTMKGTPFE	15	65[a]
ASP **28**	VFLHTMKGTPFETPD	15	81[a]
ASP **29**	DRARREQERICLFSA	15	79[a]
ASP **30**	RREQERICLFSADPF	15	73[a]
ASP **31**	QERICLFSADPFDLE	15	96[b]
ASP **32**	SGSGVVSLHCLQHVV	15	76[a]
ASP **33**	VVSLHCLQHVVAVEA	15	86[b]
ASP **34**	HCLQHVVAVEAYTRE	15	84[b]
ASP **35**	LPHCSLIFPATNWIS	15	80[a]
ASP **36**	CSLIFPATNWISGGQ	15	97[b]
ASP **37**	IFPATNWISGGQNIT	15	86[a]
ASP **38**	SHEVLSHIFRYLSLQ	15	89[a]
ASP **39**	SHIFRYLSLQDIMCME	16	78[a]
ASP **40**	LSLQDIMCMESLSRK	15	64[a]
ASP **41**	RFNLIANQHLLAPGF	15	85[a]
ASP **42**	AAAFPSQRTSWEFLQ	15	84[a]
ASP **43**	SQRTSWEFLQSLVSIK	16	92[a]
ASP **44**	EFLQSLVSIKQEKPA	15	71[a]
ASP **45**[c]	DVFLSTTVFLMLSTT	15	
ASP **46**[c]	TVFLMLSTTCFLKYE	15	
ASP **47**	LHFIMPEKFSFWEDF	15	87[a]

ASP **48**	HFIMPEKFSFWEDFE	15	88 [a]

[a]Determined by analytical RP-HPLC by integrating the peptide and impurity peaks at 214 nm.

[b]Determined by LC/MS by integrating the peptide and impurity ions observed in the mass spectrum.

[c]Efforts to synthesize and purify this peptide were unsuccessful.

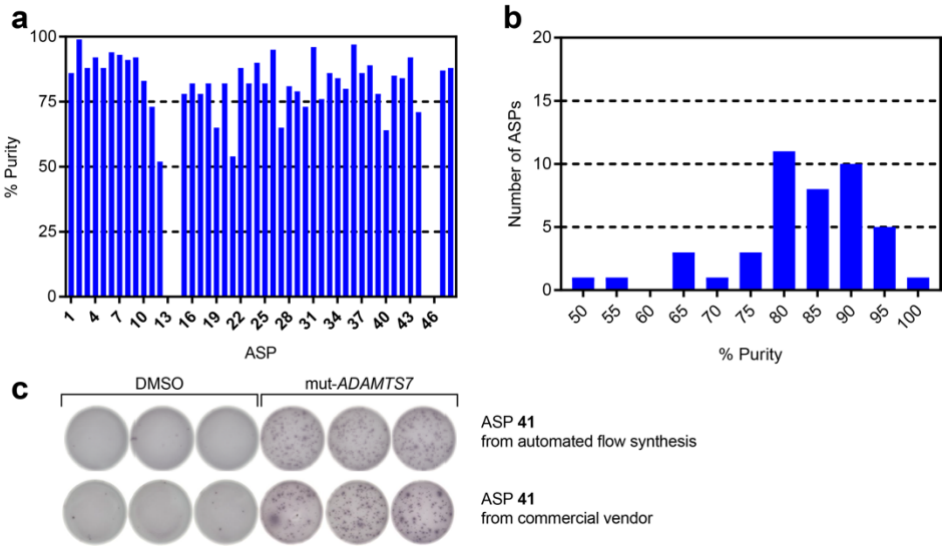

Figure 2.10. Characterization of purified ASPs produced by automated flow peptide synthesis. The graphs show (a) the individual purity and (b) the distribution of purity for ASPs **1**–**48** after purification. (c) IFN-γ secretion by neoantigen-specific T cells against mutated *ADAMTS7* (ASP **41**) peptide. The PBMCs were cultured with 2 μg/mL mut-*ADAMTS7* peptide for 14 days. $5\times10_3$ T cells were then co-cultured overnight in ELISPOT wells with $1\times10_4$ antigen presenting cells and with either DMSO or an mut-*ADAMTS7* peptide (10 μg/mL), followed by performing the IFN-γ ELISPOT assay.

We then directly purified the ASPs by preparative RP-HPLC. After the purification, 39 of 48 ASPs were obtained in sufficient purity (>70%) and amounts (>1 mg) to use for *ex vivo* characterization of immune responses. The individual purity varied, where 10 were obtained with a purity >90%, 20 with a purity between 80 and 90%, 9 with a purity between 70 and 80%, and 5 with a purity <70%; only 4 peptides were not recovered (after purification).

We further evaluated the ASP quality by performing an immune monitoring assay. We selected ASP **41**, which was used in a previous clinical trial to analyze a patient immune response after administration of the corresponding neoantigen-targeting vaccine.[13] We performed an IFN-γ enzyme-linked immune absorbent spot (ELISPOT) assay to compare the ASP **41** produced by flow synthesis with an identical peptide produced by a commercial peptide

vendor. Patient-derived peripheral blood mononuclear cells (PBMCs) were stimulated with ASP **41** peptides from flow synthesis or the commercial vendor for 14 days. The ELISPOTs indicated that the ASP **41** from both flow synthesis and the commercial vendor generated an equivalent antigen-specific T cell response (see Fig. 2.10C, Fig. 2.11). This finding establishes that the quality of ASPs produced by flow synthesis is sufficient for use in immune monitoring assays.

2.3 Materials and Methods

2.3.1 Materials

All reagents were purchased from commercial sources and used as received. *N*-α-Fmoc amino acids were purchased from CreoSalus or Novabiochem. *O*-(7-azabenzotriazol-1-yl)-*N,N,N′,N′*-tetramethyluronium hexafluorophosphate (HATU), (7-azabenzotriazol-1-yloxy)tripyrrolidinophosphonium hexafluorophosphate (PyAOP), *N*,*N*′-diisopropylcarbodiimide (DIC) were purchased from Chem-Impex. *N,N*-Dimethylformamide (DMF) was purchased from EMD Millipore. To each DMF bottle was added an AldraAmine trapping packet (Sigma-Aldrich) to minimize the accumulation of water and amine impurities. *N*,*N*-diisopropylethylamine (DIPEA), 4-(dimethylamino)pyridine (DMAP), piperidine, trifluoroacetic acid, triisopropylsilane, acetonitrile and 1,2-ethanedithiol (EDT) were purchased from Sigma-Aldrich. HMPB-ChemMatrix polyethylene glycol resin with a loading of ca. 0.5 mmol/g was purchased from Pcas Biomatrix.

2.3.2 Resin Loading

HMPB-ChemMatrix resin (200 mg, 0.5 mmol/g, 100–200 mesh) was suspended in ca. 5 mL of CH_2Cl_2 in a 6-mL fritted syringe and allowed to swell (15 min). The solution was drained, and the resin was rinsed three times with DMF and a solution was added of the first amino acid (1.0 mmol) with DIC (0.5 mmol, 78 µL) and DMAP (0.01 mmol, 50 µL of a 0.2 M solution in DMF) in 3.17 mL of DMF. The suspension was mixed gently and allowed to sit overnight (12–24 h). The solution was then drained and the resin was rinsed three times with DMF (5 mL).

2.3.3 Automated Flow Peptide Synthesis

We performed automated flow peptide synthesis on a ca. 0.1 mmol scale by manually loading the C-terminal amino acid residue onto HMPB-ChemMatrix resin, and by adding the subsequent amino acids by automated flow peptide synthesis.[20]

The reagent storage bottles on the synthesizer contain stock solutions in DMF of amino acids (0.4 M), activating agents (0.38 M HATU or PyAOP), and the deprotecting agent (40% piperidine), as well as the activating base (DIPEA, neat). The amino acid and activating agent stock solutions are mixed during each coupling step to deliver 10 equiv. of activated amino acid to the resin. The concentrations of these stock solutions can be reduced (0.2 M amino acid and 0.19 M activating agent (HATU or PyAOP)) to deliver 5 equiv. of activated amino acid, which does not extend the synthesis time and only marginally reduces the synthesis quality for ~30-mer peptides.[27]

The three pumps are Varian Prostar 210 HPLC pumps, of which two are fitted with 50 mL/min pump heads (400 μL of liquid per pump stroke) and deliver the amino acids and activating agents, whereas the third is fitted with a 5 mL/min pump head (40 μL of liquid per pump stroke) and delivers DIPEA. The two heating loops are a 10-ft stainless-steel loop at 90 °C and a 5-ft stainless-steel loop at 25 °C, which heat the solutions prior to flowing over the resin. The reactor is a stainless steel chamber for holding a fritted syringe and is heated to 90 °C. The UV-vis spectrophotometer monitors the absorbance at 312 nm, which allows relative quantitation of Fmoc removal during each coupling and deprotection step. The coupling and deprotection cycles are described in Table 2.4.

Table 2.4. Summary of coupling and deprotection steps performed during automated flow peptide synthesis.

step #	standard coupling and deprotection	arginine[a] deprotection and coupling	histidine[b] deprotection and coupling
1	amino acid (5 strokes, 1.6 mL) HATU (5 strokes, 1.6 mL) 90 °C heating loop; 90 °C reactor 80 mL/min	arginine (5 strokes, 1.6 mL) PyAOP (5 strokes, 1.6 mL) 90 °C heating loop; 90 °C reactor 40 mL/min	amino acid (5 strokes, 1.6 mL) HATU (5 strokes, 1.6 mL) 25 °C heating loop; 90 °C reactor 40 mL/min
2	amino acid (7 strokes, 2.8 mL) HATU (7 strokes, 2.8 mL) DIPEA (7 strokes, 0.28 mL) 90 °C heating loop; 90 °C reactor 80 mL/min	arginine (14 strokes, 5.6 mL) PyAOP (14 strokes, 5.6 mL) DIPEA (14 strokes, 0.56 mL) 90 °C heating loop; 90 °C reactor 40 mL/min	amino acid (7 strokes, 2.8 mL) HATU (7 strokes, 2.8 mL) DIPEA (7 strokes, 0.28 mL) 25 °C heating loop; 90 °C reactor 40 mL/min
3	DMF (35 strokes, 28 mL) 90 °C heating loop; 90 °C reactor 80 mL/min	DMF (35 strokes, 28 mL) 90 °C heating loop; 90 °C reactor 80 mL/min	DMF (35 strokes, 28 mL) 90 °C heating loop; 90 °C reactor 80 mL/min
4	40% Piperidine (13 strokes, 5.2 mL) DMF (13 strokes, 5.2 mL) 90 °C heating loop; 90 °C reactor 80 mL/min	40% Piperidine (13 strokes, 5.2 mL) DMF (13 strokes, 5.2 mL) 90 °C heating loop; 90 °C reactor 80 mL/min	40% Piperidine (13 strokes, 5.2 mL) DMF (13 strokes, 5.2 mL) 90 °C heating loop; 90 °C reactor 80 mL/min
5	DMF (35 strokes, 28 mL) 90 °C heating loop; 90 °C reactor 80 mL/min	DMF (35 strokes, 28 mL) 90 °C heating loop; 90 °C reactor 80 mL/min	DMF (35 strokes, 28 mL) 90 °C heating loop; 90 °C reactor 80 mL/min

[a]Arginine was coupled using a double coupling cycle, because the coupling efficiency of arginine is lower upon its formation of a γ-lactam.
[b]Histidine was coupled at lower temperatures to minimize epimerization.

The automated flow synthesis begins by prewashing the resin with DMF (80 mL/min, 20 s, 90 °C) and performing an initial deprotection of the first amino acid, followed by automated steps that perform coupling, deprotection, and washing as follows: (1) This step primes the lines with the corresponding amino acid and coupling agent. Two pumps simultaneously flow at 40 mL/min for 5 strokes and a volume of 1.6 mL each (total volume of 3.2 mL); (2) This step performs the standard coupling. Amino acid, coupling agent, and activator base solution flow to the resin using three pumps, two pumps simultaneously flow amino acid (11 equiv.) and coupling agent (10 equiv.) solutions at 40 mL/min for 7 strokes and a volume of 2.8 mL each (total volume of 5.6 mL), and one pump delivers DIPEA at 4 mL/min for 7 strokes and a volume of 0.28 mL; (3) This step washes the lines with DMF. Two pumps simultaneously flow DMF through the lines at 40 mL/min for 35 strokes and a volume of 14 mL each (total volume of 28 mL); (4) This step performs the deprotection. Two pumps

simultaneously flow at 40 mL/min for 13 strokes, one pump delivers a solution of 40% piperidine (5.2 mL) and the other delivers DMF (5.2 mL). These solutions combine to give 20% piperidine at a flow rate of 80 mL/min and a volume of 10.4 mL; (5) This step washes the lines with DMF (same as step 3). Two pumps simultaneously flow through the lines at 40 mL/min for 35 strokes and a volume of 14 mL each (total volume of 28 mL).

These five steps were repeated for each amino acid until the peptide total synthesis was complete. At the end of the synthesis, the resin was manually washed four times with DMF (5 mL) and four times with CH_2Cl_2 (5 mL).

Table 2.5. Summary of coupling and deprotection steps performed during microwave peptide synthesis.

step #	standard deprotection and coupling	arginine[a] deprotection and coupling	histidine[b] deprotection and coupling
1	20% Piperidine (4 mL) 75 °C for 15 s; 90 °C for 50 s	20% Piperidine (4 mL) 75 °C for 30 s	20% Piperidine (4 mL) 75 °C for 15 s; 90 °C for 50 s
2	DMF (4 mL × 4)	20% Piperidine (4 mL) 75 °C for 180 s	DMF (4 mL × 4)
3	amino acid (2.5 mL) HATU (1 mL); DIPEA (1 mL) 75 °C for 15 s; 90 °C for 110 s	DMF (4 mL × 4)	amino acid (2.5 mL) HATU (1 mL); DIPEA (1 mL) 25 °C for 120 s; 50 °C for 480 s
4	DMF (4 mL × 2)	amino acid (2.5 mL) HATU (1 mL); DIPEA (1 mL) 75 °C for 15 s; 90 °C for 110 s	DMF (4 mL × 2)
5		DMF (4 mL)	
6		amino acid (2.5 mL) HATU (1 mL); DIPEA (1 mL) 75 °C for 15 s; 90 °C for 110 s	

[a]Arginine was coupled using a double coupling cycle, because the coupling efficiency of arginine is lower upon formation of a γ-lactam.
[b]Histidine was coupled at lower temperatures to minimize epimerization.

2.3.4 Microwave Peptide Synthesis

We performed the microwave peptide syntheses on a ca. 0.1 mmol scale by manually loading the C-terminal amino acid residue onto HMPB-ChemMatrix resin, and by adding the subsequent amino acids by microwave peptide synthesis.[25] The syntheses were performed on a CEM Liberty Blue peptide synthesizer with optimized conditions: amino acid solutions (0.2 M

in DMF); activator base DIPEA (0.5 M in DMF); coupling reagent HATU (0.5 M in DMF), and washing solvent DMF. The deprotection and coupling steps were performed according to the recommended sequences from the CEM Corporation Liberty Blue User Guide (Rev. 4), which guided the amount of coupling reagents used for the amino acids (5 equiv.) and HATU (5 equiv.). The coupling and deprotection cycles are described in Table 2.5. At the end of the synthesis, the resin was manually washed four times with DMF (5 mL) and four times with CH_2Cl_2 (5 mL).

2.3.5 Resin Cleavage

After each synthesis was complete, we cleaved the peptides from the resin and removed acid-labile protecting groups under acidic conditions. The cleavages were performed on half of the resin from each synthesis (ca. 0.05 mmol of peptide) with the treatment of a 94/2.5/2.5/1 mixture of trifluoroacetic acid (TFA), triisopropyl silane, ethane dithiol, and water for 1 h at room temperature. More material can be obtained, if needed, after performing an additional resin cleavage and purification of the remaining ~0.05 mmol. The peptides were then washed three times by adding cold diethyl ether (40 mL, chilled to -80 °C in dry ice), mixing well, centrifuging (4000 rpm, 5 min), and decanting the supernatant. The remaining pellets were resuspended in 50% CH_3CN in H_2O with 0.1% TFA, filtered through a 0.2 µm nylon filter, frozen in liquid nitrogen, and lyophilized to give the unpurifed peptides as a white or yellow powder.

2.3.6 RP-HPLC analysis of IMPs by the commercial peptide vendor

The IMPs previously produced by the commercial vendor for in-human use were analyzed at 0.4 mg/mL on an Agilent 1200 HPLC system with a Phenomenex Luna 5 µm C18(2) column (4.6 mm × 250 mm) with a 0–70% gradient of CH_3CN in H_2O with 0.1% TFA and a flow rate of 1.5 mL/min.

2.3.7 RP-HPLC and LC/MS analysis of unpurified and purified IMPs

Lyophilized peptides were resuspended at 1 mg/mL in a 1:1 solution of H_2O/CH_3CN with 0.1% TFA, then analyzed on an Agilent 1200 HPLC system using an Agilent Zorbax 5 µm 300SB-C3 column (2.1 mm × 150 mm) with a 5–65% gradient of CH_3CN with 0.08% TFA in H_2O with 0.1% TFA and a flow rate of 0.8 mL/min. Representative IMPs were also characterized using a: Phenomenex Aeris 3.6 µm WIDEPORE C4 column (4.6 mm × 150 mm) with a 5–65% gradient of CH_3CN with 0.08% TFA in H_2O with 0.1% TFA and a flow rate of 0.8 mL/min; and Phenomenex Luna 5 µm C18(2) column (4.6 mm × 250 mm) with a 0–70% gradient of CH_3CN in H_2O with 0.1% TFA and a flow rate of 1.5 mL/min.

A 1:100 dilution of each 1 mg/mL peptide solution was prepared and analyzed by LC/MS on an Agilent 6550 ESI-Q-TOF mass spectrometer equipped with an Agilent Poroshell 5µm 300SB-C3 column (1 mm × 75 mm) with a 1–91% gradient of CH_3CN in H_2O with 0.1% formic acid and a flow rate of 0.4 mL/min.

2.3.8 RP-HPLC purification of IMPs

The peptides were purified with an Agilent Zorbax 7 µM SB-C18 Prep HT column (21.2 mm × 250 mm) with a 10–59% gradient over 98 min of CH_3CN in H_2O with 0.1% TFA and a flow rate of 15.0 mL/min. The pure fractions were combined, frozen in liquid nitrogen, and lyophilized to give the peptides as a white powder in 2–27% yield (3–47 mg) based on recovery from cleaving 50% of resin from a 0.1 mmol scale synthesis.

2.3.9 Patient samples

Patients with high-risk melanoma provided informed consent and were enrolled between April 2014 and October 2015 to a single center, phase I clinical trial approved by the Dana-Farber/Harvard Cancer Center Institutional Review Board (NCT01970358).[13] This study was conducted in accordance with the Declaration of Helsinki. Heparinized blood samples were obtained from study participants on Institutional Review Board-approved protocols at the DFCI. Patient PBMCs were isolated by Ficoll/Hypaque density-gradient centrifugation (GE Healthcare) and cryopreserved with 10% DMSO in FBS (Sigma-Aldrich). Cells from patients were stored in vapour-phase liquid nitrogen until the time of analysis.

2.3.10 Generation and detection of patient neoantigen-specific T cells

These experiments were performed as described in a previous publication.[13] PBMCs were cultured in RPMI-1640 medium supplemented with L-glutamine, nonessential amino acids, HEPES, β-mercaptoethanol, sodium pyruvate, penicillin/streptomycin (Gibco), and 10% AB-positive heat-inactivated human serum (Gemini Bioproduct). For *in vitro* expansion of antigen-specific T cells, PBMCs were stimulated in 24-well cell culture plates at 5×10^6 cells per well with individual peptides (each at 2 µg/mL) in the presence of IL-7 (20 ng/mL; R&D Systems). On day 3, low-dose IL-2 (20 U/mL; Amgen) was added. Half-medium change and supplementation of cytokines were performed every 3 days. After 14 days, T-cell specificity was tested against the peptide by interferon (IFN)-γ ELISPOT.

2.3.11 IFN-γ ELISPOT assay

These experiments were also performed as described in a previous publication.[13] IFN-γ ELISPOT assays were performed using 96-well MultiScreen Filter Plates (Millipore), coated with 2 µg/mL anti-human IFN-γ mAb overnight (1-D1K, Mabtech). Plates were washed with PBS and blocked with complete RPMI before use. 5×10^3 T cells were co-cultured with 1×10^4

autologous CD4+ and CD8+ T cell-depleted PBMCs (APC). Peptides (10 μg/mL) were directly added to the ELISPOT wells with APCs and incubated with T cells overnight in complete RPMI at 37 °C. The plates were rinsed with PBS containing 0.05% Tween-20 and then 1 μg/mL anti-human IFN-γ mAb (7-B6-1-Biotin, Mabtech) was added, followed by Streptavidin-ALP (Mabtech). After rinsing, SIGMA FAST BCIP/NBT (5-bromo-4-chloro-3-indolyl phosphate/nitro blue tetrazolium; Sigma-Aldrich) was used to develop the immunospots, then the spots were imaged and counted (Cellular Technology Limited).

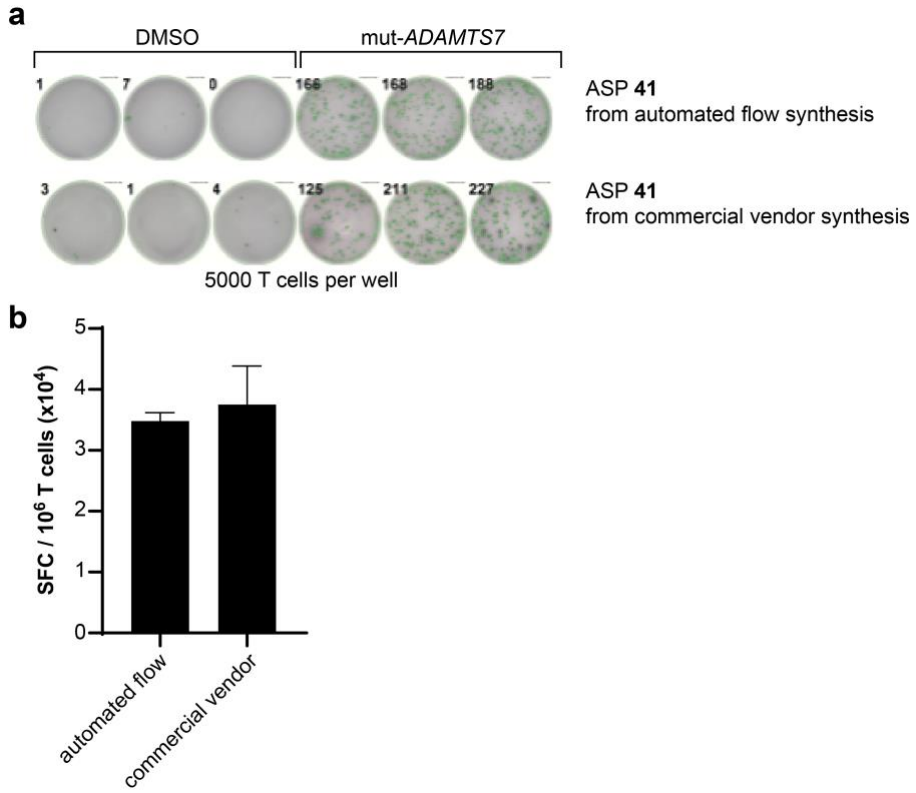

Figure 2.11. IFN-γ secretion by neoantigen-specific T cell lines against mutated *ADAMTS7* (ASP 41) peptide. (a) The PBMCs were cultured with 2 μg/ml mut-*ADAMTS7* peptide for 14 days. $5\times10_3$ T cells were co-cultured with $1\times10_4$ antigen presenting cells with DMSO or mut-*ADAMTS7* peptide (10 μg/ml in ELISPOT wells overnight followed by IFN-γ ELISPOT assay. (b) Graph of the enumerated spot forming cells (SFCs) per 1 million cells. A two-sample two-tailed *t*-test with Welch correction indicated no statistical difference ($P > 0.05$).

2.4 Conclusions

We set out to facilitate production of peptides for personalized medicine, specifically in the context of neoantigen vaccines. We evaluated each step throughout the synthesis, cleavage, and purification of neoantigen peptides to establish a high-throughput workflow. Our efforts

show that automated flow peptide synthesis can increase the rate and quality of peptide synthesis for IMP and ASP production. Flow synthesis produced IMPs with comparable or higher purity than either microwave or batch synthesis. Flow synthesis also permitted the production of a full set of neoantigen immunizing peptides, in addition to a full set of assay peptides that are of sufficient quality for use in immune monitoring assays.

Although automated flow peptide synthesis addresses the synthetic challenge of producing neoantigen peptides, obstacles in subsequent steps still prevent rapid production. The first challenge we encountered involved high-throughput cleavage of peptides from resin. Although we introduced a procedure for cleaving 24 peptides in parallel, further optimization is needed to implement this procedure on a larger scale. A second challenge is limited peptide solubility, which often delayed purification. A third challenge is peptide purification by preparative RP-HPLC, which sometimes requires multiple rounds to achieve high purity (≥95% purity). Although these challenges are a standard part of peptide production, they can delay the manufacturing of neoantigen vaccines and ultimately postpone patient treatment. Creative solutions to these challenges are urgently needed to fully address the peptide production and scalability problems for personalized neoantigen vaccines.

Our work illustrates how automated flow technology can enable rapid peptide synthesis for personalized neoantigen vaccines, which is useful in broader contexts. The advent of rapid and affordable genome-sequencing technology is likely to enable other classes of personalized medicine that use peptides, oligonucleotides, or artificial biopolymers. We anticipate that automated flow synthesis can be leveraged to produce these treatments by tailoring the solid-phase conditions to perform the corresponding coupling steps, which is part of ongoing work in our laboratory.

2.5 Acknowledgements and Conflict Statements

N.L.T. thanks the Koch Institute Ludwig Foundation for funding support. R.L.H. thanks the National Science Foundation Graduate Research Fellowship under Grant No. 1122374 for funding support. We acknowledge support from the Bridge Project between the Koch Institute and Dana-Farber/Harvard Cancer Center (to B.L.P., C.J.W., and P.O.), the National Institutes of Health (NCI-1RO1CA155010-02 (to C.J.W.)), NHLBI-5R01HL103532-03 (to C.J.W.), NIH/NCI R21 CA216772-01A1 (to D.B.K.), NCI-SPORE-2P50CA101942-11A1 (to D.B.K). C.J.W. is a scholar of the Leukemia and Lymphoma Society. The authors thank Jesús M. Dones and Prof. Ronald T. Raines for assistance with the microwave peptide synthesis experiments

and for providing feedback on the manuscript. The authors also thank A. Loas for critically reading this manuscript and providing detailed feedback.

B.L.P. is a founder of Amide Technologies and Resolute Bio. C.J.W. is a founder of Neon Therapeutics and member of its scientific advisory board. D.B.K. has previously advised Neon Therapeutics and owns equity in Aduro Biotech, Agenus, Ampliphi BioSciences, Biomarin Pharmaceutical, Bristol-Myers Squibb, Celldex Therapeutics, Editas Medicine, Exelixis, Gilead Sciences, IMV, Lexicon Pharmaceuticals, Sangamo Therapeutics and Stemline Therapeutics. N.H. is a founder of Neon Therapeutics and member of its scientific advisory board and an advisor for IFM therapeutics. P.A.O. has received research funding from and has advised Neon Therapeutics, Bristol-Myers Squibb, Merck, CytomX, Pfizer, Novartis, Celldex, Amgen, Array, AstraZeneca/MedImmune, Armo BioSciences and Roche/Genentech.

2.6 References

1 Wheeler, D. A. *et al.* The complete genome of an individual by massively parallel DNA sequencing. *Nature* **452**, 872-876, https://doi.org/10.1038/nature06884 (2008).
2 Verma, M. Personalized medicine and cancer. *Journal of personalized medicine* **2**, 1-14, https://doi.org/10.3390/jpm2010001 (2012).
3 Weiss, S. T. & Shin, M. S. Infrastructure for personalized medicine at partners healthcare. *Journal of personalized medicine* **6**, https://doi.org/10.3390/jpm6010013 (2016).
4 Shendure, J., Findlay, G. M. & Snyder, M. W. Genomic medicine-progress, pitfalls, and promise. *Cell* **177**, 45-57, https://doi.org/10.1016/j.cell.2019.02.003 (2019).
5 Fornaguera, C. & Garcia-Celma, M. J. Personalized nanomedicine: A revolution at the nanoscale. *Journal of personalized medicine* **7**, https://doi.org/10.3390/jpm7040012 (2017).
6 Cohen, J. P. & Felix, A. E. Personalized medicine's bottleneck: Diagnostic test evidence and reimbursement. *Journal of personalized medicine* **4**, 163-175, https://doi.org/10.3390/jpm4020163 (2014).
7 Hu, Z., Ott, P. A. & Wu, C. J. Towards personalized, tumour-specific, therapeutic vaccines for cancer. *Nature Reviews Immunology* **18**, 168–182, https://doi.org/10.1038/nri.2017.131 (2018).
8 Schumacher, T. N. & Schreiber, R. D. Neoantigens in cancer immunotherapy. *Science* **348**, 69–74, https://doi.org/10.1126/science.aaa4971 (2015).
9 Hirayama, M. & Nishimura, Y. The present status and future prospects of peptide-based cancer vaccines. *International Immunology* **28**, 319-328, https://doi.org/10.1093/intimm/dxw027 (2016).
10 Linette, G. P. & Carreno, B. M. Neoantigen vaccines pass the immunogenicity test. *Trends in molecular medicine* **23**, 869-871, https://doi.org/10.1016/j.molmed.2017.08.007 (2017).
11 Sahin, U. & Tureci, O. Personalized vaccines for cancer immunotherapy. *Science* **359**, 1355-1360, https://doi.org/10.1126/science.aar7112 (2018).

12 Keskin, D. B. *et al.* Neoantigen vaccine generates intratumoral t cell responses in phase ib glioblastoma trial. *Nature* **565**, 234-239, https://doi.org/10.1038/s41586-018-0792-9 (2019).
13 Ott, P. A. *et al.* An immunogenic personal neoantigen vaccine for patients with melanoma. *Nature* **547**, 217–221, https://doi.org/10.1038/nature22991 (2017).
14 Hilf, N. *et al.* Actively personalized vaccination trial for newly diagnosed glioblastoma. *Nature* **565**, 240-245, https://doi.org/10.1038/s41586-018-0810-y (2019).
15 Carreno, B. M. *et al.* A dendritic cell vaccine increases the breadth and diversity of melanoma neoantigen-specific t cells. *Science* **348**, 803-808, https://doi.org/10.1126/science.aaa3828 (2015).
16 Sahin, U. *et al.* Personalized rna mutanome vaccines mobilize poly-specific therapeutic immunity against cancer. *Nature* **547**, 222-226, https://doi.org/10.1038/nature23003 (2017).
17 Kenter, G. G. *et al.* Vaccination against hpv-16 oncoproteins for vulvar intraepithelial neoplasia. *N Engl J Med* **361**, 1838-1847, https://doi.org/10.1056/NEJMoa0810097 (2009).
18 Kenter, G. G. *et al.* Phase i immunotherapeutic trial with long peptides spanning the e6 and e7 sequences of high-risk human papillomavirus 16 in end-stage cervical cancer patients shows low toxicity and robust immunogenicity. *Clinical cancer research* **14**, 169-177, https://doi.org/10.1158/1078-0432.CCR-07-1881 (2008).
19 Hoof, I. *et al.* Netmhcpan, a method for mhc class i binding prediction beyond humans. *Immunogenetics* **61**, 1-13, https://doi.org/10.1007/s00251-008-0341-z (2009).
20 Mijalis, A. J. *et al.* A fully automated flow-based approach for accelerated peptide synthesis. *Nature chemical biology* **13**, 464–466, https://doi.org/10.1038/nchembio.2318 (2017).
21 Mong, S. K., Vinogradov, A. A., Simon, M. D. & Pentelute, B. L. Rapid total synthesis of darpin pe59 and barnase. *ChemBioChem* **15**, 721-733, https://doi.org/10.1002/cbic.201300797 (2014).
22 Vinogradov, A. A., Evans, E. D. & Pentelute, B. L. Total synthesis and biochemical characterization of mirror image barnase. *Chemical Science* **6**, 2997-3002, https://doi.org/10.1039/c4sc03877k (2015).
23 Luhmann, T., Mong, S. K., Simon, M. D., Meinel, L. & Pentelute, B. L. A perfluoroaromatic abiotic analog of h2 relaxin enabled by rapid flow-based peptide synthesis. *Organic & Biomolecular Chemistry* **14**, 3345-3349, https://doi.org/10.1039/c6ob00208k (2016).
24 Simon, M. D. *et al.* Rapid flow-based peptide synthesis. *ChemBioChem* **15**, 713-720, https://doi.org/10.1002/cbic.201300796 (2014).
25 Palasek, S. A., Cox, Z. J. & Collins, J. M. Limiting racemization and aspartimide formation in microwave-enhanced fmoc solid phase peptide synthesis. *Journal of peptide science* **13**, 143-148, https://doi.org/10.1002/psc.804 (2007).
26 Coin, I., Beyermann, M. & Bienert, M. Solid-phase peptide synthesis: From standard procedures to the synthesis of difficult sequences. *Nature Protocols* **2**, 3247-3256, https://doi.org/10.1038/nprot.2007.454 (2007).
27 Wolfe, J. M. *et al.* Machine learning to predict cell-penetrating peptides for antisense delivery. *ACS Central Science* **4**, 512–520, https://doi.org/10.1021/acscentsci.8b00098 (2018).

Chapter 3: Sequences that promote both lymphatic and intracellular delivery enhance the efficacy of peptide cancer vaccines

The work presented in this chapter was adapted from a manuscript in preparation:

Holden, R.L.,* Backlund, C.M.,* Moynihan, K.D., Garafola, D.; Mehta, N.K., Farquar, C.E.; Irvine, D.J.; Pentelute, B.L. Sequences that promote both lymphatic and intracellular delivery enhance the efficacy of peptide cancer vaccines. *In preparation.*

**These authors contributed equally to this work.*

Author contributions:

R.L.H., C.M.B., K.D.M., B.L.P., and D.J.I. designed the study. R.L.H. synthesized the peptides and peptide conjugates for each experiment, with the assistance of C.E.F. for the design variants in Figure 3.2. C.M.B., K.D.M., and D.G., collected and analyzed animal data. R.L.H., C.M.B., and K.D.M. interpreted animal data; collected, analyzed, and interpreted *in vitro* data; and performed statistical analyses. N.M. collected and analyzed serum stability data. R.L.H. and C.M.B. wrote the manuscript in preparation reproduced here.

3.1 Introduction

Therapeutic peptide vaccines are a promising class of cancer immunotherapy with the potential to initiate, strengthen and guide the anti-tumor T cell response.[1,2] They have been demonstrated to be immunogenic in a clinical setting, but their therapeutic efficacy has been limited.[3–7] Several diverging methods are currently being explored to address these shortcomings, including streamlining antigen identification and design, optimizing vaccine format and administration, and exploring combinations with immune checkpoint blockade and other immunotherapies.[1,2,8–13] Another complementary approach is to improve the delivery of vaccine molecules to the appropriate lymphatic tissue and cell types. This is particularly relevant for peptide vaccines, which have several advantages—peptides are synthetically accessible, easy to handle, readily amenable to chemical modification, and generally have a good safety profile—but are notorious for their short half-life *in vivo*.[14,15] Designing peptide vaccines with more efficient delivery can significantly boost their immunogenicity and anti-tumor efficacy.

In order to prime an efficient T cell response, vaccine antigens must first traffic to the lymphatic tissue where immune responses are primed, namely the lymph nodes or spleen.[16] Vaccine molecules can be transported to the draining lymph node from the injection site via tissue resident antigen presenting cells, i.e. active trafficking, or simply enter the lymphatic vessels and be carried to the draining node via passive trafficking.[16] Notably, relative size is a key factor determining whether material injected subcutaneously enters to the blood or lymphatic vasculature, with increasing size correlating to lymphatic partitioning.[17] We have previously demonstrated that binding serum albumin can promote vaccine molecule trafficking to the draining lymph node in a phenomenon we have termed ‘albumin hitchhiking’ (see Chapter 1.5 and Chapter 4).[18] Conjugating an albumin-binding moiety to a vaccine antigen or adjuvant can significantly enhance vaccine immunogenicity and efficacy.[18,19]

After reaching the lymph node, vaccine molecules must then be internalized and presented by antigen-presenting cells, namely dendritic cells (DCs).[16] Antigen presentation to $CD8^+$ T cells occurs via cross-presentation. The canonical cross-presentation pathway requires that endocytosed antigen proteins or peptides reach the cytosol, where they undergo proteasomal degradation and transport to the endoplasmic reticulum to be further trimmed, loaded onto newly-synthesized major histocompatibility complex (MHC)-I molecules, and shuttled to the cell surface.[16,20] Some approaches to improve vaccine efficiency use antibodies

or other targeting moieties to boost delivery to cross-presenting DC subsets.[21,22] Others focus on directly enhancing cell uptake, in particular cytosolic delivery.

Previous work has demonstrated that covalent attachment to a cell penetrating peptide (CPP) can facilitate vaccine antigen presentation and enhance anti-tumor efficacy.[23–26] CPPs are sequences that have been shown to increase the intracellular and in some cases cytosolic delivery of a variety of cargo molecules. They range in their length, which is generally ~5-40 amino acid residues; origin, derived from natural proteins, rationally design, or chimeras of existing CPPs; hydrophobicity; and net charge, with dense cationic residue content generally correlating with high uptake.[27–29] Their delivery efficiency depends on a number of factors, including the aforementioned CPP properties, as well as the treatment concentration, cell type, and cargo. CPPs have been demonstrated to promote uptake of antigen peptides into DCs and to enhance vaccine immunogenicity in animal models, including non-human primates, and to improve anti-tumor efficacy in mice.[30–38] One peptide vaccine that includes a covalently attached CPP recently entered a phase I clinical trial.[39] However, the majority of studies using CPPs to promote peptide vaccine delivery are limited to one or two CPP sequences, preventing a thorough characterization of the CPP properties that contribute to vaccine efficacy.[35–38] They are generally also limited to a handful of model antigens, making it difficult to evaluate the generalizability of this approach, with many studies only employing the highly immunogenic ovalbumin epitope SIINFEKL.[32–35] Perhaps most importantly, the mechanism by which CPPs enhance vaccine efficacy is largely uncharacterized. There is evidence supporting increased intracellular delivery as a key mechanism, in keeping with their design, and one study employs a variety of small molecule inhibitors to evaluate the role of different endocytic routes and canonical proteolytic processing.[40] However, the dependence on cross-presentation and the ability of CPPs to promote cytosolic delivery are unknown and the impact of CPPs on vaccine accumulation in lymph nodes and on their stability *in vivo* are poorly characterized.

We have sought to address these limitations and explore the generality and mechanism by which CPPs enhance peptide vaccine efficacy. We screen a set of CPPs for their ability to promote T cell priming *in vitro* and *in vivo*, then probe the generality of a top CPP to other antigens from several different tumor models and confirm its impact on anti-tumor efficacy. Having established CPP conjugation as a general strategy to improve peptide vaccines, we then delve into their mechanism of action. We demonstrate that CPPs increase relative uptake into DCs. We then explore the impact of CPP conjugation on lymphatic trafficking, serum stability, and the duration of antigen presentation *in vivo*, revealing new mechanisms by which CPPs can enhance peptide vaccine efficacy.

3.2 Results and Discussion

Antigen-CPP vaccine design and in vitro efficacy. To provide greater insight into the efficacy, generalizability, and mechanism of improving immune responses with CPPs, we selected eight previously reported sequences that ranged in hydrophobicity, net charge, length, and origin (Figure 3.1A). Using our automated flow synthesis technology, we synthesized several antigen peptides along with the chosen CPPs to rapidly generate a series of antigen-CPPs using copper(I)-catalyzed click chemistry (Figure 3.1A). Applying this facile synthesis strategy, we were able to conjugate any CPP onto any antigen sequence with high yield and minimal purification.

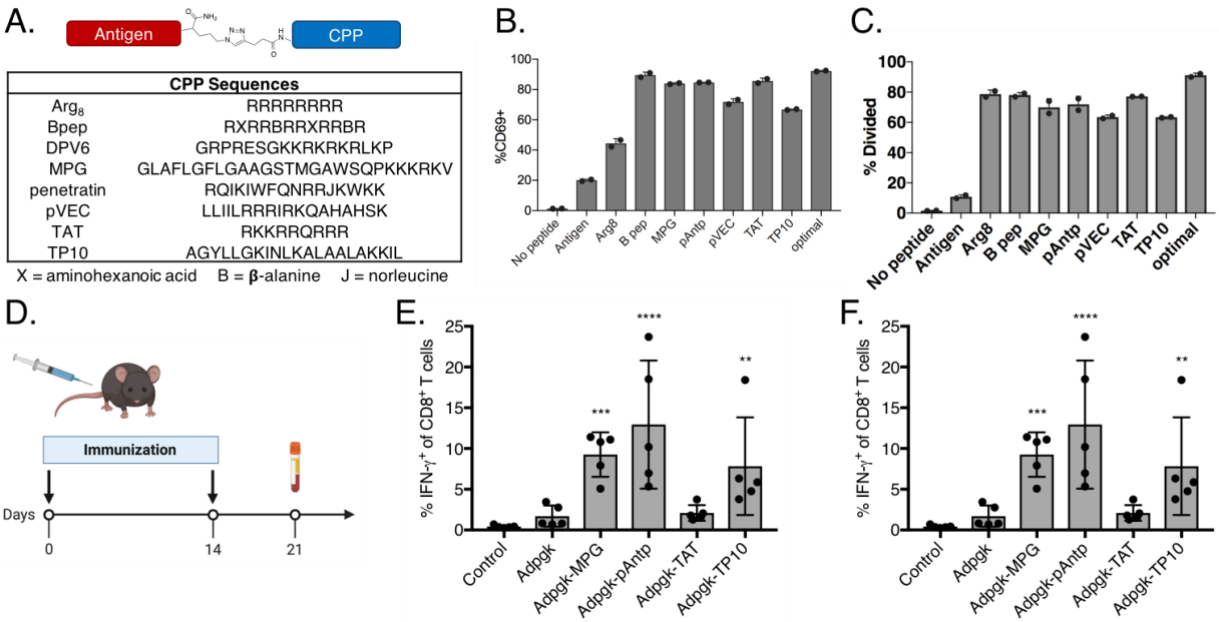

Figure 3.1 Conjugation to various CPPs increases T cell activation *in vitro* and improves immunogenicity of vaccine antigens. A) Eight CPPs varying in length, charge, hydrophobicity, and origin were selected and conjugated to two different model tumor antigens using copper(I)-catalyzed azide/alkyne cycloaddition. **B)** Primary splenocytes treated with the various antigen-CPP conjugates facilitate more effective reporter T cell activation than splenocytes treated with the antigen alone. **C)** Similarly, splenocytes treated with the antigen-CPPs promote proliferation of reporter T cells than those treated with the antigen alone. **D)** Schematic overview of endogenous priming experiment. Mice (n = 4-5) were immunized with 5 nmol of the antigen construct and 25 μg cyclic-di-GMP as an adjuvant on Day 0 and again with an identical vaccine on Day 14. On Day 21, the antigen-specific T cell response was analyzed directly from a blood draw using intracellular IFN-γ staining. **E)** CPPs increased the immunogenicity of the melanoma antigen EGP by up to 20-fold. F) CPPs also enhanced

endogenous T cell priming to the colon carcinoma antigen Adpgk. **** $p < 0.0001$, *** $p < 0.001$, ** $p < 0.01$.

To evaluate the ability of the chosen CPPs to enable T cell priming in vitro, we employed the gp100 antigen EGP, from B16F10 melanoma, as a model antigen. Murine splenocytes were treated with either EGP-CPP or EGP alone, then co-cultured with pmel-1 T cells, with transgenic TCRs for EGP. The EGP-CPP peptides induced ~10x higher upregulation of CD69 on the pmel-1 T cells than the antigen alone indicating higher levels of activation in the presence of the CPPs (Figure 3.1B). Additionally, the splenocytes treated with EGP-CPPs enabled pmel-1 proliferation, whereas those treated with EGP were unable to stimulate expansion of the T cell population (Figure 3.1C). While there was some variation between the ability of the different CPPs to stimulate T cell activation and presentation, they were all statistically different from the EGP alone. This suggests that CPPs promote increased T cell responses by improving antigen delivery to APCs.

CPPs vaccines increase in vivo T cell priming and delay tumor outgrowth. We evaluated the ability of the CPP conjugated antigens to prime an immune response in vivo by immunizing c57b6 mice with EGP-CPP and cyclic di-GMP, a potent STING agonist, using a prime boost strategy (Figure 3.1D). Seven days after the boost, we assessed the level of circulating antigen specific CD8 T cell in the peripheral blood by quantifying the cells producing IFN- γ and TNF- α in response to ex vivo stimulation with the minimal epitope. While all of the CPPs tested here enhanced T cell priming toward EGP, MPG and pAntp increased the EGP specific CD8 T cell response around 20-fold (Figure 3.1E). To test the translation of CPP efficacy to another antigen, we tested a subset of CPPs conjugated to the neoantigen Adpgk from the colorectal cancer line MC-38. Similarly, MPG and pAntp outperformed the other CPPs in their ability to generate a T cell response (Figure 3.1F). Taken together, the enhanced in vivo T cell priming toward both EGP and Adpgk suggests that MPG and pAntp should be readily translatable boosting responses against other antigens.

To screen optimal conditions, as well as construct design, we evaluated the in vivo performance of MPG and pAntp with and without the triazole linker using the same prime boost strategy above to ensure the conjugation did not play a role in the mechanism (Figure 3.2A). Both pAntp and MPG generated a robust CD8 T cell response against EGP regardless of attachment. Additionally, we noted that the adjuvant delivered in formulation with the peptides had a large impact on the ability of these antigen-CPPs to promote T cell priming (Figure 3.2B). After observing some precipitation after mixing the antigen and cyclic di-GMP, we explored

several approaches to support their solubility including formulation in 75 mM $MgCl_2$, a chaotropic salt, with the pH adjusted to 7.4 rather than the typical phosphate-buffered saline. This formulation effectively minimized precipitation without impacting vaccine immunogenicity (Figure 3.2C). Consequently, we narrowed our investigation to the use of pAntp formulated with cyclic di-GMP suspended in 75 mM $MgCl_2$.

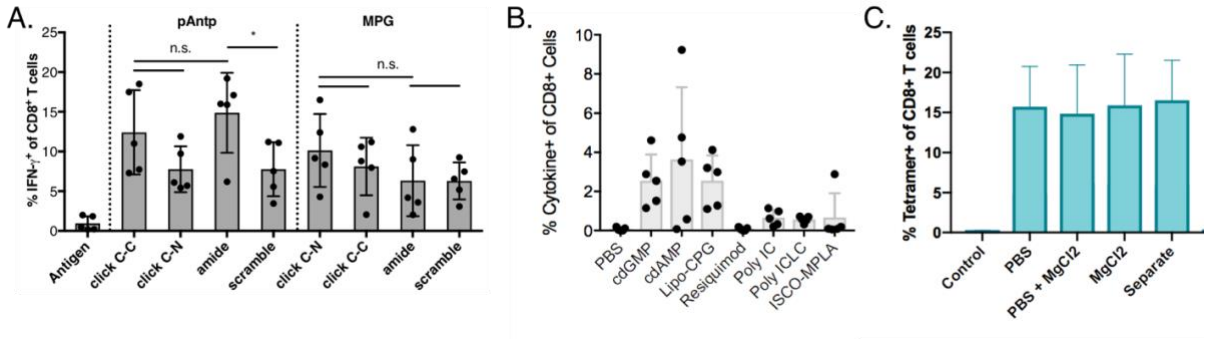

Figure 3.2. Evaluating vaccine design and formulation. A) Comparison of variants of EGP-pAntp and EGP-MPG with the CPP conjugating at its N- or C-terminus (to the C-terminus of the antigen peptide; variants with the antigen and CPP linked through an amide bond or the triazole linkage shown in Figure 3.1A; and scrambled versions of the two CPPs. While the vaccine with the scrambled pAntp exhibited lower immunogenicity, no difference was observed for either CPP based on linker type or placement. **B)** Screen of a series of adjuvants for their ability to promote endogenous T cell priming against our vaccine antigen, ultimately settling on cyclic di-GMP, a potent STING agonist. **C)** No difference in immunogenicity was observed for vaccines comprised of Trp1 or Trp1-pAntp and c-di-GMP when formulated in phosphate-buffered saline ("PBS"), 75 mM $MgCl_2$ ("MgCl2"), a 75 mM $MgCl_2$ in PBS ("PBS + MgCl2"), or a separate injection of the antigen and adjuvant in PBS ("Separate"). $*p < 0.01$; n.s., not significant.

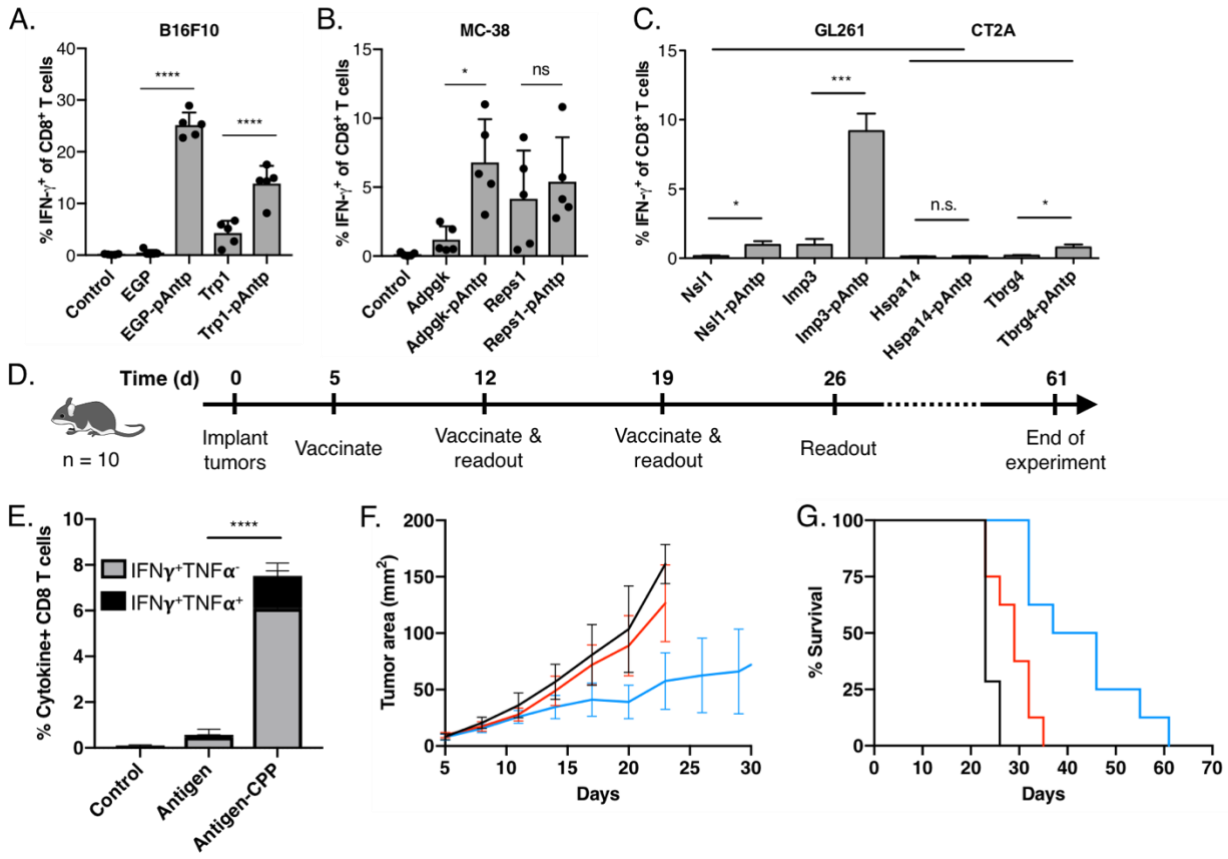

Figure 3.3. CPPs are a general strategy to enhance vaccine immunogenicity and therapeutic efficacy. Endogenous T cell priming for **A)** two antigens from the b16f10 melanoma model, EGP and Trp1. **B)** Adpgk and Reps1, neoantigens from the MC-38 colon adenocarcinoma model. **C)** Nsl, Imp3, Hspa14 and Tbrg4 from the GL261 and CT2A glioblastoma models. **D)** Timeline for therapeutic efficacy study using the TC-1 tumor model. **E)** T cell responses to the vaccine antigen E7 seven days after the third and final immunization. **F)** Tumor growth curves and **G)** survival curves. **** $p < 0.0001$; *** $p < 0.001$; * $p < 0.05$; n.s., not significant.

To further explore the generalizability of CPPs, we assessed a series of antigens from several tumor models. Similar to EGP, the addition of pAntp increased the response to the B16F10 antigen Trp1 by over 10x (Figure 3.3A). While gains in efficacy were observed for the neoantigen Adpgk, with a 5.7x increase in T cell response, T cell priming against Reps1, a different neoantigen identified from the MC-38 model, did not increase significantly with pAntp conjugation (Figure 3.3B). We also observed that the addition of pAntp increased responses toward three of the four antigens identified from GL261 and CT2A murine glioma models, by 4.2x to 9.5x (Figure 3.3C). In general, the addition of pAntp enhanced antigen

specific CD8 T cell responses toward a variety of tumor model antigens, suggesting its versatility.

To confirm the functionality of these newly formed antigen specific CD8 T cells, we tested the therapeutic, anti-tumor efficacy of a vaccine using the antigen E7. Mice were implanted with subcutaneous TC-1 tumors and then immunized with either the unmodified E7 antigen or E7-pAntp three times at one week intervals (Figure 3.3D). We longitudinally monitored the T cell responses toward E7 over the course of treatment. The E7-CPP construct facilitated a 10x increase in T cell priming over the antigen only vaccine, with 6% of CD8 T cells producing IFN-γ in response to stimulation with the minimal E7 epitope (Figure 3.3E). The vaccine containing E7-pAntp also afforded significantly reduced tumor growth than the antigen alone, prolonging survival by over 30 days (Figure 3.3F-G). Combination with other immunotherapies, such as checkpoint blockade or IL-2, may provide further therapeutic benefit and may be required for other tumor types. Having demonstrated that antigen conjugation to a CPP is a general strategy to improve the efficacy of peptide vaccines, we aimed to characterize their mechanism of action.

CPPs promote intracellular delivery into antigen presenting cells. In accordance with previous reports on the mechanism of action of CPPs, we hypothesized that they enhanced T cell priming through efficient delivery of the vaccine antigens into DC2.4 cells, both through endosomal and cytosolic uptake. To confirm this, we synthesized a set of fluorophore-labeled EGP-CPPs (fluor-Ag-CPP) using Thiol-Michael addition. To evaluate intracellular delivery, we incubated DC2.4 cells with 2.5 μM of each labeled vaccine construct for 1 hour, then treated with trypsin to release cells and remove any surface associated extracellular peptide and analyzed via flow cytometry. Cells treated with fluor-Ag-CPPs exhibited at least a 20x increase in median fluorescence intensity (MFI) relative to those treated with the labeled antigen (Figure 3.4A), confirming that the addition of any of the assessed CPPs increases antigen uptake by over an order of magnitude. We corroborated these findings by confocal microscopy of the treated DC2.4 cells, where the samples treated with fluor-Ag-CPPs significantly enhanced vaccine antigen uptake and revealed some co-localization with endosomes (Figure 3.4B). It is worth noting that the antigen-CPPs exhibiting the highest uptake in DC2.4s were not necessarily the most effective at enhancing vaccine immunogenicity. While the top sequence, MPG, also facilitated highly efficient T cell priming, the second two sequences, Arg_8 and TP10, were significantly less effective in vivo. Part of the observed discrepancy in uptake and cytosolic access might be attributed to the notion that CPP sequences that are most efficiently endocytosed are not necessarily the best at promoting delivery across the cell and/or endosomal

membrane. It may also suggest that additional mechanisms beyond enhanced cell uptake and direct cytosolic access could play a critical role in increasing CPP vaccine efficacy.

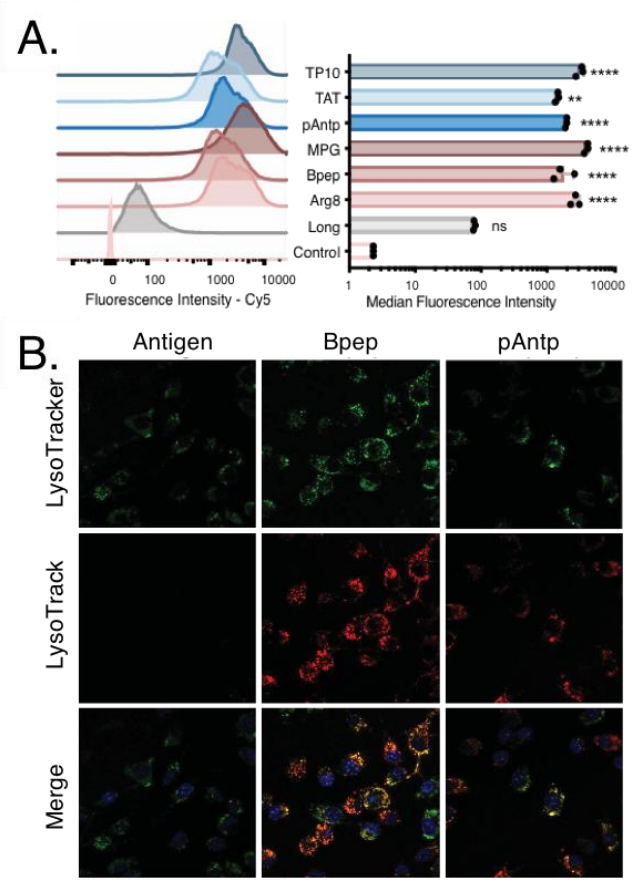

Figure 3.4. CPPs increase intracellular delivery. A) Uptake of SulfoCy5-labeled EGP and EGP-CPPs into DC2.4 cells after incubation for 1 hour at 2.5 μM, analyzed via flow cytometry. **B)** Confocal imaging of SulfoCy5-labeled EGP and EGP-CPP delivery into DC2.4 cells after 2.5 μM incubation for 1 hour. Cells were also stained with Hoescht and a lysosomal marker. **** $p < 0.0001$; ** $p < 0.01$; n.s., not significant.

CPPs enhance lymphatic trafficking of a vaccine antigen. Prior to DC uptake and presentation *in vivo*, antigen-CPPs must reach a lymph node where they can closely interact with naïve T cells to stimulate formation of an antigen specific response. Implementing a set of fluor-EGP-CPPs labeled with Bodipy-Texas Red (BDP-TR), we observed an increase in the amount of vaccine construct present in the inguinal and axillary lymph nodes 24 hours after immunization (Figure 3.5A). All of the CPP constructs resulted in some accumulation of BDP-TR signal relative to the fluor-EGP alone, with several fluor-EGP-CPPs showing up to a 5-fold increase (Figure 3.5B). It is worth noting that two of the CPPs that trafficked most efficiently, pAntp and MPG, were most effective at promoting endogenous T cell priming (Figure 3.1).

Although increased lymph node trafficking is not a complete predicator of T cell priming, such as the case with TP10, it does suggest one mechanism by which CPP conjugation improves vaccine efficacy. Given that lymphatic trafficking was not an explicit design consideration in these antigen-CPP constructs, we next sought to explain the high accumulation of signal in the lymph nodes.

Association with serum proteins may facilitate passive trafficking. Amphiphilic lipids have been previously shown to increase association with albumin increasing the effective molecular weight resulting in more efficient trafficking via the lymphatic system. Due to the cationic and hydrophobic nature of CPPs, we hypothesized that these peptides might inadvertently facilitate passive lymphatic trafficking through a similar mechanism. To evaluate serum protein binding, we performed a pulldown assay from which CPP association with several proteins of different molecular weights were detected (Figure 3.5C). In particular, a band at 25-30 kDa was observed for nearly all antigen-CPPs, but minimal protein binding was observed for the antigen alone. The intensity of the band was highest for EGP-pAntp and EGP-MPG, paralleling their increased signal in the lymph nodes and their high T cell priming. This band was excised, subjected to an in-gel trypsin digest, and analyzed via LC-MS/MS to identify fragment peptides. A database search revealed it to be murine apolipoprotein A1, a 30.6 kDa murine serum protein. Several larger molecular weight bands were also observed for several of the EGP-CPPs with higher cationic residue content; these bands will be similarly identified. Faint bands corresponding to a multitude of proteins were also present for many antigen-CPPs, indicating weak association with a range of serum proteins. All identified serum proteins will be confirmed by measuring binding to the relevant antigen-CPP conjugates via bio-layer interferometry and a pulldown assay using isolated samples of the relevant proteins. These findings suggest a new mechanism for CPP-mediated vaccine immunogenicity that takes advantage of serum protein binding to aid in transport to the draining lymph node.

CPP conjugation enhances vaccine antigen serum stability. In addition to promoting lymph node trafficking, we hypothesized that association with serum proteins could prolong the serum stability of our vaccine antigens. We pulsed splenocytes with either serum-treated constructs or fresh material to determine the concentrations required to activate pmel-1s, with a lower fold change in the EC_{50} serving as an indicator of increased stability. The change in EC_{50} for the EGP-CPPs ranged from 0.8-fold to 3.5-fold, indicating that CPP conjugation significantly increased antigen serum stability as compared with the 16-fold change observed for EGP alone (Figure 3.5D).

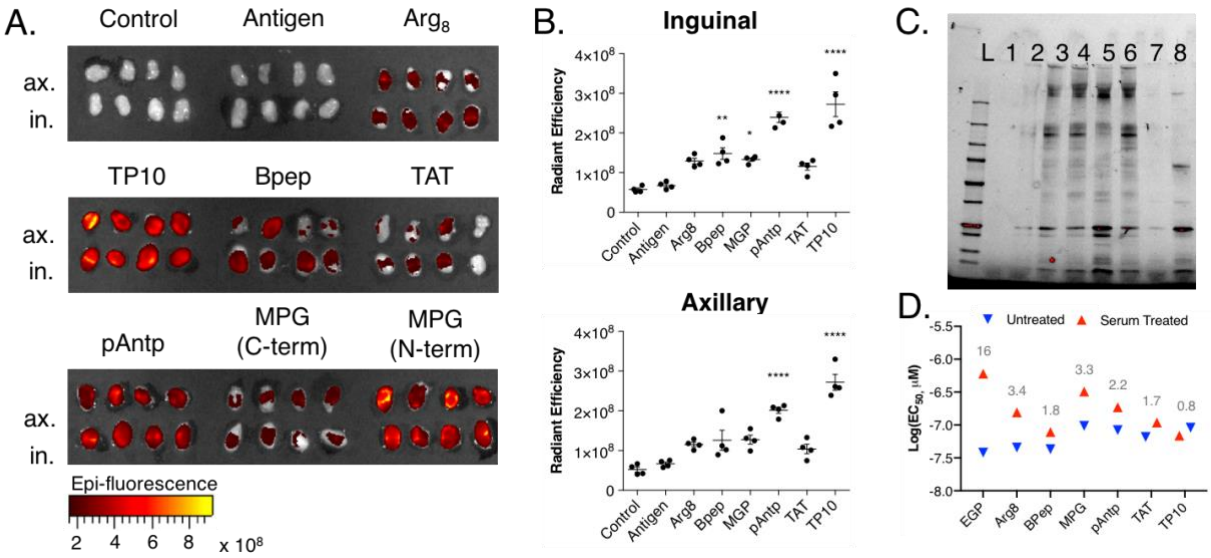

Figure 3.5. CPP conjugation promotes lymph node trafficking and enhances serum stability, likely due to association with serum proteins. A) Epifluorescence of the whole axillary and inguinal lymph nodes were analyzed by IVIS at 24 hours (n=2). **B)** Quantification of epifluorescence from **A)** in terms of radiant efficiency (photons/sec/steradian/ μW). **C)** Protein gel of eluted serum protein after association with CPPs. **D)** Serum stability of antigen constructs as determined by the EC_{50} for both the fresh and serum-treated samples, with a smaller EC_{50} fold-change corresponding to greater protection in serum. **** $p < 0.0001$; ** $p < 0.01$.

CPP conjugation extends the duration of T cell priming. Considering this enhanced serum stability and more efficient trafficking, we hypothesized that CPP conjugation could extend the duration of T cell activation against a vaccine antigen. To this end, we adoptively transferred pmel-1s into mice vaccinated with either EGP or EGP-pAntp over a period of 15 days (Figure 3.6A). The axillary and inguinal lymph nodes along with the spleen were harvested 24 hours after the AT and upregulation of CD69 on the pmel-1s was measured. We observed similar levels of activation for both EGP and EGP-pAntp when the mice were boosted the day before the AT. If the mice were boosted 4 or more days prior to AT, the level of activation dropped in the axillary lymph node for both EGP and EGP-pAntp and in the inguinal lymph node for the antigen alone, suggesting transient, short lived priming and activation (Figure 3.6B). The EGP-pAntp, on the other hand, was still able to induce CD69 upregulation in the inguinal lymph node even when it was injected up to 15 days prior (Figure 3.6B). This extended activation suggests that, in addition to increasing uptake by APCs and promoting lymph node trafficking, there is a temporal component to the mechanism by which CPPs enhance vaccine efficacy.

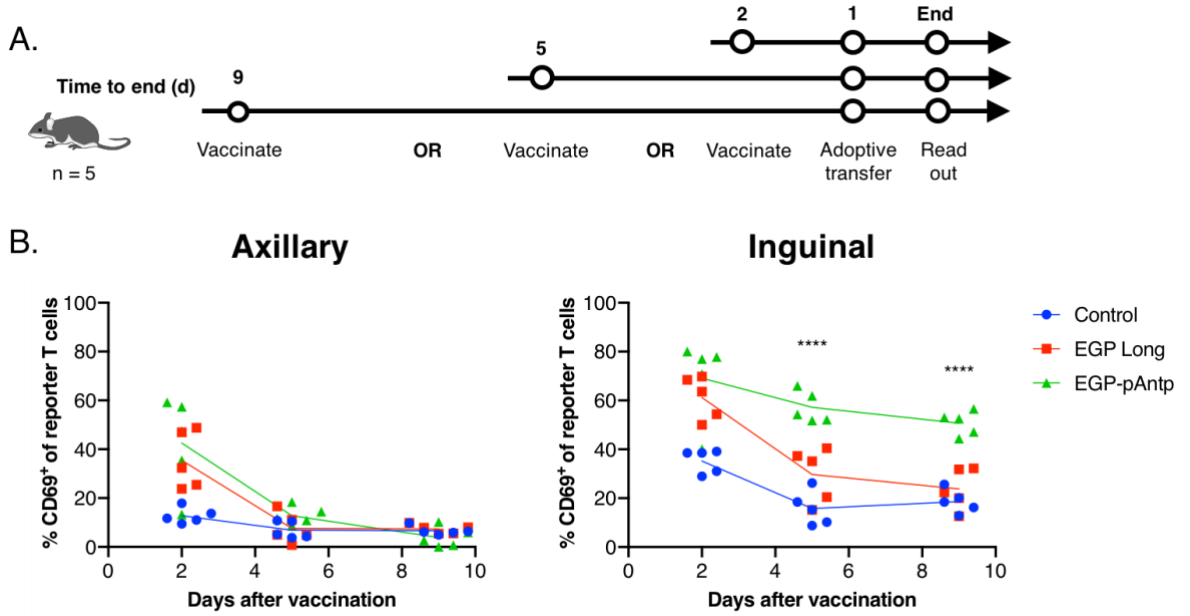

Figure 3.6. CPP conjugation extends antigen presentation in the draining lymph node. A) Timeline of experiment. Mice (n=5) were immunized either 2, 5, or 9 days prior to analysis. One day prior to analysis, pmel-1 T cells were adoptively transferred. Axillary and inguinal (draining) lymph nodes were resected and analyzed via flow cytometry to determine the extent of pmel-1 T cell activation within the relevant lymphatic compartment. **B)** T cell activation in the indicated lymph nodes measured as CD69 upregulation. Statistical analysis conducted using the student's *t*-test. **** $p < 0.0001$.

3.3 Materials and Methods

3.3.1 Reagents

H-Rink Amide-ChemMatrix and HMPB-ChemMatrix resins were obtained from PCAS BioMatrix Inc. (St-Jean-sur-Richelieu, Quebec, Canada). 1-[Bis(dimethylamino)methylene]-1H-1,2,3-triazolo[4,5-b]pyridinium-3-oxid- hexafluorophosphate (HATU), 4-pentynoic acid and Fmoc-(azido)ornithine-OH were purchased from Chem-Impex International (Wood Dale, IL). Fmoc-L-Arg(Pbf)-OH, Fmoc-L-His(Trt)-OH, Fmoc-L-Lys(Boc)-OH, Fmoc-L-Asp(tBu)-OH, Fmoc-L-Glu(tBu)-OH, Fmoc-L-Ser(tBu)-OH, Fmoc-L-Thr(tBu)-OH, Fmoc-L-Asn(Trt)-OH, Fmoc-L-Gln(Trt)-OH, Fmoc-L-Cys(Trt)-OH, Fmoc-L-Gly-OH, Fmoc-L-Ala-OH, Fmoc-L-Val-OH, Fmoc-L-Leu-OH, Fmoc-L-Ile-OH, Fmoc-L-Met-OH, Fmoc-L-Phe-OH, Fmoc-L-Pro-OH, Fmoc-L-Tyr(tBu)-OH, and Fmoc-L-Trp(Boc)-OH were purchased from EMD Millipore (Burlington, MA). 7-Azabenzotriazol-1-yloxy)trispyrrolidinophosphonium hexafluorophosphate (PyAOP) was purchased from P3 BioSystems (Louisville, KY). Peptide synthesis-grade N,N-dimethylformamide (DMF), CH_2CL_2, diethyl ether, and HPLC-grade acetonitrile were obtained from VWR International (Radnor, PA). Sulfo-

Cyanine5-maleimide and BODIPY-Texas Red-maleimide (BODIPY-TR-maleimide) were purchased from LumiProbe. All other reagents involved in peptide preparation were purchased from Sigma-Aldrich (St. Louis, MO). Milli-Q water was used exclusively.

3.3.2 Peptide synthesis

The antigen peptides and the CPPs indicated Figure 3.1A were produced using an automated solid-phase peptide synthesizer as previously described.[15] Briefly, equal volumes of a protected amino acid monomer (0.4 M in dimethyl formamide, DMF) and 1-[Bis(dimethylamino)methylene]-1H-1,2,3-triazolo[4,5-b]pyridinium 3-oxide hexafluorophosphate (HATU, 0.38 M in DMF) were combined to form an active ester then mixed with diisopropylethylamine (DIEA, neat, final concentration 1 M), heated to 90 □C, and flowed at 20 mL/min across 150 mg of H-Rink amide ChemMatrix resin contained within a fritted syringe which served as a single-use reactor. After a DMF wash, the N-terminus of the coupled monomer was de-protected with 20% piperidine, 2% formic acid in DMF (v/v) to regenerate the N-terminus, then the resin was washed again with DMF. This cycle was repeated until the entire sequence was completed. For sequences conjugated using copper(I)-catalyzed azide/alkyne cycloaddition (CuAAC), batch couplings were used to couple azido-ornithine at the C-terminus of the antigen peptides and 4-pentynoic acid at the N-terminus of each CPP, with the exception of the 'C-C' design variants of pAntp and MPG, in which propargyl glycine was coupled at the C-terminus. For batch couplings, the indicated monomer was dissolved in DMF along with HATU (0.4 M and 0.38 M respectively, final volume 2.5 mL), then the solution was mixed with 500 μL neat DIEA and added to the appropriate peptidyl resin. The reaction was incubated at room temperature for thirty minutes, then washed with DMF. After synthesis was complete, peptidyl resins were washed with dichloromethane and dried under vacuum. Peptides were cleaved from resin by incubating in 5% water, 5% thioanisole, 5% phenol, and 2.5% ethane dithiol in trifluoroacetic acid (TFA, v/v). Peptides were triturated in cold diethyl ether, resuspended in 50:50 water: acetonitrile (v/v) with 0.1% TFA as an additive, and lyophilized.

3.3.3 Peptide purification

Crude peptides (~200 mg) were suspended in 20 mL of either 5% or 15% acetonitrile in water (v/v) with 0.1% TFA as an additive and filtered through a 0.22 μm syringe filter. Peptides were then purified via preparative mass-directed reversed-phase HPLC (MD RP-HPLC) using water with 0.1% TFA as mobile phase A and acetonitrile with 0.1% TFA as mobile phase B. For each purification, solvent was flowed at 20 mL/min over an Agilent Zorbax

300SB-C3 column (21.2 x 250 mm, 7 μm) using a linear gradient ramping from either 5 to 35% B or 15 to 45% B over 60 minutes, with fractions collected in 10 mL increments. Fractions were pooled according to data from the instrument's in-line quadrupole mass spectrometer and lyophilized.

Antigen-CPP click conjugates and fluorophore-labeled conjugates were purified in a similar manner post-reaction using semi-preparative (MD RP-HPLC). Solvent was flowed at 4 mL/min over an Agilent Zorbax 300SB-C3 column (9.4 x 250 mm, 5 μm) using a linear gradient ramping from either 5 to 35% B or 15 to 45% B over 60 minutes, with fractions collected in 4 mL increments. Fractions were pooled and analyzed as above. All peptides and peptide conjugates were characterized via LC-MS to verify identity and purity.

3.3.4 Antigen conjugation

The indicated azide-containing long antigens were conjugated to each alkyne-CPP via Cu(I)-catalyzed click chemistry. Approximately 1 μmol of each reagent was dissolved in 30:70 water: dimethyl sulfoxide (DMSO, v/v) that had been sparged with N_2. Reactions were incubated for 1 hour on a nutating mixer, then quenched with the addition of 10 mL water with 0.1% TFA additive. Conjugates were then purified via reversed-phase HPLC as described above and isolated with >90% purity. Product identity and purity were verified via LC-MS.

Antigen or antigen-azide peptides (20 mg) were massed out into a 50 mL conical vial and dissolved in 45 mL water, then combined with equimolar BDP-TR-maleimide or SulfoCy5-maleimide (50 mM stock in DMSO). Reactions were incubated for 30 minutes at room temperature on a nutating mixer, then filtered with a 0.22 μm syringe filter and purified by RP-HPLC as described above. Alternately, for the antigen-azide peptides, which were subsequently conjugated to various alkyne-CPPs and purified, the reaction mixture was lyophilized immediately without purification in order to minimize loss of material. Product identity and purity were verified via LC-MS.

3.3.5 LC-MS analysis

Unless otherwise stated, LC-MS analyses were performed on an Agilent 6520 ESI-QTOF mass spectrometer with an Agilent Zorbax column (300SB C3, 2.1 x 150 mm, 5 μm). Mobile phase A was 0.1% formic acid in water and mobile phase B was 0.1% formic acid in LC-MS grade acetonitrile. The LC-MS method was as follows: 1% B from 0 to 2 min, linear ramp from 1% B to 61% B from 2 to 11 min, 61% B to 99% B from 11 to 12 min and finally 3 min of post-time at 1% B for equilibration, flow rate: 0.8 mL/min. Some LC-MS analyses were performed on Agilent 6550 ESI-QTOF mass spectrometer with an Agilent Zorbax column (300SB-C3 2.1 x 150mm, 5μm). Mobile phases were same as previous and the gradient was as

follows: 1% B from 0 to 2min with a linear gradient from 1 to 95% B over 10 minutes, then 95% B for 1 minute with the MS on from 4 to 12 minutes and a flow rate of 0.5 mL/min. All data were processed using the Agilent MassHunter software package. Y-axis in all chromatograms represents total ion current (TIC) unless noted.

3.3.6 Serum stability LC-MS assay

Peptides were incubated at 5 µM in PBS with 5% mouse serum (Gibco) at 37 °C for 24 hours. At the indicated time points, a 5 µL aliquot of the reaction mixture was removed, transferred to a fresh 1.5 mL microcentrifuge tube, and lyophilized. These aliquots were then re-suspended in water with 0.1% TFA and analyzed via LC-MS using an Agilent 6550 ESI-QTOF and the method described above.

3.3.7 Cells

DC2.4 cells were provided by K. Rock (UMass Medical School) and TC-1 cells were provided by T.C. Wu (Johns Hopkins University). All cell lines were cultured in complete RPMI-1640 medium (GE Healthcare Life Sciences; supplemented with 10% FBS, 100 units/ml penicillin, and 100 µg/mL streptomycin). T cells and splenocytes were cultured in complete RPMI with 20 mM HEPES, 1 mM sodium pyruvate, 0.05 mM B-mercaptoethanol, and 1X non-essential amino acids. Cells were maintained at 37 °C and 5% CO_2 and DC2.4 cells were split at a 1:8 ratio every three days or at 80% confluency.

3.3.8 **In vitro** *activation assay*

Splenocytes were harvested from wild-type c57bl6 mice and plated with 10_5 cells per well in a 98-well plate. Splenocytes were treated for one hour with 0.5 µM peptide, then fresh media was exchanged and splenocytes were co-cultured with $5x10_4$ CFSE-stained pmel-1 T cells. Activation of the pmel-1 T cells was measured at 24 hours via staining with Thy1.1 as a co-injection marker and upregulation of CD69. Pmel-1 proliferation was assessed at 72 hours by flow cytometry.

3.3.9 Serum protein pulldown

Protein binding to the CPPs was assessed using the Pierce™ Biotinylated Protein Interaction Kit (Thermo Scientific). Briefly, biotinylated CPPs were bound to the provided streptavidin beads. Excess peptide was washed from the column by centrifugation. 50% mouse serum in PBS was applied to the column for 1 hour. The serum proteins were washed off the column using PBS and centrifugation until elute produced undetectable levels of protein as assessed by protein gel electrophoresis. Proteins bound to the CPP-Beads were then eluted using a mild acid and assessed by gel electrophoresis. Bands were excised and lyophilized, then reconstituted in a digestion solution (50 mM NH_4HCO_3 with 12.5 ng/µL trypsin) and incubated

on ice for 45 min, then another 10 μL of the digestion solution was added and samples were incubated overnight at 37 °C. Solution was exchanged by adding 15 μL 20 mM NH_4HCO_3, then spinning and removing and saving supernatant. Peptides were extracted three times by treating with 20 μL water: acetonitrile (v/v) with 5% formic acid for 20 minutes at room temperature. Extracted fractions were added to supernatant from previous step, then combined sample was concentrated and de-salted using a C18 zip-tip. Samples were analyzed using a Thermo Oribtrap Fusion Lumos Tribrid Mass Spectrometer and data was processed using PEAKS proteomics software to perform *de novo* sequencing and a database search.

3.3.10 Activation-based serum stability assay

Following prime and boost of mice with EGP peptides, CD8+ T cell responses were confirmed on day -1. On the day of the experiment, spleens from vaccinated animals were excised, mashed through 70 μm filters (Corning), lysed in ACK buffer, pooled, and plated in 96 well V-bottom plates (1 spleen per 30 wells). 24 hours before *ex vivo* stimulation, mouse serum from naïve animals was freshly collected in collection tubes with Z-Gel to remove clotting factors (Sarstedt) and used to prepare RPMI-1640 + 10% mouse serum media. 30 μM antigen solutions were prepared in RPMI-1640 + 10% mouse serum and incubated at 37 °C. After a 24 hour incubation, fresh antigen was similarly prepared at 30 μM in RPMI-1640 + 10% mouse serum and both solutions were immediately diluted 4x with RPMI-1640 + 10% FBS; serial dilutions were prepared and used to re-stimulate the aforementioned splenocytes from vaccinated animals. $CD69^+ CD8^+$ T cell responses were measured by flow cytometry.

3.3.11 DC2.4 uptake assay

For confocal analysis, $5x10^4$ cells were seeded 48 hour prior to treatment in glass bottomed plates, such that cells were 50% confluent at the time of experiment. Each plate was treated with 2.5 μM fluor-peptide for 1 hour, then extensively washed with PBS to remove surface bound peptide and fluorophores. Samples were stained with Hoechst 33342 Solution (BD Biosciences) in complete RPMI at 37 °C for 30 min, washed with PBS, and stained with Lysotracker Green DND-26 (Invitrogen) in PBS at 37 °C for 5 min. Cells were then washed and reconstituted in Live Cell Imaging Solution (Invitrogen).

For analysis by flow cytometry, 10^5 cells were seeded 24 hours prior to treatment in a 24-well plate. Samples were treated with 2.5 μM peptide for 1 hour, then extensively washed with PBS to remove surface bound peptide and fluorophores. Cells were lifted using trypsin, cleaving off any remaining peptide, stained with a viability dye and uptake was assessed on 50,000 events.

3.3.12 Mice

B6 mice (C57BL/6NTac) were purchased from Taconic. Batf3-/- knockout mice and transgenic pmel-1 mice were bred in-house. Mice were used between 6-8 weeks of age and female mice were used unless otherwise noted. All animal work was conducted under the approval of the Massachusetts Institute of Technology Division of Comparative Medicine (MIT DCM) in accordance with federal, state, and local guidelines.

3.3.13 Prophylactic vaccination

Wild type and Batf3-/- mice were primed with 5 nmol of peptide vaccine and 25 µg c-di-GMP s.c. at the tail base, with half of the dose given at each side, followed by a boost of the same strategy 14 days later. For some experiments, a second boost vaccine was given at 21 days after the initial prime as noted. Peripheral blood was analyzed 7 days after the boost by ICS.

3.3.14 Tumor inoculation and therapy

An inoculum of 300,000 TC-1 tumor cells, suspended in 50 µL of sterile PBS were injected subcutaneously on the shoulder of mice. Mice were randomized on day 5 prior to treatment with and average tumor size ~20 mm_2, then vaccinated with 5 nmol of peptide vaccine and 25 µg c-di-GMP s.c. at the tail base, with half of the dose given at each side. Subsequent vaccinations were performed on day 12 and day 19. Peripheral blood was analyzed 7 days after each vaccination by ICS. Tumor size was measured as area (longest dimension times the perpendicular dimension) every 3 days and mice were euthanized when the tumor area exceeded 200 mm_2 or met other euthanasia criteria as assessed by MIT DCM.

3.3.15 Pmel-1 **in vivo** *activation assay*

Wild type mice were injected s.c. at the tailbase with 25 µg c-di-GMP along with 5 nmol of either EGP or EGP-pAntp in 100 µL of 75 mM $MgCl_2$, 50 µL per side on day 1, 6, 10, or 13 (one group per time point). On day 14, 10_6 pmel-1 T cells were injected retro-orbitally. 24 hours later, axillary and inguinal lymph nodes, along with the spleen were harvested and stained with the congenic marker Thy1.1, CD69, CD8, CD3, and zombie fixable viability dye. Upregulation of CD69 on pmel-1 T cells in each tissue was assessed by flow cytometry.

3.3.16 Confocal imaging

Images were acquired using an Olympus Fluoview FV1200 microscope equipped with 10X, 30X, 60X, and 100X objectives, and optimum lasers and filter sets. The images within each data set were acquired under identical settings and subsequently processed using Fiji image analysis software.

3.3.17 Lymph node trafficking

Mice were immunized with 25 nmol fluor-peptide and 25 µg c-di-GMP s.c. at the tail base, with half of the dose given at each side, then axillary and inguinal lymph nodes were resected 24 hours later. Whole lymph nodes were imaged using an *in vivo* imaging system (IVIS) to measure epifluorescence. Radiant efficiency was quantified using XX software.

3.3.18 Flow cytometry

Antibodies to CD8a, IFN-γ, TNF- α, CD3, B220, F4/80, CD11b, CD11c, CD103 were purchased from Biolegend. Viability was assessed by live/dead fixable aqua (Biolegend).

Intracellular cytokine staining (ICS) was performed as described previously. Peptides used for restimulation were 10 µg/mL of the minimal epitope (defined in Figure 3.1A). Briefly, peripheral blood was collected, lysed, and plated with restimulation peptide. After 2 hours of stimulation at 37 ˚C and 5% CO_2, brefeldin A (BFA) was added and samples were returned to incubation for an additional 4 hours. Samples were stained with a fixable viability dye followed by extracellular staining for 20 minutes. Using a fixation/permeabilization kit (BD biosciences), samples were prepared for intracellular antibody staining for 35 minutes and assessed by flow cytometry.

3.3.19 Statistical analysis

Experiments were not performed in a blinded fashion. Sample sizes were chosen based on estimates from pilot experiments and previously published results, such that appropriate statistical tests could yield significant results. Data was analyzed using a one-way ANOVA with a Bonferroni post hoc test using GraphPad Prism software. Survival curves were analyzed using the log-rank (Mantel-Cox) test.

3.4 Conclusions

While CPPs have been described as simple and versatile delivery modalities for antigens in prophylactic and therapeutic vaccines, their behavior *in vivo* has been largely unexplored. Previous investigations have also typically been limited to a small handful of CPPs and model antigens. Herein, we screened a set of CPPs to evaluate their impact of vaccine efficacy, as well as their mechanism of action. We demonstrate that the addition of a CPP is a general strategy to generate higher T cell responses both *in vitro* and *in vivo*, with penetratin enhancing vaccine immunogenicity up to 20x for a range of tumor antigens. These antigen-CPP vaccines can be used to induce a therapeutic T cell response that is able to mitigate tumor outgrowth. Turning towards mechanistic characterization, we demonstrate that CPPs increase uptake by DCs by an

order of magnitude. We then determine that, although not part of the initial design, CPPs aid in vaccine antigen lymphatic trafficking likely due at least in part to association with apolipoprotein A1 and other serum proteins. CPPs enhance antigen proteolytic stability in serum, likely due to a similar mechanism. They also prolonged antigen residence in the lymph node allowing for extended priming of antigen-specific T cells and a more robust immune response than achieved using the peptide antigen alone.

Further effort will be required to optimize CPP design that takes into consideration all of the factors outlined here. Based on these findings, we anticipate that 'universal' top sequences could be developed that would improve vaccine efficacy for the majority of antigens; however, considering the cargo-dependent nature of CPP activity and the broad diversity of antigen sequences, it is possible that some vaccine antigens may require a tailored approach. We anticipate that the rapid production and ease of modification afforded by flow peptide synthesis will streamline this optimization process. Follow up studies will also be needed to confirm whether the mechanistic factors outlined here are recapitulated in larger animals. In these studies, careful evaluation of immune responses over time will be required to ensure that prolonged use of CPPs does not result in off-target immunogenicity.

Our findings identify several key, previously uncharacterized factors to consider in the selection and design of CPPs for vaccine delivery. We highlight the importance of taking a holistic approach to the delivery challenge and considering lymphatic trafficking, serum stability, and the duration of presentation *in vivo* in addition to cell uptake and cytosolic delivery. We anticipate that this knowledge will help guide future design of CPPs and other delivery modalities for cancer vaccines.

3.5 Acknowledgements and Conflict Statements

D.J.I is a Howard Hughes Medical Institute investigator. We thank the Koch Institute Swanson Biotechnology Center for technical support, namely the whole-animal imaging facility, the histology facility, the microscopy facility, and the flow cytometry facility. The U.S. Army Research Office, the U.S. Army Medical Research and Materiel Command, and Northwestern University provided funding to develop this core facility and ongoing support is being received from the Soft and Hybrid Nanotechnology Experimental (SHyNE) Resource (NSF ECCS-1542205). R.L.H. is supported by an NSF Graduate Research Fellowship. This work was supported in part the Bridge Project partnership between the Koch Institute for Integrative

Cancer Research and the Dana Farber/Harvard Cancer Center (DF/HCC). The authors declare no conflicts.

3.6 References

(1) Hollingsworth, R. E.; Jansen, K. Turning the Corner on Therapeutic Cancer Vaccines. *npj Vaccines* **2019**, *4* (1), 1–10. https://doi.org/10.1038/s41541-019-0103-y.

(2) Sahin, U.; Türeci, Ö. Personalized Vaccines for Cancer Immunotherapy. *Science* **2018**, *359* (6382), 1355–1360. https://doi.org/10.1126/science.aar7112.

(3) Ott, P. A.; Hu, Z.; Keskin, D. B.; Shukla, S. A.; Sun, J.; Bozym, D. J.; Zhang, W.; Luoma, A.; Giobbie-Hurder, A.; Peter, L.; Chen, C.; Olive, O.; Carter, T. A.; Li, S.; Lieb, D. J.; Eisenhaure, T.; Gjini, E.; Stevens, J.; Lane, W. J.; Javeri, I.; Nellaiappan, K.; Salazar, A.; Daley, H.; Seaman, M.; Buchbinder, E. I.; Yoon, C. H.; Harden, M.; Lennon, N.; Gabriel, S.; Rodig, S. J.; Barouch, D. H.; Aster, J. C.; Getz, G.; Wucherpfennig, K.; Neuberg, D.; Ritz, J.; Lander, E. S.; Fritsch, E. F.; Hacohen, N.; Wu, C. J. An Immunogenic Personal Neoantigen Vaccine for Melanoma Patients. *Nature* **2017**, *547* (7662), 217–221. https://doi.org/10.1038/nature22991.

(4) Keskin, D. B.; Anandappa, A. J.; Sun, J.; Tirosh, I.; Mathewson, N. D.; Li, S.; Oliveira, G.; Giobbie-Hurder, A.; Felt, K.; Gjini, E.; Shukla, S. A.; Hu, Z.; Li, L.; Le, P. M.; Allesøe, R. L.; Richman, A. R.; Kowalczyk, M. S.; Abdelrahman, S.; Geduldig, J. E.; Charbonneau, S.; Pelton, K.; Iorgulescu, J. B.; Elagina, L.; Zhang, W.; Olive, O.; McCluskey, C.; Olsen, L. R.; Stevens, J.; Lane, W. J.; Salazar, A. M.; Daley, H.; Wen, P. Y.; Chiocca, E. A.; Harden, M.; Lennon, N. J.; Gabriel, S.; Getz, G.; Lander, E. S.; Regev, A.; Ritz, J.; Neuberg, D.; Rodig, S. J.; Ligon, K. L.; Suvà, M. L.; Wucherpfennig, K. W.; Hacohen, N.; Fritsch, E. F.; Livak, K. J.; Ott, P. A.; Wu, C. J.; Reardon, D. A. Neoantigen Vaccine Generates Intratumoral T Cell Responses in Phase Ib Glioblastoma Trial. *Nature* **2019**, *565* (7738), 234–239. https://doi.org/10.1038/s41586-018-0792-9.

(5) Sahin, U.; Derhovanessian, E.; Miller, M.; Kloke, B.-P.; Simon, P.; Löwer, M.; Bukur, V.; Tadmor, A. D.; Luxemburger, U.; Schrörs, B.; Omokoko, T.; Vormehr, M.; Albrecht, C.; Paruzynski, A.; Kuhn, A. N.; Buck, J.; Heesch, S.; Schreeb, K. H.; Müller, F.; Ortseifer, I.; Vogler, I.; Godehardt, E.; Attig, S.; Rae, R.; Breitkreuz, A.; Tolliver, C.; Suchan, M.; Martic, G.; Hohberger, A.; Sorn, P.; Diekmann, J.; Ciesla, J.; Waksmann, O.; Brück, A.-K.; Witt, M.; Zillgen, M.; Rothermel, A.; Kasemann, B.; Langer, D.; Bolte, S.; Diken, M.; Kreiter, S.; Nemecek, R.; Gebhardt, C.; Grabbe, S.; Höller, C.; Utikal, J.; Huber, C.; Loquai, C.; Türeci, Ö. Personalized RNA Mutanome Vaccines Mobilize Poly-Specific Therapeutic Immunity against Cancer. *Nature* **2017**, *547* (7662), 222–226. https://doi.org/10.1038/nature23003.

(6) Yutani, S.; Komatsu, N.; Yoshitomi, M.; Matsueda, S.; Yonemoto, K.; Mine, T.; Noguchi, M.; Ishihara, Y.; Yamada, A.; Itoh, K.; Sasada, T. A Phase II Study of a Personalized Peptide Vaccination for Chemotherapy-Resistant Advanced Pancreatic Cancer Patients. *Oncology Reports* **2013**, *30* (3), 1094–1100. https://doi.org/10.3892/or.2013.2556.

(7) Noguchi, M.; Moriya, F.; Koga, N.; Matsueda, S.; Sasada, T.; Yamada, A.; Kakuma, T.; Itoh, K. A Randomized Phase II Clinical Trial of Personalized Peptide Vaccination with Metronomic Low-Dose Cyclophosphamide in Patients with Metastatic Castration-Resistant Prostate Cancer. *Cancer Immunol. Immunother.* **2016**, *65* (2), 151–160. https://doi.org/10.1007/s00262-015-1781-6.

(8) Ilyas, S.; Yang, J. C. Landscape of Tumor Antigens in T-Cell Immunotherapy. *J Immunol* **2015**, *195* (11), 5117–5122. https://doi.org/10.4049/jimmunol.1501657.
(9) Sarkizova, S.; Klaeger, S.; Le, P. M.; Li, L. W.; Oliveira, G.; Keshishian, H.; Hartigan, C. R.; Zhang, W.; Braun, D. A.; Ligon, K. L.; Bachireddy, P.; Zervantonakis, I. K.; Rosenbluth, J. M.; Ouspenskaia, T.; Law, T.; Justesen, S.; Stevens, J.; Lane, W. J.; Eisenhaure, T.; Lan Zhang, G.; Clauser, K. R.; Hacohen, N.; Carr, S. A.; Wu, C. J.; Keskin, D. B. A Large Peptidome Dataset Improves HLA Class I Epitope Prediction across Most of the Human Population. *Nat. Biotechnol.* **2020**, *38* (2), 199–209. https://doi.org/10.1038/s41587-019-0322-9.
(10) Grenier, J. M.; Yeung, S. T.; Khanna, K. M. Combination Immunotherapy: Taking Cancer Vaccines to the Next Level. *Front Immunol* **2018**, *9*, 610. https://doi.org/10.3389/fimmu.2018.00610.
(11) Collins, J. M.; Redman, J. M.; Gulley, J. L. Combining Vaccines and Immune Checkpoint Inhibitors to Prime, Expand, and Facilitate Effective Tumor Immunotherapy. *Expert Rev Vaccines* **2018**, *17* (8), 697–705. https://doi.org/10.1080/14760584.2018.1506332.
(12) Moynihan, K. D.; Opel, C. F.; Szeto, G. L.; Tzeng, A.; Zhu, E. F.; Engreitz, J. M.; Williams, R. T.; Rakhra, K.; Zhang, M. H.; Rothschilds, A. M.; Kumari, S.; Kelly, R. L.; Kwan, B. H.; Abraham, W.; Hu, K.; Mehta, N. K.; Kauke, M. J.; Suh, H.; Cochran, J. R.; Lauffenburger, D. A.; Wittrup, K. D.; Irvine, D. J. Eradication of Large Established Tumors in Mice by Combination Immunotherapy That Engages Innate and Adaptive Immune Responses. *Nat Med* **2016**, *22* (12), 1402–1410. https://doi.org/10.1038/nm.4200.
(13) Hos, B. J.; Tondini, E.; van Kasteren, S. I.; Ossendorp, F. Approaches to Improve Chemically Defined Synthetic Peptide Vaccines. *Front. Immunol.* **2018**, *9*. https://doi.org/10.3389/fimmu.2018.00884.
(14) Fosgerau, K.; Hoffmann, T. Peptide Therapeutics: Current Status and Future Directions. *Drug Discov. Today* **2015**, *20* (1), 122–128. https://doi.org/10.1016/j.drudis.2014.10.003.
(15) Mijalis, A. J.; Thomas, D. A.; Simon, M. D.; Adamo, A.; Beaumont, R.; Jensen, K. F.; Pentelute, B. L. A Fully Automated Flow-Based Approach for Accelerated Peptide Synthesis. *Nat. Chem. Biol.* **2017**, *13* (5), 464–466. https://doi.org/10.1038/nchembio.2318.
(16) Abbas, A.; Lichtman, A. H.; Pillai, S. *Cellular and Molecular Immunology*, 9th ed.; Elsevier, 2017.
(17) McLennan, D. N.; Porter, C. J. H.; Charman, S. A. Subcutaneous Drug Delivery and the Role of the Lymphatics. *Drug Discov Today Technol* **2005**, *2* (1), 89–96. https://doi.org/10.1016/j.ddtec.2005.05.006.
(18) Liu, H.; Moynihan, K. D.; Zheng, Y.; Szeto, G. L.; Li, A. V.; Huang, B.; Van Egeren, D. S.; Park, C.; Irvine, D. J. Structure-Based Programming of Lymph-Node Targeting in Molecular Vaccines. *Nature* **2014**, *507* (7493), 519–522. https://doi.org/10.1038/nature12978.
(19) Moynihan, K. D.; Holden, R. L.; Mehta, N. K.; Wang, C.; Karver, M. R.; Dinter, J.; Liang, S.; Abraham, W.; Melo, M. B.; Zhang, A. Q.; Li, N.; Gall, S. L.; Pentelute, B. L.; Irvine, D. J. Enhancement of Peptide Vaccine Immunogenicity by Increasing Lymphatic Drainage and Boosting Serum Stability. *Cancer Immunol Res* **2018**, *6* (9), 1025–1038. https://doi.org/10.1158/2326-6066.CIR-17-0607.
(20) Joffre, O. P.; Segura, E.; Savina, A.; Amigorena, S. Cross-Presentation by Dendritic Cells. *Nat Rev Immunol* **2012**, *12* (8), 557–569. https://doi.org/10.1038/nri3254.

(21) Keler, T.; He, L.; Ramakrishna, V.; Champion, B. Antibody-Targeted Vaccines. *Oncogene* **2007**, *26* (25), 3758–3767. https://doi.org/10.1038/sj.onc.1210375.
(22) Tsuji, T.; Matsuzaki, J.; Kelly, M. P.; Ramakrishna, V.; Vitale, L.; He, L.-Z.; Keler, T.; Odunsi, K.; Old, L. J.; Ritter, G.; Gnjatic, S. Antibody-Targeted NY-ESO-1 to Mannose Receptor or DEC-205 in Vitro Elicits Dual Human CD8+ and CD4+ T Cell Responses with Broad Antigen Specificity. *J. Immunol.* **2011**, *186* (2), 1218–1227. https://doi.org/10.4049/jimmunol.1000808.
(23) Walker, P. R.; Belnoue, E.; Dietrich, P.-Y.; Derouazi, M. Cell-Penetrating Peptides-the Swiss Army Knife of Cancer Vaccines. *Oncoimmunology* **2016**, *5* (3), e1095435. https://doi.org/10.1080/2162402X.2015.1095435.
(24) Skwarczynski, M.; Toth, I. Cell-Penetrating Peptides in Vaccine Delivery: Facts, Challenges and Perspectives. *Ther Deliv* **2019**, *10* (8), 465–467. https://doi.org/10.4155/tde-2019-0042.
(25) Yang, J.; Luo, Y.; Shibu, M. A.; Toth, I.; Skwarczynskia, M. Cell-Penetrating Peptides: Efficient Vectors for Vaccine Delivery. *Curr Drug Deliv* **2019**, *16* (5), 430–443. https://doi.org/10.2174/1567201816666190123120915.
(26) Brooks, N. A.; Pouniotis, D. S.; Tang, C.-K.; Apostolopoulos, V.; Pietersz, G. A. Cell-Penetrating Peptides: Application in Vaccine Delivery. *Biochim. Biophys. Acta* **2010**, *1805* (1), 25–34. https://doi.org/10.1016/j.bbcan.2009.09.004.
(27) Milletti, F. Cell-Penetrating Peptides: Classes, Origin, and Current Landscape. *Drug Discov. Today* **2012**, *17* (15–16), 850–860. https://doi.org/10.1016/j.drudis.2012.03.002.
(28) Copolovici, D. M.; Langel, K.; Eriste, E.; Langel, Ü. Cell-Penetrating Peptides: Design, Synthesis, and Applications. *ACS Nano* **2014**, *8* (3), 1972–1994. https://doi.org/10.1021/nn4057269.
(29) Kauffman, W. B.; Fuselier, T.; He, J.; Wimley, W. C. Mechanism Matters: A Taxonomy of Cell Penetrating Peptides. *Trends Biochem. Sci.* **2015**, *40* (12), 749–764. https://doi.org/10.1016/j.tibs.2015.10.004.
(30) Belnoue, E.; Mayol, J.-F.; Carboni, S.; Di Berardino Besson, W.; Dupuychaffray, E.; Nelde, A.; Stevanovic, S.; Santiago-Raber, M.-L.; Walker, P. R.; Derouazi, M. Targeting Self and Neo-Epitopes with a Modular Self-Adjuvanting Cancer Vaccine. *JCI Insight* **2019**, *5*. https://doi.org/10.1172/jci.insight.127305.
(31) Belnoue, E.; Di Berardino-Besson, W.; Gaertner, H.; Carboni, S.; Dunand-Sauthier, I.; Cerini, F.; Suso-Inderberg, E.-M.; Wälchli, S.; König, S.; Salazar, A. M.; Hartley, O.; Dietrich, P.-Y.; Walker, P. R.; Derouazi, M. Enhancing Antitumor Immune Responses by Optimized Combinations of Cell-Penetrating Peptide-Based Vaccines and Adjuvants. *Mol. Ther.* **2016**, *24* (9), 1675–1685. https://doi.org/10.1038/mt.2016.134.
(32) Derouazi, M.; Di Berardino-Besson, W.; Belnoue, E.; Hoepner, S.; Walther, R.; Benkhoucha, M.; Teta, P.; Dufour, Y.; Yacoub Maroun, C.; Salazar, A. M.; Martinvalet, D.; Dietrich, P.-Y.; Walker, P. R. Novel Cell-Penetrating Peptide-Based Vaccine Induces Robust CD4+ and CD8+ T Cell-Mediated Antitumor Immunity. *Cancer Res.* **2015**, *75* (15), 3020–3031. https://doi.org/10.1158/0008-5472.CAN-14-3017.
(33) Pouniotis, D. S.; Esparon, S.; Apostolopoulos, V.; Pietersz, G. A. Whole Protein and Defined CD8(+) and CD4(+) Peptides Linked to Penetratin Targets Both MHC Class I and II Antigen Presentation Pathways. *Immunol. Cell Biol.* **2011**, *89* (8), 904–913. https://doi.org/10.1038/icb.2011.13.
(34) Wu, H.; Zhuang, Q.; Xu, J.; Xu, L.; Zhao, Y.; Wang, C.; Yang, Z.; Shen, F.; Liu, Z.; Peng, R. Cell-Penetrating Peptide Enhanced Antigen Presentation for Cancer Immunotherapy. *Bioconjug. Chem.* **2019**, *30* (8), 2115–2126. https://doi.org/10.1021/acs.bioconjchem.9b00245.

(35) Brooks, N.; Esparon, S.; Pouniotis, D.; Pietersz, G. A. Comparative Immunogenicity of a Cytotoxic T Cell Epitope Delivered by Penetratin and TAT Cell Penetrating Peptides. *Molecules* **2015**, *20* (8), 14033–14050. https://doi.org/10.3390/molecules200814033.
(36) Brooks, N.; Hsu, J.; Esparon, S.; Pouniotis, D.; Pietersz, G. A. Immunogenicity of a Tripartite Cell Penetrating Peptide Containing a MUC1 Variable Number of Tandem Repeat (VNTR) and A T Helper Epitope. *Molecules* **2018**, *23* (9). https://doi.org/10.3390/molecules23092233.
(37) Batchu, R. B.; Gruzdyn, O.; Potti, R. B.; Weaver, D. W.; Gruber, S. A. MAGE-A3 with Cell-Penetrating Domain as an Efficient Therapeutic Cancer Vaccine. *JAMA Surg* **2014**, *149* (5), 451–457. https://doi.org/10.1001/jamasurg.2013.4113.
(38) Granadillo, M.; Vallespi, M. G.; Batte, A.; Mendoza, O.; Soria, Y.; Lugo, V. M.; Torrens, I. A Novel Fusion Protein-Based Vaccine Comprising a Cell Penetrating and Immunostimulatory Peptide Linked to Human Papillomavirus (HPV) Type 16 E7 Antigen Generates Potent Immunologic and Anti-Tumor Responses in Mice. *Vaccine* **2011**, *29* (5), 920–930. https://doi.org/10.1016/j.vaccine.2010.11.083.
(39) Phase 1b Study to Evaluate ATP128, With or Without BI 754091, in Patients With Stage IV Colorectal Cancer - Full Text View - ClinicalTrials.gov https://clinicaltrials.gov/ct2/show/NCT04046445 (accessed Jul 2, 2020).
(40) Pouniotis, D.; Tang, C.-K.; Apostolopoulos, V.; Pietersz, G. Vaccine Delivery by Penetratin: Mechanism of Antigen Presentation by Dendritic Cells. *Immunol. Res.* **2016**, *64* (4), 887–900. https://doi.org/10.1007/s12026-016-8799-5.

Chapter 4: Enhancement of peptide vaccine immunogenicity by increasing lymphatic drainage using diverse albumin binders

The work presented in this chapter has been adapted from the following publication:

Moynihan, K. D., Holden, R. L., Mehta, N. K., Wang, C., Karver, M. R., Dinter, J., Liang, S., Abraham, W., Melo, M. B., Zhang, A. Q., Li, N., Gall, S. L., Pentelute, B. L. & Irvine, D. J. Enhancement of Peptide Vaccine Immunogenicity by Increasing Lymphatic Drainage and Boosting Serum Stability. *Cancer Immunol. Res.* **6,** 1025–1038 (2018).

A portion of the work presented in the chapter also appears in the following patent:

Moynihan, K. D., Holden, R. L., Irvine, D. J. & Pentelute, B. L. Albumin binding peptide conjugates and methods thereof. (2019).

Author contributions:

R.L.H., K.D.M., B.L.P., and D.J.I. designed this project. R.L.H. synthesized the peptides and peptide conjugates for each experiment. K.D.M. collected and analyzed animal data and R.L.H. collected and analyzed LC-MS characterization data. R.L.H. K.D.M., B.L.P., and D.J.I. interpreted data and wrote the relevant manuscript sections and corresponding patent application.

4.1 Introduction

The capacity of anti-tumor T cell responses to be curative in cancer patients is known from clinical studies of adoptive cell therapy, but the induction of qualitatively and quantitatively potent anti-tumor T cell responses through therapeutic vaccination remains a challenge.[1,2] The poor lymphatic drainage and short *in vivo* half-life of linear peptides likely contribute to the low potency of peptide vaccines.[3–6] We previously reported that enhanced lymph node targeting of peptides can be achieved by covalently modifying peptides and molecular adjuvants with diacyl lipids (with the peptides linked through a poly(ethylene glycol), PEG, spacer), and this trafficking enhancement results in a corresponding increase in T cell priming.[6] The mechanism of action is thought to involve binding of the lipid tails to endogenous albumin, allowing peptides and molecular adjuvants to "hitchhike" on albumin to the draining lymph node, similar to the mechanism of action of sentinel lymph node mapping dyes in clinical use.[7,8] We hypothesized that covalent linkage to other albumin-binding moieties, namely albumin binding peptides and α-tocopherol, could promote favorable lymphatic trafficking of vaccine antigens in a similar manner.

Albumin binding peptides, unlike lipid albumin binders, remain largely unexplored in the context of vaccinology. They have previously been used to improve the serum stability and extend the pharmacokinetics of therapeutically-relevant proteins, but have not been examined for their potential to direct peptide vaccines to the lymphatic system via albumin hitchhiking, a novel application for these under-utilized sequences.[9] They could provide several technical advances over lipidic albumin binders that could be translationally desirable. An "all on resin" synthesis is easier to envision for GMP production than synthesis methods requiring solution coupling (which is how the diacyl lipid-PEG-peptides are currently synthesized). Additionally, libraries of albumin-binding peptides (ABPs) have been characterized that could allow for precise control over albumin-binding affinity, which may be important for the resulting immune response. One study utilizing phage display identified the cyclized peptide DICLPRWGCLW as the minimal core sequence for achieving binding to serum albumin from multiple species, including mice and humans.[9] We chose to use this albumin-binding peptide as a model sequence to explore this hypothesis.

In addition to peptide albumin binders, several small molecules have been identified to associate with serum albumin. In particular, α-tocopherol, the most biologically active form of Vitamin E, has been demonstrated to bind albumin (K_D ~ 7 μM).[10,11] Its abundance and high safety profile could make α-tocopherol a potentially useful candidate in vaccine design.

Evaluating the impact of a small molecule albumin binder on vaccine efficacy could serve to underscore the generalizability of albumin hitchhiking as a strategy to enhance vaccine efficacy. Here, we demonstrate that a model albumin-binding sequence and α-tocopherol enhance lymph node trafficking and boost vaccine efficacy for a melanoma antigen.

4.2 Results

We previously reported that peptide antigens conjugated to 1,2-distearoyl-sn-glycero-3-phosphoethanolamine (DSPE) through a poly(ethylene glycol) spacer (Fig. 4.1A) could exhibit greatly increased lymphatic trafficking following immunization, and thereby 20-30-fold increased immunogenicity in mice.[6] This enhanced lymphatic trafficking and vaccine potency was associated with the ability of the conjugates to bind serum albumin, suggesting that albumin serves as an *in situ* molecular chaperone delivering amph-vaccines to lymph nodes. If this proposed mechanism of action is correct, other albumin-binding moieties might be equally well suited to target peptide vaccines to lymphoid tissues. To test this idea, we prepared cyclized albumin-binding peptides linked via either a PEG_{2000} spacer or a Gly_4Ser spacer to the melanoma gp100 antigen EGP_{20} (ABP-PEG-EGP_{20} and ABP-G4S-EGP_{20}, respectively, Fig. 4.1A).[9] These constructs were prepared as a single unit via automated rapid-flow solid-phase peptide synthesis, cleaved, and purified via reversed-phase high performance liquid chromatography (RP-HPLC). Disulfide formation was then accomplished via incubation in mild basic conditions (0.1 mg/mL in 0.1 M $NaHCO_3$, pH 8.0) at ambient temperature for 48 hours in order to cyclize the ABP component of each construct.

We then evaluated the impact of our albumin binding peptide on vaccine lymph node trafficking. We generated variants of EGP20 and ABP-PEG-EGP20 with tetramethylrhodamine (TAMRA) conjugated at the C-terminus via Cu(I)-catalyzed click chemistry. Mice were injected subcutaneously with TAMRA-labeled EGP_{20} peptide or ABP-PEG-EGP_{20} and lymph nodes were resected 24 hr later for whole tissue fluorescence imaging. We observed that the ABP-conjugated peptide resulted in 13.6-fold and 18.2-fold higher fluorescence in inguinal and axillary lymph nodes, respectively, compared to unmodified EGP_{20} (Fig. 4.1B-C). Our ABP sequence therefore boosts lymph node trafficking of a vaccine antigen, likely via interaction with serum albumin.

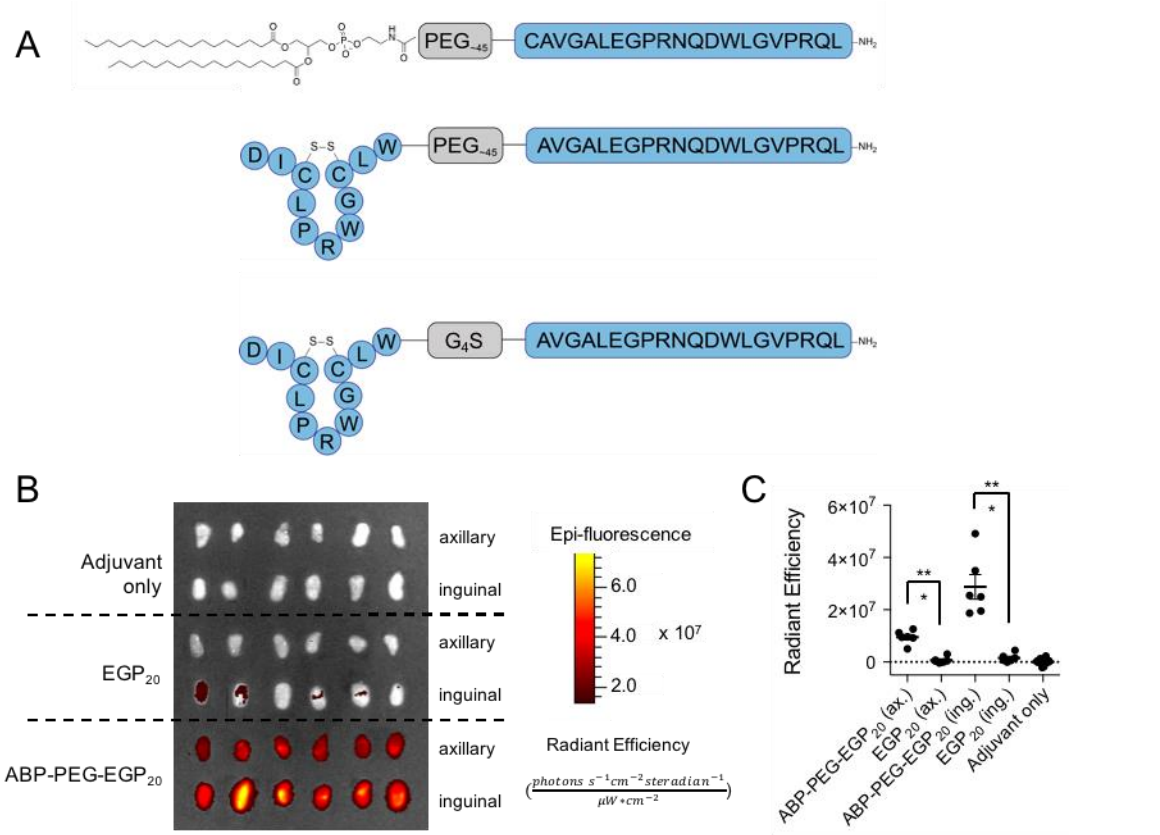

Figure 4.1. Albumin-binding peptide conjugation enhances lymph node targeting of peptide antigens. A) Chemical structures of DSPE conjugated to EGP20 via PEG spacer, cyclized albumin-binding peptide conjugated to EGP20 peptide via PEG spacer, and cyclized albumin-binding peptide conjugated to EGP20 peptide via a Gly_4Ser (G_4S) spacer. **B-C)** 8-week old C57BL6/J female mice were injected s.c. at the tail base with 15nmol TAMRA labeled EGP20 peptide or ABP-PEG-EGP20 and 25µg c-di-GMP adjuvant. Lymph nodes were resected 24h later and imaged using IVIS. **B)** Images of resected nodes; **C)** Quantification of background-subtracted radiant efficiency, (photons*s^{-1}*cm^{-2}*$steradian^{-1}$)/(µW*cm^2), (n = 6, student's t-test, representative of 2 independent experiments). $^{**}P < 0.01$.

After demonstrating the ability of our ABP to facilitate lymph node accumulation, we determined whether this corresponded to more effective T cell priming. Mice were immunized with the indicated antigen or antigen conjugate and cyclic-di-GMP as an adjuvant at Day 0 and Day 14, then antigen-specific T cell priming was determined via tetramer staining on Day 21 (Fig. 4.2A). The response to unmodified peptide was 1.45%, which was not statistically different from background in unimmunized mice, at 0.82%. The ABP-G_4S-EGP construct primed a mean response of 4.56%, or approximately 4-fold higher responses than unmodified peptide. The ABP- PEG_{2000}-EGP construct primed an even more impressive response: 8.58%,

or approximately 6-fold higher than unmodified peptide (Figure 4.2B-C). The addition of an albumin-binding peptide linked through either a G_4S or PEG_{2000} spacer to a peptide antigen showed dramatic enhancement in T cell priming relative to unmodified peptide for a clinically relevant tumor sequence.

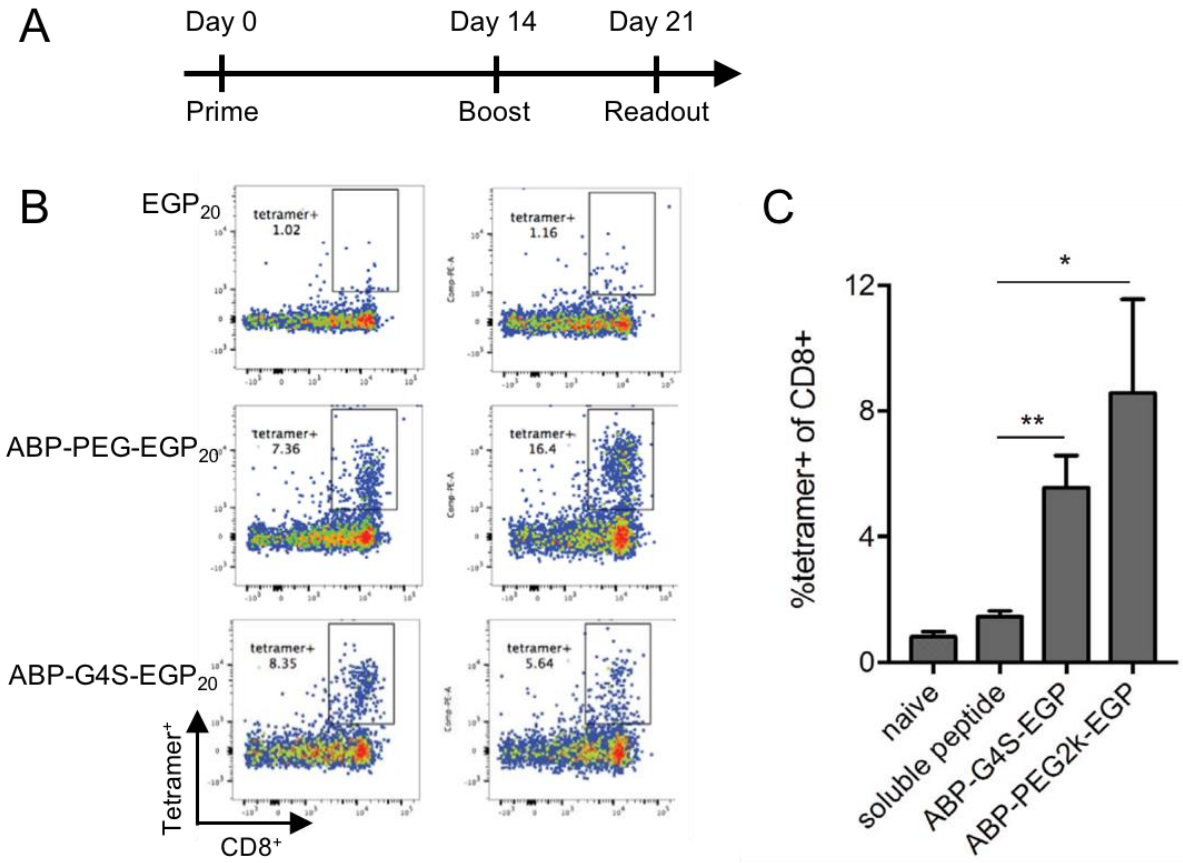

Figure 4.2. Albumin-binding peptides enhance vaccine immunogenicity. A) 8-week old C57BL6/J female mice were primed on day 0 and boosted on day 14 with 5nmol EGP_{20} peptide or EGP_{20}-conjugate as indicated and 25µg c-di-GMP, and tetramer staining was performed on day 21. **B)** Representative flow plots, (gated on live single $CD8_+$ T cells. **C)** Mean tetramer responses quantified as % $tetramer_+$ of $CD8_+$ (n = 5, ANOVA with Bonferroni correction for shown preplanned comparisons of interest, representative of 2 independent experiments). $*P < 0.05$, $**P < 0.01$.

We then explored the design criteria of vaccine constructs containing this ABP by generating variants of the constructs from Figure 4.2 and comparing their *in vivo* immunogenicity. We first assessed variants with the ABP conjugated to either the N- or C-terminus of the antigen sequence, connected by either the PEG or the Gly_4Ser linker (Figure 4.3A). The N-terminal linkage, the original design tested in Figure 4.2, was significantly more

immunogenic than the C-terminal linkage for both linkers (Figure 4.3C). It is possible that this ABP sequence is sensitive to the point of conjugation such that attaching cargo at its N-terminus (i.e., at the C-terminus of the antigen) impairs albumin binding; however, further investigation with different antigen sequences as well as other ABPs would be required to determine whether this is a general trend. We also evaluated whether cyclization of the ABP was required in order to mediate albumin binding, testing a variant of the ABP-G4S-EGP construct in which the cysteines were alkylated by treatment with 2-bromoacetamide (Figure 4.3B). Interestingly, no statistically meaningful difference in immunogenicity was observed between the cyclized and linear variants (Figure 4.3C). This could suggest that albumin-binding is mediated by the primary sequence, without requiring cyclization. However, it would be useful to determine whether trend is consistent for ABP-PEG-EGP, as this linker variant was significantly more immunogenic. It would be interesting to test other ABPs to determine whether cyclization can help mediate albumin binding for other sequences. Altogether, we determined that cyclization may not be required and that the linker placement significantly impacts the immunogenicity of vaccine constructs using this ABP. Modification with an albumin-binding peptide can enhance lymph node targeting and immunogenicity in an approach we anticipate could be versatile for a range of albumin binding peptides and peptide antigens.

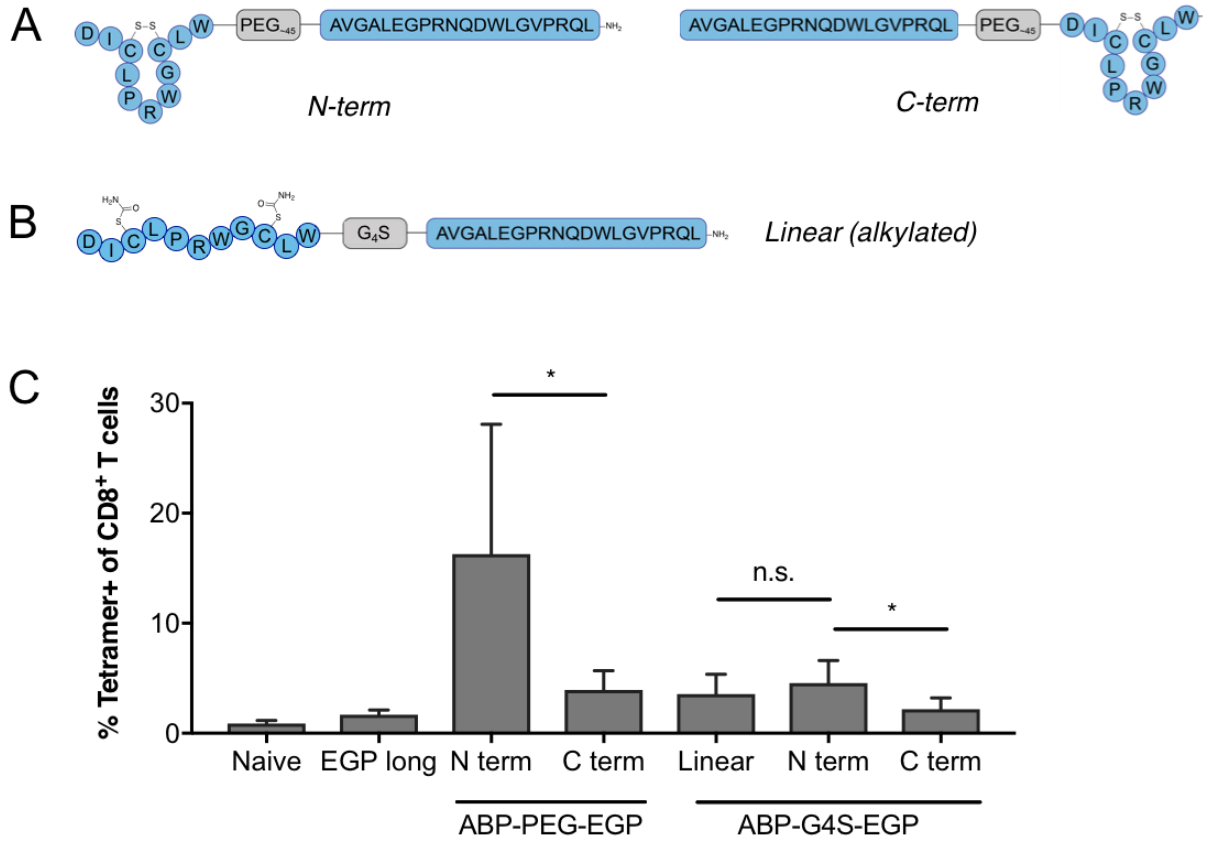

Figure 4.3 Linker placement but not cyclization impacts immunogenicity of ABP-containing vaccine constructs. A) ABPs were linked to a 20-mer vaccine antigen via either ~2000 kDa PEG or Gly_4Ser connecting either the C-terminus of the ABP with the N-terminus of the antigen ('N-term') or the N-terminus of the ABP with the C-terminus of the antigen ('C-term'). **B)** A linear variant of ABP-G4S-EGP was generated by treating the vaccine construct with 2-bromoacetamide to alkylate the ABP cysteines and prevent disulfide formation. **C)** 8-week old C57BL6/J female mice were primed on day 0 and boosted on day 14 with 5nmol of the indicated vaccine antigen construct and 25µg c-di-GMP, and tetramer staining was performed on day 21. Mean tetramer responses were quantified as % $tetramer^+$ of $CD8^+$ ($n = 5$, ANOVA with Bonferroni correction for shown preplanned comparisons of interest). $*P < 0.05$, n.s. not significant.

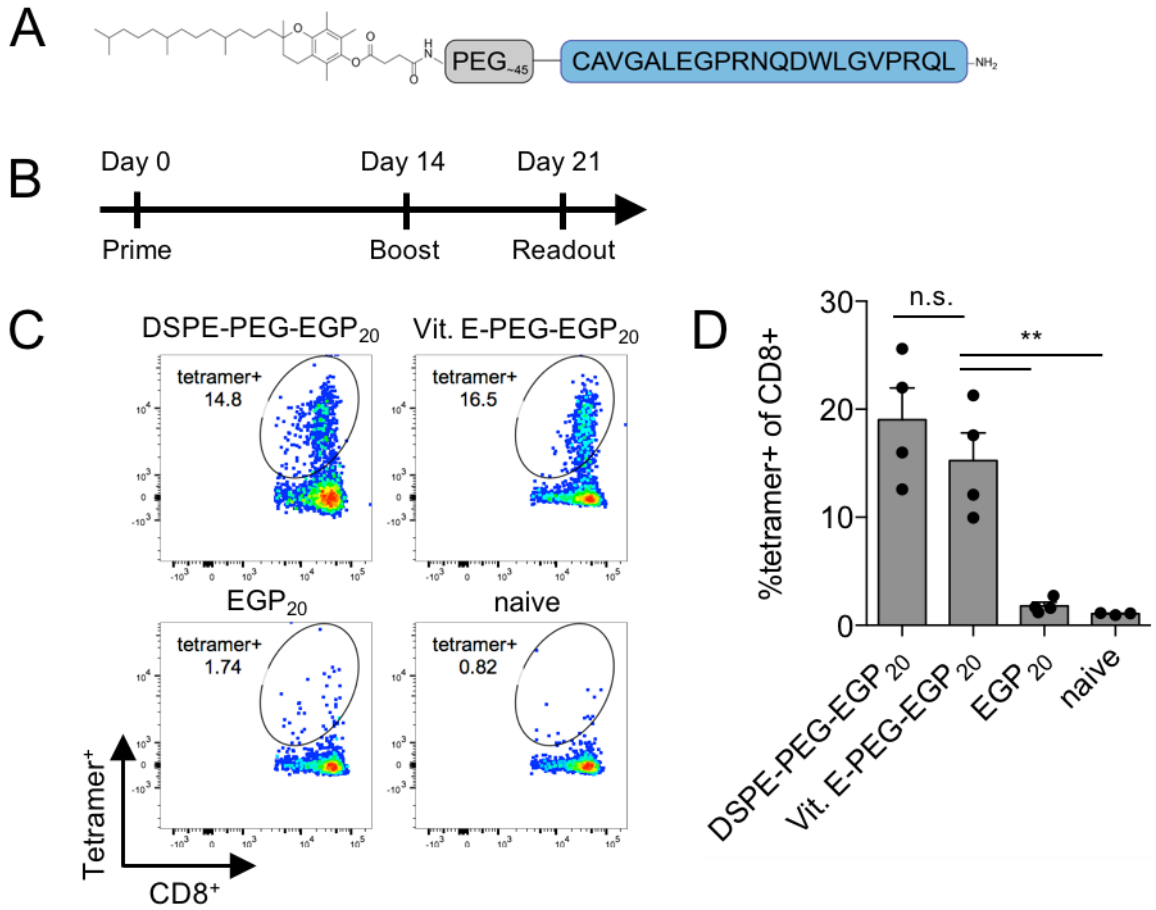

Figure 4.4. Conjugation to α-tocopherol enhances immunogenicity of a vaccine antigen. **A)** gp100 EGP_{20} peptide linked to vitamin E via PEG spacer. **B)** Mice were primed on day 0 and boosted on day 14 with 5 nmol EGP_{20} peptide or EGP_{20}-conjugate as indicated and 25 μg c-di-GMP, and tetramer staining was performed on day 21. **C)** Representative flow plots (gated on live single $CD8^+$ T cells); **D)** mean tetramer responses quantified as % $tetramer^+$ of $CD8^+$ (n = 4, ANOVA with Tukey post-test, representative of 3 independent experiments). n.s. $P \geq 0.05$, $^{**}P < 0.01$.

As a second test of the generality of albumin binding as a mechanism for targeting vaccine antigens to lymph nodes, we evaluated conjugates of the most biologically active form of vitamin E, α-tocopherol, which has been shown to bind to serum albumin with an affinity of $K_D \sim 7$ μM.[10] To see if α-tocopherol enhanced peptide vaccine efficacy, α-tocopherol-PEG-maleimide was conjugated to the gp100 antigen EGP_{20} long via an N-terminal cysteine (Vit. E-PEG-EGP_{20}, Fig. 4.4A). Mice were immunized with the indicated construct on Day 0, boosted on Day 14, and the antigen-specific T cell response was measured on Day 21 via tetramer staining. Mice immunized with Vit. E-PEG-EGP_{20} showed T cell responses approximately 10-

fold higher than unmodified peptides. This response was statistically equivalent the leading lipid albumin binder, DSPE (Fig. 4.4B-D).[6] Conjugation to α-tocopherol therefore improves the immunogenicity of peptide antigens.

4.3 Materials and Methods

4.3.1 Peptide and peptide conjugate synthesis

Peptides were synthesized on a rapid-flow automated peptide synthesizer as described.[12] Fmoc-protected amino acids were purchased from ChemImpex. For the ABP-antigen constructs, following synthesis of the antigen component, the PEG2k linker (Creative PEGworks) was coupled manually onto peptidyl resin containing the antigen peptide; the resin was then transferred back to the synthesizer to complete the construct. Crude peptides were cleaved overnight at room temperature (by volume, 82.5% trifluoroacetic acid, 5% water, 5% thioanisole, 5% phenol, and 2.5% ethane dithiol), triturated with -80 °C diethyl ether, and purified via mass-directed RP-HPLC (mobile phase A: water with 0.1% trifluoroacetic (TFA) acid additive, B: acetonitrile with 0.1% TFA additive with a 5-35% B gradient over 60 minutes). The ABP moieties were cyclized by incubating the purified constructs (0.1 mg/mL) in 0.1 M $NaHCO_3$, pH 8.0 for 24h to facilitate disulfide formation. The cyclized constructs were desalted via solid phase extraction, lyophilized, and analyzed via LC-MS to verify identity, purity, and disulfide formation (Figure 4.5). For the linear ABP-G4S-EGP, alkylation was performed by incubating the isolated peptide in 6 M guanidine-HCl, 0.2 M sodium phosphate, 50 mM 2-bromoacetamide, and 20 mM tris(2-carboxyethyl)phosphine (TCEP)-HCl, pH 7.4 to a final concentration of 1 mM peptide for 1 hour, then quenching with 6 M HCl (final pH 2) and purifying via mass-directed RP-HPLC. Peptide antigen sequences used are as follows: gp100 EGP long, EGP_{20} ($gp100_{20\text{-}39}$): AVGALEGPRNQDWLGVPRQL; Cys-EGP_{20}: CAVGALEGPRNQDWLGVPRQL.[13] The ABP sequence chosen was the minimal core sequence identified in a phage display library of albumin binders: DICLPRWGCLW.[9]

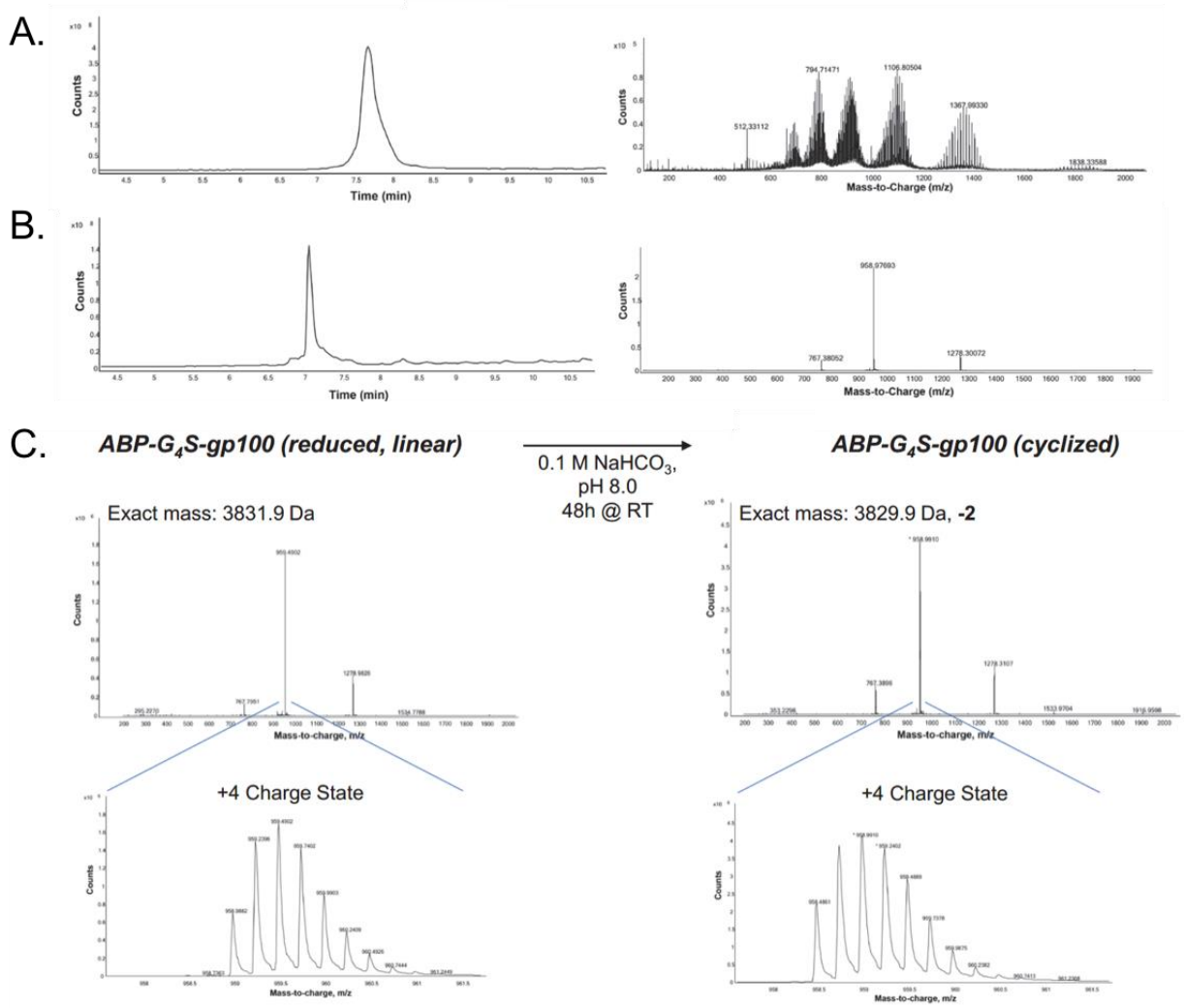

Figure 4.5. ABP vaccine construct characterization. A) Characterization of ABP-PEG-EGP$_{20}$, synthesized as a single unit. Shown are LC-MS chromatogram and corresponding mass spectrum generated via ESI-MS. **B**) Characterization of ABP-G$_4$S-EGP$_{20}$, synthesized as a single unit. Shown are LC-MS chromatogram and corresponding mass spectrum generated via ESI-MS. **C)** confirmation of ABP cyclization via disulfide formation, using ABP-G$_4$S-EGP$_{20}$ construct. Shown are mass spectra of ABP-G$_4$S-EGP$_{20}$ prior to cyclization and after cyclization as indicated in reaction scheme, with +4 charge state enlarged for clarity and calculated exact mass given. Loss of 2 Da upon cyclization corresponds to disulfide formation.

For the labeled constructs, EGP long and ABP-PEG$_{2000}$-EGP were synthesized as described above, incorporating a C-terminal propargylglycine to serve as a chemical 'handle.' Prior to disulfide cyclization, purified EGP long and ABP-PEG$_{2000}$-EGP long peptides were coupled to TAMRA-azide (tetramethylrhodamine, 5-isomer, Lumiprobe) via Cu(I)-catalyzed click chemistry. Briefly, ~0.5 μmol of each peptide was dissolved in 720 μL of 50:50 b.v. solution of *t*-butanol (Sigma) and water. The following reagents were then added (final

concentration in parentheses): TAMRA-azide (500 μM), Tris (pH 8.0, final concentration 50 mM, Roche), ascorbic acid (100 mM, Sigma), TCEP (1 mM, Hampton Research), TBTA (100 μM, Alfa Aeser), and copper sulfate (5 mM, Sigma) to a final volume of 1.00 mL. The reactions were mixed thoroughly and incubated at room temperature for one hour. The reactions were quenched in 20 mL 95:5 water: acetonitrile with 0.1% TFA additive, purified via RP-HPLC as described above, and lyophilized. The TAMRA-labeled constructs were cyclized and desalted as described above.

DSPE-PEG-EGP_{20} or α-tocopherol-PEG-EGP_{20} conjugations were carried out as follows. Equimolar amounts of either DSPE-PEG-maleimide or α-tocopherol-PEG-maleimide (both from Nanocs) and Cys-EGP_{20} (5 mg) were massed into a septum vial and flushed with N_2 for 5 min. Separately, 50 mM phosphate buffer, pH 7.0 with N_2 was also flushed with N_2 for 10 min. Reagents were then dissolved in 5 mL of the degassed phosphate buffer in a septum vial, sonicated briefly to dissolve, and incubated at room temperature for one hour on a nutating mixer. Reactions were then quenched in 20 mL 95:5 water: acetonitrile with 0.1% TFA additive, purified via RP-HPLC as described above, and lyophilized. LC-MS analysis indicated that the desired conjugates were successfully obtained. Reagents were purchased from Sigma unless otherwise noted.

4.3.2 Mice and immunizations

All animal studies were carried out under an institute-approved IACUC protocol following federal, state, and local guidelines for the care and use of animals. C57BL6/J mice were procured from Jackson Laboratory; 6- to 12- week old female mice were used for these studies.

Immunizations comprised of peptides or peptide-conjugates mixed with adjuvant were administered subcutaneously at the base of the tail in 100 μL total, 50 μL on each side, with sterile saline diluent. Peptides and peptide conjugates were dosed at ~ 5 nmol. Adjuvants c-di-GMP (InvivoGen) was dosed at 25 μg. For lymph node trafficking studies using the Spectrum In Vivo Imaging System (IVIS, PerkinElmer), the peptide dose was 15 nmol.

4.3.3 Evaluation of murine immune responses and flow cytometry

Anti-CD8α antibody (53-6.7) was purchased from BioLegend, and anti-CD4 (RM4-5) was purchased from eBioscience. Gp100 tetramer (iTAg Tetramer/PE H-$2D_b$ gp100) was purchased from MBL. Tetramer staining was performed in buffer containing 50 nM dasatinib at room temperature for 30 min, followed by surface staining at 4°C for 15 minutes. Viability

was assessed by LIVE/DEAD Fixable Aqua (Life Technologies) or DAPI. Cells were analyzed using BD LSR Fortessa and BD FACSCanto flow cytometers. Data was analyzed using FlowJo.

4.3.4 Statistical analysis

Statistical methods were not used to determine sample size, but sample numbers were chosen based on estimates from pilot studies and published results such that appropriate statistical tests may yield statistically significant results. Unless otherwise stated, tetramer results were analyzed by using one-way ANOVA with a Tukey post-test using GraphPad Prism software. Where ANOVA was used, variance between groups was found to be similar by Bartlett's test. Where comparisons were predetermined as indicated in figure legends, ANOVA with Bonferroni correction was used. No samples were excluded from analysis.

4.4 Discussion

We have previously shown that conjugation of peptide antigens with diacyl lipids (through a PEG spacer) significantly enhances lymph node accumulation of these vaccine agents following parenteral vaccination, and thereby augments T cell priming.[6] Here we extend those results to show that substitution of the diacyl lipid with α-tocopherol as the albumin-binding moiety similarly enhances both antigen and adjuvant activity. Further, we show that non-lipid modifications, namely fusion of antigens with albumin-binding peptides, also allows for enhancement of lymph node delivery and T cell priming. The former result is particularly striking, given that α-tocopherol has a low affinity for albumin ($K_D \sim 7$ μM).[10] Effective lymphatic delivery even with low affinity binders is likely facilitated by the very high concentrations of albumin in interstitial fluid.[14] Our data suggest that amphiphilic peptides utilizing lipid albumin binding domains, DSPE-PEG-EGP20 and Vit. E-PEG-EGP20, are superior to compositions incorporating an ABP (Fig. 4.2B-C and Fig. 4.4C-D). However, we cannot rule out that further optimization of the affinity of these ABPs for albumin or their linkages to the peptide antigens might further increase activity of ABP-PEG-peptide conjugates[9]. By expanding on previous findings using acyl and diacyl lipids, we demonstrate that directing molecular vaccines to bind albumin may be a general design principle to increase lymph node accumulation and immunogenicity. Further, we provide evidence to support an additional class of biomolecules, albumin binding peptides, that can be further developed as an alternative to currently employed lipid albumin binding moieties.

4.5 Acknowledgements and Conflict Statements

D.J.I is an investigator of the Howard Hughes Medical Institute. We thank the Koch Institute Swanson Biotechnology Center for technical support, specifically the applied therapeutics and whole-animal imaging facility, the histology facility, and the flow cytometry facility. The U.S. Army Research Office, the U.S. Army Medical Research and Materiel Command, and Northwestern University provided funding to develop this core facility and ongoing support is being received from the Soft and Hybrid Nanotechnology Experimental (SHyNE) Resource (NSF ECCS-1542205). K.D.M. is supported by the Fannie & John Hertz Foundation Fellowship, the NSF Graduate Research Fellowships, and the Siebel Scholarship. R.L.H. is supported by an NSF Graduate Research Fellowship. This work was supported in part by the Ragon Institute of MGH, MIT, and Harvard, the Mayo Clinic-Koch Institute Collaboration, the Koch Institute Support (core) grant P30-CA14051 from the National Cancer Institute, the Marble Center for Cancer Nanomedicine, the Bridge Project partnership between the Koch Institute for Integrative Cancer Research and the Dana Farber/Harvard Cancer Center (DF/HCC), the V Foundation, and the NIH (awards EB022433, CA174795, CA206218, and CA172164).

D.J.I. holds equity in Vedantra Pharmaceuticals, which holds a license to the amphiphile–vaccine technology used in these studies.

4.6 References

(1) Melief, C. J. M.; Hall, T. van; Arens, R.; Ossendorp, F.; Burg, S. H. van der. Therapeutic Cancer Vaccines. *J. Clin. Invest.* **2015**, *125* (9), 3401–3412. https://doi.org/10.1172/JCI80009.

(2) Rosenberg, S. A. Decade in Review-Cancer Immunotherapy: Entering the Mainstream of Cancer Treatment https://pubmed.ncbi.nlm.nih.gov/25311350/ (accessed Mar 20, 2020). https://doi.org/10.1038/nrclinonc.2014.174.

(3) Mathur, D.; Prakash, S.; Anand, P.; Kaur, H.; Agrawal, P.; Mehta, A.; Kumar, R.; Singh, S.; Raghava, G. P. S. PEPlife: A Repository of the Half-Life of Peptides. *Sci. Rep.* **2016**, *6*. https://doi.org/10.1038/srep36617.

(4) Fan, Q.; Leuther, K. K.; Holmes, C. P.; Fong, K. I.; J, J.; Velkovska, S.; Chen, M. J.; Mortensen, R. B.; Leu, K.; Green, J. M.; Schatz, P. J.; Woodburn, K. W. Preclinical Evaluation of Hematide, a Novel Erythropoiesis Stimulating Agent, for the Treatment of Anemia https://pubmed.ncbi.nlm.nih.gov/16982323/ (accessed Mar 20, 2020). https://doi.org/10.1016/j.exphem.2006.05.012.

(5) Nguyen, L. T.; Chau, J. K.; Perry, N. A.; de Boer, L.; Zaat, S. A.; Vogel, H. J. Serum Stabilities of Short Tryptophan- And Arginine-Rich Antimicrobial Peptide Analogs https://pubmed.ncbi.nlm.nih.gov/20844765/ (accessed Mar 20, 2020). https://doi.org/10.1371/journal.pone.0012684.

(6) Liu, H.; Moynihan, K. D.; Zheng, Y.; Szeto, G. I.; Li, A. V.; Huang, B.; Van Egeren, D. S.; Park, C.; Irvine, D. J. Structure-based Programming of Lymph-Node Targeting in Molecular Vaccines https://pubmed.ncbi.nlm.nih.gov/24531764/ (accessed Mar 20, 2020). https://doi.org/10.1038/nature12978.
(7) Lindner, V.; Heinle, H. Binding Properties of Circulating Evans Blue in Rabbits as Determined by Disc Electrophoresis. *Atherosclerosis* **1982**, *43* (2–3), 417–422. https://doi.org/10.1016/0021-9150(82)90040-5.
(8) Tsopelas, C.; Sutton, R. Why Certain Dyes Are Useful for Localizing the Sentinel Lymph Node. *J. Nucl. Med.* **2002**, *43* (10), 1377–1382.
(9) Dennis, M. S.; Zhang, M.; Meng, Y. G.; Kadkhodayan, M.; Kirchhofer, D.; Combs, D.; Damico, L. A. Albumin Binding as a General Strategy for Improving the Pharmacokinetics of Proteins. *J. Biol. Chem.* **2002**, *277* (38), 35035–35043. https://doi.org/10.1074/jbc.M205854200.
(10) Fanali, G.; Fasano, M.; Ascenzi, P.; Zingg, J.-M.; Azzi, A. α-Tocopherol Binding to Human Serum Albumin. *BioFactors* **2013**, *39* (3), 294–303. https://doi.org/10.1002/biof.1070.
(11) Li, X.; Chen, D.; Wang, G.; Lu, Y. Study of Interaction between Human Serum Albumin and Three Antioxidants: Ascorbic Acid, α-Tocopherol, and Proanthocyanidins. *Eur. J. Med. Chem.* **2013**, *70*, 22–36. https://doi.org/10.1016/j.ejmech.2013.09.033.
(12) Mijalis, A. J.; Thomas, D. A.; Simon, M. D.; Adamo, A.; Beaumont, R.; Jensen, K. F.; Pentelute, B. L. A Fully Automated Flow-Based Approach for Accelerated Peptide Synthesis. *Nat. Chem. Biol.* **2017**, *13* (5), 464–466. https://doi.org/10.1038/nchembio.2318.
(13) Stipdonk, M. J. B. van; Badia-Martinez, D.; Sluijter, M.; Offringa, R.; Hall, T. van; Achour, A. Design of Agonistic Altered Peptides for the Robust Induction of CTL Directed towards H-2Db in Complex with the Melanoma-Associated Epitope Gp100. *Cancer Res.* **2009**, *69* (19), 7784–7792. https://doi.org/10.1158/0008-5472.CAN-09-1724.
(14) Poulsen, H. L. Interstitial Fluid Concentrations of Albumin and Immunoglobulin G in Normal Men. *Scand. J. Clin. Lab. Invest.* **1974**, *34* (2), 119–122. https://doi.org/10.1080/00365517409050824.

Chapter 5: A direct elution and targeted analysis approach to characterize antigen presentation and design peptide vaccines

The work presented in this chapter was adapted from a manuscript in preparation:

Holden, R.L.; Backlund, C.M.; Quartararo, A.J.; Irvine, D.J.; Pentelute, B.L. A straightforward direct elution and targeted analysis approach to quantify antigen presentation. *In preparation.*

Author contributions:

R.L.H. and B.L.P. designed the study and developed the methodology. R.L.H. synthesized peptides and collected, analyzed, and interpreted data. C.M.B. helped with data interpretation and provided the cd11c+ splenocytes. A.J.Q. contributed to method development. D.J.I. provided input interpreting results. R.L.H. wrote the manuscript in preparation that appears here.

5.1 Introduction

Antigen presentation by the major histocompatibility complex (MHC) is of fundamental importance to the initiation, maintenance, and execution of a T cell response.[1] It is crucial to the anti-cancer immune response, both to prime tumor-specific T cells and to facilitate recognition of tumor cells.[1,2] We are particularly interested in antigen presentation by MHC class I (MHC-I), which presents antigen to $CD8^+$ or cytotoxic T cells. This process must be considered when interrogating the anti-tumor immune response or designing cancer immunotherapies, particularly vaccines.[1–3] While peptide-based vaccines, as well as nucleic acid- and dendritic cell-based platforms, have been demonstrated to prime an anti-tumor T cell response in humans, their immunogenicity is generally low and their therapeutic efficacy is unclear.[3–8] These vaccines require further development to reach their full potential. The ability to reliably and accurately measure antigen presentation could facilitate the development of strategies to improve vaccine design, for example by identifying those that increase the level of presentation. It could also provide fundamental insight into the dynamics of vaccine antigen presentation. Existing methods to measure antigen presentation have proven valuable but are generally limited either in their generalizability or their throughput.[9–13]

Approaches that use reporter T cells or antibodies represent valuable tools to study antigen presentation and develop immunotherapies, but are sharply limited in their generalizability and capacity for absolute quantitation. Reporter T cells require either a transgenic mouse model or an engineered T cell line that expresses T cell receptors against a specific antigen of interest, effectively limiting this approach to a handful of model antigens.[9,12,14] Activation of the antigen-specific T cell population can then be quantified as an indirect metric of antigen presentation. Additionally, absolute quantitation requires a labor-intensive serial T cell dilution technique, generally limiting this approach to relative quantitation.[9,14] Similarly, quantification via antibody staining requires the generation and validation of monoclonal antibodies against unique peptide-MHCs, which prohibits routine screening of diverse antigens.[9,13,16] While this approach directly reports on antigen presentation, rather than a downstream process, it provides relative quantitation. While this is sufficient in many cases, there is a need for broadly applicable techniques that provide direct, absolute quantitation of an antigen(s) of interest.

More recently, direct and generalizable quantification of MHC-bound peptides has been accomplished via mass spectrometry (MS).[9-10,17–22] MS-based quantification of MHC antigens typically involves affinity purification of peptide-MHC complexes from cell lysate, dissociation

and separation of antigen peptides from MHCs, then analysis of these antigen peptides via high sensitivity MS techniques, with MS_2 or MS_3 fragmentation increasing sensitivity and providing high confidence identification.[9,10,20] A number of strategies exist to enable quantitation, but the addition of a sequence-matched isotopically labeled standard peptide for each antigen of interest remains the gold standard for absolute quantitation.[10,17] This approach measures antigen presentation directly and, with an MS readout, generalizing between antigens is a matter of adjusting instrument detector settings or simply tweaking data analysis. It has been used to identify new epitopes, monitor the kinetics of viral antigen presentation, and screen for antigen-specific T cells The main drawback associated with this technique is its sensitivity. This is generally attributed to sample loss occurring during the workup steps, in particular the affinity purification, with one estimate indicating a loss of up to 99% of antigen peptides.[23] It must be noted, however, that others have contradicted this report, asserting that sample loss during the affinity purification workup is minimal.[17] Although they did not directly quantify sample loss, they measured antigen presentation down to the hundreds of attomoles, or 10_5 cells with a copy number of ~730/cell. Nonetheless, studies using this method routinely report using 10_7 cells or more per replicate, or approximately 10-fold higher than each well in a 6-well plate at confluency.[18–22,24] As a result, the throughput of this technique is limited in practice due to its sensitivity, which is likely limited at least in part by sample loss during workup.

A variation of this technique has also been reported that excludes the lysis and affinity purification steps, eluting antigen peptides directly from MHC at the surface of intact cells by incubating with a mild acid buffer.[9,25] This approach has the added advantage of only surveying peptide-MHCs present at the cell surface—rather than those undergoing loading in the ER, for example—providing a more precise and relevant picture of antigen presentation. It has been primarily used for ‘immunopeptidomics’ studies, which sought to characterize the global set of MHC-presented peptides.[25–27] However, it is less commonly used due to several concerns, namely contamination from non-MHC presented peptides and proteins at the cell surface and elution efficiency.[9]

We reasoned that this mild acid elution approach could be developed to quantify the presentation of designated antigen(s) of interest in a straightforward and generalizable manner. Direct elution of MHC peptides from the cell surface using mild acidic incubation might increase sensitivity by avoiding potential sample loss during lysis, affinity purification, and separation of antigen peptides from MHC. We further reasoned that targeted MS analysis of designated antigen(s) of interest could, along with the appropriate untreated controls, sidestep concerns about contamination from non-MHC peptides. A targeted analysis method has the

additional benefit of increasing sensitivity over a full scan for some classes of detectors, including the orbitrap-based instrument used in these experiments. We hypothesized that this technique would increase sensitivity and allow for a higher throughput than is generally reported for methods involving affinity purification while maintaining the advantages of an MS-based approach, namely direct measurement of antigen presentation, absolute quantitation, and generalizability between antigens. Additionally, this approach only measures cell surface peptide-MHCs and is non-destructive, allowing for the possibility of coupling antigen presentation measurements with other types of analysis such as bulk transcriptomics or proteomics.

Here, we develop and validate a straightforward, reproducible, and generalizable method based on mild acid elution and targeted MS analysis to obtain absolute quantitation of MHC-presented peptide antigens. We demonstrate its ability to examine the kinetics and concentration-dependence of vaccine antigen presentation. We then employ this technique to screen two different approaches to enhancing cancer vaccine efficacy: substitution with D-amino acids and conjugation to cell-penetrating peptides.

5.2 Results

We set out to develop a straightforward, sensitive method to quantify antigen presentation. The general workflow for our approach is given in Figure 5.1A. Briefly, cells are treated with an antigen, then washed with phosphate-buffered saline and incubated for 60 seconds with 0.1 M citrate buffer, pH 3.0, to liberate MHC-bound peptides directly from the surface of intact cells. At this point, isotopically labeled standard(s) corresponding to the antigen(s) of interest is added to this MHC eluate. The eluate is then de-salted and concentrated during a single zip-tip cleanup step and analyzed via LC-MS/MS. For these experiments, analysis was performed on an Orbitrap Fusion Lumos using a method that alternated between a targeted selected ion monitoring scan (to analyze the most prominent precursor ion, typically the +2 charge state) and a full MS_2 scan of fragment ions from the targeted precursor. Data are then processed using the Skyline software from the MacCoss lab, which identify and integrate our antigen(s) of interest using both precursor and fragment ions for confident assignment. The antigen of interest can then be quantified via comparison with its corresponding isotopically labeled standard.

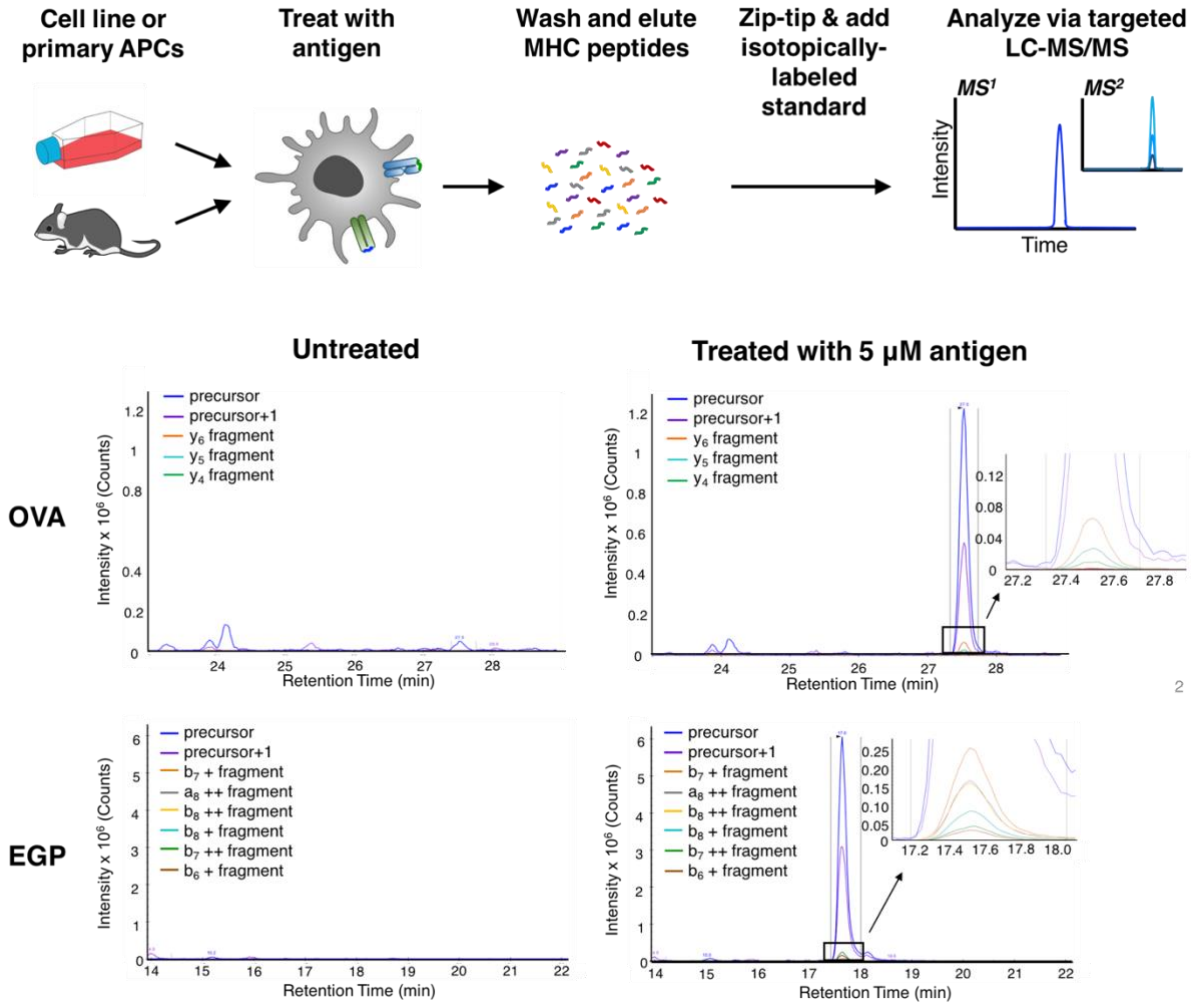

Figure 5.1. Direct elution followed by targeted LC-MS/MS analysis enables detection of MHC-presented antigens. A) Schematic of direct elution and targeted analysis workflow for detecting MHC-bound antigen peptides. Briefly, cells are incubated with a 'long' peptide antigen containing a minimal epitope 'short' sequence, then these MHC-bound epitope peptides are eluted by incubating for 60 seconds with 0.1 M citrate buffer, pH 3.0. An isotopically labeled standard is added for each peptide to be analyzed, and the eluted peptides are concentrated and de-salted using C18 zip-tips. Targeted LC-MS/MS analysis is then performed using an instrument like the Orbitrap Fusion Lumos with attomole sensitivity. **B, C)** The expected short antigen sequence is detectable in MHC eluate from cells treated with the corresponding long antigen, but absent in untreated cells. Data was analyzed using the proteomics software Skyline. Overlaid extracted ion chromatograms for precursor and fragment ions are given for both antigens tested, the ovalbumin antigen SIINFEKL ('OVA,' B) and the gp100 antigen EGPRNQDWL ('EGP', C).

As a proof of concept, DC2.4 cells were treated with 5 μM of the 20-residue 'long' versions of either a model antigen from ovalbumin (OVA) or a murine tumor antigen from the gp100 protein (EGP), or media only, for six hours, then the corresponding minimal epitope or 'short' antigen presented at the cell surface was eluted and analyzed according to the above workflow. Each antigen was readily detected in the corresponding treated condition but absent in the untreated condition (Figure 5.1B). Addition of labeled standards enabled quantification of antigen presentation, both in terms of absolute amount and, considering the seeding density and growth time, the estimated copy number (Figure 5.2A). Under these conditions, 1.4 ± 0.4 fmol of OVA and 25 ± 6 fmol EGP were detected, or around 15,000 or 840 copies per cell, respectively. This experiment was also performed with isolated cd11c+ murine splenocytes to confirm its applicability to different cell types, including primary cells (Figure 5.2B). Several additional parameters were evaluated, including duration of mild acid incubation and the point in the workflow at which standard was added, and ultimately the optimal conditions were determined to be those described above (Section 5.3.7).

We then assessed whether the presentation of exogenous antigen observed using this technique was energy dependent, and thereby dependent on cell uptake. We are interested in measuring the level of presentation of antigen peptides that have been endocytosed, then proteolytically processed and presented, as this is the process that occurs *in vivo* with vaccine antigens. Halting endocytosis by depleting cellular ATP with sodium azide allows us to distinguish antigen presented due to this process from artefactual antigen presentation due to extracellular processing by serum proteases and surface loading of empty MHC molecules. DC2.4 cells were pre-incubated for 1 hour with 10 mM sodium azide and 25 mM 2-deoxy-D-glucose in media at 37 °C, then media was exchanged for treatment media containing 5 μM of the indicated long antigen peptide as well as the previous treatment.[28] After two hours, MHC-presented antigens were eluted and quantified as described above. Treatment with sodium azide significantly reduced but did not entirely ablate presentation of both antigens tested (Figure 5.2C). The antigen observed with sodium azide treatment could indicate extracellular antigen processing and loading, but could also be due in part to incomplete depletion of cellular ATP. These results indicate that the majority of antigen detected using this detection method and treatment with a synthetic peptide stems from internalization, processing, and presentation of the vaccine peptide rather than extracellular loading.

To probe whether the observed antigens are indeed presented by MHC, we assessed presentation of several allele-matched and -mismatched antigens in DC2.4 cells. As this cell

line is derived from bl6 mice, it expresses $H2_b$ MHC alleles. DC2.4 cells were treated either with two matched antigens—EGP, which binds the murine allele H2-D_b, and OVA, which binds H2-K_b—or two mis-matched antigens—one from the HIV-1 protein gp160 ('gp160'), which binds H2-D_d, and one from Influenza A nucleoprotein ('NP'), which binds H2-K_d. Thus, gp160 and NP should be absent in MHC eluate from DC2.4 cells, as they lack the appropriate MHC alleles to bind and present these antigens. After treating with 5 μM of the indicated antigens for six hours, antigens were analyzed as described. Both allele-matched antigens, EGP and OVA, were readily detected in MHC eluate from DC2.4 cells as expected based on previous experiments. However, the level of antigen detected from cells treated with NP was indistinguishable from the untreated control (Figure 5.2D). A minor increase in gp160 was observed for treated cells relative to untreated, but the overall level was low and could be due to a minimal level of presentation by the H2-D_b allele (Figure 5.2D). Overall, this indicates that only allele-matched antigens are efficiently presented, suggesting that antigen detection with this method is MHC-dependent. However, these findings should be confirmed by performing this experiment in an $H2_d$ cell line, to verify that gp160 and NP are detectable in an allele-matched cell line and determine whether OVA and EGP presentation is ablated when the appropriate MHC are absent.

We then assessed the generalizability of our method. We selected several additional murine tumor antigens, including Trp1 from the b16f10 melanoma model and two neoantigens, Reps1 and Adpgk, from the MC-38 adenocarcinoma model. DC2.4 cells were treated with 5 μM of each antigen for 6 hours. Four of the five antigens tested were readily detected and quantified (Figure 5.2E). Note that the antigen that was not observed, Adpgk, appears to not be easily detected by LC-MS. Detection of the synthetic Adpgk standard was challenging even at orders of magnitude higher concentrations. Sequence-specific factors such as poor ionization likely impair its analysis, indicating that some peptide sequences will not be well-suited to this detection method. However, as the majority of short antigen peptides are anticipated to be readily detectable using LC-MS/MS, we determined that our technique is generalizable between antigen sequences. Having demonstrated that this approach is a straightforward and

generalizable technique capable of quantifying MHC-presented antigen directly from the surface of intact cells, we then applied it to measure antigen presentation kinetics and concentration dependence.

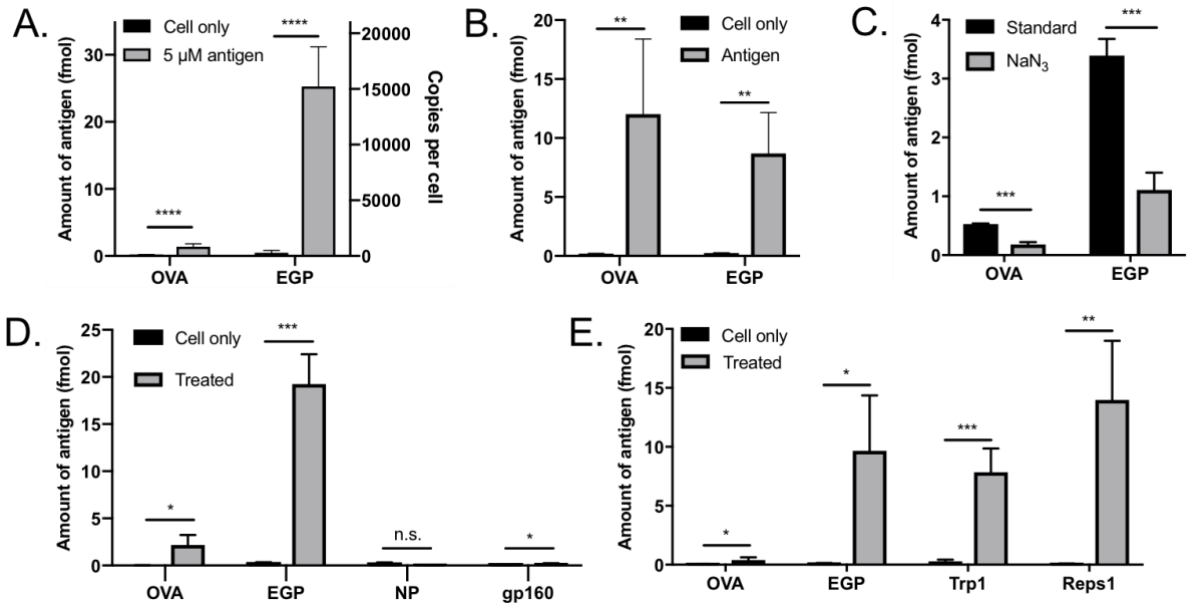

Figure 5.2. Our assay enables quantitation of MHC-presented antigens in a sensitive and generalizable manner. A) Quantification of OVA and EGP antigen presentation by DC2.4 cells after treatment with the corresponding long antigen peptides at 5 μM for 6 hours. Peak areas of the predominant precursor ion for the antigen of interest and corresponding standard were determined using Skyline, and the ratio of the peak areas was used to calculate the absolute amount of antigen present based on the amount of standard added (typically 1 or 10 fmol). Copy number per cell was estimated based on the plating density and growth time. Data from two independent experiments (n = 5-6). **B)** OVA and EGP presentation can also be quantified in primary Cd11c+ murine splenocytes. Cells were isolated from primary splenocytes using a positive cd11c+ isolation kit, then treated and analyzed as in A. Data from two independent experiments (n = 4-6). **C)** DC2.4 cells were pre-treated with 10 mM sodium azide and 25 mM 2-deoxy-D-glucose ('NaN_3) or standard media ('Standard') for 1 hour, then treated with these conditions and 5 μM of the indicated long antigen for 2h. MHC-bound peptides were then eluted and analyzed as in A. Data from a single experiment (n = 3). **D)** DC2.4 cells were treated with 5 μM of two antigens that bind MHC alleles present in this cell line (OVA and EGP) and two that bind MHC alleles absent in this cell line (NP and gp160) for six hours, then MHC-bound peptides were eluted and quantified as in A. Data represent one experiment (n = 3). **E)** DC2.4 cells were treated with 5 μM of the indicated antigen for 6 hours, then MHC-presented peptides were analyzed as in A. Results represent the mean of two independent experiments (n

= 5-6). All results are given with an error of one standard deviation (SD). Statistical significant was calculated using the student's *t*-test; **** denotes $p < 0.0001$, *** $p < 0.001$, ** $p < 0.01$, * $p < 0.05$, n.s. $p \geq 0.05$ (not significant).

Characterizing the kinetics of antigen presentation provides insight into this fundamental process that could help guide vaccine development. While several studies have examined changes in antigen presentation over time *in vitro*, no one has characterized the kinetics of presentation for exogenous peptide antigens such as vaccine antigens. We therefore set out to use the assay we developed to evaluate presentation over time for the model vaccine antigen OVA.

We first evaluated antigen presentation over various treatment times. DC2.4 cells were treated with 5 μM OVA in media continuously for the indicated duration, then MHC-bound peptides were quantified as described above. Combined data from three independent experiments indicate that antigen presentation tends to increase with treatment time, but in a non-linear manner (Figure 5.3A). Note that although these results combine three independent experiments, each time point was not included in each experiment due to constraints related to the instrument time required for each analysis. Each time point in Figure 5.3A combines data from at least two experiments and between three and six technical replicates.

Examining the decay in antigen presentation over time after treatment ended provided further insight into the kinetics of exogenous peptide antigen presentation. We were curious to determine whether presentation drops immediately after ending treatment with the exogenous antigen, or whether there might be a period with consistent or even increasing presentation levels. To test this, we treated DC2.4 cells with 5 μM OVA in media for two hours. The treatment media was then exchanged for fresh media without OVA and incubated for the remaining time indicated. Antigen presentation was measured at two hours (end of treatment) and then at two-hour intervals until eight hours after the beginning of the experiment. The level of OVA presentation appears to decrease as soon as treatment ends and continues to drop steadily with time, as demonstrated in three independent experiments (Figure 5.3B). Performing a linear regression indicated that OVA presentation decreased by 0.13 ± 0.2 fmol per hour, with an R_2 of 0.996 (or 0.808, if calculated using each individual data point rather than the average for each time point).

We then assessed the impact of treatment concentration on presentation by treating DC2.4 cells with the 20-residue OVA antigen at a range of concentrations from 0.5 to 10 μM

for six hours and quantifying MHC-presented peptides as described. The level of OVA presentation correlated linearly with treatment concentration, with an increase of 0.573 ± 0.003 fmol per μM and an R_2 of 0.989 (0.966 when considering each data point individually, Figure 5.3C). It could be interesting to further examine whether antigen presentation plateaus at higher concentrations, and whether these trends vary between different antigen sequences.

We demonstrate that this direct elution and targeted analysis technique can be used to measure the kinetics of antigen presentation and the response to treatment with different concentrations of antigen peptide. Understanding the dynamics of antigen presentation at the cellular level, in particular for extracellular peptide antigens, could provide valuable insight into the development of peptide-based vaccines. However, a more thorough analysis was hindered by challenges with assay throughput, due in part to the analysis time required per sample. Fluctuations in instrument sensitivity also required some experiments to be repeated.

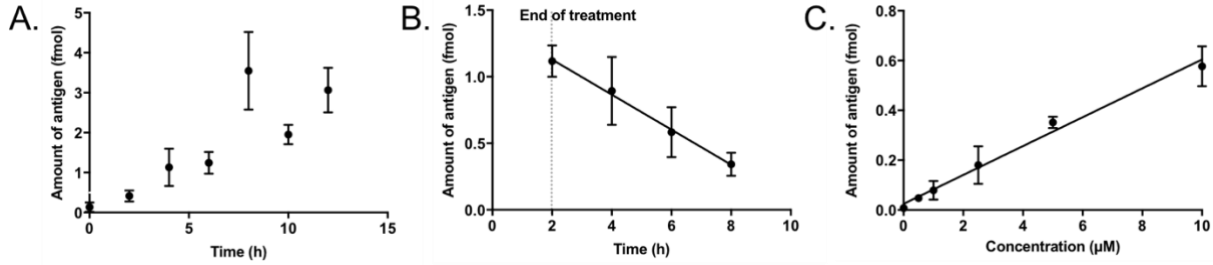

Figure 5.3. This technique enables characterization of various treatment parameters on antigen presentation. A) DC2.4 cells were treated continuously with 5 μM OVA long for the indicated time, then MHC-bound peptides were eluted, de-salted, and quantified. Results from two-three independent experiments per time point (n = 4-6). **B)** DC2.4 cells were treated with 5 μM OVA long for 2 hours, then media was aspirated, cells were washed with warm PBS, and cells were incubated in fresh media (without OVA) for the remainder of the indicated time, after which MHC-bound peptides were then quantified. Results from three independent experiments (n = 3). **C)** DC2.4 cells were treated with the indicated concentration of OVA long for 6 hours, then MHC-bound peptides were quantified. Results from two independent experiments (n = 3-4).

Screening different approaches to improve vaccine design *in vitro* could streamline their development, but this is challenging with existing techniques due to their low throughput and difficulty generalizing beyond a handful of model antigens. We hypothesized that our direct elution and targeted analysis method could at least in part address these shortcomings. We

explore the use of this technique to assess two potential strategies to improve vaccine design: single residue substitution with D-amino acids and conjugation to a cell-penetrating peptide.

D-amino acids (D-AAs) are enantionmers of the native L-amino acids, with opposite chirality around the alpha carbon. They are therefore similar in many key respects to their natural counterparts, but their incorporation into peptides and proteins tends to increase their proteolytic stability, as proteases often fail to recognize and cleave D-AAs. We hypothesized that incorporating a single D-AA substitution into the minimal epitope region of an antigen peptide could help stabilize this crucial sequence to destruction by proteolysis, while minimally impacting MHC binding. We used Trp1, with the minimal epitope sequence TAPDNLGYM, as a starting point. Guided by recent work exploring the impact of single amino acid substitutions on Trp1 immunogenicity, we selected three positions to substitute within the epitope sequence that we suspected would not impact MHC binding—T1, P3, and D4.[29] We began by generating variants of the 20-mer long Trp1 antigen (and the corresponding isotopically labeled short standard, for quantification) with each of these residues substituted for D-alanine, which we hoped would minimally disruptive. We then compared the level of Trp1 antigen presentation for each of these variants—termed T1a, P3a, and D4a—with the original Trp1 sequence (Figure 5.4A). Surprisingly, substituting D-alanine at the T1 or D4 positions dramatically decreased antigen presentation, almost ablating it entirely. The level of MHC-presented antigen after treatment with the P3a and the original sequence were not statistically different. Although D-alanine substitution did not increase presentation, the P3 position appeared to be amenable to substitution.

We then synthesized a Trp1 variant with D-proline substituted at the P3 position (P3p) and a variant with the 'anchor residue' A2 substituted for D-alanine (A2a). We were curious to determine whether P3 would be amenable to substitution with D-proline, in addition to D-alanine. We suspected that, as an anchor residue providing key interactions with the MHC binding pocket, A2 would not be amenable to substitution with the corresponding D-amino acid. However, at three different concentrations tested—0.5, 1.0, and 5.0 μM—there was no statistically significant difference between the level of antigen presented between P3p, A2a, or the original Trp1 sequence (Figure 5.4B). However, it should be noted that the results for each condition came from a single experiment with only 2-3 technical replicates.

While none of the D-AA substitutions studied increased the level of presented antigen relative to the original sequence, the residue P3 and, at least to some extent, the anchor residue A2, demonstrated tolerance to D-AA substitution without a loss in presentation levels. It could be interesting to examine whether these D-AA substitutions impact other aspects of antigen immunogenicity, namely cognate T cell receptor signaling, and to further probe the tolerance of different antigens to D-AA substitution.

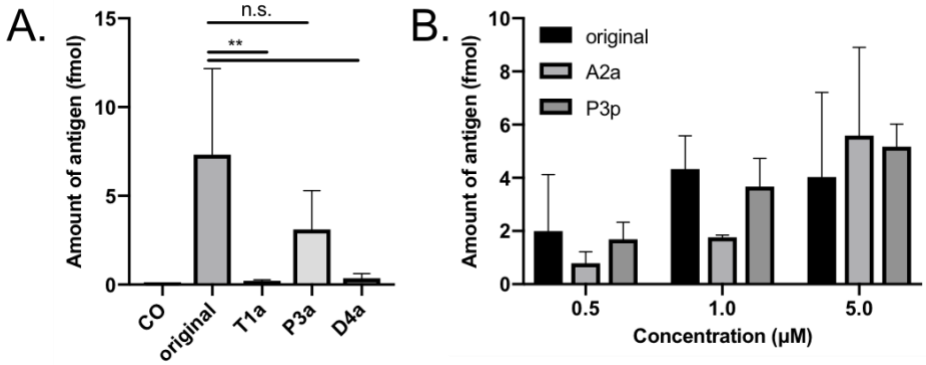

Figure 5.4. Single residue substitutions with a D-amino acid impacted the presentation of a murine tumor antigen in a position-dependent manner. A) DC2.4 cells were treated with 5 μM of the indicated 'long' Trp1 variant for 6 hours, then MHC-bound peptides were eluted and analyzed. Results from three replicate experiments (n = 6-7). Statistical significant was determined using the student's *t*-test; ** denotes $p < 0.01$, n.s. denotes $p \geq 0.05$ (not significant). **B)** DC2.4 cells were treated with the indicated 'long' Trp1 variant at the indicated concentration for 6 hours, then MHC-bound peptides were eluted and analyzed. Each condition includes results from one experiment (n = 2-3). Results are reported with an error of one SD. A one-way ANOVA performed using Tukey's multiple comparisons test indicated that for each concentration, no statistically significant difference existed between the Trp1 variants tested.

Another approach to enhance the efficacy of peptide vaccines is to covalently attach antigens to a cell-penetrating peptide (CPP). CPPs represent a diverse set of sequences that are capable of delivering various cargo into cells via endocytosis and, in some cases, direct translocation across the cell or endosomal membrane. CPPs have been used to successfully enhance the immunogenicity of peptide vaccines. However, the impact of CPP conjugation on the absolute level of antigen presented at the cell surface remains uncharacterized. This knowledge could provide insight into the mechanism by which CPPs enhance vaccine efficacy and potentially guide the design of more effective CPPs.

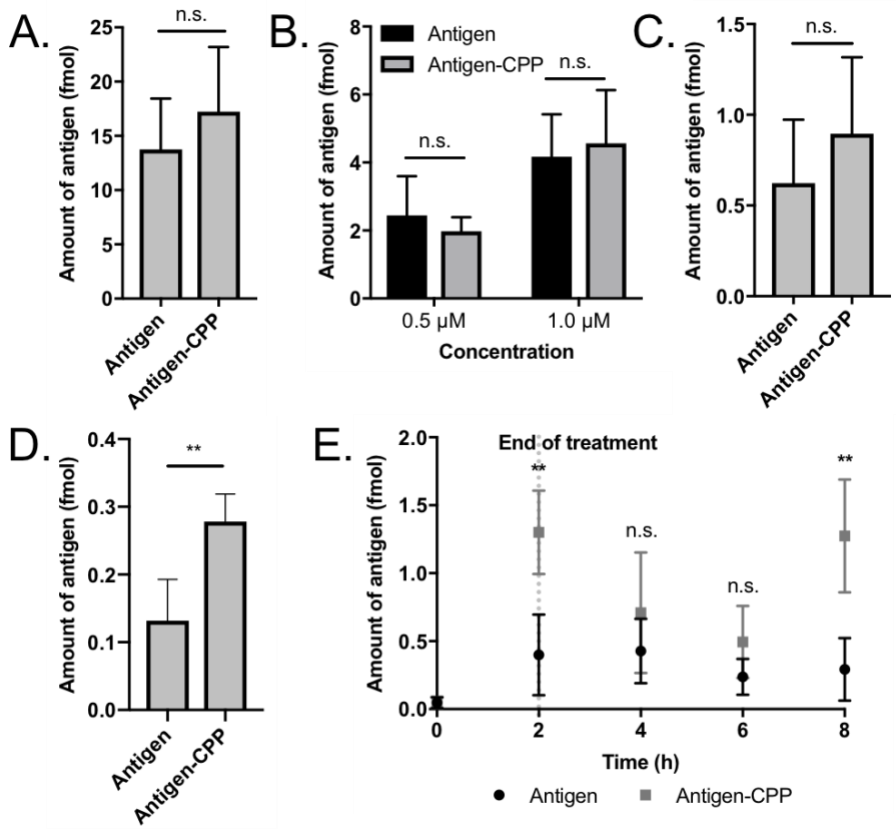

Figure 5.5. Conjugation to a cell-penetrating peptide increased presentation of a murine tumor antigen under certain treatment conditions. A-D) DC2.4 cells were treated with EGP long ('Antigen') or EGP long conjugated to the CPP penetratin ('Antigen-CPP') for 5 μM and 6 hours (**A**), the indicated concentration for 6 hours (**B**), 1 μM for 2 hours (**C**) or 1 μM for 1 hour (**D**). **E)** DC2.4 cells were treated with 0.5 μM Antigen or Antigen-CPP for 2 hours, then the treatment media was aspirated, cells were washed with warm PBS and incubated in fresh media (without the antigen construct) for the remainder of the indicated time, at which point MHC-bound peptides were quantified. Results in A, C-E are from two independent experiments and results in B are from a single experiment. All comparisons were calculated using the student's *t*-test; ** denotes $p < 0.01$ and n.s. denotes $p \geq 0.05$ (not significant).

We compared the absolute level of presentation of the murine melanoma antigen EGP after treating DC2.4 cells with either the 20-mer EGP peptide ("antigen") or the 20-mer EGP peptide conjugated to a model CPP, penetratin ("antigen-CPP") at a range of concentrations and times. We have previously demonstrated that conjugation to penetratin increases this antigen's immunogenicity *in vivo* by approximately 20-fold. Surprisingly, the majority of treatment conditions tested did not yield a difference in the absolute amount of antigen presented by cells treated with either the antigen or the antigen-CPP (Figure 5.5A-C). It was

only with a low concentration and treatment time, 1 μM for 1 hour, that we saw a significant increase in the amount of antigen presented by cells treated with the antigen-CPP (Figure 5.5D). We would expect physiologically-relevant concentrations of vaccine antigens to be low, so it is quite possible that this observed increase in presentation with CPP conjugation is representative of vaccine antigen presentation by dendritic cells *in vivo*. However, these results also suggest that, all else being equal, any gain in antigen presentation achieved with CPP conjugation may be short lived. To further investigate this possibility, we performed a pulse-chase style experiment to study the impact of CPP conjugation on antigen presentation kinetics. After treating with 0.5 μM of either the antigen or antigen-CPP for two hours, the treatment media was exchanged for fresh media without the antigen construct and cells were incubated for the remainder of the indicated time. As expected, cells treated with the antigen-CPP exhibited higher presentation at two hours, but this dropped at four and six hours to the same level as cells treated with the antigen alone (Figure 5.5E). Interestingly, antigen presentation for cells treated with the antigen-CPP increased again at eight hours (six hours after treatment ended). It would be pertinent to confirm these findings and to monitor later time points to better capture the impact of CPP conjugation on antigen presentation kinetics.

5.3 Materials and Methods

5.3.1 Reagents

H-Rink Amide-ChemMatrix and HMPB-ChemMatrix resins were obtained from PCAS BioMatrix Inc. (St-Jean-sur-Richelieu, Quebec, Canada). 1-[Bis(dimethylamino)methylene]-1H-1,2,3-triazolo[4,5-b]pyridinium-3-oxid- hexafluorophosphate (HATU), 4-pentynoic acid and Fmoc-(azido)ornithine-OH were purchased from Chem-Impex International (Wood Dale, IL). Fmoc-L- Arg(Pbf)-OH, Fmoc-L-His(Trt)-OH, Fmoc-L-Lys(Boc)-OH, Fmoc-L-Asp(tBu)-OH, Fmoc-L- Glu(tBu)-OH, Fmoc-L-Ser(tBu)-OH, Fmoc-L-Thr(tBu)-OH, Fmoc-L-Asn(Trt)-OH, Fmoc-L-Gln(Trt)- OH, Fmoc-L-Cys(Trt)-OH, Fmoc-L-Gly-OH, Fmoc-L-Ala-OH, Fmoc-L-Val-OH, Fmoc-L-Leu-OH, Fmoc-L-Ile-OH, Fmoc-L-Met-OH, Fmoc-L-Phe-OH, Fmoc-L-Pro-OH, Fmoc-L-Tyr(tBu)-OH, and Fmoc-L-Trp(Boc)-OH were purchased from EMD Millipore (Burlington, MA). Fmoc-D-Alanine-OH, Fmoc-D-Thr(tBu)-OH, Fmoc-D-Pro-OH, and Fmoc-D-Asp(tBu)-OH were obtained from Advanced Chem Tech. Fmoc-L-Pro-OH ($^{13}C_5$, ^{15}N), Fmoc-L-Phe-OH ($^{13}C_9$, ^{15}N), Fmoc-L-Val-OH (D_8), and Fmoc-L-Ala-OH (2,3,3,3-D_4) were obtained from Cambridge Isotopes. 7-Azabenzotriazol-1-yloxy)trispyrrolidinophosphonium hexafluorophosphate (PyAOP) was purchased from P3

BioSystems (Louisville, KY). Peptide synthesis-grade N,N-dimethylformamide (DMF), CH_2CL_2, diethyl ether, and HPLC-grade acetonitrile were obtained from VWR International (Radnor, PA). RPMI 1640 media with L-glutamine, fetal bovine serum, 10,000 units/mL penicillin/streptomycin, and 0.25% trypsin were obtained from Gibco. 1X PBS was purchased from Corning. DC2.4 cells were a gift from Darrell Irvine at the Koch Institute, MIT. All other reagents were purchased from Sigma-Aldrich (St. Louis, MO). Milli-Q water was used exclusively.

5.3.2 Synthesis

Peptide synthesis was performed in house on a custom-built automated flow synthesizer as previously described. The majority of sequences were produced via automated flow synthesis. However, non-natural amino acids were coupled in batch at room temperature using previously reported conditions. Long peptides (~20-mer antigens) were synthesized on RINK-amide Chemmatrix resin, such that the final product contained a C-terminal amide. Minimal epitope peptides, including isotopically-labeled standards, were synthesized on HMPB Chemmatrix resin such that the final product contained a C-terminal acid.

Peptides were synthesized on a 0.1 mmol scale on an automated flow synthesizer. For each sequence, 100-150 mg of either ChemMatrix Rink Amide resin (0.5 mmol/g loading) or ChemMatrix HMPB resin (0.44 mmol/g loading) was transferred into a fritted syringe and loaded onto a reactor heated to 90 °C. For all couplings, reagents were drawn up, sent through a heating loop at 90 °C, and flowed across the resin at 40 mL/min via HPLC pumps. For each coupling, 10 mL of a solution containing 0.2 M amino acid in DMF, 0.17 M HATU in DMF was mixed with 200 μL diisopropylethylamine (DIEA) and delivered to the reactor. The resin was then washed with 15 mL DMF. To remove the Fmoc protecting group and regenerate the free N-terminus, 10.4 mL of 20% piperidine (v/v) was flowed across the peptidyl resin. The resin was then washed with an additional 15 mL of DMF. These steps were performed iteratively for each amino acid in the sequence until the synthesis was complete. Batch couplings for non-natural (including isotopically-labeled) amino acids were performed by incubating peptidyl resin for 30 minutes at room temperature with 0.2 mmol of the indicated amino acid, 0.98 mmol HATU, and 100 μL DIEA in DMF (3 mL total volume). For capping with 4-pentynoic acid, peptidyl resin was incubated with 1 mmol 4-pentynoic acid, 0.98 mmol HATU, and 500 μL DIEA in DMF (3 mL total volume). After synthesis was complete, peptidyl resins were washed three times with DCM and dried under vacuum.

5.3.3 Cleavage and Deprotection

Peptides were subjected to global deprotection and cleavage from resin by treatment with 5 mL of 94% trifluoroacetic acid (TFA), 2.5% water, 2.5% ethane dithiol, 1% triisopropyl silane (v/v) for two hours at room temperature. For sequences containing an azide, thioanisole was substituted for ethane dithiol. Solutions were then filtered through a fritted syringe to remove resin, triturated in cold diethyl ether, then re-suspended in 50:50 water: acetonitrile containing 0.1% TFA and lyophilized.

5.3.4 Purification

Lyophilized crude peptides were suspended in water containing acetonitrile and 0.1% TFA and filtered through a 0.22 μm syringe filter, then purified via preparative mass-directed reversed-phase high performance liquid chromatography (RP-HPLC) using water with 0.1 % TFA additive as mobile phase A and acetonitrile with 0.1% TFA additive as mobile phase B. For each purification, solvent was flowed at 20 mL/min over an Agilent Zorbax 300SB-C3 column (21.2 x 250 mm, 7 μm) using a linear gradient ramping from either 5 to 35% B or 15 to 45% B over 60 minutes, with fractions collected in 10 mL increments. Fractions were pooled according to data from the instrument's in-line quadrupole mass spectrometer and lyophilized. An aliquot of each purified peptide was each analyzed as described in 5.3.5.

5.3.5 LC-MS Characterization

LC-MS analyses were performed on an Agilent 6520 ESI-QTOF mass spectrometer using an Agilent Zorbax column (300SB C3, 2.1 x 150 mm, 5 μm). The following mobile phases were used: 0.1% formic acid in water (solvent A) and 0.1% formic acid in LC-MS grade acetonitrile (solvent B). The following LC-MS method was used for characterization: 1% B from 0 to 2 min, linear ramp from 1% B to 61% B from 2 to 11 min, 61% B to 99% B from 11 to 12 min and finally 3 min of post-time at 1% B for equilibration, flow rate: 0.8 mL/min. Representative chromatograms and mass spectra are given in section 5.6. All data were processed using the Agilent MassHunter software package. Y-axis in all chromatograms represents total ion current (TIC) unless noted.

5.3.6 Mammalian tissue culture and $CD11c^+$ isolation

DC2.4 cells were maintained in Roswell Park Memorial Institute (RPMI) media with 10 mM HEPES, 10% (v/v) fetal bovine serum (FBS), and 100 units/mL each penicillin/ streptomycin at 37 °C and 5% CO_2. Cells were split at a 1:10 ratio every three days or at 80% confluency.

Primary splenocytes from were obtained from C57BL6/J mice procured from Jackson Laboratory. This was carried out by collaborators in the Irvine Lab at the Koch Institute, MIT, under an institute-approved IACUC protocol following federal, state, and local guidelines for the care and use of animals. Splenocytes were processed to yield a cell suspension and CD11c+ cells were isolated using a positive isolation kit (STEMCELL Technologies), according to the manufacturer's protocol. Isolated $CD11c^+$ splenocytes were plated in a 6-well plate (2.5×10^5 cells/well) and immediately used in the MHC presentation assay described in 5.3.7.

5.3.7 MHC presentation assay

The following protocol was used unless otherwise indicated: 24 hours prior to treatment, DC2.4 cells were plated at a density of 5×10^5/well in a 6-well plate. Media was then exchanged for fresh media containing the indicated long antigen at the indicated concentration in 1 mL media and cells were treated for six hours or the indicated time. After the treatment was complete, media was aspirated and cells were washed in-well with 2 x 1 mL sterile phosphate-buffered saline (PBS) warmed to 37 °C. Cells were then incubated in-well for 60 seconds with 37 °C, sterile-filtered 0.1 M citrate buffer, pH 3.0 to elute MHC-bound peptides. This MHC eluate was then transferred to a 96-well plate (each sample spanning several wells as needed), either 1 or 10 fmol of the corresponding isotopically-labeled standard peptide was added to each sample, and samples were de-salted using C18 ziptips (EMD Millipore). MHC peptides were eluted from zip-tips with 5 μL 50:50 water: acetonitrile 0.1% formic acid (FA) directly into LC-MS vials with glass inserts containing 15 μL water with 0.1 % FA. Samples were mixed briefly by pipetting.

Antigens of interest were then quantified via targeted LC-MS/MS using a Thermo Scientific Orbitrap Fusion Lumos. Mobile phase A was water with 0.1% formic acid and mobile phase B was a 4:1 (v/v) mixture of acetonitrile and water, with 0.1% formic acid as an additive. The following LC Method was used: 2% B from 0 to 2 min, followed by a linear gradient from 2 to 60% B from 2 to 52 min, a linear gradient from 60% B to 95% B from 52 to 55 min and then 4 min of 95% B, flow rate: 300 nL /minc. For MS detection, alternating MS_1 and MS_2 experiments were performed: selected ion monitoring (SIM) scans for the +1 or +2 charge state associated with the peptide of interest and its isotopically labeled standard, with an isolation window of ± 2 m/z; and full scans (350 to 1200 m/z) of the fragment ions obtained from HCD fragmentation (HCD collision energy 25%) of the same species as the SIM scan, isolating these precursors with a window of ± 1.2 m/z. Data was analyzed using the open-source proteomics software Skyline from the MacCoss Lab. Identity of relevant peptides was confirmed by the

presence of corresponding fragment ions and the predominant precursor peak was used for quantification.

We tested several variations of the treatment and workup parameters to identify optimal conditions. First, we compared the signal obtained when the isotopically labeled standard was added to the MHC eluate immediately after elution and prior to zip-tip cleanup and concentration, compared to adding this standard to the concentrated and de-salted sample immediately prior to analysis. Comparing both versions of this workflow for OVA and EGP, the signal was approximately 5x higher when the standard was added at elution, rather than at analysis, and the error between replicates was consistent relative to the value (Figure 5.6A). This was presumably because as any sample loss occurring during the workup should be consistent for both the analyte and the standard. We determined to add the standard immediately after elution.

Incubating cells with mild acidic buffer (0.1 M citrate, pH 3.0) is a reported technique that allowed us to elute MHC-bound peptides directly from the cell surface. However, reported incubation times varied and we did not find a direct comparison. We therefore compared the amount of antigen measured after incubating cells with the citric acid buffer for 30, 60, or 90 seconds in order to determine whether longer elution times could more efficiently elute MHC peptides. No meaningful difference was observed between any of these incubation times for either OVA or EGP (Figure 5.6B). We therefore selected 60 second as the incubation time, as this was the most practical for assay handling. We also compared the level of presentation measured after treating cells with OVA and EGP individually or a pooled treatment with both antigens, observing no difference between these treatment conditions (Figure 5.6C). This was unsurprising, as each antigen is presented by a different MHC allele and the presentation of one antigen should not be affected by the other. We therefore used these conditions interchangeably, treating cells individually or with the pooled antigens as needed.

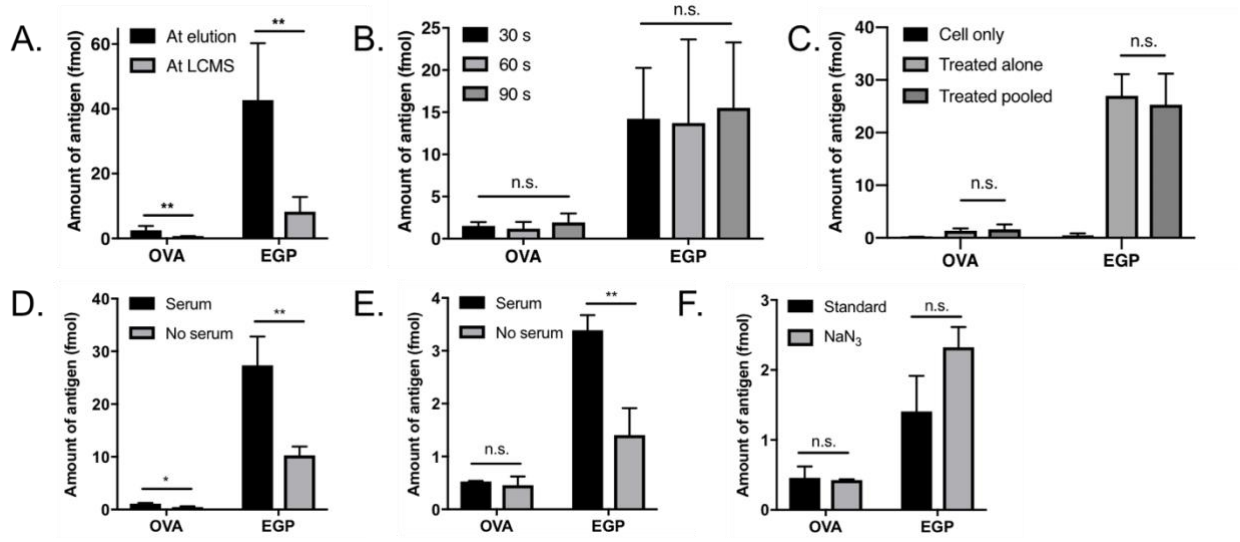

Figure 5.6. Testing treatment and elution conditions. A) DC2.4 cells were treated with EGP long or OVA long at 5 μM for 6 hours, then MHC-bound peptides were eluted and worked up as described. Isotopically labeled standards were added either immediately after elution ("At elution") or after workup and immediately prior to analysis ("At analysis"). **B)** DC2.4 cells were treated with EGP long or OVA long at 5 μM for 6 hours, then MHC-bound peptides were eluted by incubating with 0.1 M citrate, pH 3.0 for 30, 60, or 90 seconds. Eluate was then worked up and analyzed as described. **C)** DC2.4 cells were treated for 6 hours with either 5 μM EGP long alone, 5 μM OVA long alone, or 5 μM each EGP long and OVA long pooled. MHC-bound peptides were then eluted, worked up, and analyzed as described. **D)** DC2.4 cells were treated for 6 hours with 5 μM EGP long and OVA long in media containing 10% fetal bovine serum or in serum-free media, then MHC-bound peptides were eluted, worked up, and analyzed as described. **E)** Same as D, but treatment was 2 hours; F) DC2.4 cells were pre-treated with 10 mM sodium azide and 25 mM 2-deoxy-D-glucose ('NaN_3) or standard, serum-free media ('Standard') for 1 hour, then treated with these conditions and 5 μM of the indicated long antigen for 2h. MHC-bound peptides were then eluted and analyzed as in A. Student's *t*-test was used to determine statistical significance, ** $p < 0.01$, * $p < 0.05$, n.s. $p \geq 0.05$ (not significant).

We the compared presentation levels when the treatment was performed with standard media (10% serum) or serum-free media in an effort to provide further insight beyond the sodium azide treatment into whether extracellular processing by serum proteases might be responsible for some of the measured MHC-bound antigen. After treating with antigen peptides for six hours at 5 μM, significantly more antigen was presented by cells treated with media

containing 10% serum than by cells treated with serum-free media; a similar trend was observed after a two hour treatment for the antigen EGP, while the presence of serum made no difference in the level of OVA antigen presented after a two hour treatment (Figure 5.6D-E). This suggests that some extracellular processing and loading may occur in the presence of serum and that treating in serum-free media could provide a better representation of antigen presentation after uptake and intracellular processing. To confirm this, we compared antigen presentation by cells treated using serum-free media with or without cell energy depletion using sodium azide. While sodium azide treatment significantly diminished antigen presentation by cells treated in serum-containing media (Figure 5.2C), we expected that sodium azide treatment would entirely ablate presentation, which should in this case be entirely dependent on cell uptake. However, there was no meaningful difference after energy depletion (Figure 5.6F). Although the precise cause is unclear, this suggests that the canonical route by which DCs present exogenous antigen—uptake, proteolytic processing, loading on MHC, then presentation at the cell surface—may not occur as expected in the absence of serum. We therefore decided, despite the possibility of some extracellular antigen loading, to perform the antigen treatments in serum-containing media.

5.4 Discussion

Here, we report a straightforward and generalizable technique to directly measure MHC-I-presented antigen(s) of interest. We achieve absolute quantification using isotopically labeled standards and demonstrate that we can detect less than 1 femtomole of an antigen peptide. We further demonstrate that these measurements require energy-dependent processes, including uptake, and appear to be restricted to antigens matching the expressed MHC alleles. Taken together, this suggests that this approach measures MHC-bound antigens that are presented only after internalization and intracellular processing. However, further experiments are needed to confirm this hypothesis and to compare quantitation using this method to established methods, in particular MS-based techniques involving affinity purification.

We applied this technique to monitor the presentation dynamics of an exogenous peptide antigen and to screen two strategies designed to enhance cancer vaccine efficacy. We obtained insight into the kinetics of vaccine antigen presentation at the cellular level, which has not previously been studied, demonstrating that presentation levels rise with continuous treatment in a non-linear manner, and begin to drop immediately after treatment ends. We also observed a linear relationship between treatment concentration and presentation. Turning towards vaccine design, we demonstrated that D-amino acids can be substituted within the minimal

presented epitope sequence without perturbing presentation in a position-dependent manner. We also interrogated the impact of CPP conjugation, a technique previously demonstrated to dramatically enhance efficacy in mouse models, on antigen presentation at the cellular level. We saw that CPP conjugation increased presentation primarily for low concentrations and short treatment times; however, some preliminary evidence suggests that conjugation to a CPP may prolong presentation after exposure has ended. Follow-up experiments are needed to confirm these findings and further articulate the relationship between CPP conjugation and presentation kinetics. We demonstrated that this technique can be used to monitor antigen presentation on a fundamental level and to interrogate the effectiveness of different strategies to improve vaccine design.

However, several limitations were encountered in developing and testing this technique. The throughput was more limited than initially anticipated, due in part to the instrument time required for each targeted analysis. A full scan approach could help address this by allowing analysis of multiple precursor ions in a single run. However, this targeted MS analysis was necessary to achieve sufficient sensitivity. Still, the sensitivity was not as consistently high as expected, with fluctuations in the limit of detection occasionally requiring experiments to be repeated. Other MS methods that have been applied to measure MHC peptides exhibit similar detection and throughput limits.[10] While our approach provides a simple, generalizable technique to measure MHC-presented peptides, the full potential of this and other approaches may not be met until MS instrumentation can permit an order of magnitude or more increase in sensitivity. Nonetheless, this approach enabled us to obtain insight into the presentation dynamics of exogenous peptide antigens and screen several approaches to vaccine design. Our direct elution and targeted analysis approach provides a straightforward, generalizable, and non-destructive method to measure antigen presentation, but does not fully address the limitations of existing techniques.

5.5 References

(1) Abbas, A.; Lichtman, A.; Pillai, S. *Cellular and Molecular Immunology*, 9th ed.; Elsevier, 2017.

(2) Janeway, C. A.; Travers, P.; Walport, M.; Shlomchik, M. J. *Immunobiology: The Immune System in Health and Disease*, 5th ed.; Garland Science: New York, 2001.

(3) Sahin, U.; Türeci, Ö. Personalized Vaccines for Cancer Immunotherapy. *Science* **2018**, *359* (6382), 1355–1360. https://doi.org/10.1126/science.aar7112.

(4) Carreno, B. M.; Magrini, V.; Becker-Hapak, M.; Kaabinejadian, S.; Hundal, J.; Petti, A. A.; Ly, A.; Lie, W.-R.; Hildebrand, W. H.; Mardis, E. R.; Linette, G. P. A Dendritic Cell

Vaccine Increases the Breadth and Diversity of Melanoma Neoantigen-Specific T Cells. *Science* **2015**, *348* (6236), 803–808. https://doi.org/10.1126/science.aaa3828.
(5) Calmeiro, J.; Carrascal, M. A.; Tavares, A. R.; Ferreira, D. A.; Gomes, C.; Falcão, A.; Cruz, M. T.; Neves, B. M. Dendritic Cell Vaccines for Cancer Immunotherapy: The Role of Human Conventional Type 1 Dendritic Cells. *Pharmaceutics* **2020**, *12* (2). https://doi.org/10.3390/pharmaceutics12020158.
(6) Ott, P. A.; Hu, Z.; Keskin, D. B.; Shukla, S. A.; Sun, J.; Bozym, D. J.; Zhang, W.; Luoma, A.; Giobbie-Hurder, A.; Peter, L.; Chen, C.; Olive, O.; Carter, T. A.; Li, S.; Lieb, D. J.; Eisenhaure, T.; Gjini, E.; Stevens, J.; Lane, W. J.; Javeri, I.; Nellaiappan, K.; Salazar, A. M.; Daley, H.; Seaman, M.; Buchbinder, E. I.; Yoon, C. H.; Harden, M.; Lennon, N.; Gabriel, S.; Rodig, S. J.; Barouch, D. H.; Aster, J. C.; Getz, G.; Wucherpfennig, K.; Neuberg, D.; Ritz, J.; Lander, E. S.; Fritsch, E. F.; Hacohen, N.; Wu, C. J. An Immunogenic Personal Neoantigen Vaccine for Patients with Melanoma. *Nature* **2017**, *547* (7662), 217–221. https://doi.org/10.1038/nature22991.
(7) Sahin, U.; Derhovanessian, E.; Miller, M.; Kloke, B.-P.; Simon, P.; Löwer, M.; Bukur, V.; Tadmor, A. D.; Luxemburger, U.; Schrörs, B.; Omokoko, T.; Vormehr, M.; Albrecht, C.; Paruzynski, A.; Kuhn, A. N.; Buck, J.; Heesch, S.; Schreeb, K. H.; Müller, F.; Ortseifer, I.; Vogler, I.; Godehardt, E.; Attig, S.; Rae, R.; Breitkreuz, A.; Tolliver, C.; Suchan, M.; Martic, G.; Hohberger, A.; Sorn, P.; Diekmann, J.; Ciesla, J.; Waksmann, O.; Brück, A.-K.; Witt, M.; Zillgen, M.; Rothermel, A.; Kasemann, B.; Langer, D.; Bolte, S.; Diken, M.; Kreiter, S.; Nemecek, R.; Gebhardt, C.; Grabbe, S.; Höller, C.; Utikal, J.; Huber, C.; Loquai, C.; Türeci, Ö. Personalized RNA Mutanome Vaccines Mobilize Poly-Specific Therapeutic Immunity against Cancer. *Nature* **2017**, *547* (7662), 222–226. https://doi.org/10.1038/nature23003.
(8) Ma, M.; Liu, J.; Jin, S.; Wang, L. Development of Tumour Peptide Vaccines: From Universalization to Personalization. *Scandinavian Journal of Immunology n/a* (n/a), e12875. https://doi.org/10.1111/sji.12875.
(9) Croft, N. P.; Purcell, A. W.; Tscharke, D. C. Quantifying Epitope Presentation Using Mass Spectrometry. *Mol. Immunol.* **2015**, *68* (2 Pt A), 77–80. https://doi.org/10.1016/j.molimm.2015.06.010.
(10) Reinhold, B.; Keskin, D. B.; Reinherz, E. L. Molecular Detection of Targeted Major Histocompatibility Complex I-Bound Peptides Using a Probabilistic Measure and Nanospray MS3 on a Hybrid Quadrupole-Linear Ion Trap. *Anal. Chem.* **2010**, *82* (21), 9090–9099. https://doi.org/10.1021/ac102387t.
(11) Dolan, B. P. Quantitating MHC Class I Ligand Production and Presentation Using TCR-Like Antibodies. In *Antigen Processing: Methods and Protocols*; van Endert, P., Ed.; Methods in Molecular Biology™; Humana Press: Totowa, NJ, 2013; pp 169–177. https://doi.org/10.1007/978-1-62703-218-6_14.
(12) Antón, L. C.; Yewdell, J. W.; Bennink, J. R. MHC Class I-Associated Peptides Produced from Endogenous Gene Products with Vastly Different Efficiencies. *Journal of Immunology* **1997**, *158* (6), 2535–2542.
(13) Porgador, A.; Yewdell, J. W.; Deng, Y.; Bennink, J. R.; Germain, R. N. Localization, Quantitation, and In Situ Detection of Specific Peptide–MHC Class I Complexes Using a Monoclonal Antibody. *Immunity* **1997**, *6* (6), 715–726. https://doi.org/10.1016/S1074-7613(00)80447-1.
(14) Chen, W.; Antón, L. C.; Bennink, J. R.; Yewdell, J. W. Dissecting the Multifactorial Causes of Immunodominance in Class I–Restricted T Cell Responses to Viruses. *Immunity* **2000**, *12* (1), 83–93. https://doi.org/10.1016/S1074-7613(00)80161-2.

(15) Smith, K. B.; Ellis, S. A. Standardisation of a Procedure for Quantifying Surface Antigens by Indirect Immunofluorescence. *Journal of Immunological Methods* **1999**, *228* (1), 29–36. https://doi.org/10.1016/S0022-1759(99)00087-3.
(16) Princiotta, M. F.; Finzi, D.; Qian, S.-B.; Gibbs, J.; Schuchmann, S.; Buttgereit, F.; Bennink, J. R.; Yewdell, J. W. Quantitating Protein Synthesis, Degradation, and Endogenous Antigen Processing. *Immunity* **2003**, *18* (3), 343–354. https://doi.org/10.1016/S1074-7613(03)00051-7.
(17) Tan, C. T.; Croft, N. P.; Dudek, N. L.; Williamson, N. A.; Purcell, A. W. Direct Quantitation of MHC-Bound Peptide Epitopes by Selected Reaction Monitoring. *Proteomics* **2011**, *11* (11), 2336–2340. https://doi.org/10.1002/pmic.201000531.
(18) Testa, J. S.; Shetty, V.; Hafner, J.; Nickens, Z.; Kamal, S.; Sinnathamby, G.; Philip, R. MHC Class I-Presented T Cell Epitopes Identified by Immunoproteomics Analysis Are Targets for a Cross Reactive Influenza-Specific T Cell Response. *PLoS ONE* **2012**, *7* (11), e48484. https://doi.org/10.1371/journal.pone.0048484.
(19) Croft, N. P.; Smith, S. A.; Wong, Y. C.; Tan, C. T.; Dudek, N. L.; Flesch, I. E. A.; Lin, L. C. W.; Tscharke, D. C.; Purcell, A. W. Kinetics of Antigen Expression and Epitope Presentation during Virus Infection. *PLOS Pathogens* **2013**, *9* (1), e1003129. https://doi.org/10.1371/journal.ppat.1003129.
(20) Reinherz, E. L.; Keskin, D. B.; Reinhold, B. Forward Vaccinology: CTL Targeting Based upon Physical Detection of HLA-Bound Peptides. *Front. Immunol.* **2014**, *5*. https://doi.org/10.3389/fimmu.2014.00418.
(21) Keskin, D. B.; Reinhold, B. B.; Zhang, G. L.; Ivanov, A. R.; Karger, B. L.; Reinherz, E. L. Physical Detection of Influenza A Epitopes Identifies a Stealth Subset on Human Lung Epithelium Evading Natural CD8 Immunity. *Proc. Natl. Acad. Sci. U.S.A.* **2015**, *112* (7), 2151–2156. https://doi.org/10.1073/pnas.1423482112.
(22) Ternette, N.; Block, P. D.; Sánchez-Bernabéu, Á.; Borthwick, N.; Pappalardo, E.; Abdul-Jawad, S.; Ondondo, B.; Charles, P. D.; Dorrell, L.; Kessler, B. M.; Hanke, T. Early Kinetics of the HLA Class I-Associated Peptidome of MVA.HIVconsv-Infected Cells. *J. Virol.* **2015**, *89* (11), 5760–5771. https://doi.org/10.1128/JVI.03627-14.
(23) Hassan, C.; Kester, M. G. D.; Oudgenoeg, G.; de Ru, A. H.; Janssen, G. M. C.; Drijfhout, J. W.; Spaapen, R. M.; Jiménez, C. R.; Heemskerk, M. H. M.; Falkenburg, J. H. F.; van Veelen, P. A. Accurate Quantitation of MHC-Bound Peptides by Application of Isotopically Labeled Peptide MHC Complexes. *Journal of Proteomics* **2014**, *109*, 240–244. https://doi.org/10.1016/j.jprot.2014.07.009.
(24) Useful Numbers for Cell Culture - US https://www.thermofisher.com/us/en/home/references/gibco-cell-culture-basics/cell-culture-protocols/cell-culture-useful-numbers.html (accessed Jun 1, 2020).
(25) Storkus, W. J.; Zeh, H. J., III; Salter, R. D.; Lotze, M. T. Identification of T-Cell Epitopes: Rapid Isolation of Class i-Presented Peptides from Viable Cells by Mild Acid Elution. *Journal of Immunotherapy* **1993**, *14* (2), 94–103. https://doi.org/10.1097/00002371-199308000-00003.
(26) Herr, W.; Ranieri, E.; Gambotto, A.; Kierstead, L. S.; Amoscato, A. A.; Gesualdo, L.; Storkus, W. J. Identification of Naturally Processed and HLA-Presented Epstein-Barr Virus Peptides Recognized by CD4+ or CD8+ T Lymphocytes from Human Blood. *Proceedings of the National Academy of Sciences of the United States of America* **1999**, *96* (21), 12033–12038. https://doi.org/10.1073/pnas.96.21.12033.
(27) Fortier, M.-H.; Caron, É.; Hardy, M.-P.; Voisin, G.; Lemieux, S.; Perreault, C.; Thibault, P. The MHC Class I Peptide Repertoire Is Molded by the Transcriptome. *Journal of Experimental Medicine* **2008**, *205* (3), 595–610. https://doi.org/10.1084/jem.20071985.

(28) Hällbrink, M.; Oehlke, J.; Papsdorf, G.; Bienert, M. Uptake of Cell-Penetrating Peptides Is Dependent on Peptide-to-Cell Ratio Rather than on Peptide Concentration. *Biochimica et Biophysica Acta (BBA) - Biomembranes* **2004**, *1667* (2), 222–228. https://doi.org/10.1016/j.bbamem.2004.10.009.
(29) Clancy-Thompson, E.; Devlin, C. A.; Tyler, P. M.; Servos, M. M.; Ali, L. R.; Ventre, K. S.; Bhuiyan, M. A.; Bruck, P. T.; Birnbaum, M. E.; Dougan, S. K. Altered Binding of Tumor Antigenic Peptides to MHC Class I Affects CD8+ T Cell-Effector Responses. *Cancer Immunol Res* **2018**, *6* (12), 1524–1536. https://doi.org/10.1158/2326-6066.CIR-18-0348.

5.6 Appendix

OVA long
Mass expected: 2322.17 Da
Mass observed: 2322.21 Da

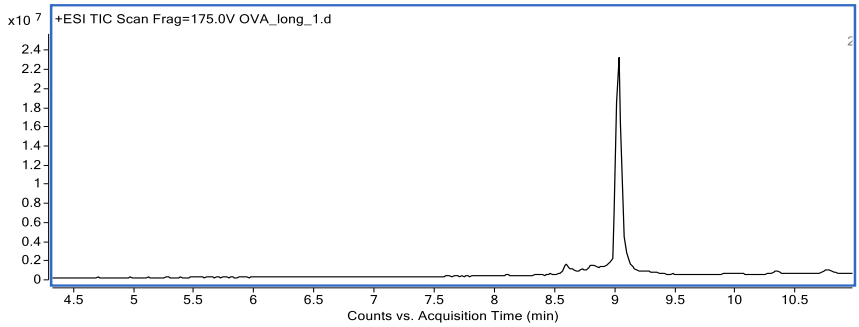

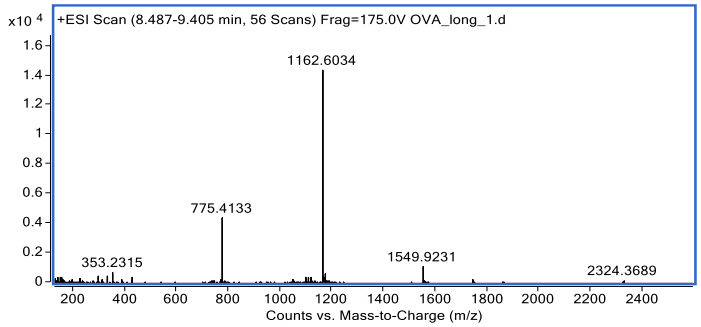

heavy-OVA short

Mass expected: 972.57 Da
Mass observed: 972.57 Da

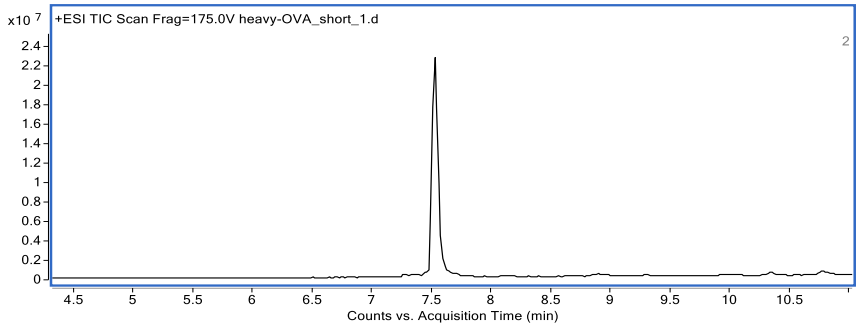

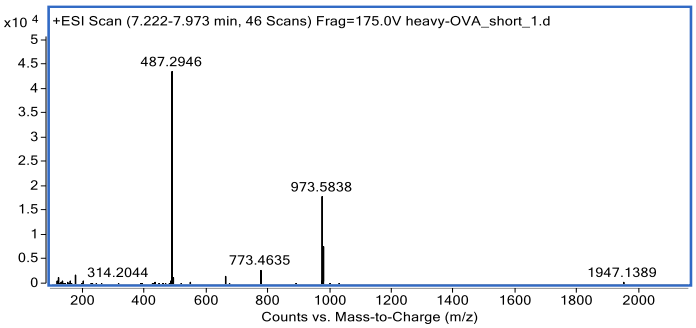

EGP long
Mass expected: 2174.17 Da
Mass observed: 2174.19 Da

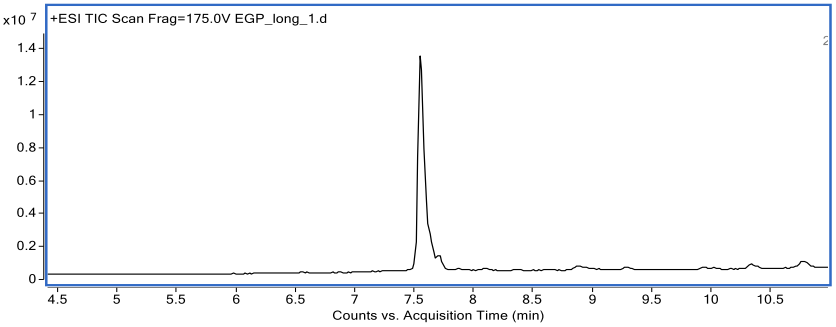

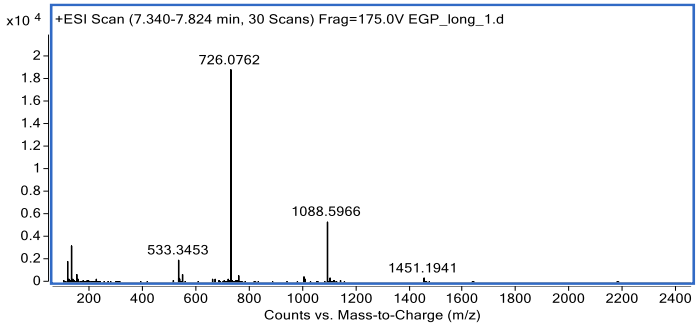

heavy-EGP short
Mass expected: 1119.53 Da
Mass observed: 1119.53 Da

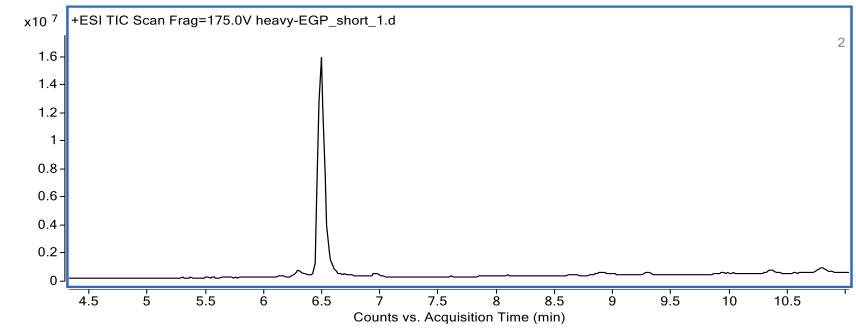

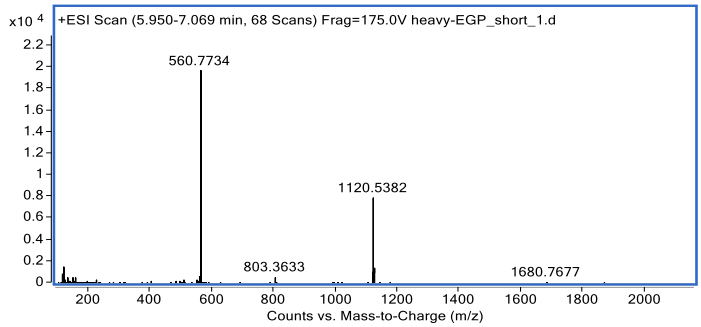

EGP-penetratin
Mass expected: 4383.48 Da
Mass observed: 4383.86 Da

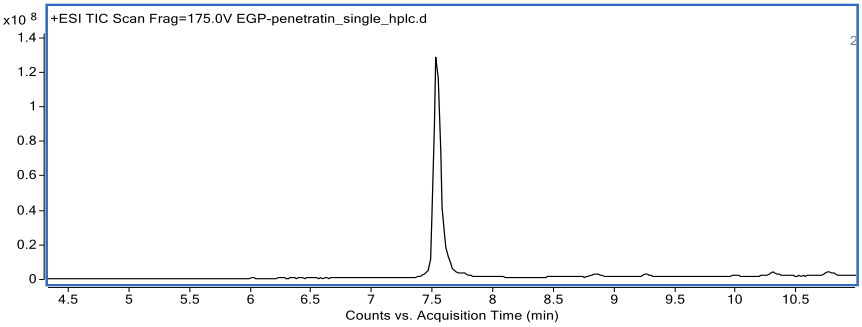

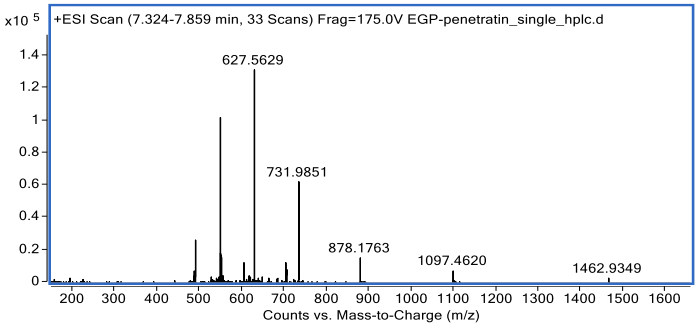

NP long

Mass expected: 2290.16 Da

Mass observed: 2290.49 Da

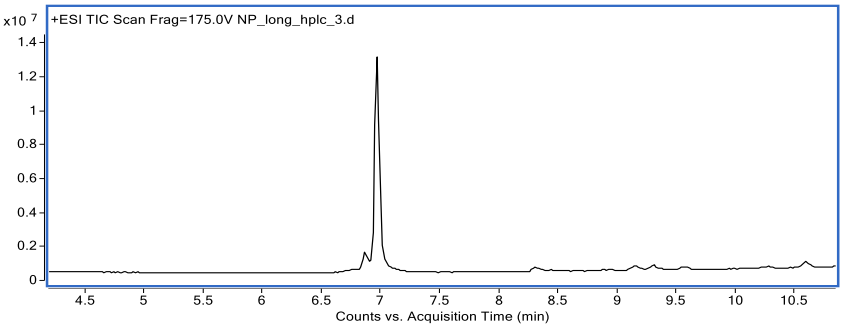

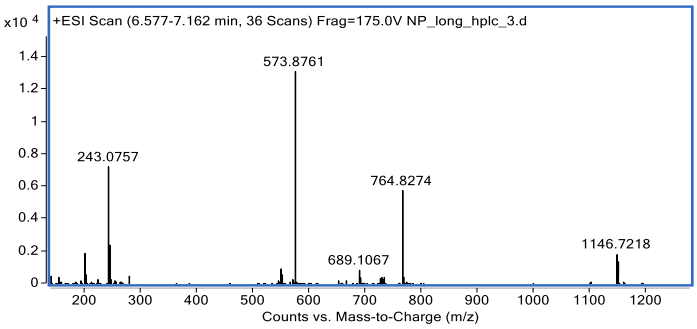

heavy-NP short

Mass expected: 1110.64 Da

Mass observed: 1110.74 Da

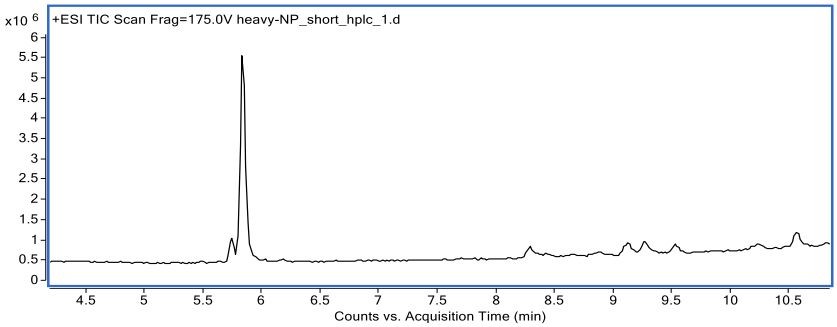

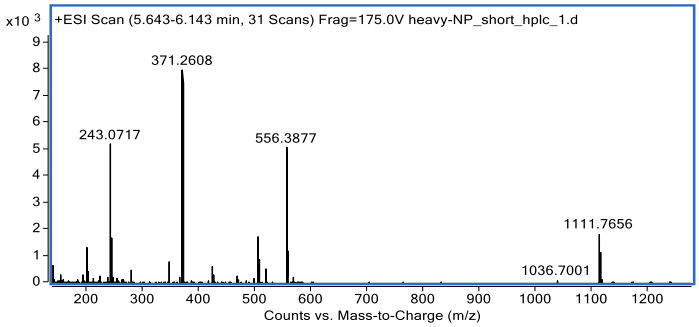

gp160 long
Mass expected: 2207.32 Da
Mass observed: 2207.65 Da

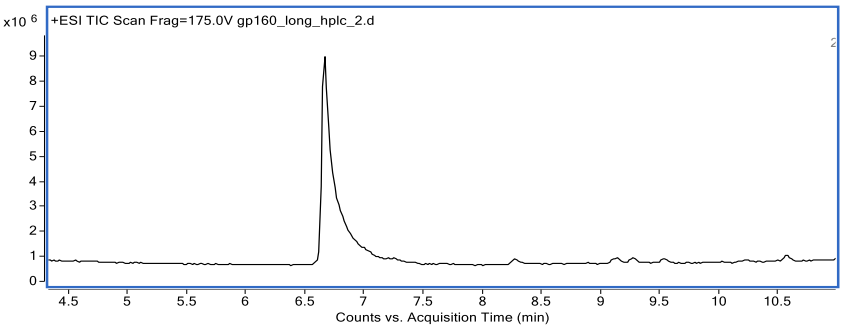

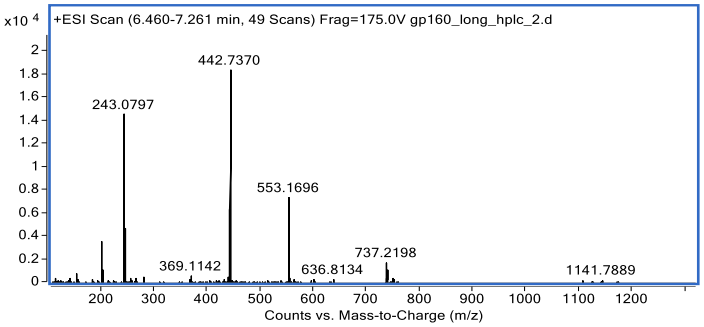

heavy-gp160 short
Mass expected: 1078.63 Da
Mass observed: 1078.75 Da

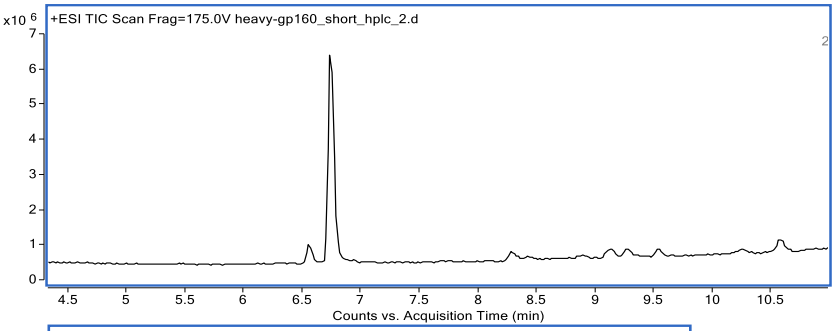

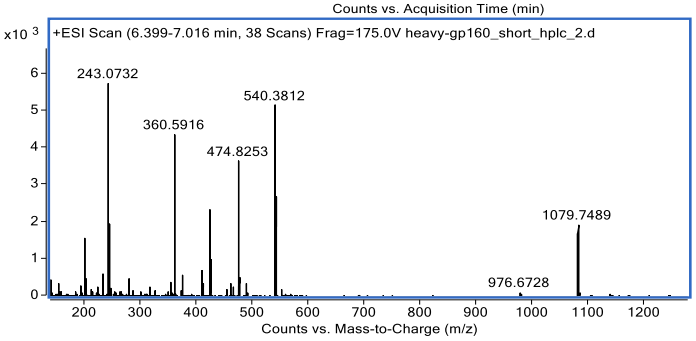

Reps1 long
Mass expected: 2284.26 Da
Mass observed: 2284.27 Da

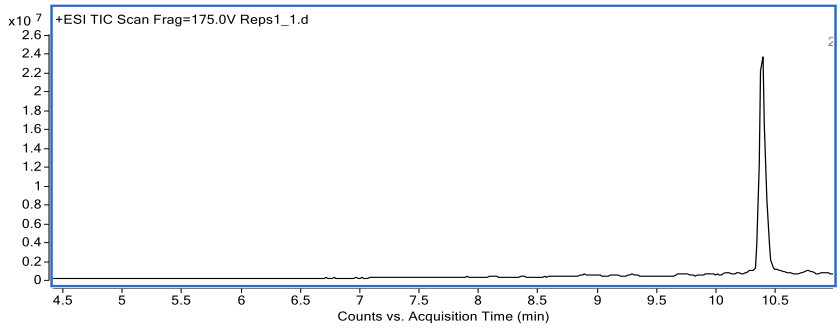

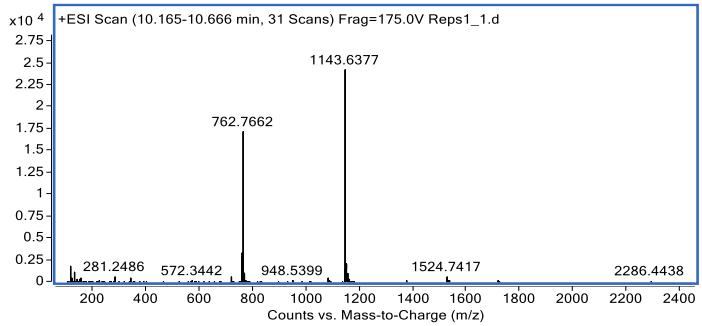

heavy-Reps1 short
Mass expected: 949.57 Da
Mass observed: 949.58 Da

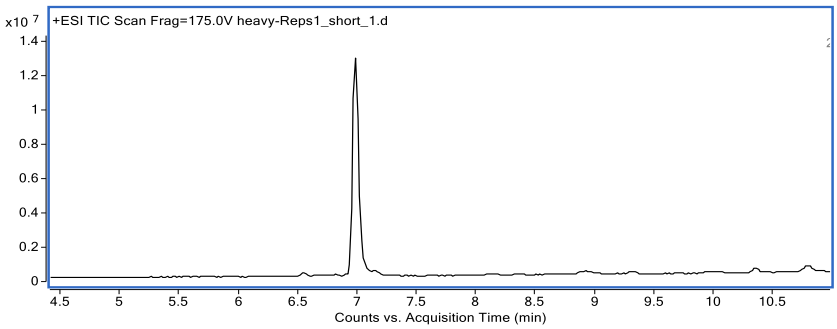

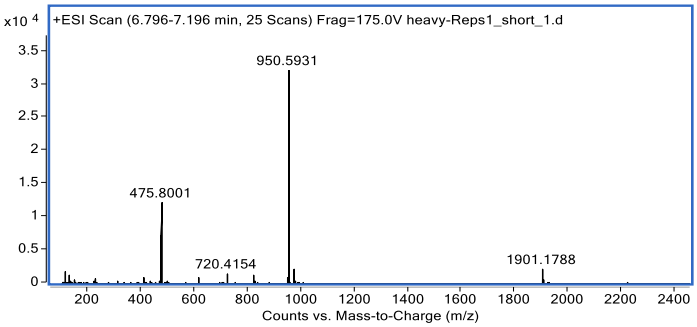

Trp1 long
Mass expected: 2389.07 Da
Mass observed: 2389.08 Da

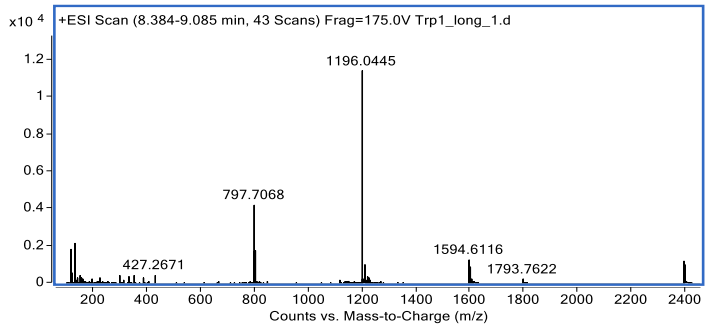

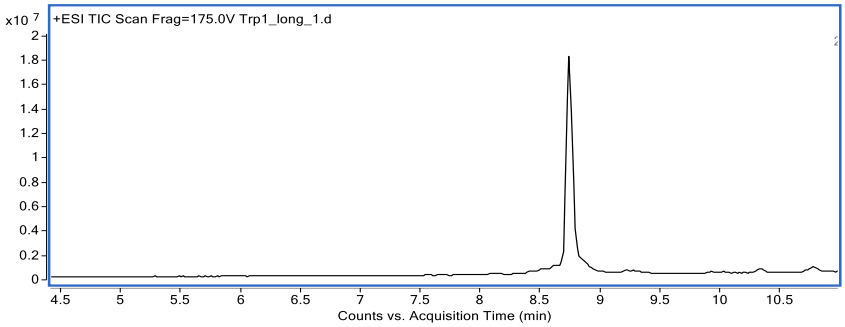

heavy-Trp1 short
Mass expected: 984.45 Da
Mass observed: 984.52 Da

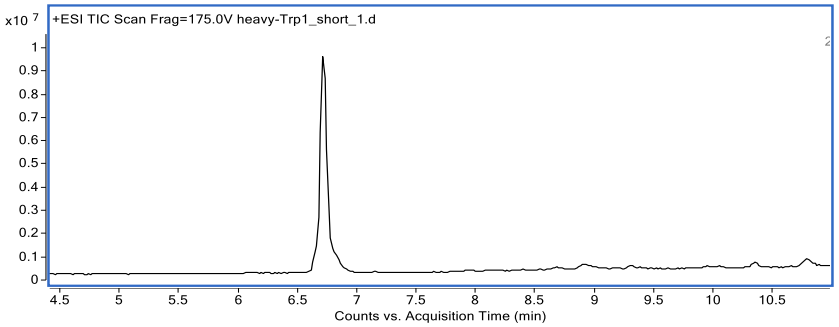

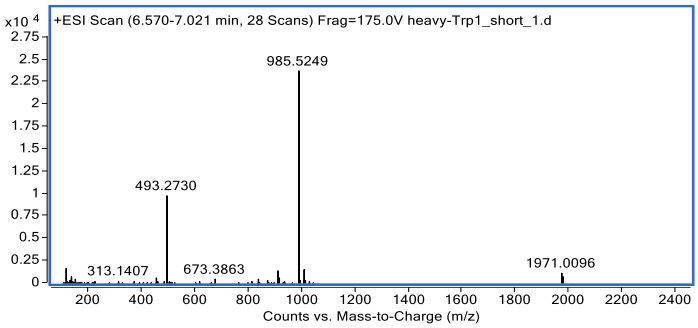

Trp1 T1a long
Mass expected: 2359.05 Da
Mass observed: 2359.14 Da

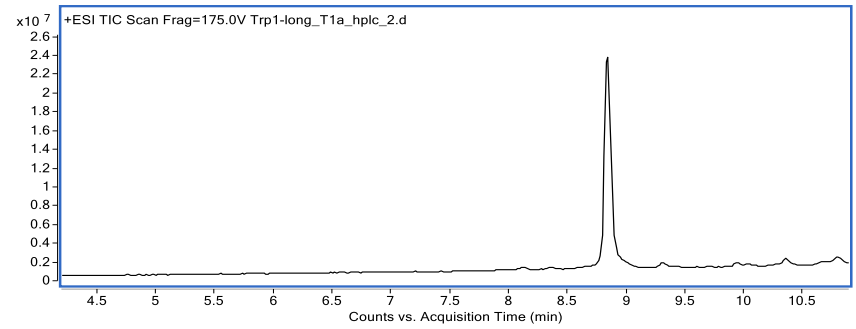

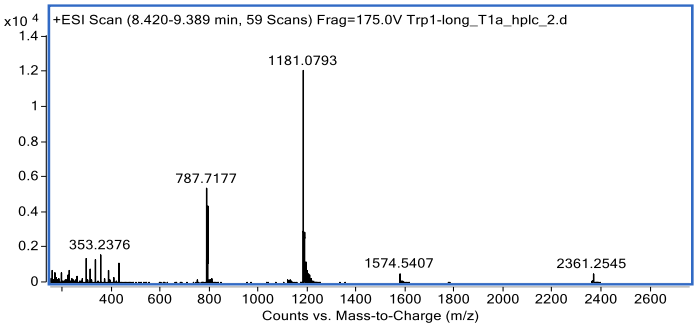

heavy-Trp1 T1a short
Mass expected: 954.44 Da
Mass observed: 954.44 Da

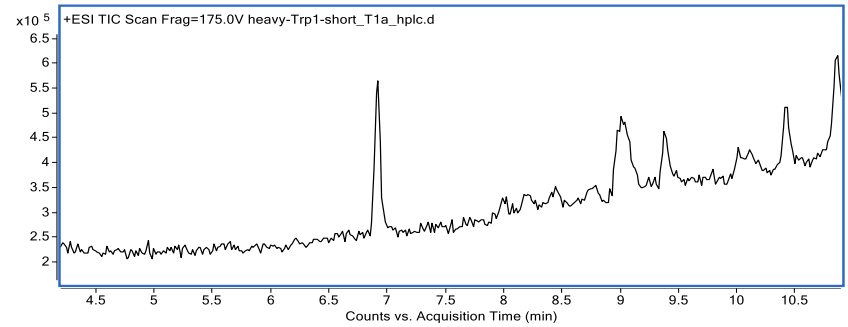

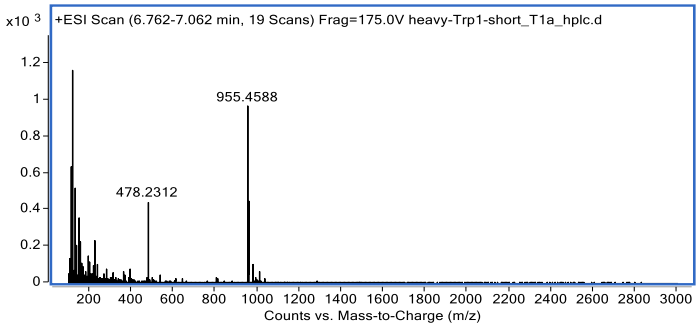

Trp1 A2a long
Mass expected: 2389.07 Da
Mass observed: 2389.22 Da

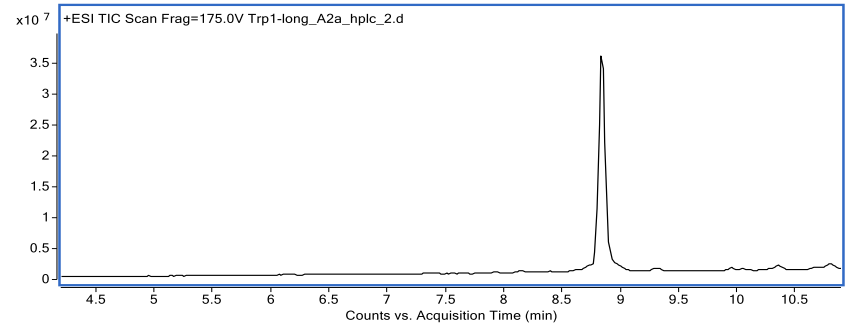

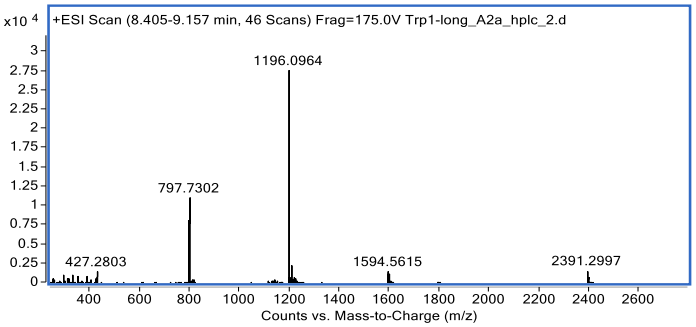

heavy-Trp1 A2a short
Mass expected: 986.44 Da
Mass observed: 986.56 Da

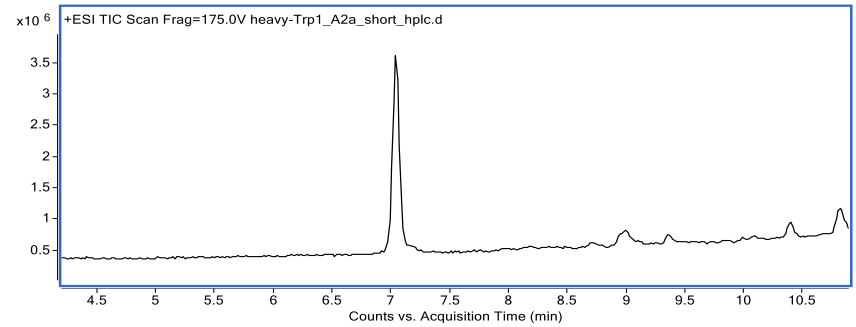

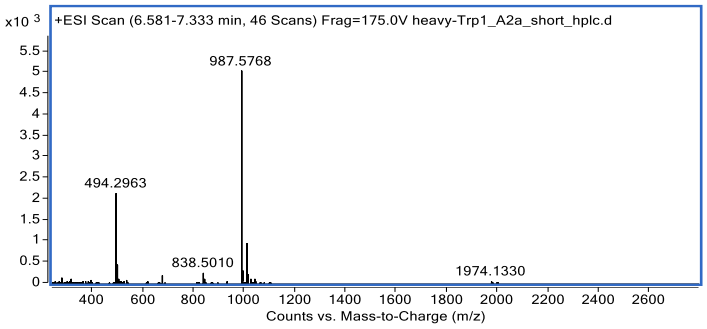

Trp1 P3a long
Mass expected: 2363.05 Da
Mass observed: 2363.05 Da

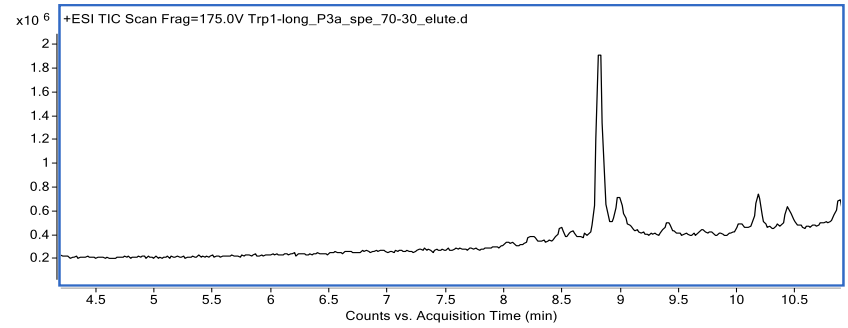

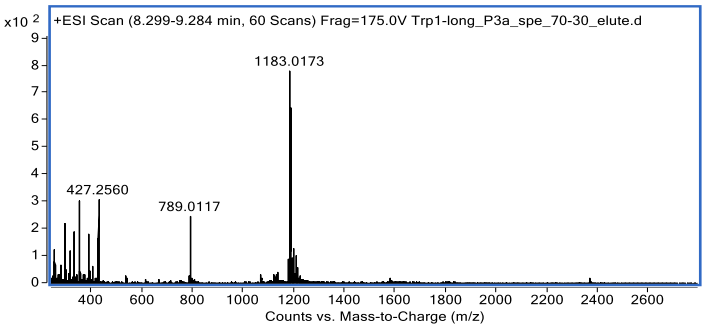

heavy-Trp1 P3a short
Mass expected: 958.43 Da
Mass observed: 958.45 Da

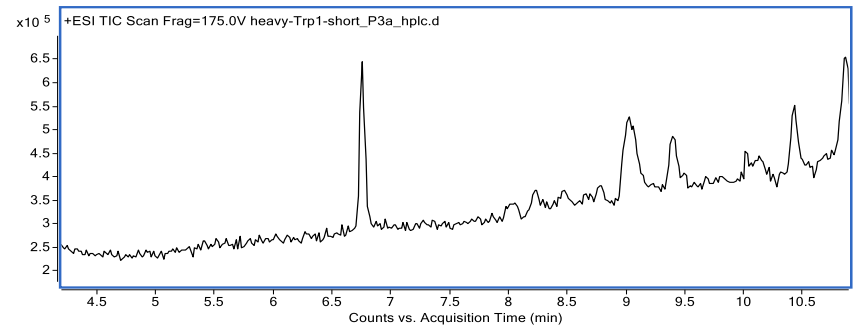

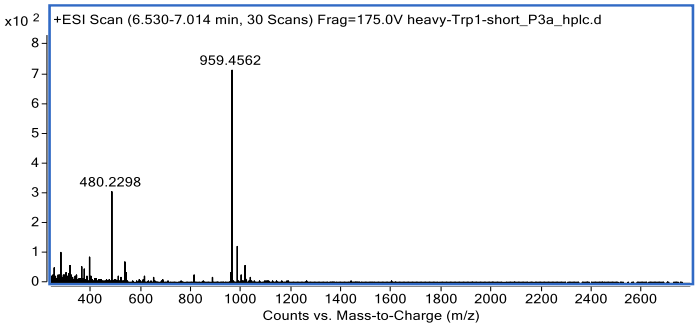

Trp1 D4a long
Mass expected: 2345.08 Da
Mass observed: 2345.29 Da

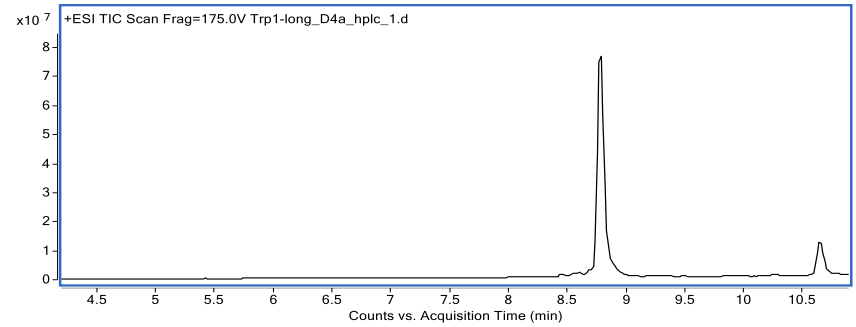

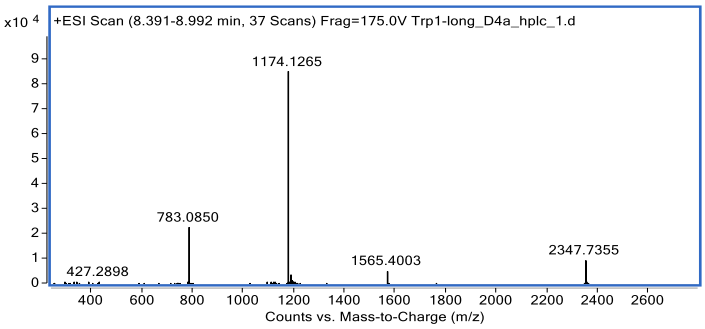

heavy-Trp1 D4a short
Mass expected: 940.46 Da
Mass observed: 940.47 Da

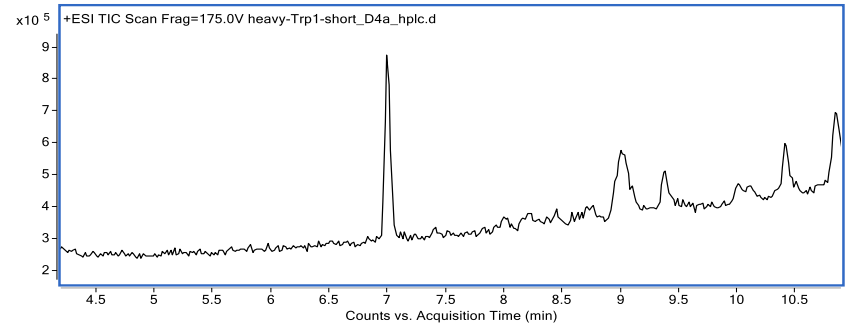

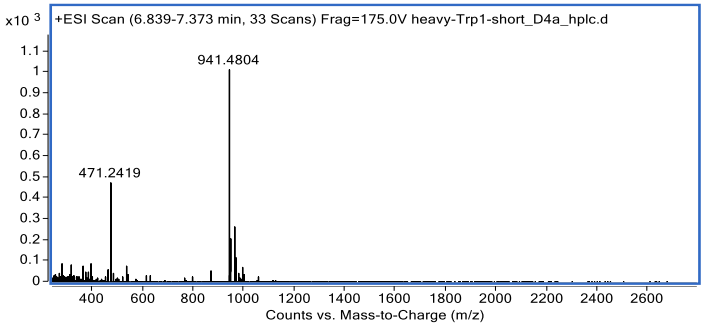

Trp1 P3p long
Mass expected: 2389.07 Da
Mass observed: 2389.04 Da

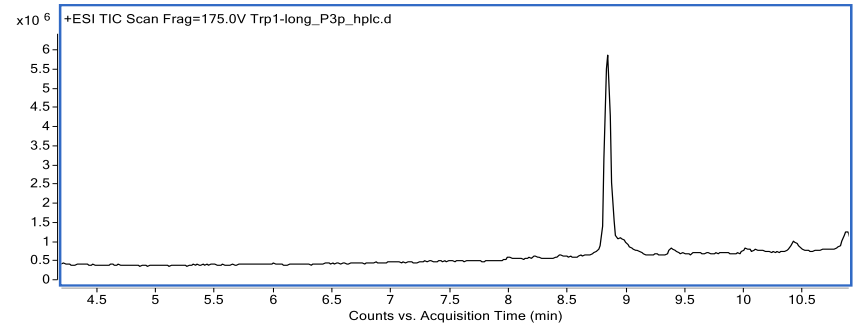

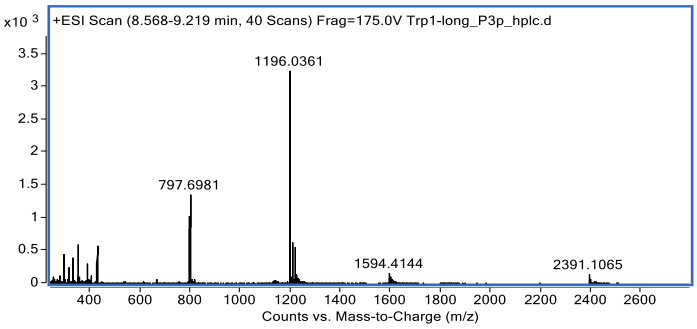

heavy-Trp1 P3p short
Mass expected: 984.45 Da
Mass observed: 984.55 Da

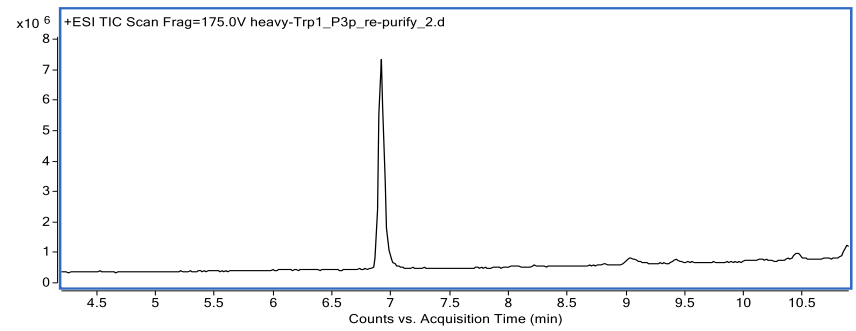

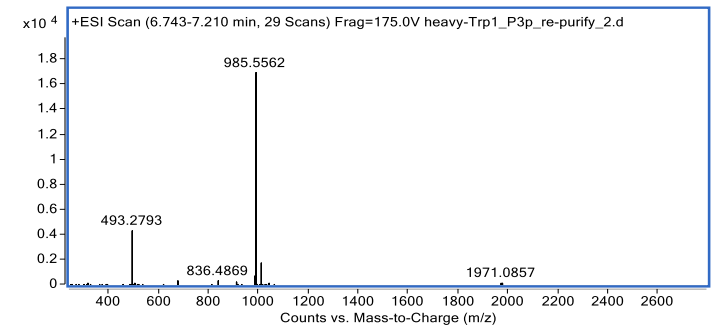

Chapter 6: Chimeras of Cell-Penetrating Peptides Demonstrate Synergistic Improvement in Antisense Efficacy

The work presented in this chapter has been adapted from the following publication:

Fadzen, C. M.;* Holden, R. L.;* Wolfe, J. M.;* Choo, Z.-N.; Schissel, C. K.; Yao, M.; Hanson, G. J.; Pentelute, B. L. Chimeras of Cell-Penetrating Peptides Demonstrate Synergistic Improvement in Antisense Efficacy. *Biochemistry* **2019**, *58* (38), 3980–3989.

**These authors contributed equally to this work.*

Author contributions:

R.L.H., C.M.F., J.M.W., and B.L.P. designed this study. R.L.H., C.M.F., J.M.W., and Z.N.C. synthesized all peptides and peptide conjugates. M.Y. and G.H. collected flow cytometry data comparing N- and C-terminal swapped variants of all chimeras. C.K.S. and R.L.H. collected and analyzed dose-response data. C.M.F. collected confocal imaging data and R.L.H. performed image analysis. R.L.H., C.M.F., and J.M.W. collected, analyzed, and interpreted all other data and performed statistical analyses. R.L.H., C.M.F., J.M.W., and B.L.P. wrote the manuscript.

6.1 Introduction

Phosphorodiamidate morpholino oligonucleotides (PMOs) are attractive therapeutic molecules for genetic diseases. Designed to recognize targets by Watson-Crick base pairing, PMOs exhibit a high level of specificity for their complementary nucleotide sequence. Depending on the type of sequence targeted, PMOs can mediate a variety of effects, including blocking protein translation or modifying pre-mRNA splicing. Eteplirsen, a PMO conditionally approved by the FDA to treat Duchenne muscular dystrophy, alters the splicing of the dystrophin pre-mRNA in order to restore the functionality of the dystrophin protein.[1]

In terms of structure, PMOs are neutral oligonucleotide analogues in which the ribosyl ring has been replaced with a morpholino ring and the negatively-charged phosphodiester backbone has been replaced with the uncharged phosphorodiamidate.[2] The altered backbone structure prevents degradation both in serum and by intracellular nucleases.[3,4] Yet the relatively large size and neutral charge of PMOs can lead to inefficient delivery to the cytosol and nucleus.[5]

Cell-penetrating peptides (CPPs) are a promising strategy to improve the delivery of PMO to the nucleus.[6–11] CPPs are relatively short sequences of 5-40 amino acids that ideally access the cytosol and can promote the intracellular delivery of cargo.[12,13] CPPs can be classified into different groups based on their physicochemical properties. One common CPP class consists of repetitive, arginine-based peptides such as R_{12} and Bpep (RXRRβRRXRRβR, in which X is aminohexanoic acid and β is β-alanine). These oligoarginine peptides are often random coils.[14] When conjugated to PMO, the oligoarginine peptides have been among the most effective peptides in promoting PMO delivery.[7–9] Other CPPs, such as Penetratin, pVEC, and melittin, are more amphipathic in nature. While these sequences do contain cationic residues, the defined separation of charged and hydrophobic residues can promote amphipathic helix formation. However, amphipathic CPPs have not been demonstrated to significantly improve PMO efficacy.

No universal mechanism of cell entry exists for CPPs or CPP-PMO conjugates.[15,16] The mechanism is often highly dependent on the treatment concentrations and the type of cargo attached.[17,18] Above a certain threshold concentration (generally low micromolar), energy-independent cytosolic uptake can be observed faster than the time scale of endocytosis and cell surface recycling.[17,19] The fast uptake rate provides evidence for a direct translocation mechanism similar to what is observed for a small molecule. However, at low, physiologically-relevant concentrations, uptake is primarily endocytic. Even within the category of endocytosis,

CPPs and CPP-PMO conjugates can enter cells using one or multiple endocytic mechanisms.[16,20] These endocytic mechanisms include macropinocytosis, clathrin-mediated endocytosis, caveolae-mediated endocytosis and clathrin/caveloae-independent endocytosis.[21] CPP-PMO conjugates are primarily endocytosed at low concentrations, and the CPPs that are poor for PMO delivery are likely trapped in endosomes or excluded from the nuclear compartment.

Given that different CPPs can engage different endocytic mechanisms and that some CPPs are better at escaping endosomes than others, each individual CPP has strengths and weaknesses. One way to harness the benefits of various peptides is to combine them into chimeric peptides and leverage the strengths of each component. Yin and coworkers created covalent chimeras between a muscle targeting peptide and Bpep to combine muscle targeting with cell-penetration for PMO delivery.[22] Abes *et al.* utilized one chimera composed of penetratin and a polyarginine peptide to improve the delivery of peptide nucleic acids, a different class of antisense oligonucleotide.[23] However, there has yet to be an extensive examination of the design space of chimeras composed of two CPPs. A thorough understanding of this space is necessary in order to apply these hybrid molecules to improve PMO delivery.

To begin our investigations, we envisioned that chimeric peptides composed of a random-coil, oligoarginine CPP with an amphipathic CPP could improve PMO activity. If each CPP utilizes distinct mechanisms of endocytosis, the chimera may be able to access multiple mechanisms of cellular entry. Further, the different CPPs may have beneficial effects on processes downstream of uptake, such as endosomal escape or nuclear entry. Here, we present several amphipathic/oligoarginine CPP chimeras that exhibit a synergistic, rather than additive, gain in PMO efficacy in a biological assay. The CPP chimeras increase PMO activity in this assay up to 70-fold over the PMO alone and outperform the potent CPP standard (Bpep). We investigate several of the design principles for the success of these conjugates and probe the mechanism of uptake for one particular conjugate.

6.2 Results and Discussion

Our initial proof-of-concept experiments were aimed at determining if chimeric CPPs could improve PMO efficacy. We designed a set of three constructs that combine an arginine-rich CPP with an amphipathic CPP. Each construct has three components: the two CPPs and the PMO. The two CPPs were linked through an amide bond to generate one long, linear peptide. The C-terminal peptide for each construct was Bpep, an arginine-rich CPP that has

consistently been one of the highest performing CPPs for PMO delivery.[9,11,24] For the N-terminal peptide, we chose three known amphipathic CPPs: pVEC, penetratin, and mellitin.[25–27] One additional construct was generated with Bpep as the N-terminal peptide to serve as a standard of comparison in which the chimera consists of two arginine-rich peptides (Figure 6.1A). The PMO cargo employed was a 6 kDa, 18-base pair PMO that can trigger increased eGFP expression in a HeLa cell line stably transfected with a split eGFP construct (Figure 6.1B).

To synthesize the constructs, the two-component, chimeric peptide was prepared by automated fast-flow solid-phase peptide synthesis.[28] The N-terminus of the peptide was capped with 4-pentynoic acid to provide a click chemistry handle. The PMO was provided by Sarepta Therapeutics and functionalized at the 3'-amine with 5-azidopentanoic acid. The PMO was conjugated to the chimeric peptide using copper-catalyzed click chemistry and the PMO-chimera conjugates were purified by reversed-phase high-performance liquid chromatography (RP-HPLC) (Figure 6.1B).

Next, the conjugates were evaluated in the HeLa-654 eGFP assay to assess if the chimeric CPPs would improve PMO efficacy. In this assay, the HeLa cells are stably transfected with an eGFP sequence that is interrupted with a mutated intron of the human β-globin gene (IVS2-654). The mutation creates a cryptic splice site that leads to retention of a β-globin fragment in the eGFP mRNA sequence. Upon translation, the eGFP is nonfluorescent. The IVS2-654 PMO utilized in the conjugates hybridizes to the mutated intron and prevents the aberrant pre-mRNA splicing, leading to an eGFP mRNA sequence that encodes for functional, fluorescent eGFP. The amount of PMO delivered is therefore correlated to the amount of functional eGFP expressed. However, multiple factors, such as endosomal escape, nuclear localization, and pre-MRNA-splicing activity, will influence the amount of eGFP fluorescence observed after treatment with a given PMO conjugate.

The HeLa-654 cells were treated with 5 μM of each conjugate in serum-containing media. After 22 hours, the fluorescence of the cells was analyzed by flow cytometry (Figure 6.1C). All four CPP chimeras performed better than Bpep, the consistently high-performing CPP for PMO delivery. Our top chimera, PMO-Penetratin-Bpep, had an approximately 70-fold increase in eGFP fluorescence compared to the background fluorescence of untreated cells. For reference, this is over a 20-fold improvement with respect to the unconjugated PMO and a 2-fold improvement with respect to PMO-Bpep.

Both PMO-Penetratin-Bpep and PMO-pVEC-Bpep displayed synergy, in which the activity of the PMO-chimeric CPP was greater than the sum of the expected activities from each of the PMO-CPPs individually. For example, PMO-Penetratin demonstrated a 7-fold increase and PMO-Bpep demonstrated a 35-fold increase in eGFP fluorescence. An additive effect would lead to a 42-fold increase in eGFP fluorescence for PMO-Penetratin-Bpep. However, the PMO-Penetratin-Bpep chimera had an almost 70-fold increase in eGFP fluorescence, meaning it performed approximately 1.5 times better than an additive effect. A similar synergy was also observed for PMO-pVEC-Bpep, in which the measured eGFP fluorescence was also 1.5 times greater than the sum of the parts.

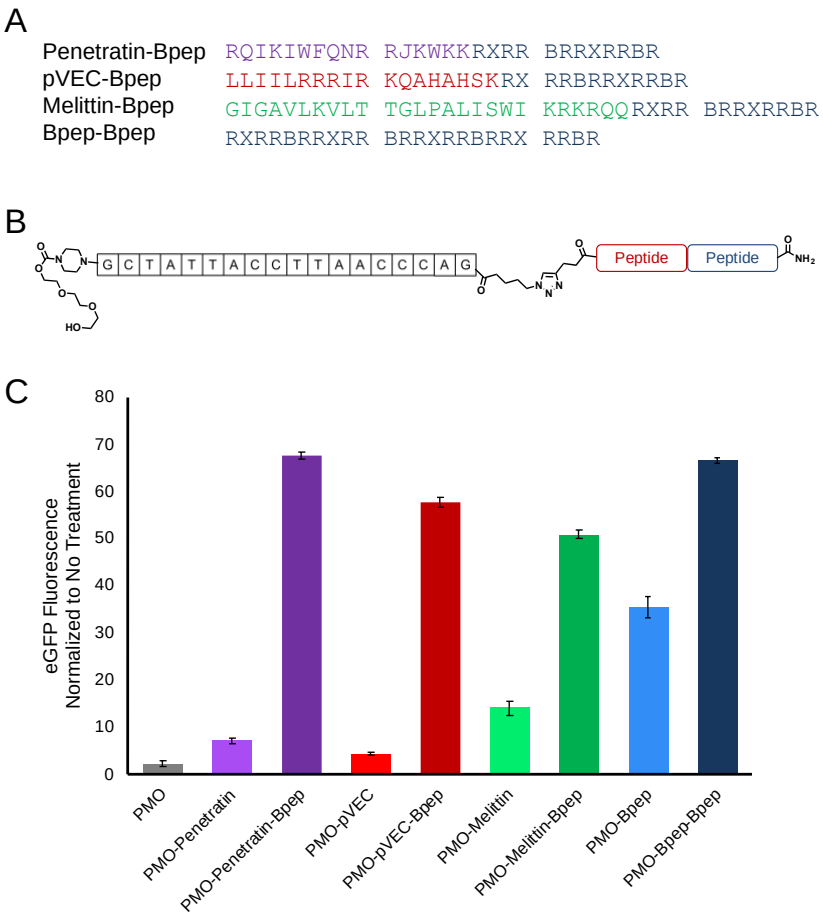

Figure 6.1. PMO-peptide chimera conjugates enhance exon skipping. A) Amino acid sequences of the four cell-penetrating peptide chimeras used in this work. Each chimera includes one cell-penetrating peptide on the N-terminus followed by Bpep on the C-terminus. X = aminohexanoic acid, B = beta-alanine and J = norleucine. B) General scheme of a PMO-chimera conjugate. C) Plot showing mean eGFP fluorescence of a population of stably transfected HeLa-654 cells after continuous treatment for 22 hours with 5 μM of each PMO-

peptide conjugate. The mean eGFP fluorescence was normalized to the eGFP fluorescence of untreated cells. Both PMO-Penetratin-Bpep and PMO-pVEC-Bpep demonstrated synergistic improvement in activity over the base PMO-peptide conjugates. Error bars are a standard deviation of a technical triplicate and the increased activity of each PMO-chimera conjugate is statistically significant compared to both PMO-CPP and PMO-Bpep. Statistical analyses were performed using a one-way ANOVA and Bonferroni's multiple comparison test ($p \leq 0.0001$ for all groups). Results are a representative example of several independent experiments that included these constructs and conditions (Figure 6.3).

The existence of a synergistic effect in two of the chimeras supports the notion that combining an arginine-rich CPP with an amphipathic CPP can improve PMO efficacy. However, other variables could be responsible for the observed effects. The order of the individual peptides may influence PMO activity. Therefore, for each construct, we synthesized the peptide sequences with the order reversed where Bpep is at the N-terminus and the other CPP is at the C-terminus. After conjugation to PMO and purification by RP-HPLC, these conjugates were tested in the eGFP assay along with their counterparts that had Bpep on the C-terminus. For both synergistic chimeras (PMO-Penetratin-Bpep and PMO-pVEC-Bpep), switching the order of the peptides decreased observed PMO activity (Figure 6.2A). This observation suggests that it is critical to have Bpep as the C-terminal component to observe synergy.

This result raises the question of whether or not the N-terminal peptide has functional significance. Alternatively, the N-terminal peptide could serve as a spacer between the PMO and Bpep that amplifies the effect of Bpep. If this were true, it would explain why all four chimeras with Bpep at the C-terminus performed similarly. To address this question, we prepared chimeras in which the N-terminal peptide was replaced by a 15-residue polyproline or polyalanine spacer. The two spacers are of identical length but will likely exhibit different structures given the rigidity of polyproline sequences. PMO-P15-Bpep and PMO-A15-Bpep were evaluated in the eGFP assay (Figure 6.2B). PMO-P15-Bpep showed no improvement over PMO-Bpep. However, PMO-A15-Bpep exhibited a mean fluorescence intensity greater than PMO-Bpep and performed almost as well as the CPP chimeras. Unfortunately, comparison of this result to PMO-A15 was prevented due to the poor synthesis and solubility of A15, which limits assessment of whether or not the effect is synergistic. P15 and A15 had divergent effects as the N-terminal peptide, indicating that while spacing may play a role in the efficacy of the

chimeric CPPs, it likely does not fully account for the effect of the N-terminal peptide in the chimeric sequence.

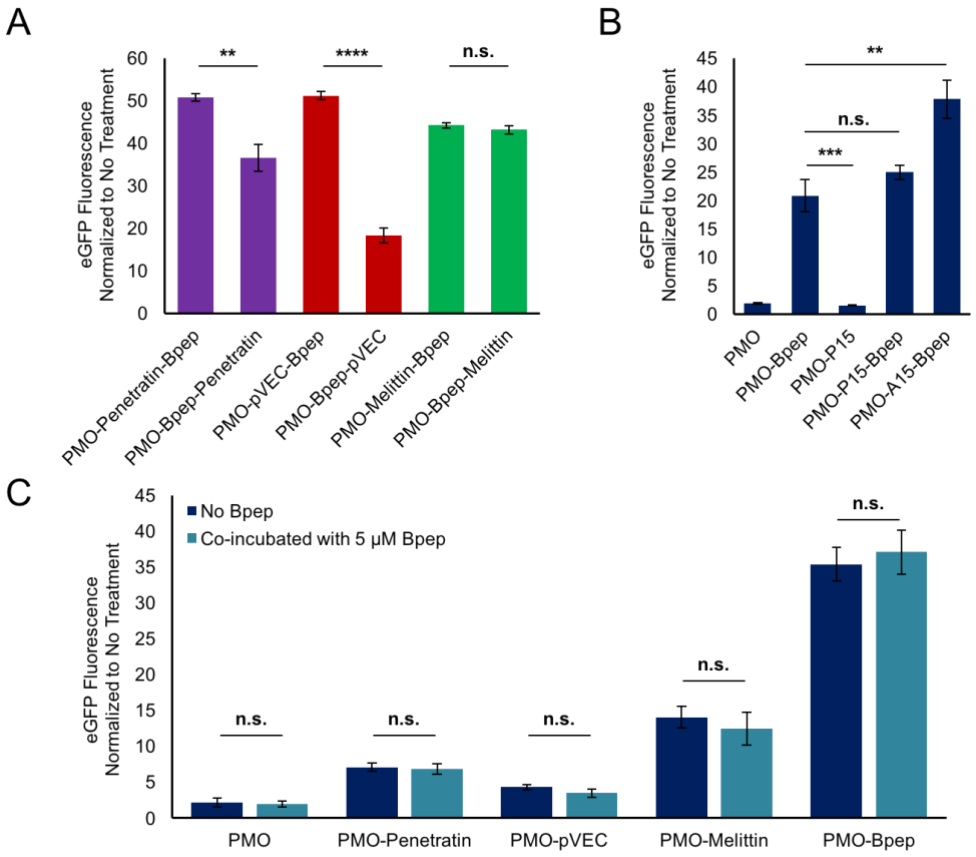

Figure 6.2. The activity of PMO-CPP chimera conjugates is influenced by specific design features. (A) For each chimera, the order of the sequences was reversed and the activity of the PMO-peptide conjugate was measured in the eGFP assay. The plot shows the fold change in eGFP fluorescence relative to the untreated control. B) Plot of the fold change in eGFP fluorescence for cells treated with 5 μM of PMO, PMO-P15, PMO-Bpep, PMO-P15-Bpep, or PMO-A15-Bpep for 22 hours. C) Comparison of the fold change in eGFP fluorescence for HeLa-654 cells treated with 5 μM of each base PMO-CPP for 22 hours in the presence or absence of 5 μM Bpep. For each construct, the difference in activity with and without B-pep co-incubation was not statistically significant. For every experiment displayed in the figure, error bars represent a standard deviation of a technical triplicate and statistical analyses were performed using a student's t-test (**** $p \leq 0.0001$, *** $p \leq 0.001$, ** $p \leq 0.01$, n.s. $p > 0.05$).

Next, we investigated the necessity of covalent attachment. The increase in PMO activity may or may not require the two component peptides of the chimera to be covalently attached. The eGFP assay was repeated with PMO-Penetratin, PMO-pVEC, PMO-Melittin and

PMO-Bpep in either the presence or absence of 5 μM Bpep (Figure 6.2C). In all cases, the PMO-CPP conjugates performed identically, regardless of whether or not Bpep was present. This result demonstrates that covalently linking the two CPPs is necessary to observe an improvement in activity. Co-incubation with Bpep did not result in any change in eGFP fluorescence.

Given concerns over the size and net charge of the constructs, a lactate dehydrogenase assay was performed to assess if the plasma membrane of the cells had been compromised in any way during treatment with the chimeric constructs (see Section 6.3.10). At 5 μM, none of the constructs except for the PMO-Melittin-Bpep construct caused additional lactate dehydrogenase release compared to untreated cells, suggesting the majority of our chimeras do not disrupt the cell membrane.

Since both efficacy and toxicity can be concentration-dependent, we also assessed the extent to which trends in exon skipping activity and toxicity were consistent across a range of concentrations. Concentrations of 0.2 μM, 1 μM, 5 μM, 10μM and 25 μM were used for treatment in the exon skipping assay described above. Non-chimeric CPP-PMO conjugates exhibited minimal activity at low concentrations and a gradual increase in efficacy with increasing dose (Figure 6.3). The PMO-chimeras exhibited poor efficacy at 0.2 μM but increased dramatically at 1 μM, with the exception of PMO-pVEC-Bpep which did not increase significantly until 5 μM. Efficacy began to plateau at 10 μM, except for PMO-Melittin-Bpep which could not be measured at 10 μM due to severe toxicity. All PMO-chimeras were toxic at 25 μM. An LDH assay confirmed these results, indicating that the PMO-chimera conjugates exhibited 70 to 100% of the maximum possible LDH release at 25 μM, with some causing significant membrane disruption at 10 μM as well (see Section 6.3.10). At lower concentrations however, most of the PMO-chimera conjugates did not exhibit cytotoxicity. Taken together, these data indicate that 5 μM is an optimal dosing window for these chimeric CPPs to mediate exon skipping.

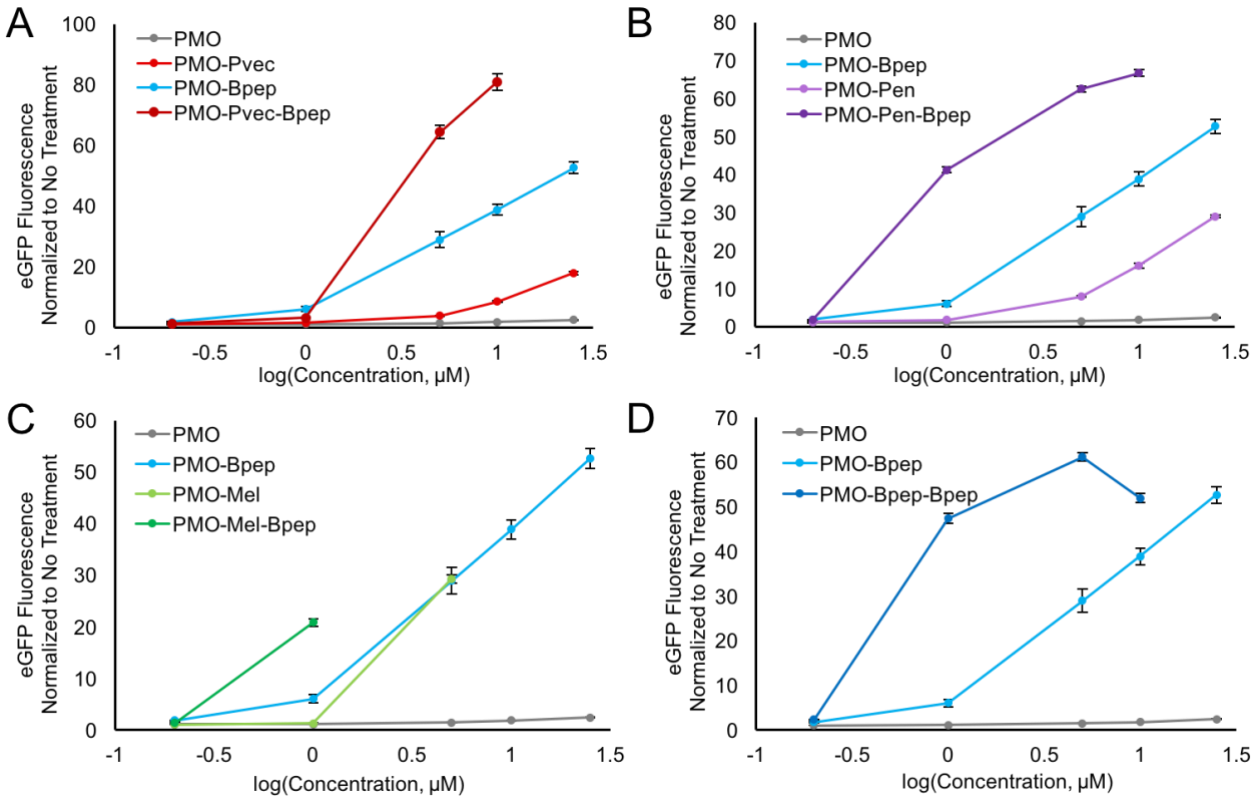

Figure 6.3. PMO-peptide chimera conjugates exhibit dose dependent activity. For each CPP chimera, HeLa-654 cells were treated with 0.2, 1, 5, 10, and 25 μM of the PMO-chimera, the related PMO-CPPs, and the unmodified PMO. After 22 hours, eGFP fluorescence was measured via flow cytometry. A) PMO-pVEC-Bpep, B) PMO-Penetratin-Bpep, C) PMO-Melittin-Bpep, D) PMO-Bpep-Bpep. All values are normalized to the eGFP fluorescence of untreated cells. Error bars are a standard deviation of a technical triplicate.

We then probed the mechanism by which these chimeric CPPs improve PMO efficacy. The eGFP HeLa cells provide a functional assay for PMO activity, yet many mechanistic steps contribute to this final read-out. The PMO conjugates must be internalized into cells, escape endosomes if endocytosed, localize to the nucleus, and bind to pre-mRNA to generate an effect. The different parts of the chimera may be aiding in one or many of these steps. While it is challenging to conclusively demonstrate the exact mechanism given the complexity of the biological processes involved, we chose one model chimera to thoroughly study to gain additional insight. PMO-pVEC-Bpep was used for this purpose, since it demonstrated synergy and did not disrupt the plasma membrane at 5 μM. Additionally, the poor performance of PMO-pVEC made the strong performance of PMO-pVEC-Bpep an intriguing result.

Mechanistic studies began with experiments to assess cellular uptake pathways. To examine if energy-dependent pathways are involved, PMO activity was measured after treatment at 4 °C vs. 37 °C. The experiments were performed in a pulse-chase format in which the eGFP HeLa cells were incubated with 5 μM PMO-pVEC, PMO-Bpep, or PMO-pVEC-Bpep for 3 hours at either 4 °C or 37 °C (Figure 6.4A). Then, the treatment media was exchanged for fresh media and the cells were allowed to grow for an additional 22 hours. For all compounds except PMO-Bpep, there was a decrease in eGFP fluorescence when treated at 4 °C. This result suggests that energy-dependent mechanisms are relevant to the uptake of the PMO-pVEC-Bpep chimera. With respect to the PMO-Bpep result, any conjugate that binds to the surface of the cells during treatment at 4 °C could be subsequently internalized and trigger eGFP expression when the cells are incubated for an additional 22 hours at 37 °C after treatment.

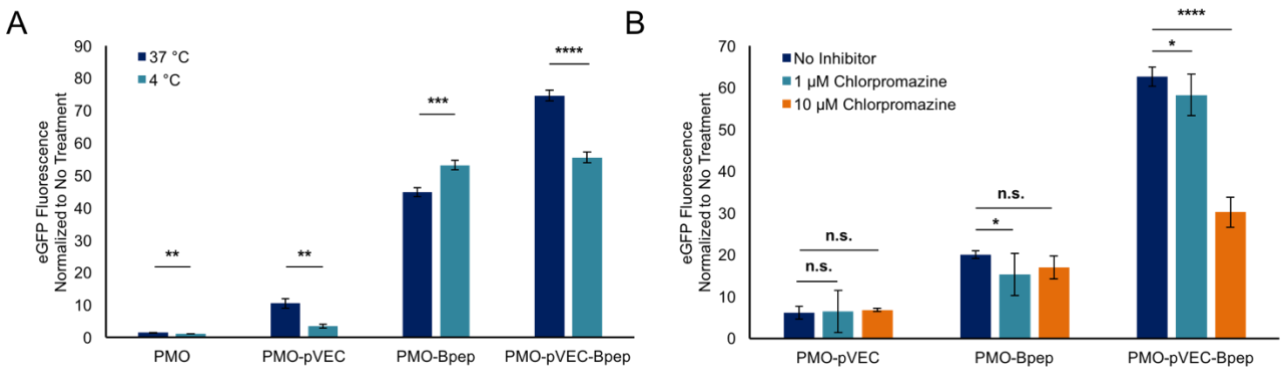

Figure 6.4. PMO-pVEC-Bpep conjugate undergoes energy-dependent uptake via a route distinct from the PMO-CPPs. A) Plot of normalized eGFP fluorescence for cells treated at either 37 ^{o}C or 4 ^{o}C, normalized to the respective untreated control. The cells were allowed to equilibrate to their respective temperatures for 30 minutes prior to treatment with 5 μM PMO, PMO-pVEC, PMO-Bpep, or PMO-pVEC-Bpep. After treatment with the constructs for 3 hours, the media was exchanged for fresh, untreated media and the cells from both conditions were incubated for another 22 hours at 37 ^{o}C. Both PMO-pVEC and PMO-pVEC-Bpep exhibited a reduction in uptake at 4 ^{o}C, suggesting that energy-dependent processes are relevant for uptake. Statistical analyses were performed using a student's t-test (**** $p \leq 0.0001$, *** $p \leq 0.001$, ** $p \leq 0.01$). B) Plot of normalized eGFP fluorescence for cells treated with different concentrations of chlorpromazine, normalized to the untreated control. The cells were pre-incubated for 30 minutes with chlorpromazine and then 5 μM PMO, PMO-pVEC, PMO-Bpep, or PMO-pVEC-Bpep was added. After treatment with the constructs for 3 hours, the media was exchanged for fresh, untreated media and the cells from both conditions were incubated for

another 22 hours at 37 ^{o}C. At 10 μM chlorpromazine, eGFP fluorescence decreased only in the cells treated with the PMO-pVEC-Bpep chimera, suggesting that clathrin-mediated endocytosis plays a unique role in the uptake of the chimera. Statistical analyses were performed using a one-way ANOVA and Sidak's multiple comparison test (**** $p \leq 0.0001$, * $p \leq 0.05$, n.s. $p > 0.05$). For both experiments, error bars are a standard deviation of a technical triplicate.

In addition, we studied the effect of multiple endocytosis inhibitors on the internalization of PMO-pVEC, PMO-Bpep, and PMO-pVEC-Bpep into cells (Figure 6.4B, Section 6.3.11). The experiments were performed in a pulse-chase format in which the eGFP HeLa cells were pre-incubated with the inhibitors. After thirty minutes of pre-incubation, the PMO-peptide conjugates were added and after three hours, the treatment media was exchanged with fresh media and the cells were left to grow for another 22 hours. The majority of the inhibitors had no effect. However, at high concentrations of chlorpromazine, eGFP fluorescence decreased in the cells treated with the PMO-pVEC-Bpep chimera. While chlorpromazine is considered an inhibitor of clathrin-mediated endocytosis, it may possibly affect downstream components of the process too.[29] Beyond the possible role of clathrin-mediated endocytosis in the uptake of the chimera, these data demonstrate that the chimera is accessing a unique internalization mechanism since no appreciable decrease was observed with either PMO-pVEC or PMO-Bpep.

Finally, the constructs were labeled with a small molecule organic dye orthogonal to eGFP to allow simultaneous monitoring of the uptake of the compounds and functional exon-skipping activity. Experiments of this format could help deconvolve cellular internalization from PMO efficacy. The compounds were designed with the dye linked to the amino acid directly adjacent to the PMO such that the dye should be reflective of the localization of the PMO even if the peptide undergoes proteolytic degradation. To prepare these compounds, pVEC, Bpep and pVEC-Bpep were synthesized with a cysteine residue on the N-terminus of the sequence and the terminus was then capped with 4-pentynoic acid as before. After purification by RP-HPLC, the peptides were dissolved in water with equimolar Sulfo-Cyanine5 maleimide and purified again by RP-HPLC. Finally, the SulfoCy5-labeled peptides were all conjugated to the PMO-azide through copper-catalyzed click chemistry and purified by RP-HPLC.

Using the SulfoCy5-labeled constructs, we performed a flow cytometry experiment with the eGFP HeLa cells. The cells were treated with 5 μM of each conjugate in serum-containing media for 22 hours and then analyzed by flow cytometry (Figure 6.5A). For eGFP fluorescence,

the 488 nm excitation laser and 530 nm emission filter were used, and for the SulfoCy5, the 561 nm excitation laser and 695 nm emission filter were used. The separation of channels enabled fluorescence from both fluorophores to be simultaneously recorded. We also treated with unlabeled PMO-pVEC, PMO-Bpep, and PMO-pVEC-Bpep to determine if the fluorophore was perturbing the effect of a given conjugate. In all cases, eGFP fluorescence was slightly decreased with the fluorophore attached suggesting that while the fluorophore may affect the efficacy of the conjugate, it does so uniformly (see Section 6.3.12).

In terms of SulfoCy5 fluorescence, PMO-SulfoCy5-Bpep exhibited less fluorescence than PMO-SulfoCy5-pVEC or PMO-SulfoCy5-pVEC-Bpep. However, PMO-SulfoCy5-Bpep had a relatively high ability to facilitate eGFP expression. This result suggests that while the overall cellular uptake of PMO-Bpep is less than PMO-pVEC, Bpep has a beneficial downstream effect. Perhaps improved endosomal escape, nuclear entry, RNA binding, or splice-modification results in the relatively high eGFP fluorescence for PMO-Bpep. On the other hand, PMO-SulfoCy5-pVEC had high SulfoCy5 fluorescence, but poor eGFP expression, which indicates that the compound has good cellular uptake but has limitations elsewhere downstream. The pVEC-Bpep chimera exhibited both the highest eGFP expression and the highest SulfoCy5 fluorescence, though the SulfoCy5 fluorescence was on a similar scale to pVEC. Therefore, our hypothesis for the basis of the chimera's synergy is that the pVEC component is improving cellular uptake without interfering with the beneficial downstream effects of Bpep.

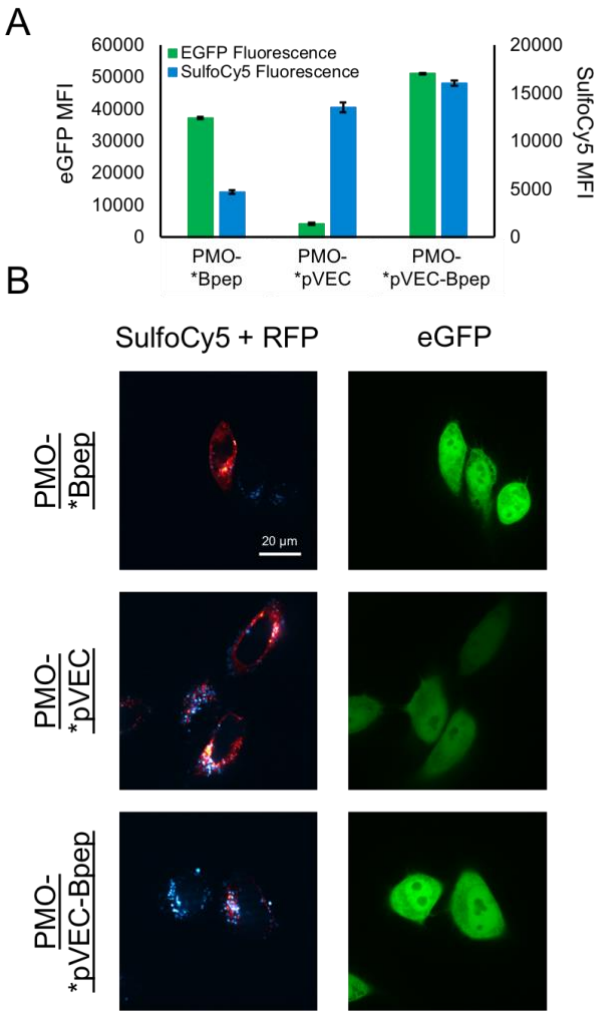

Figure 6.5. PMO-pVEC-Bpep exhibits high internalization and high exon skipping activity. A) Plot showing the mean fluorescence intensity (MFI) in each respective channel for eGFP and SulfoCy5 for HeLa-654 cells treated with 5 µM PMO-SulfoCy5-pVEC, PMO-SulfoCy5-Bpep, or PMO-SulfoCy5-pVEC-Bpep for 22 hours at 37 ^{o}C. The left axis pertains to eGFP fluorescence and the right axis pertains to SulfoCy5 fluorescence. PMO-*Peptide is a figure abbreviation for a PMO-SulfoCy5-Peptide construct. Error bars are a standard deviation of a technical triplicate. For both eGFP and SulfoCy5 fluorescence, the activity of PMO-pVEC-Bpep, PMO-pVEC, and PMO-Bpep are all statistically different ($p \leq 0.0001$, analyses performed using a one-way ANOVA and Tukey's multiple comparison test). B) Live-cell confocal microscopy images of HeLa-654 cells after treatment with the same conditions as the flow cytometry experiments. The cells were also transiently transfected with an RFP-Rab5a fusion construct to label early endosomes (green - eGFP - PMO activity, red – RFP – early endosomes, cyan – SulfoCy5 – conjugates). For visualization of nuclei and brightfield images, see Section 6.7.2.

To test the hypothesis that the pVEC component improves cellular uptake, we performed live cell confocal microscopy imaging experiments on the eGFP HeLa cells. The same treatment conditions as the flow cytometry assay were used except that a Rab5a-RFP fusion protein was used to label early endosomes and Hoechst dye was used to label nuclei. The eGFP HeLa cells were transiently transfected sixteen hours prior to imaging with a Rab5a-RFP fusion construct in order to examine the extent of localization to endosomes. We reasoned that if PMO-SulfoCy5-pVEC had poor efficacy in triggering eGFP expression due to endosomal entrapment, the RFP signal would be co-localized with the SulfoCy5 signal. In addition, labeling with Hoechst dye enabled the nuclear regions to be delineated and the nuclear SulfoCy5 signal to be quantified.

The imaging data correlate well with the flow cytometry data (Figure 6.5B). With both PMO-SulfoCy5-pVEC and PMO-SulfoCy5-pVEC-Bpep, the bright SulfoCy5 signal is mostly concentrated in punctae. Some SulfoCy5 signal is co-localized with RFP signal, with Mander's Colocalization Coefficients of 0.4 ± 0.1 and 0.4 ± 0.2 for PMO-SulfyCy5-pVEC and PMO-SulfoCy5-pVEC-Bpep, respectively (see Section 8 of SI for details). This indicates that approximately 40% of the SulfoCy5-labeled construct is co-localized with RFP, suggesting localization to the early endosome. Other SulfoCy5 punctae are likely late endosomes and lysosomes. These images provide further evidence that the primary mechanism of internalization is endocytosis and that endosomal entrapment can limit PMO activity for certain constructs, despite significant cellular uptake.

With regard to the nuclear SulfoCy5 signal, PMO-SulfoCy5-pVEC-Bpep exhibited the highest mean nuclear fluorescence (see Section 6.3.13). The nuclear fluorescence was determined by labeling the nuclei with Hoechst, outlining the nuclear regions, and quantifying SulfoCy5 signal in the nuclear regions. Intriguingly, the nuclear SulfoCy5 fluorescence of PMO-SulfoCy5-pVEC was higher than PMO-SulfoCy5-Bpep, even though PMO-SulfoCy5-Bpep exhibited more eGFP signal. Because multiple factors influence the amount of eGFP fluorescence observed after treating the HeLa-654 cells, the higher activity combined with a lower nuclear concentration suggests that the Bpep component may lead to enhanced splicing activity independent of delivery.

We then analyzed the impact of peptide conjugation on PMO binding to its complementary oligonucleotide sequence. Although the PMO exerts exon skipping activity by binding pre-mRNA, we considered single-stranded DNA to be a good proxy for comparing the relative binding affinity of these PMO-peptide conjugates *in vitro*, given that relative trends in antisense oligonucleotide binding affinity are generally conserved between RNA and DNA.[30,31]

We obtained melting curves for the unmodified PMO, PMO-Bpep, PMO-pVEC, and PMO-pVEC-Bpep each combined with DNA sequence complementary to the PMO (Figure 6.6A, Section 6.3.14). We then determined the melting temperature (T_m) for each construct from the derivative of the corresponding melting curve, where the maximum of this derivative plot corresponds to the T_m (Figure 6.6B, Section 6.3.14).

A

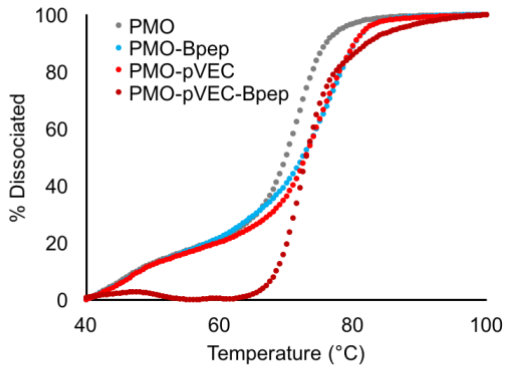

B

	T_m (°C)
PMO	71.3 ± 0.3
PMO-Bpep	77.3 ± 0.3
PMO-pVEC	75 ± 3
PMO-pVEC-Bpep	72.3 ± 0.6

Figure 6.6. Peptide conjugation slightly alters PMO binding to a complementary nucleic acid. A) Melting curves for the unmodified PMO, PMO-Bpep, PMO-pVEC, and PMO-pVEC-Bpep annealed to the complementary DNA sequence. Melting was monitored via fluorescence decrease of an intercalating dye. Fluorescence measurements were then normalized and converted to percent dissociated. Shown is one representative independent experiment of three total independent experiments, with remaining replicates shown in Figure S7. B) The T_m for each construct was calculated from the derivative of the corresponding melting curve. Values represent the average of three independent experiments with an error of one standard deviation.

The melting curves as well as the T_m values indicate that peptide conjugation slightly enhances PMO affinity for its target sequence, with a maximum increase in T_m of (6.0 ± 0.4) °C for PMO-Bpep. It is possible that this slight increase in binding affinity could contribute to the increase in exon skipping activity noted for PMO-Bpep despite its lower observed nuclear localization. However, the differences in T_m between the three PMO-peptide conjugates was relatively low, indicating that peptide identity does not have a dramatic impact on the affinity of the PMO for its complementary sequence. Further, PMO-pVEC-Bpep exhibited the smallest

increase in T_m relative to the unmodified PMO. Altogether, this suggests that the mechanism by which the pVEC-Bpep chimera enhances exon skipping is not related to improved PMO binding to its target sequence.

Further experiments will be necessary to precisely define the effects downstream of internalization that are involved in the synergistic performance of the chimeras. However, here we show with our mechanistic studies that individual CPPs may be helpful with different elements of macromolecule delivery. We show that chimeric peptides composed of CPPs can exhibit synergistic improvements in PMO delivery and exon skipping efficiency. We show that the relative position of the sequences affects the degree of uptake, that peptide identity tunes activity, and that they must be covalently attached to observe the effect. One issue with this strategy is the large molecular weight of the resultant conjugates. One way to overcome this would be to create deletion analogues to identify the minimal necessary sequence to observe synergy. These deletion constructs will be the subject of future investigations with the Penetratin-Bpep and pVEC-Bpep chimeras.

Given that poor intracellular delivery has largely limited the therapeutic application of antisense oligonucleotides, we believe this strategy could help improve conjugate therapies for the treatment of several genetic diseases, such as Duchenne muscular dystrophy. More generally, we envision that the approach of combining CPPs from different classes can be applied to the intracellular delivery of a variety of macromolecular cargoes.

6.3 Materials and Methods

6.3.1 Materials

H-Rink Amide-ChemMatrix resin was obtained from PCAS BioMatrix Inc. (St-Jean-sur-Richelieu, Quebec, Canada). 1-[Bis(dimethylamino)methylene]-1H-1,2,3-triazolo[4,5-b]pyridinium-3-oxid-hexafluorophosphate (HATU), 4-pentynoic acid, 5-azidopentanoic acid, Fmoc-β-Ala-OH, and Fmoc-6-aminohexanoic acid were purchased from Chem-Impex International (Wood Dale, IL). Fmoc-L-Arg(Pbf)-OH, Fmoc-L-His(Trt)-OH, Fmoc-L-Lys(Boc)-OH, Fmoc-L-Asp(tBu)-OH, Fmoc-L-Glu(tBu)-OH, Fmoc-L-Ser(tBu)-OH, Fmoc-L-Thr(tBu)-OH, Fmoc-L-Asn(Trt)-OH, Fmoc-L-Gln(Trt)-OH, Fmoc-L-Cys(Trt)-OH, Fmoc-L-Gly-OH, Fmoc-L-Ala-OH, Fmoc-L-Val-OH, Fmoc-L-Leu-OH, Fmoc-L-Ile-OH, Fmoc-L-Met-OH, Fmoc-L-Phe-OH, Fmoc-L-Pro-OH, Fmoc-L-Tyr(tBu)-OH, and Fmoc-L-Trp(Boc)-OH were purchased from Advanced ChemTech (Louisville, KY). PyAOP was purchased from P3 BioSystems (Louisville, KY). Sulfo-Cy5-Maleimide was purchased from Lumiprobe

Corporation (Hallandale Beach, FL). Peptide synthesis-grade N,N-dimethylformamide (DMF), CH_2Cl_2, diethyl ether, and HPLC-grade acetonitrile were obtained from VWR International (Radnor, PA). Cytochalasin D was obtained from Santa Cruz Biotech. The LDH Assay kit was purchased from Promega (Madison, WI). PMO IVS2-654 was provided by Sarepta Therapeutics. All other reagents were purchased from Sigma-Aldrich (St. Louis, MO). Milli-Q water was used exclusively. HeLa-654 cells were obtained from the University of North Carolina Tissue Culture Core facility.

6.3.2 Methods for LC-MS Analysis

LC-MS analyses were performed on an Agilent 6520 ESI-Q-TOF mass spectrometer equipped with a C_3 Zorbax column (300SB C3, 2.1 x 150 mm, 5 μm). Mobile phases were: 0.1% formic acid in water (solvent A) and 0.1% formic acid in acetonitrile (solvent B). The following LC-MS methods were used for characterization:

Method A: 5% B from 0 to 2 min, linear ramp from 5% B to 65% B from 2 to 11 min, 65% B from 11 to 12 min and finally 3 min of post-time at 5% B for equilibration, flow rate: 0.8 mL/min.

Method B: 1% B from 0 to 2 min, linear ramp from 1% B to 61% B from 2 to 11 min, 61% B to 99% B from 11 to 12 min and finally 3 min of post-time at 1% B for equilibration, flow rate: 0.8 mL/min.

Chromatograms were obtained using Method B unless otherwise noted. All data were processed using Agilent MassHunter software package. Y-axis in all chromatograms shown represents total ion current (TIC) unless noted.

6.3.3 Fast-flow Peptide Synthesis

Peptides were synthesized on a 0.1-mmol scale using an automated flow peptide synthesizer.[24] A 200 mg portion of ChemMatrix Rink Amide HYR resin was loaded into a reactor maintained at 90 ºC. All reagents were flowed at 80 mL/min with HPLC pumps through a stainless-steel loop maintained at 90 ºC before introduction into the reactor. For each coupling, 10 mL of a solution containing 0.2 M amino acid and 0.17 M HATU in DMF were mixed with 200 μL diisopropylethylamine and delivered to the reactor. Fmoc removal was accomplished using 10.4 mL of 20% (v/v) piperidine. Between each step, DMF (15 mL) was used to wash out the reactor. Special coupling conditions were used for arginine, in which the flow rate was reduced to 40 mL/min and 15 mL of a solution containing 0.2 M Fmoc-L-Arg(Pbf)-OH and 0.17 M PyAOP in DMF were mixed with 200 μL diisopropylethylamine and delivered to the reactor. To cap the peptide with 4-pentynoic acid, the resin was incubated for 30 min at room temperature with 4-pentynoic acid (1 mmol) dissolved in 2.5 mL 0.4 M HATU in DMF with

500 µL diisopropylethylamine. After completion of the synthesis, the resins were washed 3 times with DCM and dried under vacuum.

6.3.4 Peptide Cleavage and Deprotection

Each peptide was subjected to simultaneous global side-chain deprotection and cleavage from resin by treatment with 5 mL of 94% trifluoroacetic acid (TFA), 2.5% 1,2-ethanedithiol (EDT), 2.5% water, and 1% triisopropylsilane (TIPS) (v/v) for 7 min at 60 °C. For arginine-rich sequences, the resin was treated with a cleavage cocktail consisting of 82.5% TFA, 5% phenol, 5% thioanisole, 5% water, and 2.5% EDT (v/v) for 14 hours at room temperature. The TFA was evaporated by bubbling N_2 through the mixture. Then ~40 mL of cold ether (chilled at –80°C) was added to precipitate and wash the peptide. The crude product was pelleted through centrifugation for 3 min at 4,000 rpm and the ether decanted. The ether precipitation and centrifugation was repeated two more times. After the third wash, the pellet was redissolved in 50% water and 50% acetonitrile containing 0.1% TFA, filtered through a fritted syringe to remove the resin and lyophilized.

6.3.5 Peptide Purification

The peptides were redissolved in water and acetonitrile containing 0.1% TFA, filtered through a 0.22 µm nylon filter and purified by mass-directed semi-preparative reversed-phase HPLC. Solvent A was water with 0.1% TFA additive and Solvent B was acetonitrile with 0.1% TFA additive. A linear gradient that changed at a rate of 0.5%/min was used. Most of the peptides were purified on an Agilent Zorbax SB C3 column: 9.4 x 250 mm, 5 µm. Extremely hydrophilic peptides, such as the arginine-rich sequences were purified on an Agilent Zorbax SB C18 column: 9.4 x 250 mm, 5 µm. Using mass data about each fraction from the instrument, only pure fractions were pooled and lyophilized. The purity of the fraction pool was confirmed by LC-MS.

6.3.6 PMO-Azide Synthesis

PMO IVS-654 (200 mg, 32 µmol) was dissolved in 600 µL DMSO. To the solution was added a solution containing 4 equivalents of 5-azidopentanoic acid (13.6 µL, 128 µmol) activated with HBTU (320 µL of 0.4 M HBTU in DMF, 128 µmol) and DIEA (22.3 µL, 128 µmol) in 244 µL DMF (Final reaction volume = 1.2 mL). The reaction proceeded for 25 min before being quenched with 1 mL of water and 2 mL of ammonium hydroxide. The ammonium hydroxide will hydrolyze any ester formed during the course of the reaction. After 1 hour, the solution was diluted to 40 mL and purified using reversed-phase HPLC (Agilent Zorbax SB C3 column: 21.2 x 100 mm, 5 µm) and a linear gradient from 2 to 60% B (solvent A: water; solvent B: acetonitrile) over 58 min (1% B / min). Using mass data about each fraction from the

instrument, only pure fractions were pooled and lyophilized. The purity of the fraction pool was confirmed by LC-MS.

6.3.7 PMO-Peptide Conjugation with Cu(I)-Catalyzed Azide-Alkyne Cycloaddition

PMO-peptide conjugates were synthesized using Cu(I)-catalyzed azide-alkyne 1,3-dipolar cycloaddition using copper(I) bromide in DMF. PMO-azide (0.95 µmol), Peptide-alkyne (1.1 µmol), and copper(I) bromide (0.05 mmol) powders were added to a septum vial (note: the amount of PMO-azide ranged from 0.63-0.95 µmol). The vial was flushed with N_2 for 2 min, 1 mL dry DMF was added, and the vial was vortexed. The reaction was allowed to proceed for 1 hour. The reaction was quenched with the addition of 10 mL of 50 mM Tris in water (pH 8).

Our optimized purification procedure was using reversed-phase HPLC with a linear gradient from 5-45% B over 20 min (Agilent Zorbax SB C3 9.4 x 50 mm, 5 µm). Mobile phase A: 100 mM ammonium acetate pH 7.2 in water. Mobile phase B: acetonitrile. Using mass data about each fraction from the instrument, only pure fractions were pooled and lyophilized. The purity of the fraction pool was confirmed by LC-MS.

6.3.8 Fluorophore Conjugation

For fluorophore-labeled PMO-peptide conjugates, the organic dye was attached prior to conjugation to PMO. Equimolar SulfoCy5-maleimide was conjugated to cysteine-containing peptides in 1 mL of H_2O. After 30 minutes, the reactions were purified by reversed-phase HPLC using a linear gradient from 5-45% B over 80 minutes for pVEC and pVEC-Bpep and a linear gradient from 1-31% B over 60 minutes for Bpep. Mobile phase A: water with 0.1% TFA. Mobile phase B: acetonitrile with 0.1% TFA. For LC-MS characterization of SulfoCy5-peptide conjugates, please see the Supplementary Information.

6.3.9 Flow Cytometry

HeLa-654 cells were maintained in MEM supplemented with 10% (v/v) fetal bovine serum (FBS) and 1% (v/v) penicillin-streptomycin at 37 °C and 5% CO_2. Eighteen hours prior to treatment, the cells were plated at a density of 5,000 cells per well in a 96-well plate in MEM supplemented with 10% FBS and 1% penicillin-streptomycin. The day of the experiment, stocks of each PMO-peptide conjugate were prepared in phosphate-buffered saline (PBS) (Note: for experiments with PMO-SulfoCy5-peptide conjugates, the procedure was similar but the stocks were prepared in dimethylsulfoxide – see supporting information for details). The concentration of the stocks was determined by measuring the absorbance at 260 nm and using an extinction coefficient of 168,700 L mol^{-1} cm^{-1}. Cells were incubated with each respective conjugate at a concentration of 5 µM (unless otherwise indicated) in MEM supplemented with

10% FBS and 1% penicillin-streptomycin for 22 hours at 37 °C and 5% CO_2. Next, the treatment media was aspirated, the cells were incubated with Trypsin-EDTA 0.25 % for 15 min at 37 °C and 5% CO_2, washed 1x with PBS, and resuspended in PBS with 2% FBS and 2 µg/mL propidium iodide. The PMO-CPPs in Figure 6.2A were tested at Sarepta Therapeutics and all remaining experiments were performed at MIT on a BD LSRII flow cytometer using HeLa-654 cells obtained from the University of North Carolina Tissue Culture Core facility. Gates were applied to the data to ensure that cells that were highly positive for propidium iodide or had forward/side scatter readings that were sufficiently different from the main cell population were excluded. Each histogram contains at least 3,000 gated events, with the exception of cells treated with PMO-Melittin-Bpep and several of the 25 µM treatments.

6.3.10 LDH Assay

HeLa-654 cells were maintained in MEM supplemented with 10% (v/v) fetal bovine serum and 1% (v/v) penicillin-streptomycin at 37 °C and 5% CO_2. Eighteen hours before treatment, HeLa cells were plated at a density of 5,000 cells per well in a 96-well plate. The next day, fresh 1 mM stocks of each of PMO-peptide conjugate were prepared in PBS. The concentration of the stocks was determined by measuring the absorbance at 260 nm and using an extinction coefficient of 168,700 L mol^{-1} cm^{-1}. The growth media was aspirated from the cells and treatment media was added with each respective conjugate at either a concentration of 5 µM (Fig. S3) or concentrations of 0.2, 1, 5, 10 and 25 µM (Fig. S4) in MEM supplemented with 10% FBS and 1% penicillin-streptomycin. The cells were incubated with treatment-containing media for 22 hours at 37 °C and 5% CO_2. Next, the supernatant treatment media was transferred to another clear-bottom 96-well plate for the assay. The assay was performed using the CytoTox 96® Non-Radioactive Cytotoxicity Assay (Promega) according to the included technical bulletin. After completion of the assay, the final solution in each well was diluted 1:4 with PBS such that the measured absorbance was in the linear range of the instrument. The absorbance was measured on a BioTek Epoch Microplate Spectrophotometer at 490 nm. The positive control is a cell lysis and the negative control is untreated cells. The data are worked up by subtracting the absorbance of untreated cells from all of the treatment conditions, including the cell lysis, and then dividing by the corrected lysis value. A value of 0 reflects no additional LDH release over cell baseline and a value of 1 reflects total LDH release.

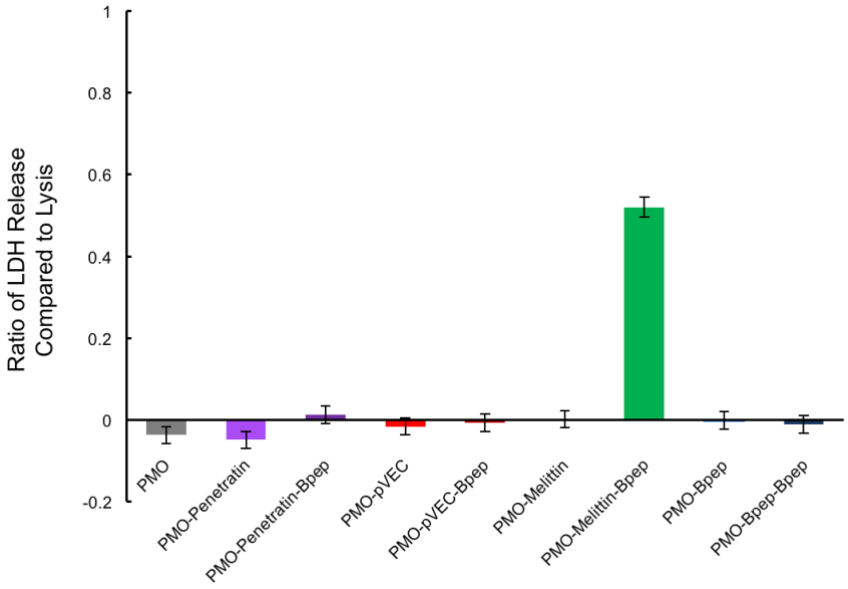

Figure 6.7. LDH Release from HeLa-654 Cells upon Treatment with 5 μM PMO-peptide conjugate. HeLa-654 cells were treated with each construct at 5 μM for twenty-two hours. The y-axis is the ratio of LDH release compared with the cell lysis control. The only construct that demonstrated compromise of the cell membrane and early signs of cytotoxicity was PMO-Melittin-Bpep. Error bars correspond to a standard deviation of a technical triplicate.

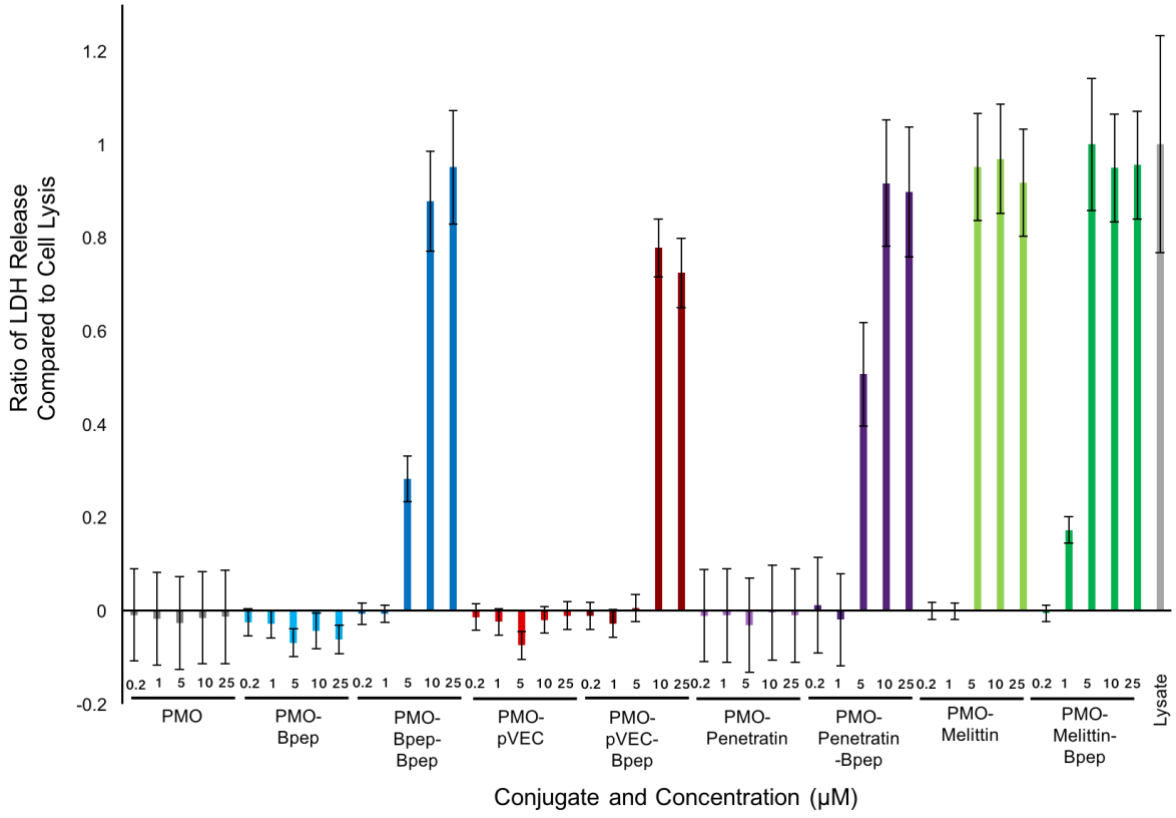

Figure 6.8. LDH Release from HeLa-654 Cells upon Treatment with PMO-peptide conjugates across a range of concentrations. HeLa-654 cells were treated with each construct

at 0.2, 1, 5, 10, or 25 μM for 22 h. Shown is ratio of LDH release relative to a cell lysis control and normalized to an untreated control for PMO-pVEC-BPEP, PMO-penetratin-Bpep, PMO-melittin-Bpep, PMO-Bpep-Bpep, their corresponding component PMO-CPPs, and unmodified PMO. Error bars correspond to a standard deviation of a technical triplicate.

6.3.11 Inhibitor Experiments

To interrogate endocytic mechanism, we performed pulse-chase experiment with a panel of endocytosis inhibitors including: chlorpromazine, which is demonstrated to interfere with clathrin-mediated endocytosis (CME); cytochalasin D, which inhibits phagocytosis and micropinocytosis; wortmannin, which alters various endocytosis pathways by inhibiting phosphatidylinositol kinases; EIPA (5-(N-ethyl-Nisopropyl) amiloride), which inhibits micropinocytosis; and Dynasore, which also inhibits CME.[299,322] HeLa-654 cells were plated at a density of 5,000 cells per well in a 96-well plate in MEM supplemented with 10% FBS and 1% penicillin-streptomycin. The next day, the cells were treated with each inhibitor at the concentration indicated on the graph (Figure 6.9). The stock solutions used for each inhibitor were as follows: chlorpromazine - 10 mM in water; cytochalasin D - 10 mM in DMSO; wortmannin - 2 mM in DMSO; EIPA - 10 mM in DMSO; dynasore - 10 mM in DMSO. After 30 min, PMO-peptide conjugate was added to each well at a concentration of 5 μM. After incubation at 37 °C and 5% CO_2 for 3 hours, the treatment media was replaced with fresh media (containing neither inhibitor nor PMO-peptide) and the cells were allowed to grow for another 22 hours at 37 °C and 5% CO_2. Sample preparation and flow cytometry was then performed as described in the main text. Each histogram contains at least 3,000 gated events, with the exception of treatment with 20 μM cytochalasin D.

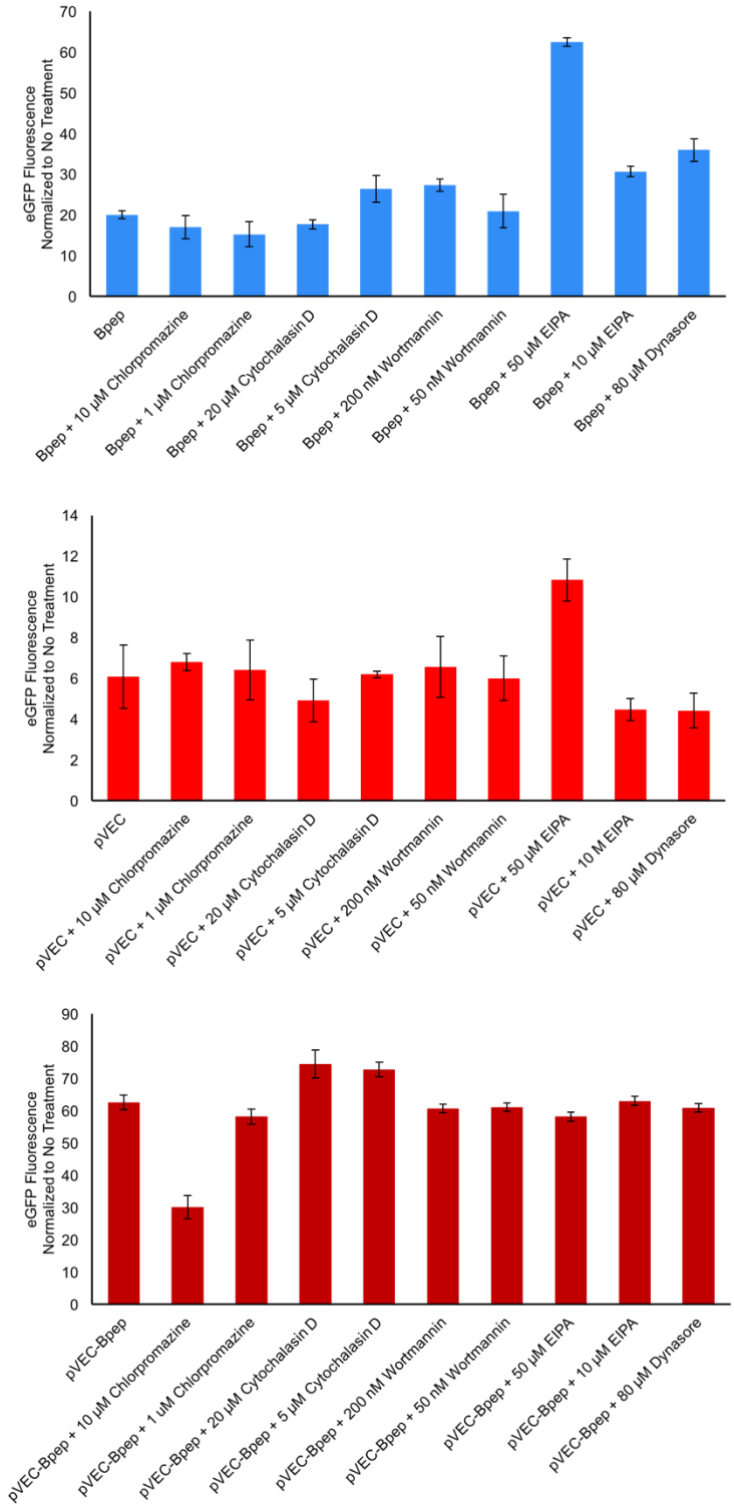

Figure 6.9. Effect of endocytosis inhibitors on PMO-Bpep, PMO-pVEC, and PMO-pVEC-Bpep efficacy. HeLa-654 cells were treated with each inhibitor in a pulse-chase experiment as described in the main text. After treatment, the mean fluorescence intensity of eGFP is measured by flow cytometry and the fold change in eGFP fluorescence with respect to the untreated control is calculated. Bpep, pVEC, and pVEC-Bpep are used as shorthand for the

PMO-Bpep, PMO-pVEC and PMO-pVEC-Bpep conjugates. EIPA is 5-(N-Ethyl-N-isopropyl)amiloride. Error bars correspond to a standard deviation of a technical triplicate.

6.3.12 Flow cytometry assay with fluorophore-labeled conjugates

HeLa-654 cells were maintained in MEM supplemented with 10% (v/v) fetal bovine serum and 1% (v/v) penicillin-streptomycin at 37 °C and 5% CO_2. Twenty-four hours before treatment, HeLa cells were plated at a density of 5,000 cells per well in a 96-well plate. The next day, fresh 1 mM stocks of each of the SulfoCy5-PMO-peptide conjugates in DMSO, as well as the respective unlabeled PMO-peptide controls in DMSO, were prepared. The concentration of the stocks was determined by measuring the absorbance at 260 nm and using an extinction coefficient of 168,700 L mol^{-1} cm^{-1}. The growth media was aspirated from the cells and treatment media consisting of each respective conjugate 5 µM concentration in MEM supplemented with 10% FBS and 1% penicillin-streptomycin was added. The cells were incubated with treatment-containing media for 22 hours at 37 °C and 5% CO_2. Next, the treatment media was aspirated. Trypsin-EDTA 0.25 % (20 µL) was added to the cells and incubated for 15 min at 37 °C and 5% CO_2. To quench the trypsin, 80 µL of MEM supplemented with 10% (v/v) fetal bovine serum and 1% (v/v) Pen Strep was added to each well. The dissociated cells in media were transferred with a multichannel pipet to a polypropylene v-bottom 96-well plate (Falcon) and centrifuged at 500 rcf for 3 min. The supernatant was removed, the cell pellets were resuspended with 200 µL of phosphate-buffered saline (PBS), and the plate was centrifuged again. The supernatant was again removed and the pellets were resuspended in 300 µL PBS with 2% FBS (v/v) and 2 µg/mL propidium iodide in water. Flow cytometry analysis was carried out on a BD LSRII flow cytometer. For eGFP fluorescence, the 488 nm excitation laser and 530 nm emission filter were used, and for the SulfoCy5, the 561 nm excitation laser and 695 nm emission filter were used. The separation of channels enabled fluorescence from both fluorophores to be simultaneously recorded. Gates were applied to the data to ensure that only data from healthy, living cells were taken into account. Cells that were highly positive for propidium iodide or had forward/side scatter readings that were sufficiently different from the main cell population were excluded. Each histogram contained at least 3,000 gated events.

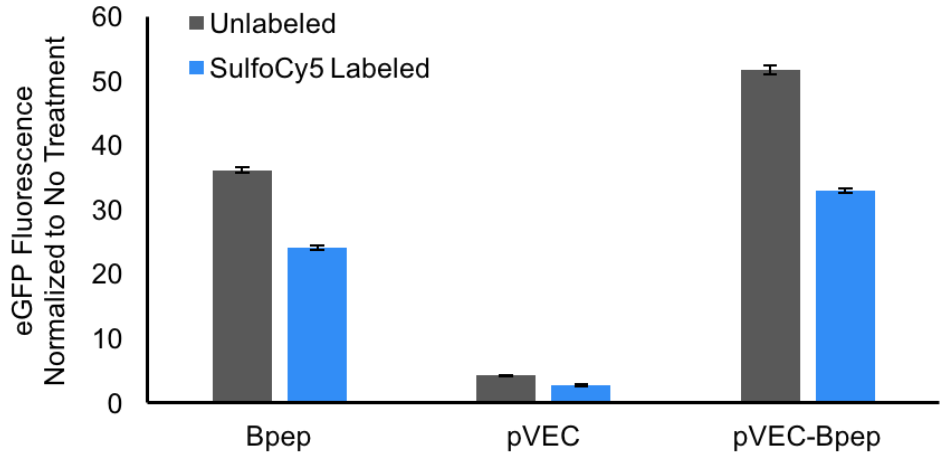

Figure 6.10. Comparison of PMO activity of unlabeled PMO-peptide conjugates with SulfoCy5-labeled PMO-peptide conjugates. The original unlabeled PMO-peptide conjugates were run side-by-side in the flow cytometry assay with the Sulfo-Cy5-labeled PMO-peptide conjugates to determine the extent to which SulfoCy5 perturbs the effect of the conjugates. In all cases, eGFP fluorescence was slightly decreased with SulfoCy5 attached, suggesting that while the fluorophore may affect the efficacy of the conjugate, it does so in a relatively uniform fashion. Error bars correspond to a standard deviation of a technical triplicate.

6.3.13 Live-Cell Confocal Imaging

HeLa-654 cells were plated at a density of 5,000 cells per well in a #1.5 coverslip glass-bottom 96-well plate in MEM supplemented with 10% (v/v) fetal bovine serum and 1% (v/v) penicillin-streptomycin. The next day, fresh 1 mM stocks of each PMO-SulfoCy5-peptide conjugate were prepared in DMSO. The concentration of the stocks was determined by measuring the absorbance at 260 nm and using an extinction coefficient of 168,700 L mol^{-1} cm^{-1}. Twenty-four hours after plating, the growth media was aspirated and the cells were treated with media containing each PMO-SulfoCy5-peptide conjugate at a concentration of 5 µM in MEM supplemented with 10% FBS and 1% penicillin-streptomycin. Six hours after that (sixteen hours prior to imaging), 3 µL of CellLight™ Early Endosomes-RFP, BacMam 2.0 was added to each well (corresponding to 30 particles per cell). After 22 hours of total PMO treatment, the treatment media was aspirated, the cells were washed twice with PBS (5 min for each wash), and the cells were stained for 10 min with 2 µg/mL Hoechst in PBS followed by two more PBS washes (5 min for each wash). Finally, the cells were imaged in PBS on a spinning disk confocal microscope composed of a Yokogawa CSU-22 spinning disk confocal scan head with Borealis modification, Zeiss AxioVert 200M inverted microscope stand with

DIC optics, six lasers, a Hamamatsu Orca-ER cooled CCD camera, and MetaMorph acquisition software. The images were acquired with the 63x objective and processed using ImageJ software (http://imagej.net/Fiji). The complete set of images can be found in Section 6.7. 2.

Co-localization was quantified in terms of the Mander's Co-localization Coefficient of SulfoCy5 fluorescence ($MCC_{SulfoCy5}$) with respect to fluorescence from the Rab5a-RFP fusion protein. The $MCC_{SulfoCy5}$ obtained for a given image thus corresponds to the proportion of the total SulfoCy5-labeled construct that co-localizes with RFP-labeled early endosomes. This value is represented according to the following equation:

$$MCC_{SulfoCy5} = \frac{\sum_i S_{i,coloc}}{\sum_i S_i}$$

Where S_i is the SulfoCy5 signal for a given pixel and $S_{i,coloc}$ is the SulfoCy5 signal of a pixel that also contains above-threshold RFP fluorescence.[33] $MCC_{SulfoCy5}$ values for each image were calculated using ImageJ, with manual thresholding to determine the regions of interest corresponding to RFP fluorescence. Images deemed unsuitable because of a low signal/background ratio were excluded. The remaining values were averaged to determine the $MCC_{SulfoCy5}$ for PMO-SulfoCy5-pVEC (0.4 ± 0.1) and PMO-SulfoCy5-pVEC-Bpep (0.4 ± 0.2), reported with an error of one standard deviation. Too few images were deemed suitable for analysis for PMO-SulfoCy5-Bpep to calculate the $MCC_{SulfoCy5}$.

To quantify the amount of nuclear SulfoCy5 fluorescence, the nuclear regions were first outlined in ImageJ. Next, the mean SulfoCy5 fluorescence intensity for these regions was calculated in ImageJ. To avoid quantifying punctate signal, a threshold intensity was set to exclude pixels with an intensity greater than 20. The process was repeated for 10-20 cells for each construct and the results were plotted using GraphPad Prism (Figure 6.11).

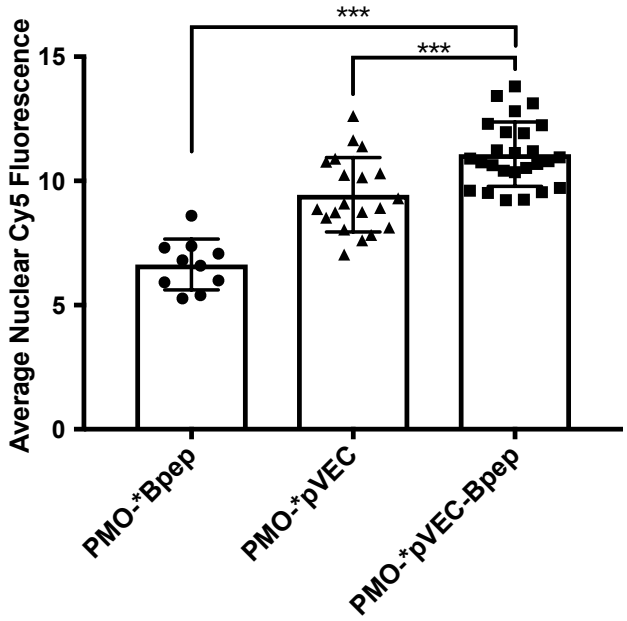

Figure 6.11. PMO-SulfoCy5-pVEC-Bpep exhibits the most nuclear SulfoCy5 fluorescence. HeLa-654 cells were treated with each construct at 5 μM for twenty-two hours. The cells were then imaged by confocal microscopy and the SulfoCy5 fluorescence in the nuclear regions were quantified. The graph shows standard deviation error bars, and statistical analyses were performed using the one-way ANOVA and Tukey's multiple comparison test (***P<0.001).

6.3.14 Melting Temperature Analysis

The melting temperature for dissociation of PMO from its complementary sequence was measured for the unmodified PMO, PMO-pVEC, PMO-Bpep, and PMO-pVEC-Bpep to assess binding. Each construct was incubated with its complementary DNA strand (Integrated DNA Technologies) in PBS for 30 minutes at room temperature (50 μM each, 20 μL total volume). An intercalating fluorescent dye (EvaGreen, Biotium) was then added and samples were incubated for 30 minutes at room temperature. A melting experiment was performed using a quantitative real-time PCR machine (BioRad CFX96 Real-Time System) by increasing the temperature from 40 °C to 100 °C in 0.5 °C increments. Fluorescence at 520 nm was measured at each increment, with PMO/DNA melting corresponding to a decrease in fluorescence. Melting temperature (T_m) was calculated from three experimental replicates.

A derivative plot was then obtained for each melting curve, in which the y-values were calculated according to the following equation:

$$y_i = \frac{dD_i}{dT_i} = \frac{(T_i) - D(T_{i-1})}{T_i - T_{i-1}}$$

D(Ti) represents the percent dissociation at temperature *Ti*. These y-values were then plotted against the corresponding temperatures to obtain a derivative plot for each melting curve (Figure 6.12). The *Tm* for each construct was then obtained by determining the temperature corresponding to the maximum of the relevant derivative plot.

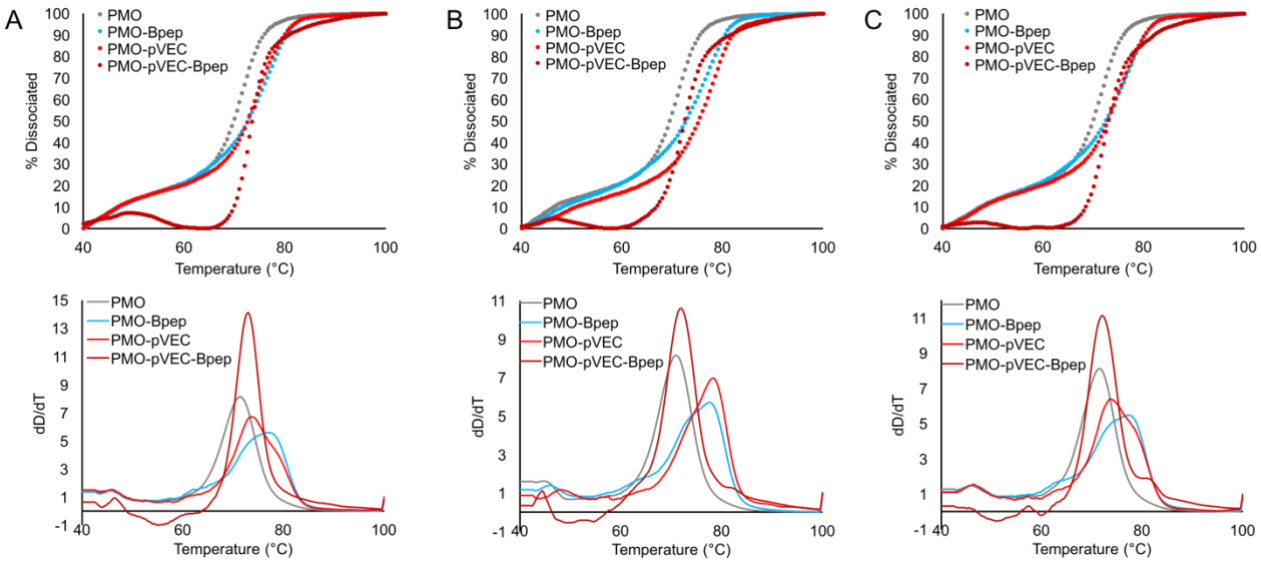

Figure 6.12. Peptide conjugation has a minor impact on PMO binding to its target sequence. Melting curves were obtained for the unmodified PMO, PMO-Bpep, PMO-pVEC, and PMO-pVEC-Bpep annealed to the complementary DNA sequence. Melting was monitored via fluorescence decrease of an intercalating dye. Fluorescence measurements were then normalized and converted to percent dissociated. The derivative of each melting curve, represented by dD/dT, was then determined and plotted with respect to temperature. Shown are the melting curves and corresponding derivative plots for each of three experimental replicates given in A, B, and C.

6.3.15 Structural Prediction

Structures of the CPPs Penetratin, pVEC, and Melittin were predicted using the online PepFold prediction tool (http://bioserv.rpbs.univ-paris-diderot.fr/services/PEP-FOLD/).[34,35] This tool provides the probability of the presence of three structural elements along the amino acid sequence of a given peptide: helical, extended, and coiled. It also provides several possible structures for each input sequence. Plots showing the probability of each structural element as well as the most likely structure for each CPP are shown in Figure 6.13. These predictions suggest that, in solution, each CPP may have some helical character with varying levels of extended and coiled regions. However, these results should be interpreted with several caveats: this tool cannot predict non-natural amino acids, so sequences containing non-natural amino

acids like Bpep and the full-length chimeras cannot be included in these structural predictions; the PMO, which constitutes a significant component of our conjugates, is likewise excluded; and finally, these predictions only relate to the CPPs in solution and do not include interaction with the cell and/or endosomal membrane, which could significantly alter their structure. These structures should therefore be interpreted as a rough first approximation of the structure of our PMO-peptide conjugates.

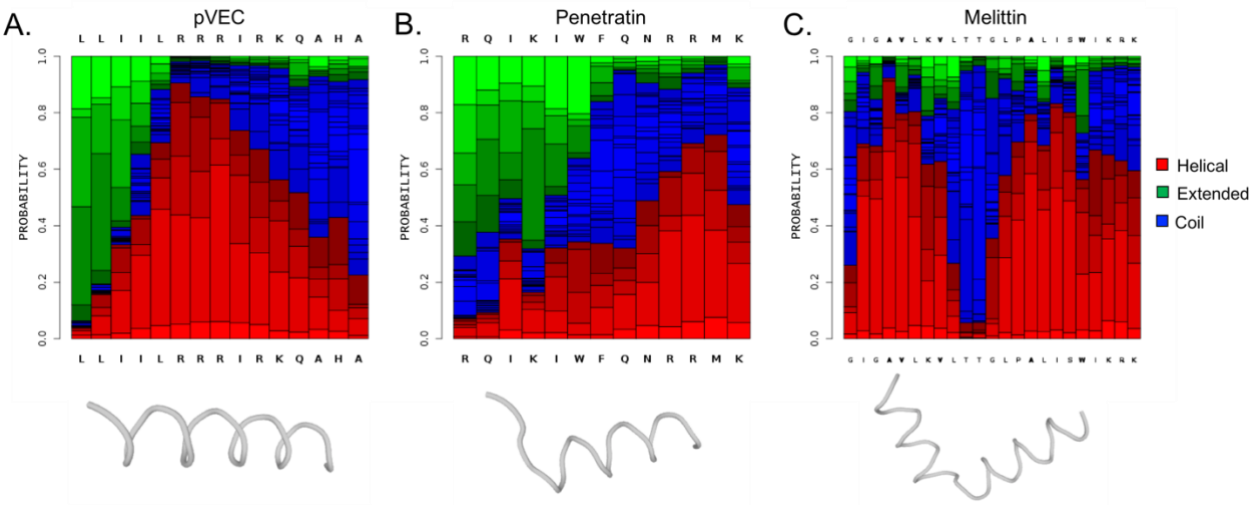

Figure 6.13. CPPs are predicted to contain significant helical character, with coiled and extended elements. The online tool PepFold was used to predict the structures of the component CPPs used to design our chimeric CPPs, with the exception of Bpep.[33,34] The structural predictions results shown include a graph displaying the probability of helical (red), extended (green), or coiled (blue) structural motifs at each amino acid along the CPP's sequence as well as a cartoon representation of the top predicted structure for **A)** pVEC, **B)** Penetratin, and **C)** Melittin.

6.4 Acknowledgements and Conflict Statements

The authors acknowledge the Swanson Biotechnology Center Flow Cytometry Facility at the Koch Institute for advice and the use of their flow cytometers. The authors also acknowledge Wendy Salmon and the W.M. Keck Biological Imaging Facility at the Whitehead Institute for advice and the use of their confocal microscope. We thank Dr. Daniel Chinnapen for his advice on image analysis. We thank Christine Isabella and Prof. Laura Kiessling for assistance with the melting temperature experiments and use of their qPCR instrument. We thank Dr. Ethan Evans and Dr. Alan Beggs for helpful discussions.

This work was supported by Sarepta Therapeutics, Cambridge MA. J.M.W. and R.L.H are supported by the National Science Foundation Graduate Research Fellowship under Grant No. 1122374. C.M.F. is supported by the David H. Koch Graduate Fellowship Fund and by the Eunice Kennedy Shriver National Institute of Child Health and Human Development of the National Institutes of Health under award number F30HD093358.

The authors declare the following competing financial interest(s): GJH and MY are employees of Sarepta Therapeutics.

6.5 References

(1) Lim, K. R. Q.; Maruyama, R.; Yokota, T. Eteplirsen in the Treatment of Duchenne Muscular Dystrophy. *Drug Des Devel Ther* **2017**, *11*, 533–545. https://doi.org/10.2147/DDDT.S97635.

(2) Summerton, J.; Weller, D. Morpholino Antisense Oligomers: Design, Preparation, and Properties. *Antisense and Nucleic Acid Drug Development* **1997**, *7* (3), 187–195. https://doi.org/10.1089/oli.1.1997.7.187.

(3) Youngblood, D. S.; Hatlevig, S. A.; Hassinger, J. N.; Iversen, P. L.; Moulton, H. M. Stability of Cell-Penetrating Peptide−Morpholino Oligomer Conjugates in Human Serum and in Cells. *Bioconjugate Chem.* **2007**, *18* (1), 50–60. https://doi.org/10.1021/bc060138s.

(4) Hudziak, R. M.; Barofsky, E.; Barofsky, D. F.; Weller, D. L.; Huang, S.-B.; Weller, D. D. Resistance of Morpholino Phosphorodiamidate Oligomers to Enzymatic Degradation. *Antisense and Nucleic Acid Drug Development* **1996**, *6* (4), 267–272. https://doi.org/10.1089/oli.1.1996.6.267.

(5) Chan, J. H.; Lim, S.; Wong, W. F. Antisense Oligonucleotides: From Design to Therapeutic Application. *Clinical and Experimental Pharmacology and Physiology* **2006**, *33* (5–6), 533–540. https://doi.org/10.1111/j.1440-1681.2006.04403.x.

(6) Hammond, S. M.; Hazell, G.; Shabanpoor, F.; Saleh, A. F.; Bowerman, M.; Sleigh, J. N.; Meijboom, K. E.; Zhou, H.; Muntoni, F.; Talbot, K.; Gait, M. J.; Wood, M. J. A. Systemic Peptide-Mediated Oligonucleotide Therapy Improves Long-Term Survival in Spinal Muscular Atrophy. *Proc. Natl. Acad. Sci. U.S.A.* **2016**, *113* (39), 10962–10967. https://doi.org/10.1073/pnas.1605731113.

(7) Betts, C.; Saleh, A. F.; Arzumanov, A. A.; Hammond, S. M.; Godfrey, C.; Coursindel, T.; Gait, M. J.; Wood, M. J. Pip6-PMO, A New Generation of Peptide-Oligonucleotide Conjugates With Improved Cardiac Exon Skipping Activity for DMD Treatment. *Mol Ther Nucleic Acids* **2012**, *1* (8), e38. https://doi.org/10.1038/mtna.2012.30.

(8) Moulton, H. M.; Nelson, M. H.; Hatlevig, S. A.; Reddy, M. T.; Iversen, P. L. Cellular Uptake of Antisense Morpholino Oligomers Conjugated to Arginine-Rich Peptides. *Bioconjugate Chem.* **2004**, *15* (2), 290–299. https://doi.org/10.1021/bc034221g.

(9) Wu, R. P.; Youngblood, D. S.; Hassinger, J. N.; Lovejoy, C. E.; Nelson, M. H.; Iversen, P. L.; Moulton, H. M. Cell-Penetrating Peptides as Transporters for Morpholino Oligomers: Effects of Amino Acid Composition on Intracellular Delivery and Cytotoxicity. *Nucleic Acids Res* **2007**, *35* (15), 5182–5191. https://doi.org/10.1093/nar/gkm478.

(10) Moulton, H. M.; Moulton, J. D. Morpholinos and Their Peptide Conjugates: Therapeutic Promise and Challenge for Duchenne Muscular Dystrophy. *Biochimica et Biophysica*

Acta (BBA) - Biomembranes **2010**, *1798* (12), 2296–2303. https://doi.org/10.1016/j.bbamem.2010.02.012.
(11) Wu, B.; Moulton, H. M.; Iversen, P. L.; Jiang, J.; Li, J.; Li, J.; Spurney, C. F.; Sali, A.; Guerron, A. D.; Nagaraju, K.; Doran, T.; Lu, P.; Xiao, X.; Lu, Q. L. Effective Rescue of Dystrophin Improves Cardiac Function in Dystrophin-Deficient Mice by a Modified Morpholino Oligomer. *PNAS* **2008**, *105* (39), 14814–14819. https://doi.org/10.1073/pnas.0805676105.
(12) *Cell-Penetrating Peptides*; Langel, Ü., Ed.; Methods in Molecular Biology; Humana Press: Totowa, NJ, 2011; Vol. 683.
(13) Copolovici, D. M.; Langel, K.; Eriste, E.; Langel, Ü. Cell-Penetrating Peptides: Design, Synthesis, and Applications. *ACS Nano* **2014**, *8* (3), 1972–1994. https://doi.org/10.1021/nn4057269.
(14) Eiríksdóttir, E.; Konate, K.; Langel, Ü.; Divita, G.; Deshayes, S. Secondary Structure of Cell-Penetrating Peptides Controls Membrane Interaction and Insertion. *Biochimica et Biophysica Acta (BBA) - Biomembranes* **2010**, *1798* (6), 1119–1128. https://doi.org/10.1016/j.bbamem.2010.03.005.
(15) Thorén, P. E. G.; Persson, D.; Esbjörner, E. K.; Goksör, M.; Lincoln, P.; Nordén, B. Membrane Binding and Translocation of Cell-Penetrating Peptides. *Biochemistry* **2004**, *43* (12), 3471–3489. https://doi.org/10.1021/bi0360049.
(16) Lundin, P.; Johansson, H.; Guterstam, P.; Holm, T.; Hansen, M.; Langel, Ü.; EL Andaloussi, S. Distinct Uptake Routes of Cell-Penetrating Peptide Conjugates. *Bioconjugate Chem.* **2008**, *19* (12), 2535–2542. https://doi.org/10.1021/bc800212j.
(17) Kosuge, M.; Takeuchi, T.; Nakase, I.; Jones, A. T.; Futaki, S. Cellular Internalization and Distribution of Arginine-Rich Peptides as a Function of Extracellular Peptide Concentration, Serum, and Plasma Membrane Associated Proteoglycans. *Bioconjugate Chem.* **2008**, *19* (3), 656–664. https://doi.org/10.1021/bc700289w.
(18) Tünnemann, G.; Martin, R. M.; Haupt, S.; Patsch, C.; Edenhofer, F.; Cardoso, M. C. Cargo-Dependent Mode of Uptake and Bioavailability of TAT-Containing Proteins and Peptides in Living Cells. *FASEB J* **2006**, *20* (11), 1775–1784. https://doi.org/10.1096/fj.05-5523com.
(19) Madani, F.; Lindberg, S.; Langel, Ü.; Futaki, S.; Gräslund, A. Mechanisms of Cellular Uptake of Cell-Penetrating Peptides https://www.hindawi.com/archive/2011/414729/ (accessed Dec 11, 2017). https://doi.org/10.1155/2011/414729.
(20) Duchardt, F.; Fotin-Mleczek, M.; Schwarz, H.; Fischer, R.; Brock, R. A Comprehensive Model for the Cellular Uptake of Cationic Cell-Penetrating Peptides. *Traffic* **2007**, *8* (7), 848–866. https://doi.org/10.1111/j.1600-0854.2007.00572.x.
(21) Mayor, S.; Pagano, R. E. Pathways of Clathrin-Independent Endocytosis. *Nature Reviews Molecular Cell Biology* **2007**, *8* (8), 603. https://doi.org/10.1038/nrm2216.
(22) Yin, H.; Boisguerin, P.; Moulton, H. M.; Betts, C.; Seow, Y.; Boutilier, J.; Wang, Q.; Walsh, A.; Lebleu, B.; Wood, M. J. Context Dependent Effects of Chimeric Peptide Morpholino Conjugates Contribute to Dystrophin Exon-Skipping Efficiency. *Mol Ther Nucleic Acids* **2013**, *2* (9), e124. https://doi.org/10.1038/mtna.2013.51.
(23) Abes, S.; Turner, J. J.; Ivanova, G. D.; Owen, D.; Williams, D.; Arzumanov, A.; Clair, P.; Gait, M. J.; Lebleu, B. Efficient Splicing Correction by PNA Conjugation to an R6-Penetratin Delivery Peptide. *Nucleic Acids Res* **2007**, *35* (13), 4495–4502. https://doi.org/10.1093/nar/gkm418.
(24) Yin, H.; Moulton, H. M.; Seow, Y.; Boyd, C.; Boutilier, J.; Iverson, P.; Wood, M. J. A. Cell-Penetrating Peptide-Conjugated Antisense Oligonucleotides Restore Systemic Muscle and Cardiac Dystrophin Expression and Function. *Hum Mol Genet* **2008**, *17* (24), 3909–3918. https://doi.org/10.1093/hmg/ddn293.

(25) Elmquist, A.; Lindgren, M.; Bartfai, T.; Langel U, null. VE-Cadherin-Derived Cell-Penetrating Peptide, PVEC, with Carrier Functions. *Exp. Cell Res.* **2001**, *269* (2), 237–244. https://doi.org/10.1006/excr.2001.5316.
(26) Derossi, D.; Joliot, A. H.; Chassaing, G.; Prochiantz, A. The Third Helix of the Antennapedia Homeodomain Translocates through Biological Membranes. *J. Biol. Chem.* **1994**, *269* (14), 10444–10450.
(27) Terwilliger, T. C.; Eisenberg, D. The Structure of Melittin. II. Interpretation of the Structure. *J. Biol. Chem.* **1982**, *257* (11), 6016–6022.
(28) Mijalis, A. J.; Thomas Iii, D. A.; Simon, M. D.; Adamo, A.; Beaumont, R.; Jensen, K. F.; Pentelute, B. L. A Fully Automated Flow-Based Approach for Accelerated Peptide Synthesis. *Nat Chem Biol* **2017**, *13* (5), 464–466. https://doi.org/10.1038/nchembio.2318.
(29) Dutta, D.; Donaldson, J. G. Search for Inhibitors of Endocytosis. *Cell Logist* **2012**, *2* (4), 203–208. https://doi.org/10.4161/cl.23967.
(30) Gryaznov, S. M.; Lloyd, D. H.; Chen, J. K.; Schultz, R. G.; DeDionisio, L. A.; Ratmeyer, L.; Wilson, W. D. Oligonucleotide N3'-->P5' Phosphoramidates. *PNAS* **1995**, *92* (13), 5798–5802. https://doi.org/10.1073/pnas.92.13.5798.
(31) Jensen, K. K.; Orum, H.; Nielsen, P. E.; Nordén, B. Kinetics for Hybridization of Peptide Nucleic Acids (PNA) with DNA and RNA Studied with the BIAcore Technique. *Biochemistry* **1997**, *36* (16), 5072–5077. https://doi.org/10.1021/bi9627525.
(32) Kjeken, R.; Mousavi, S. A.; Brech, A.; Griffiths, G.; Berg, T. Wortmannin-Sensitive Trafficking Steps in the Endocytic Pathway in Rat Liver Endothelial Cells. *Biochem. J.* **2001**, *357* (Pt 2), 497–503.
(33) Thévenet, P.; Shen, Y.; Maupetit, J.; Guyon, F.; Derreumaux, P.; Tufféry, P. PEP-FOLD: An Updated de Novo Structure Prediction Server for Both Linear and Disulfide Bonded Cyclic Peptides. *Nucleic Acids Res.* **2012**, *40* (Web Server issue), W288-293. https://doi.org/10.1093/nar/gks419.
(34) Shen, Y.; Maupetit, J.; Derreumaux, P.; Tufféry, P. Improved PEP-FOLD Approach for Peptide and Miniprotein Structure Prediction. *J Chem Theory Comput* **2014**, *10* (10), 4745–4758. https://doi.org/10.1021/ct500592m.

6.7 Appendix

6.7.1 LC-MS Characterization

Note: Chromatograms were obtained using Method B from 6.3.2 unless otherwise noted.

PMO-Azide
Mass expected: 6337.5 Da
Mass observed: 6337.9 Da

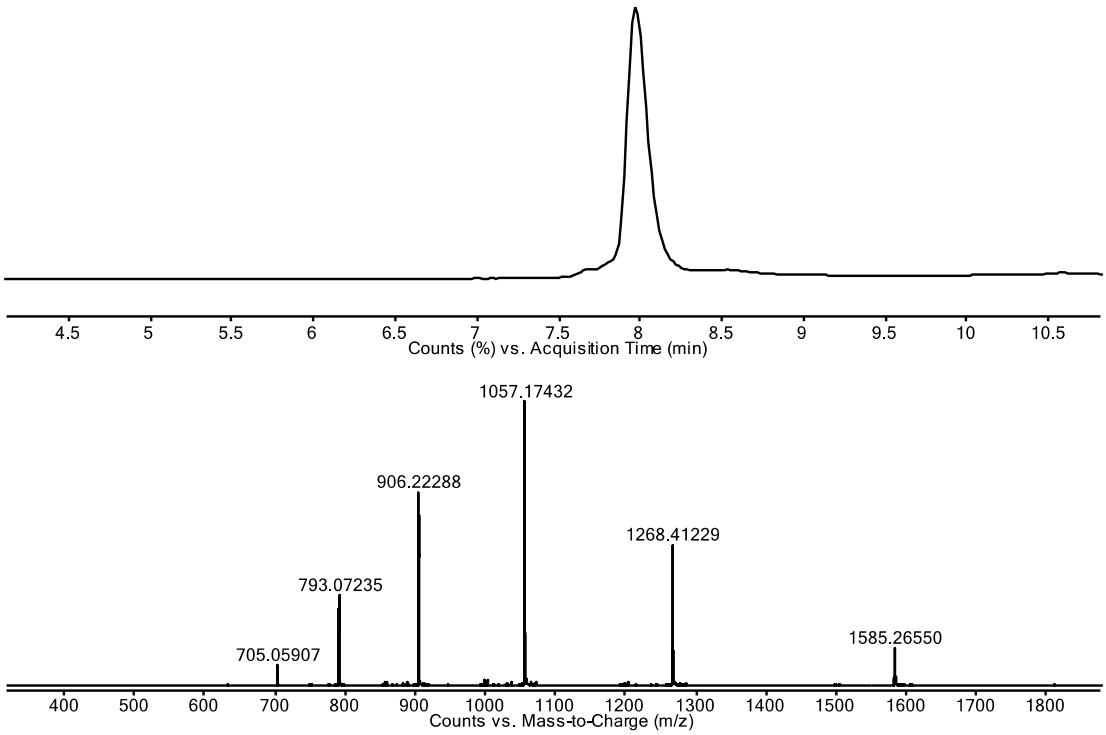

PMO-Bpep
Mass Expected: 8052.5 Da
Mass Observed: 8053.0 Da
Peptide Sequence: RXRRBRRXRRBR

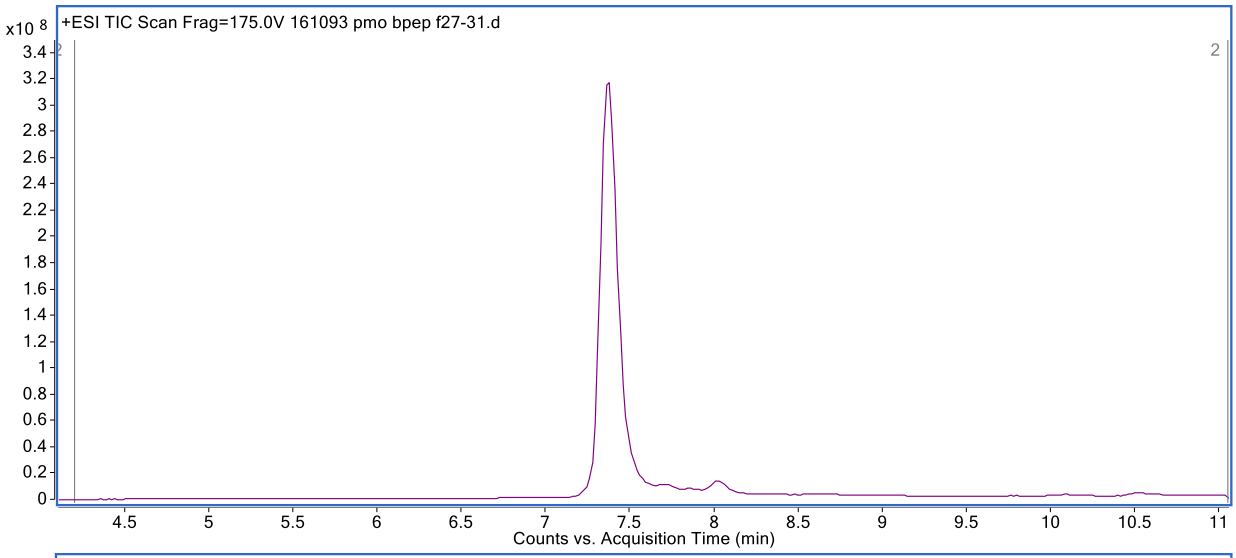

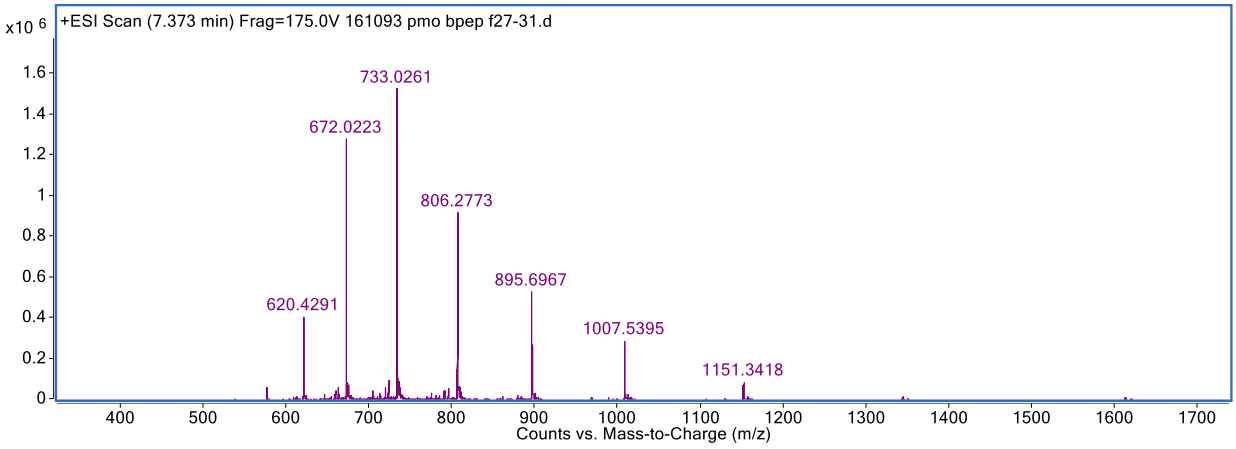

PMO-pVEC
Mass Expected: 8626.3 Da
Mass Observed: 8626.8 Da
Peptide Sequence: LLIILRRRIRKQAHAHSK

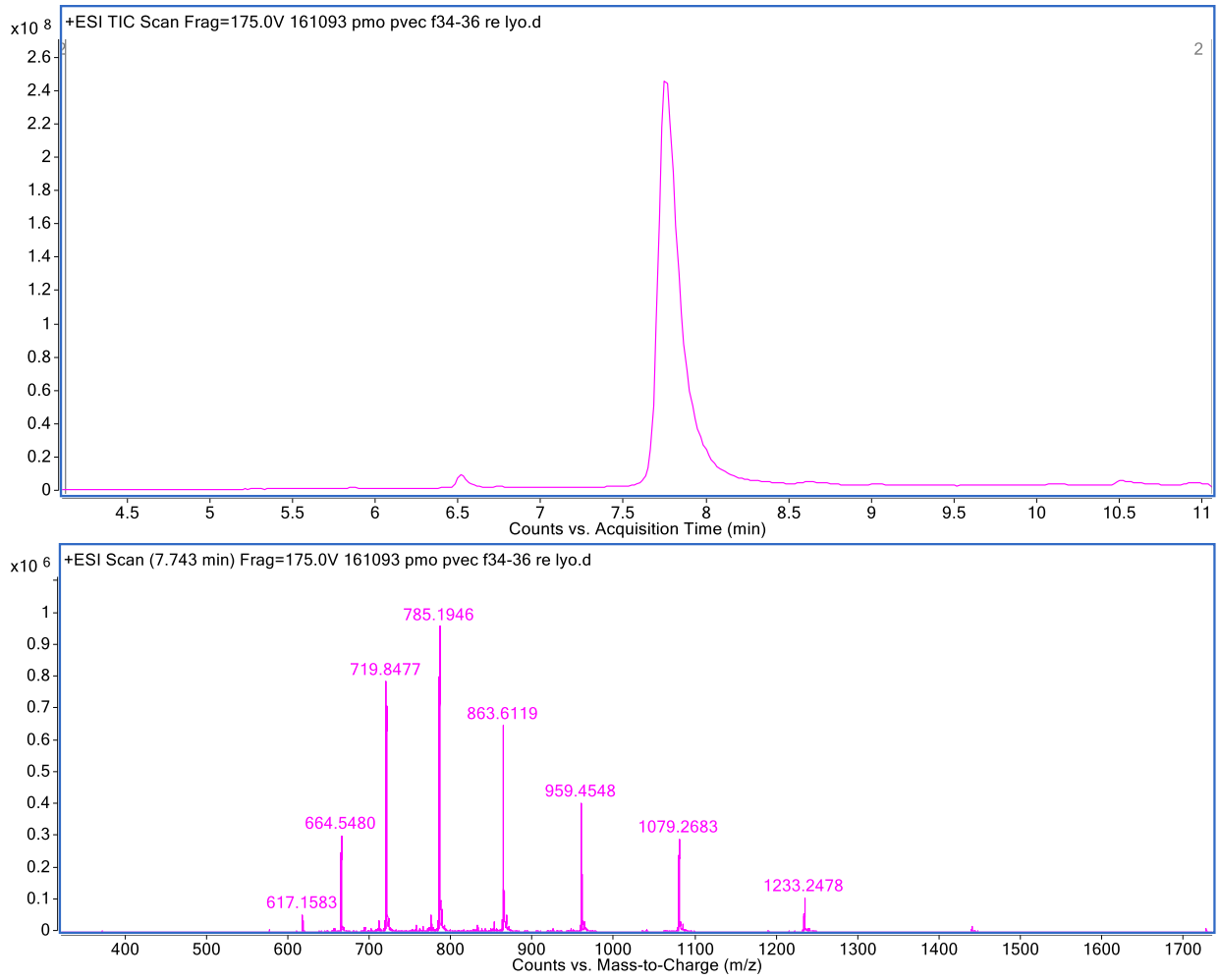

PMO-pVEC-Bpep
Mass Expected: 10244.3 Da
Mass Observed: 10244.7 Da
Peptide Sequence: LLIILRRRIRKQAHAHSKRXRRBRRXRRBR

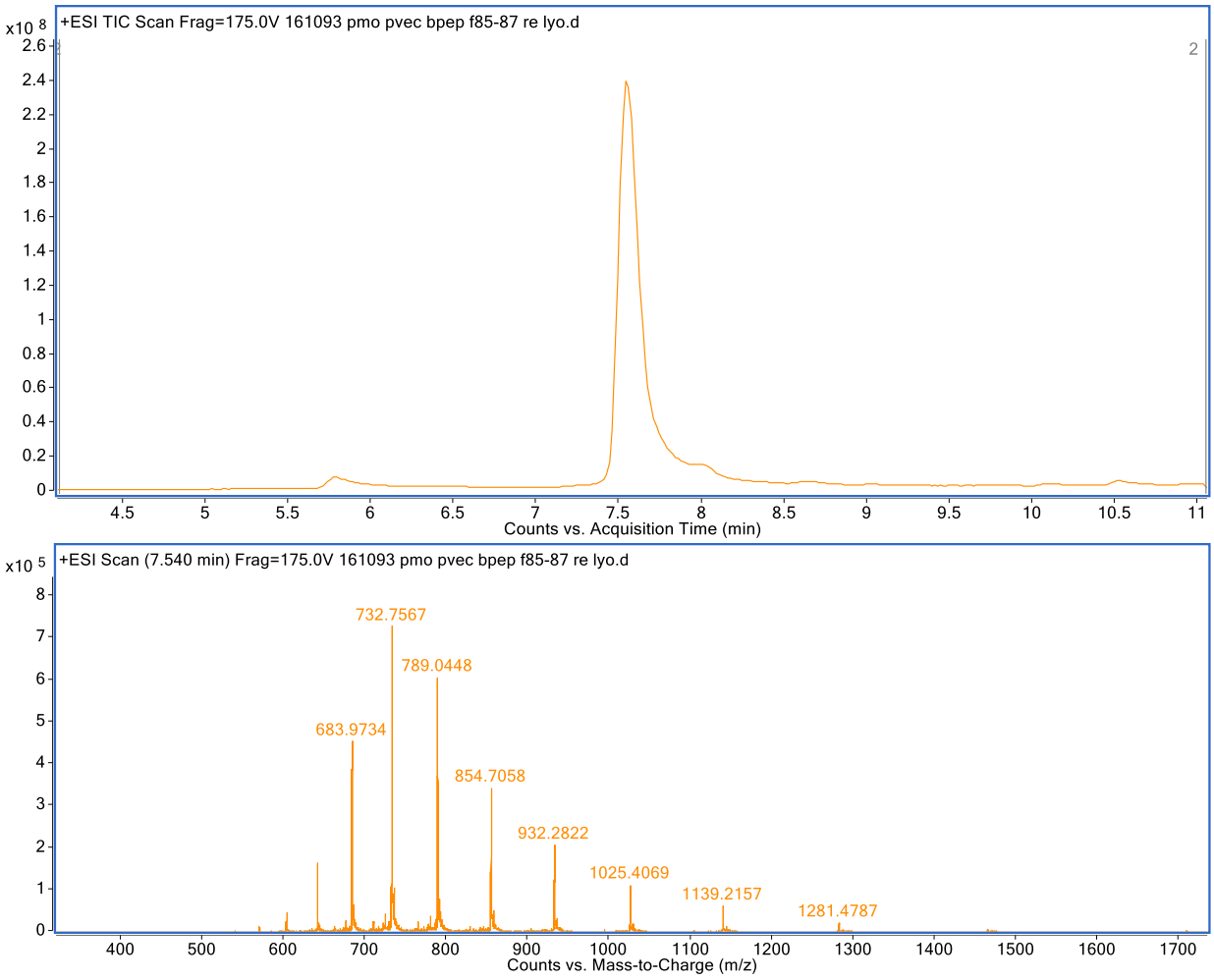

PMO-Penetratin
Mass Expected: 8645.3 Da
Mass Observed: 8645.8 Da
Peptide Sequence: RQIKIWFQNRRZKWKK

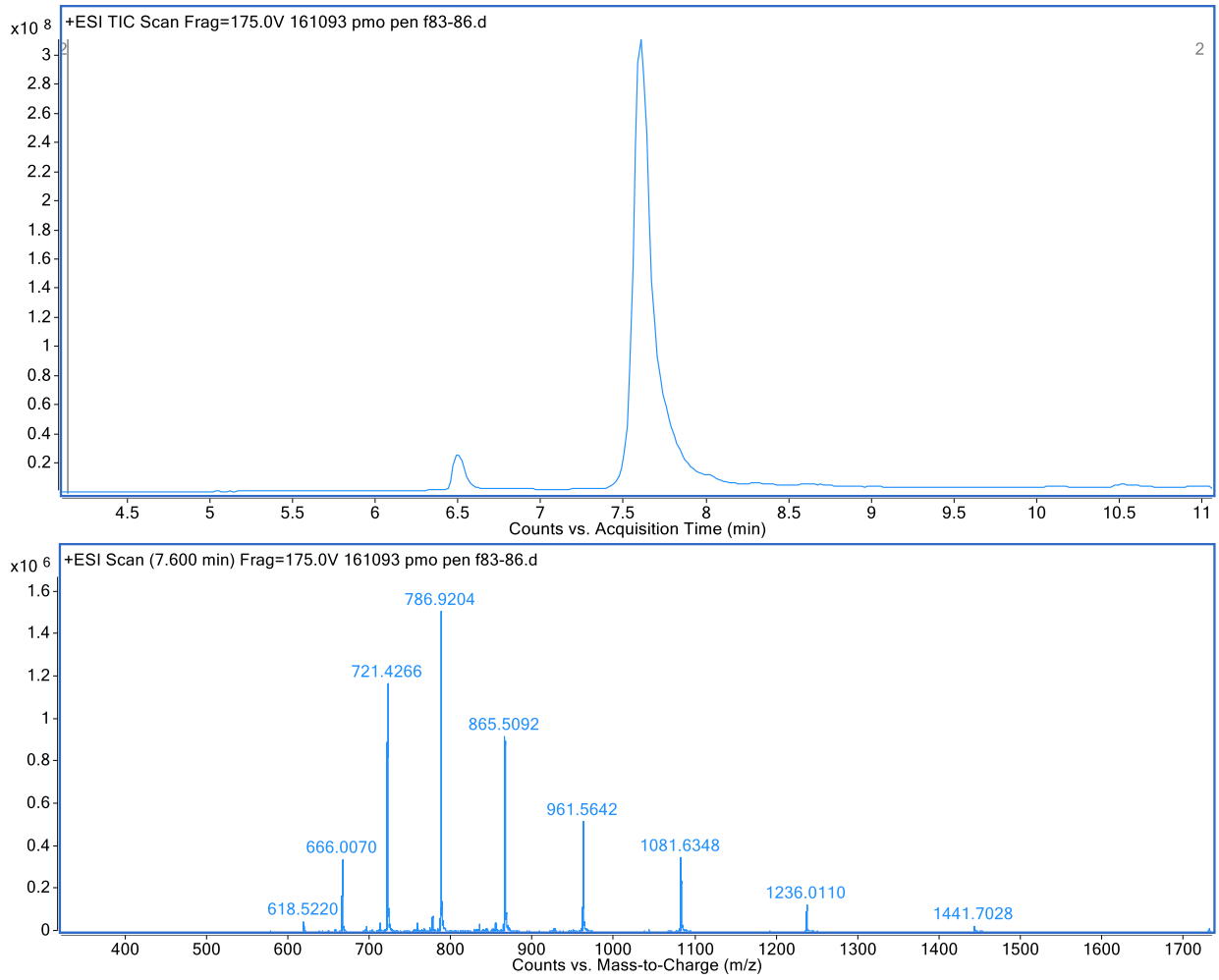

PMO-Penetratin-Bpep
Mass Expected: 10263.3 Da
Mass Observed: 10263.6 Da
Peptide Sequence: RQIKIWFQNRRZKWKKRXRRBRRXRRBR

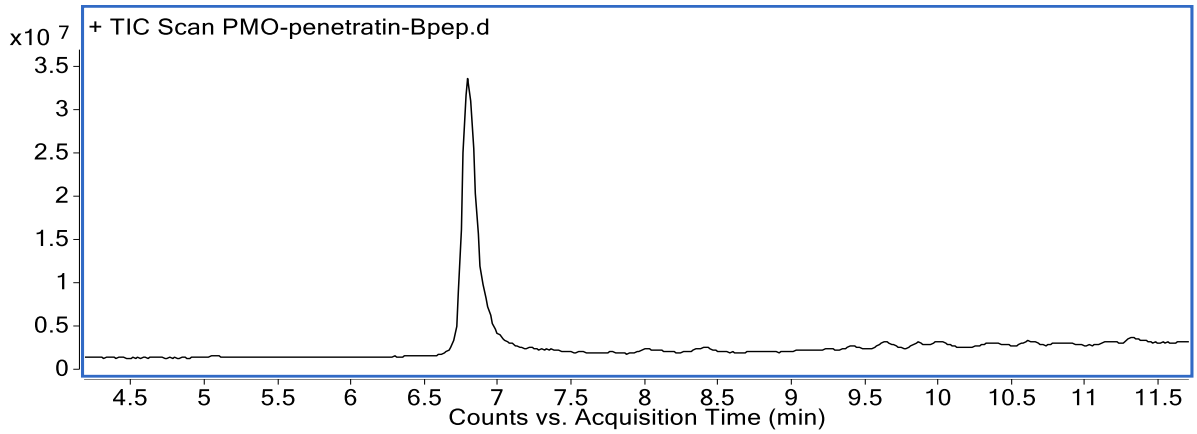

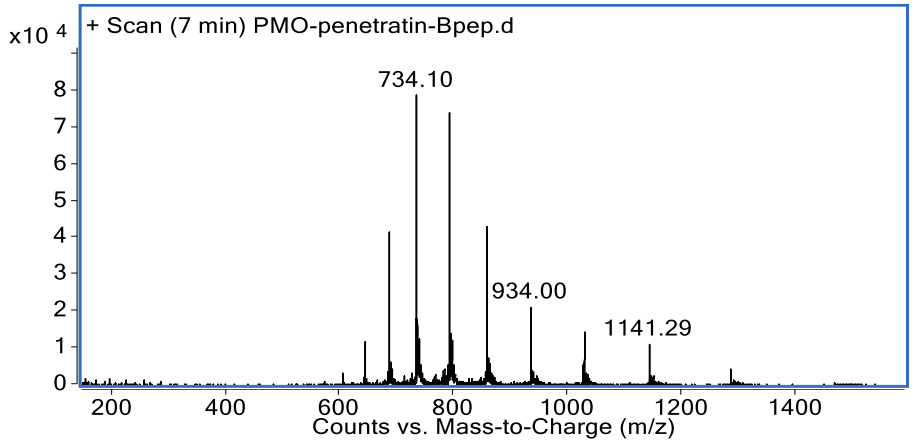

PMO-Melittin
Mass Expected: 9264.1 Da
Mass Observed: 9264.6 Da
Peptide Sequence: GIGAVLKVLTTGLPALISWIKRKRQQ

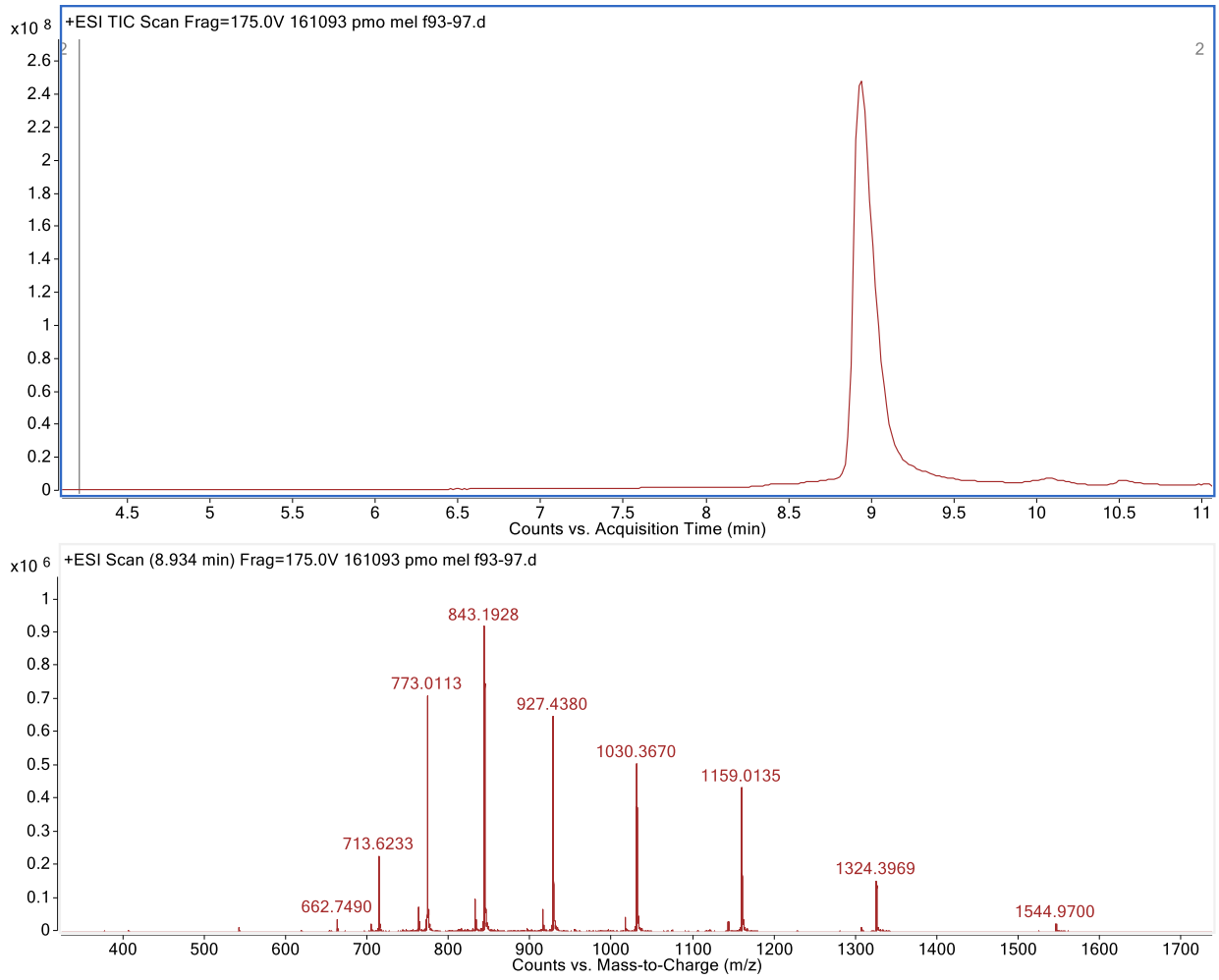

PMO-Melittin-Bpep
Mass Expected: 10882.1 Da
Mass Observed: 10882.7 Da
Peptide Sequence: GIGAVLKVLTTGLPALISWIKRKRQQRXRRBRRXRRBR

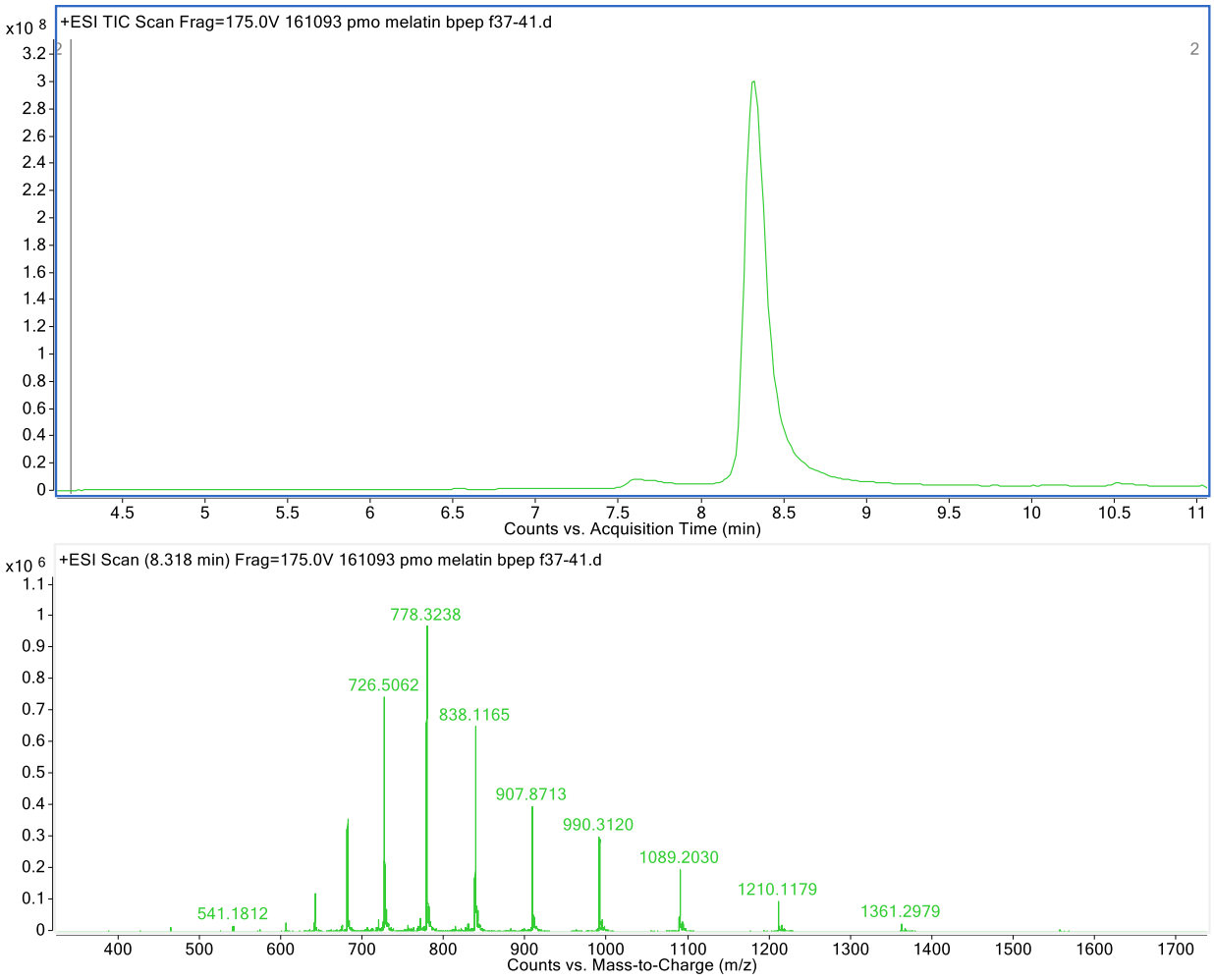

PMO-P15
Mass Expected: 7891.3 Da
Mass Observed: 7891.7 Da
Peptide Sequence: PPPPPPPPPPPPPP

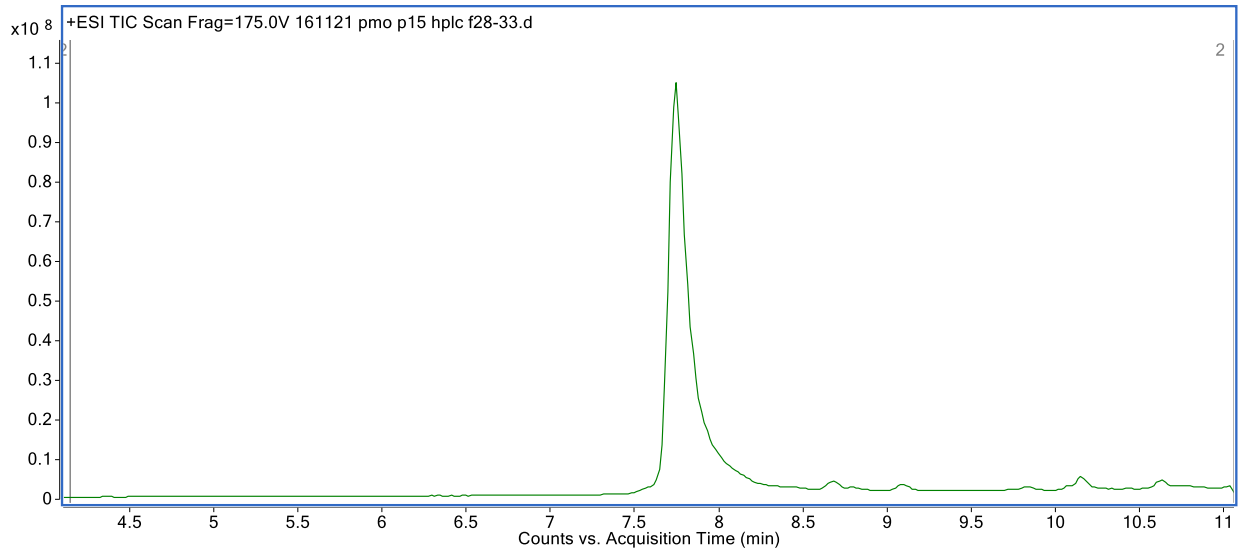

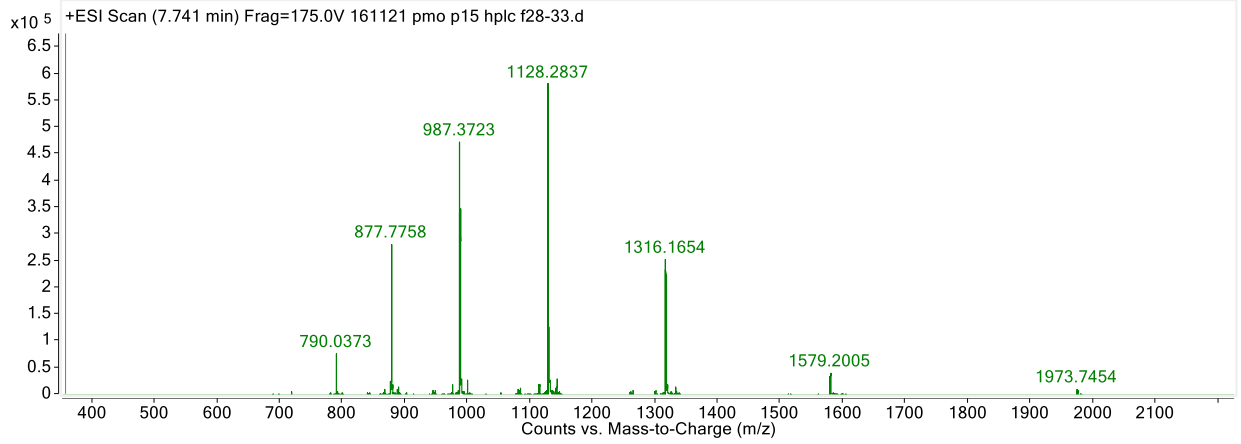

PMO-P15-Bpep
Mass Expected: 9509.2 Da
Mass Observed: 9509.7 Da
Peptide Sequence: PPPPPPPPPPPPPPRXRRBRRXRRBR

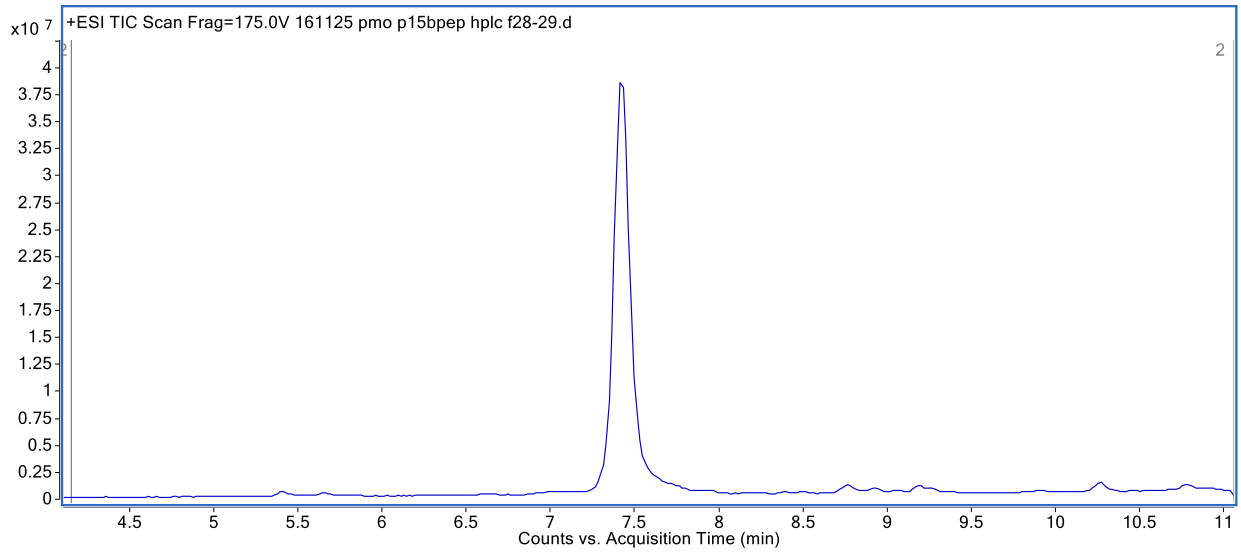

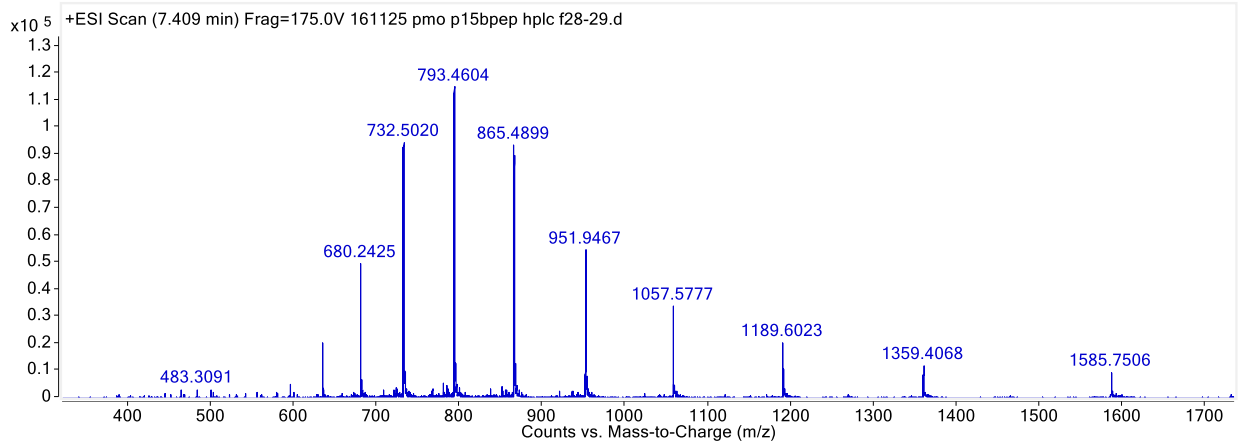

PMO-A15-Bpep
Mass Expected: 9118.7 Da
Mass Observed: 9118.9 Da
Peptide Sequence: AAAAAAAAAAAAAARXRRBRRXRRBR

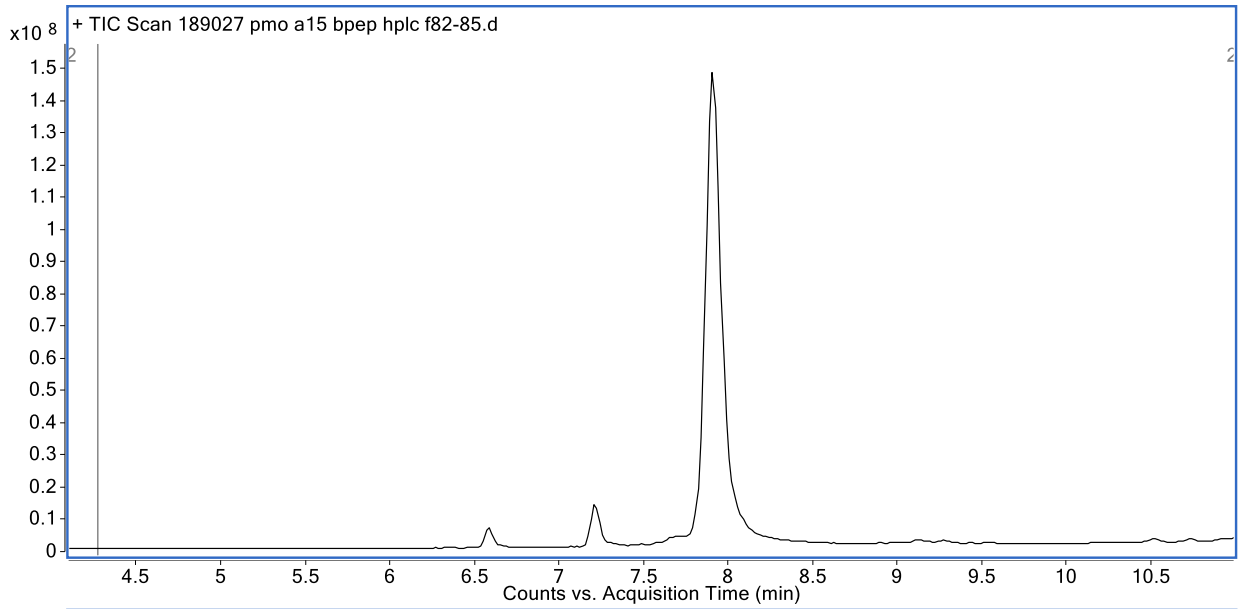

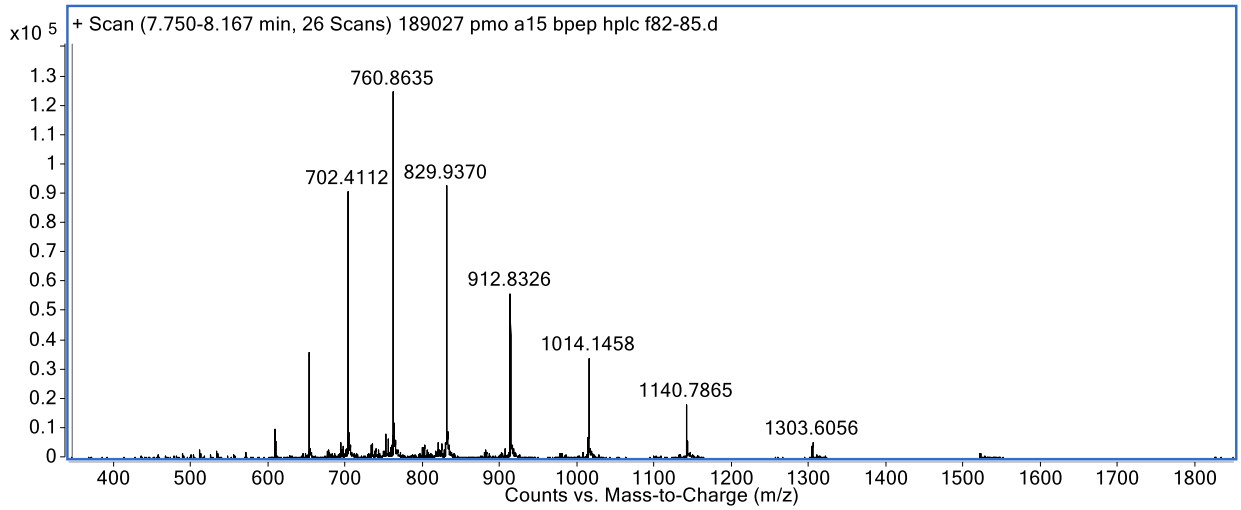

PMO-Bpep-pVEC
Mass Expected: 10244.3 Da
Mass Observed: 10244.6 Da
Peptide Sequence: RXRRBRRXRRBRLLIILRRRIRKQAHAHSK
LC-MS **Method A**

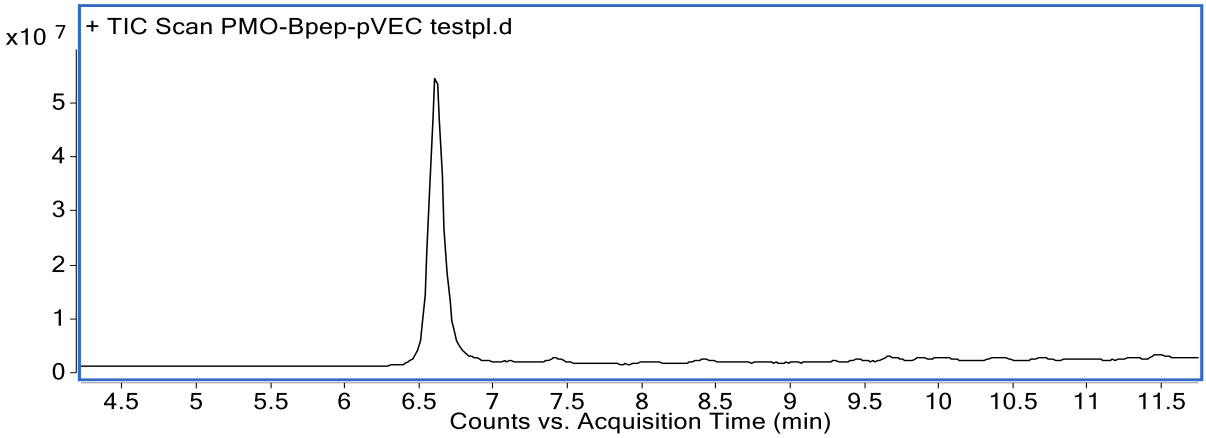

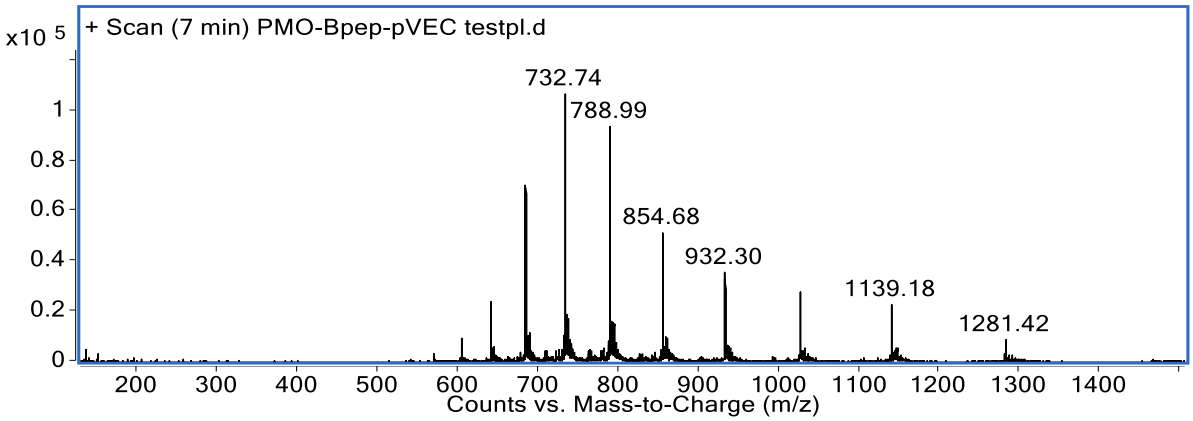

PMO-Bpep-Penetratin
Mass Expected: 10263.3 Da
Mass Observed: 10263.7 Da
Peptide Sequence: RXRRBRRXRRBRRQIKIWFQNRRZKWKK
LC-MS **Method A**

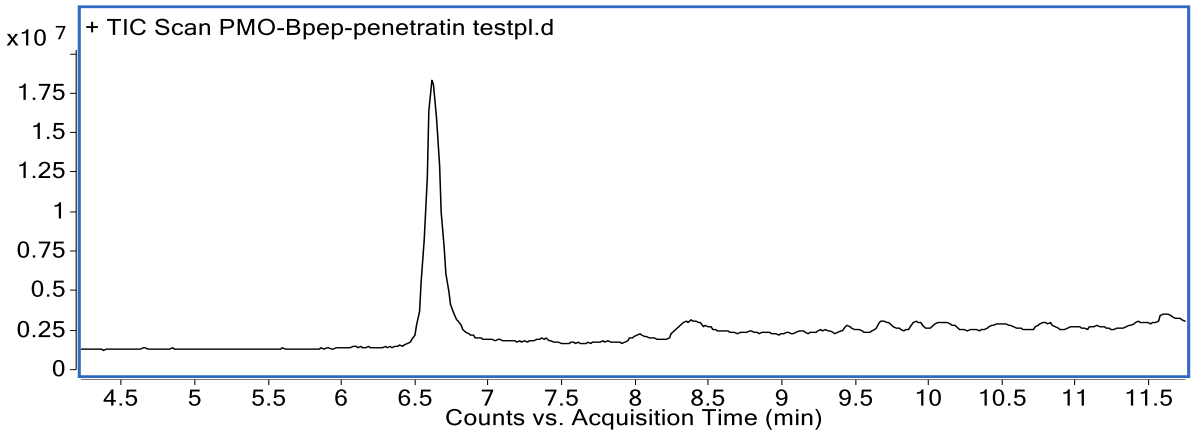

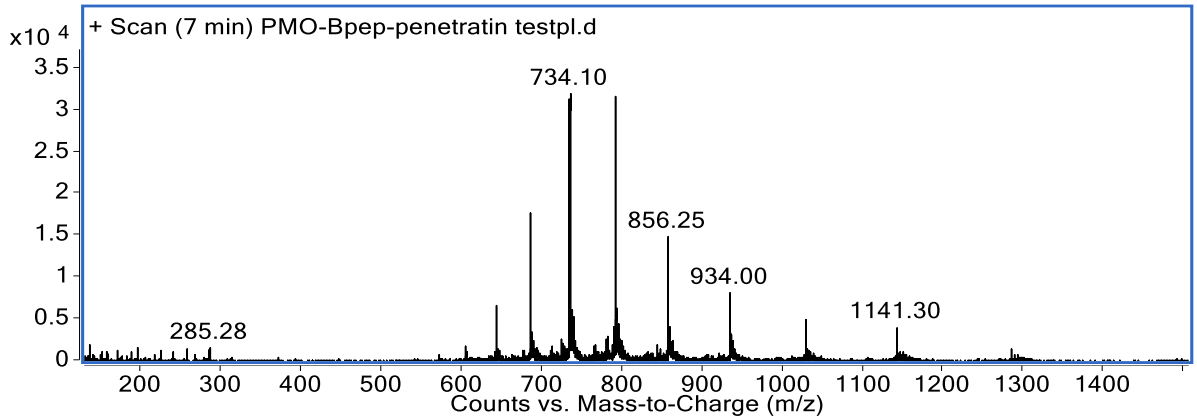

PMO-Bpep-Melittin
Mass Expected: 10882.1 Da
Mass Observed: 10882.5 Da
Peptide Sequence: RXRRBRRXRRBRGIGAVLKVLTTGLPALISWIKRKRQQ
LC-MS **Method A**

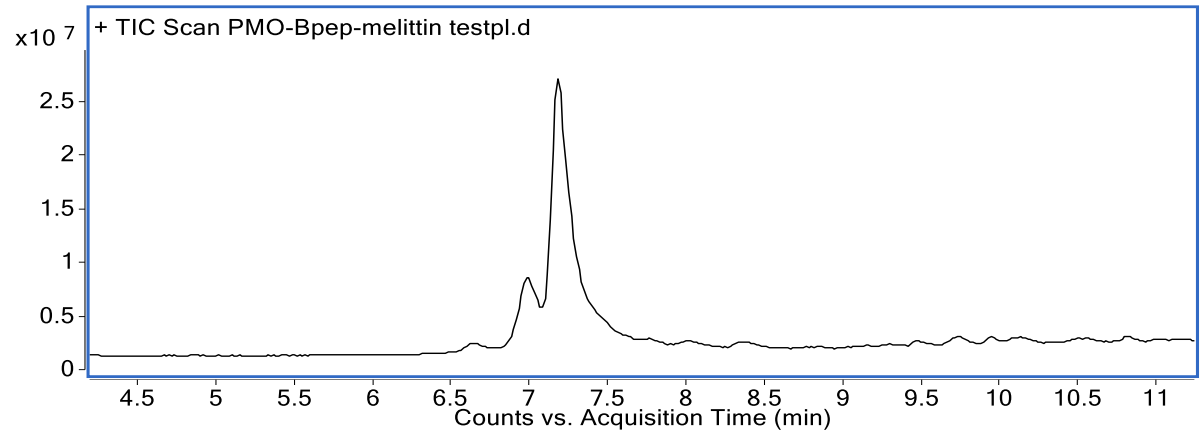

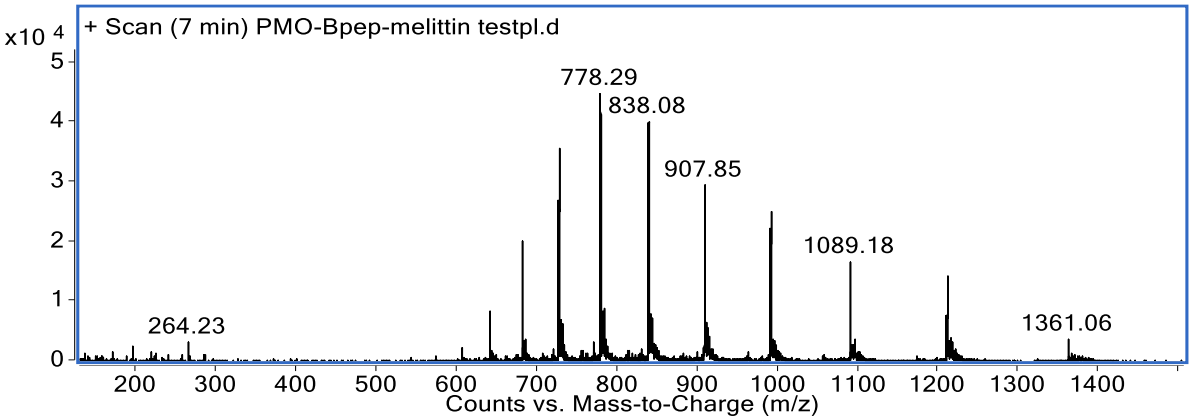

PMO-Bpep-Bpep
Mass Expected: 9670.5 Da
Mass Observed: 9672.9 Da
Peptide Sequence: RXRRBRRXRRBRRXRRBRRXRRBR
LC-MS **Method A**

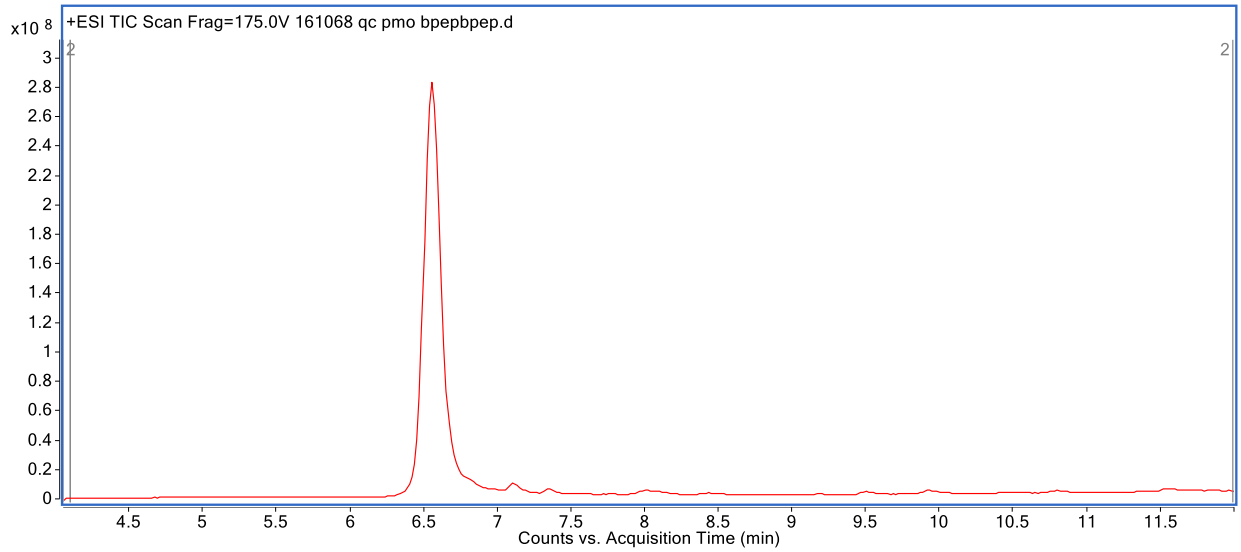

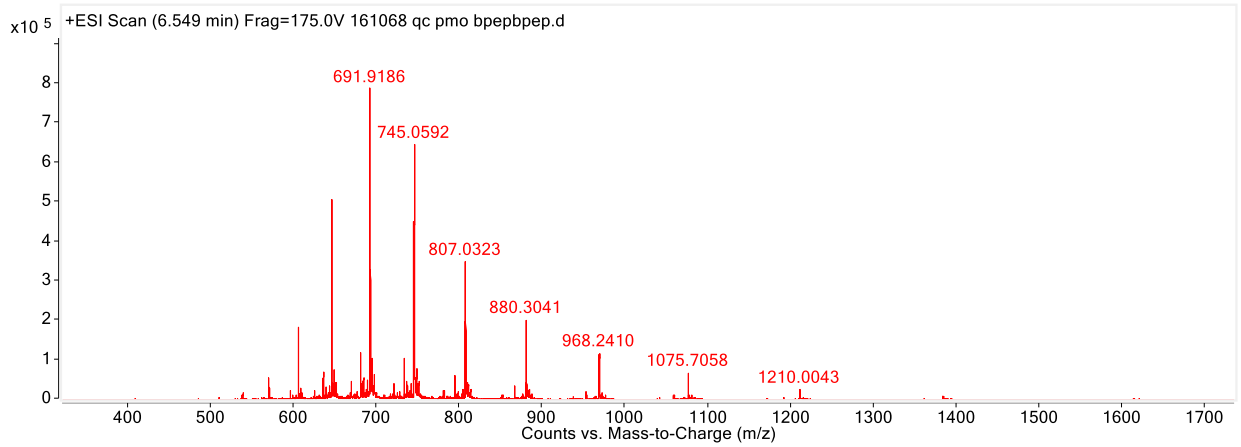

PMO-SulfoCy5-Bpep
Mass Expected: 8921.7
Mass Observed: 8921.6
Peptide Sequence: C(SulfoCy5)RXRRBRRXRRBR

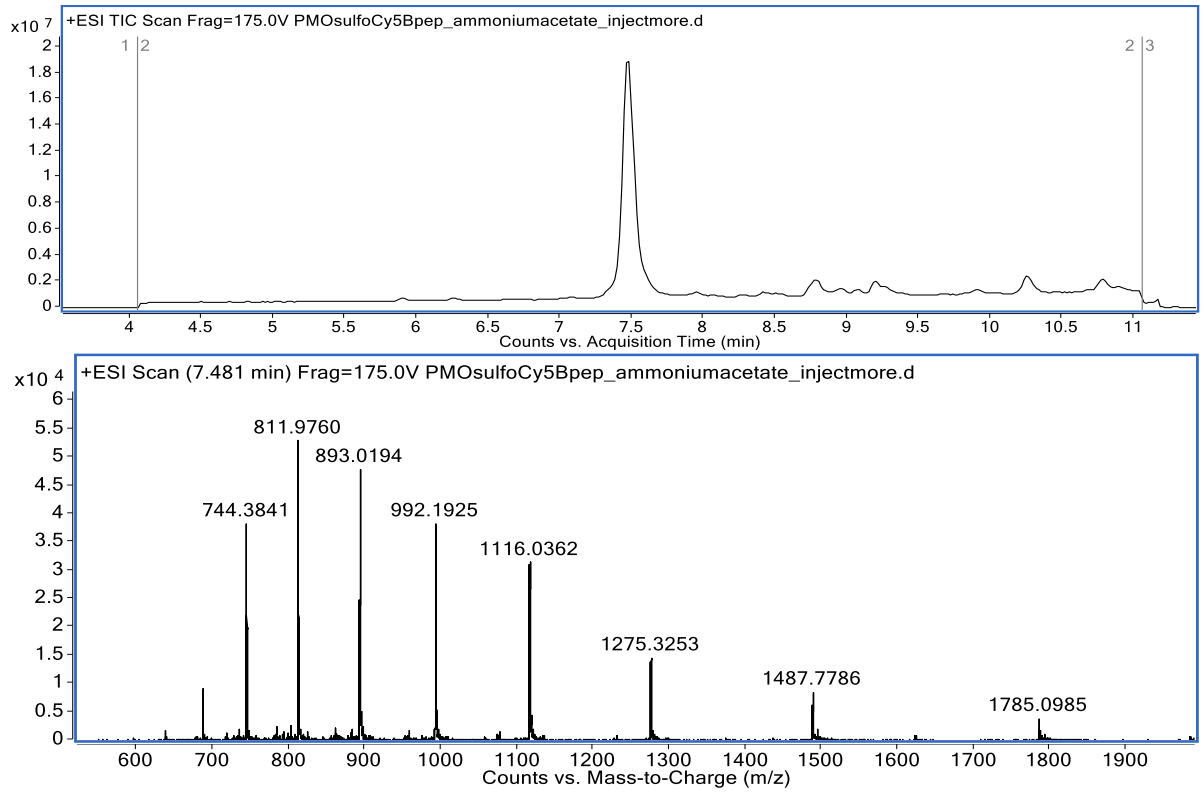

PMO-SulfoCy5-pVEC
Mass Expected: 9495.4
Mass Observed: 9495.0
Peptide Sequence: C(SulfoCy5)LLIILRRRIRKQAHAHSK

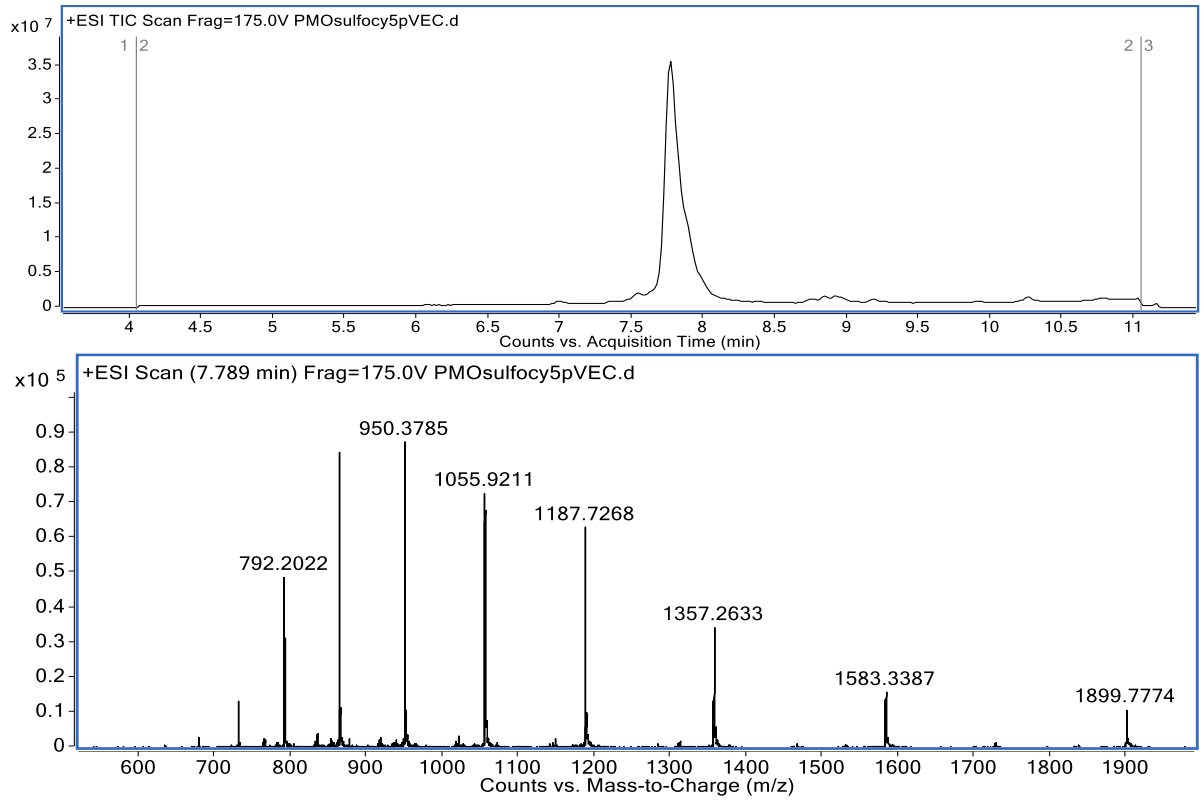

PMO-SulfoCy5-pVEC-Bpep
Mass Expected: 11112.8 Da
Mass Observed: 11112.6 Da
Peptide Sequence: C(SulfoCy5)LLIILRRRIRKQAHAHSKRXRRBRRXRRBR

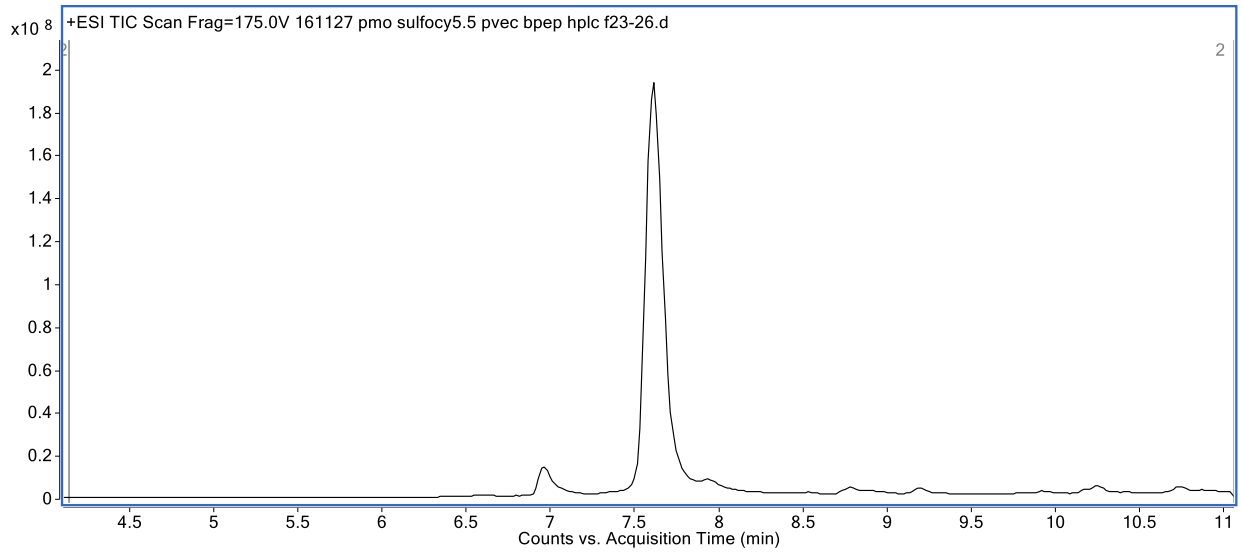

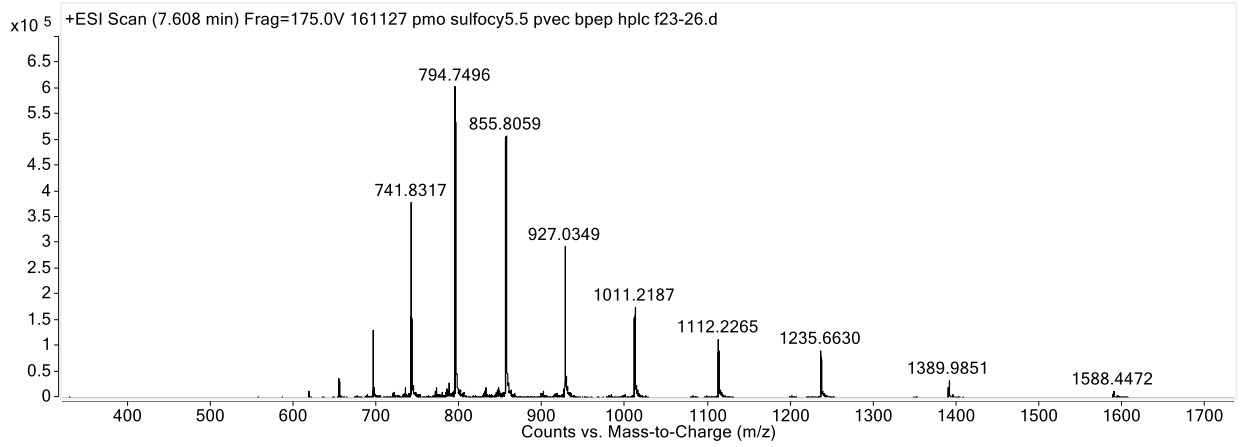

6.7.2 Cell Images

Five images are shown for each construct
PMO-SulfoCy5-pVEC-Bpep

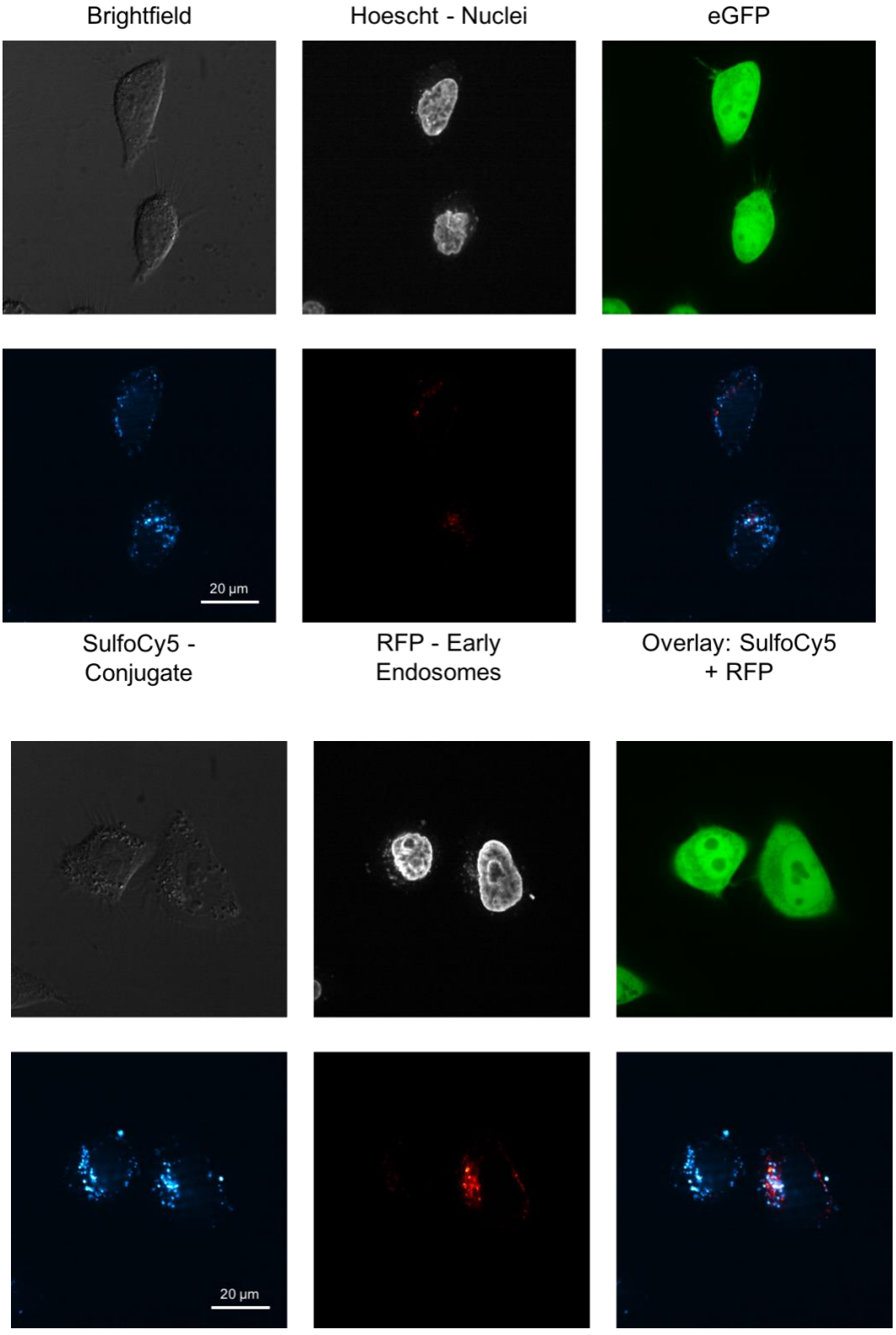

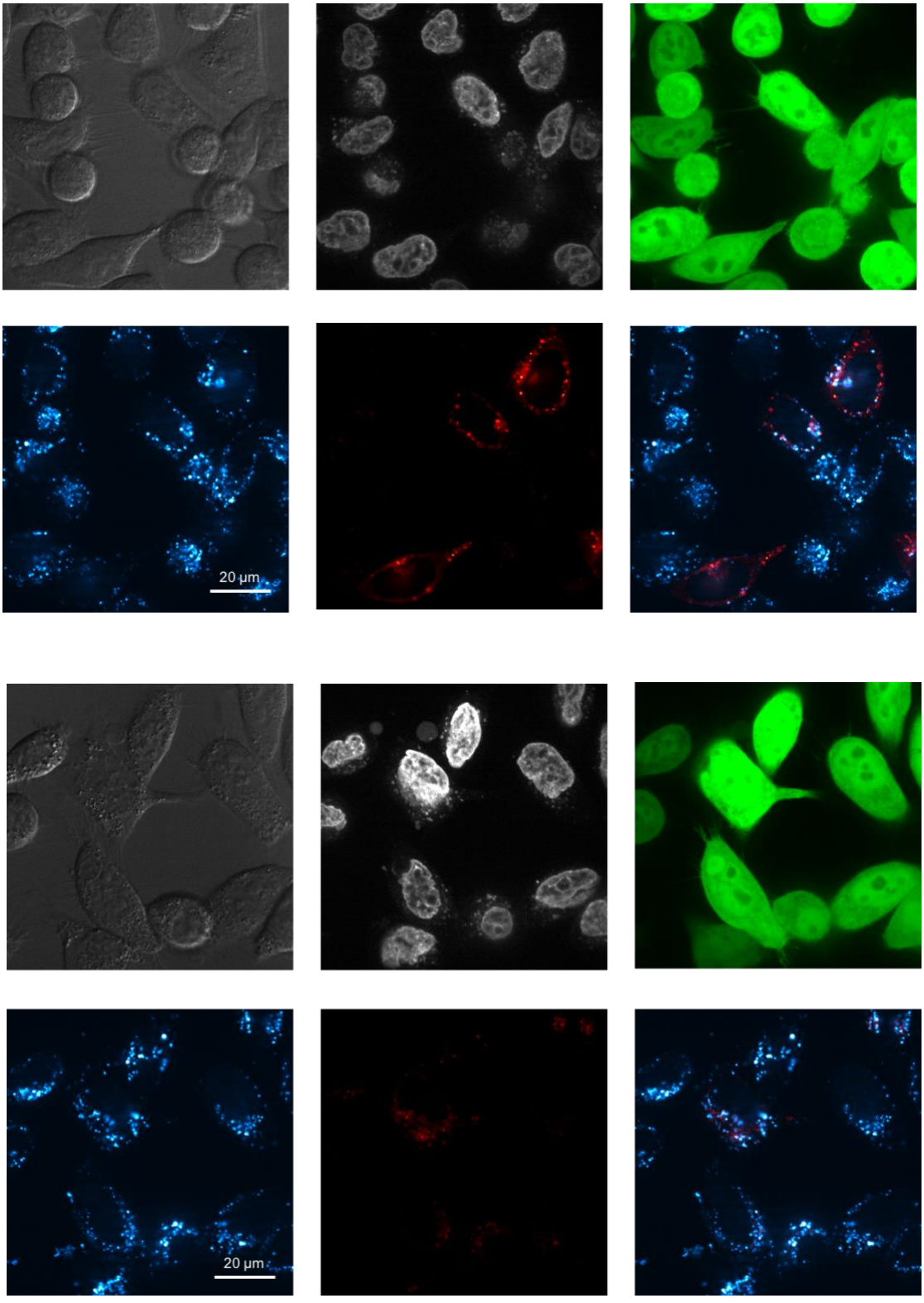
20 µm
20 µm

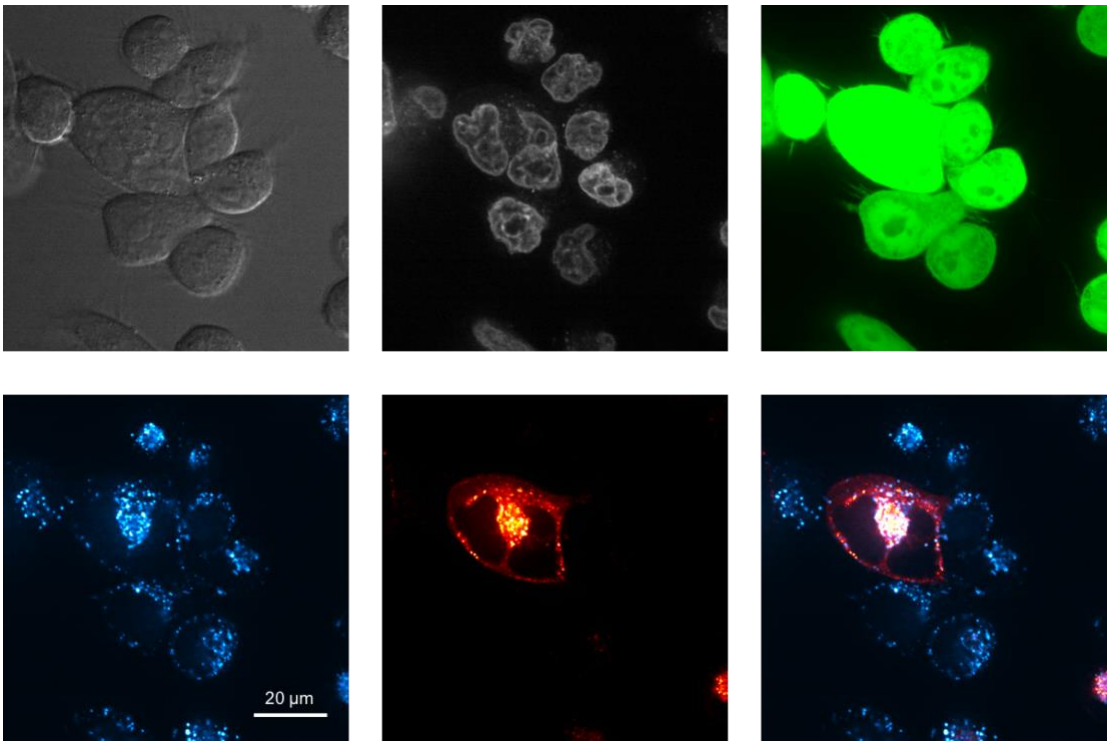

PMO-SulfoCy5-pVEC

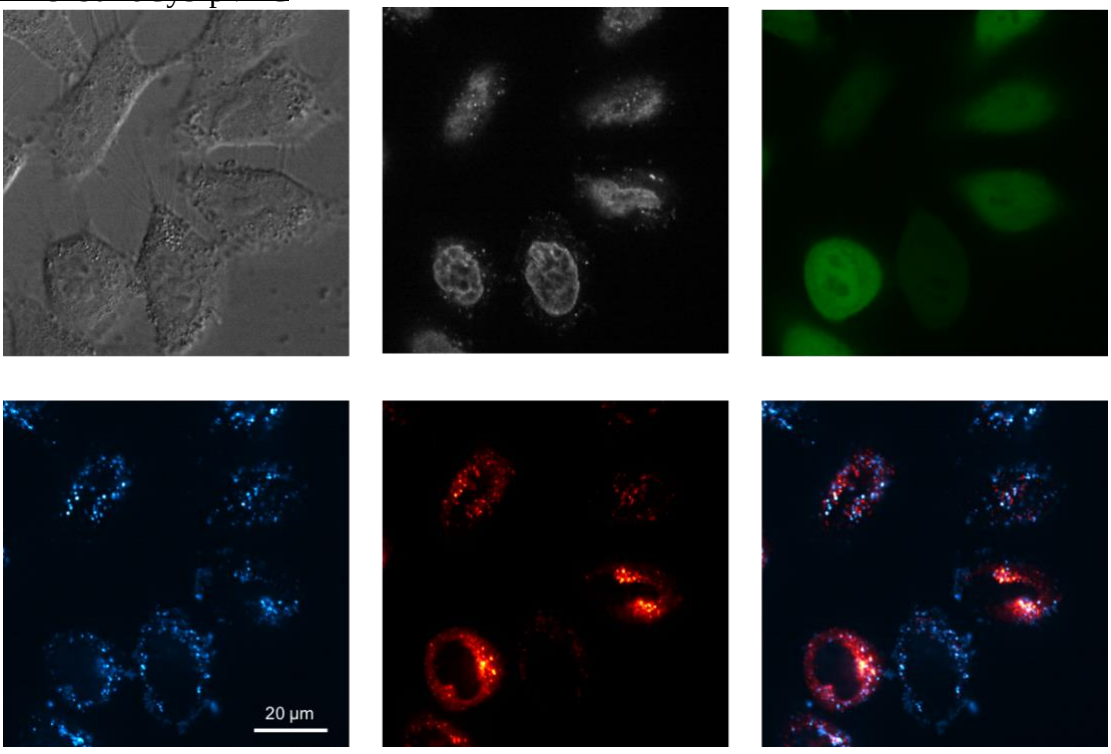

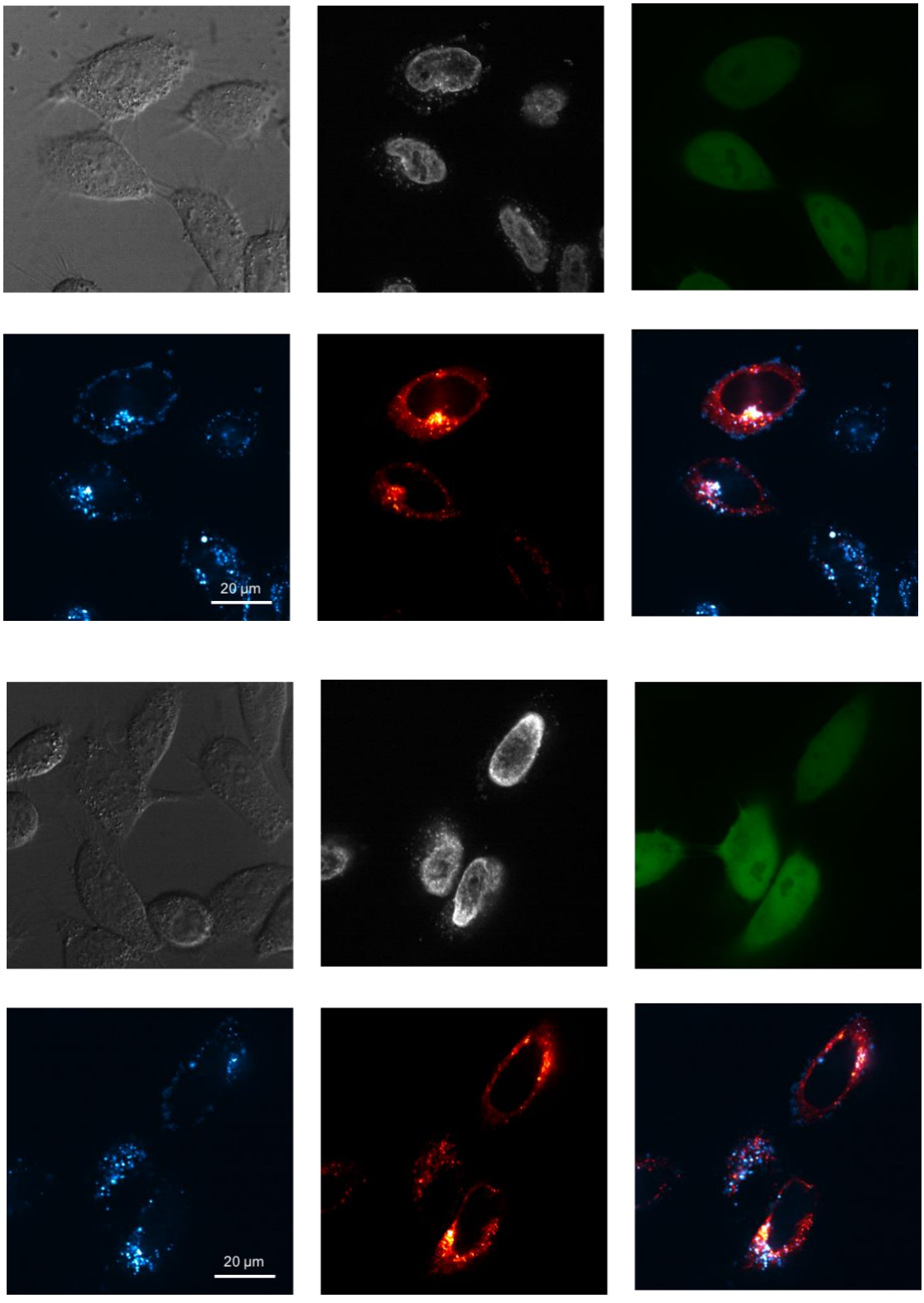
20 µm
20 µm

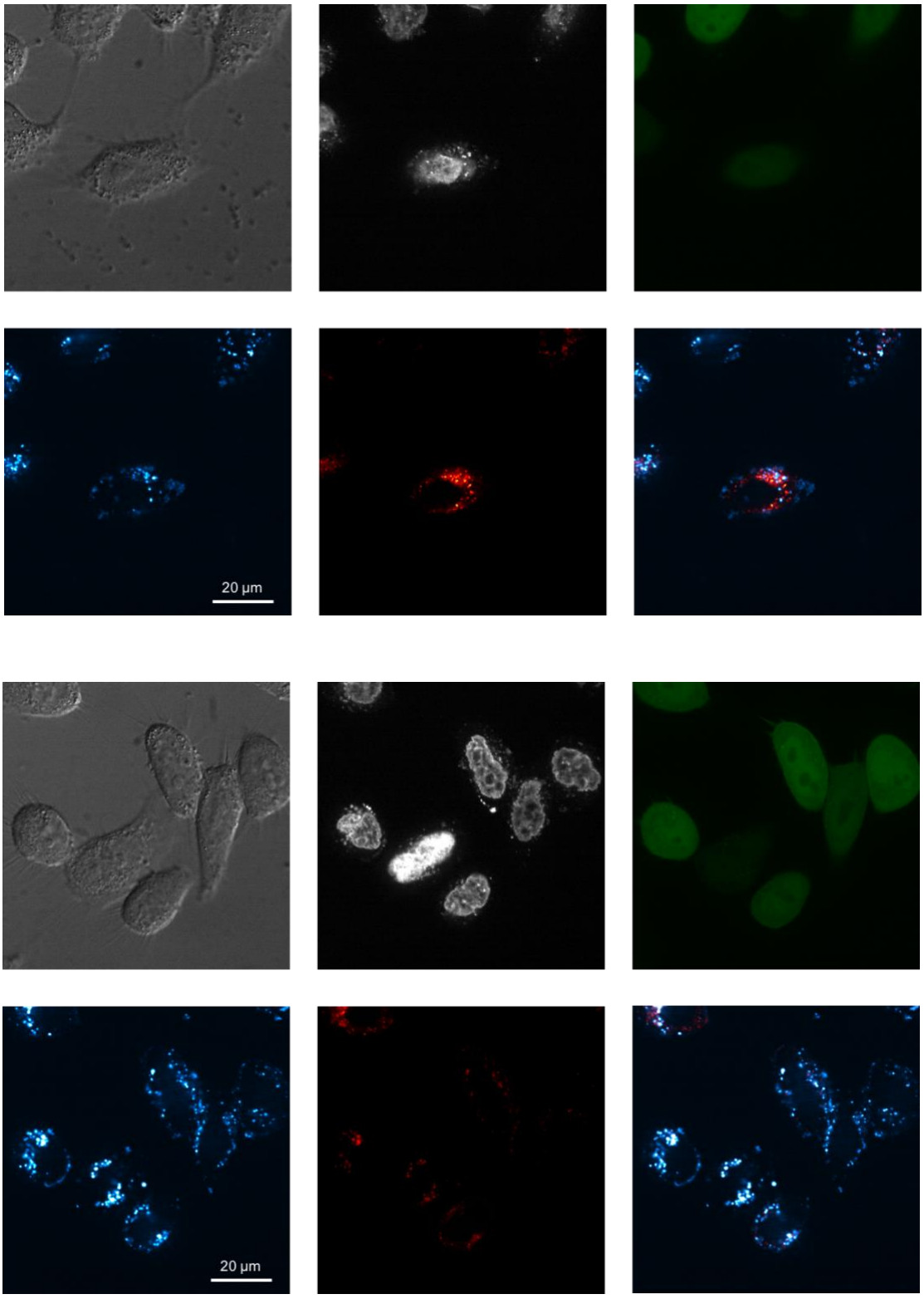
20 µm
20 µm

PMO-SulfoCy5-Bpep

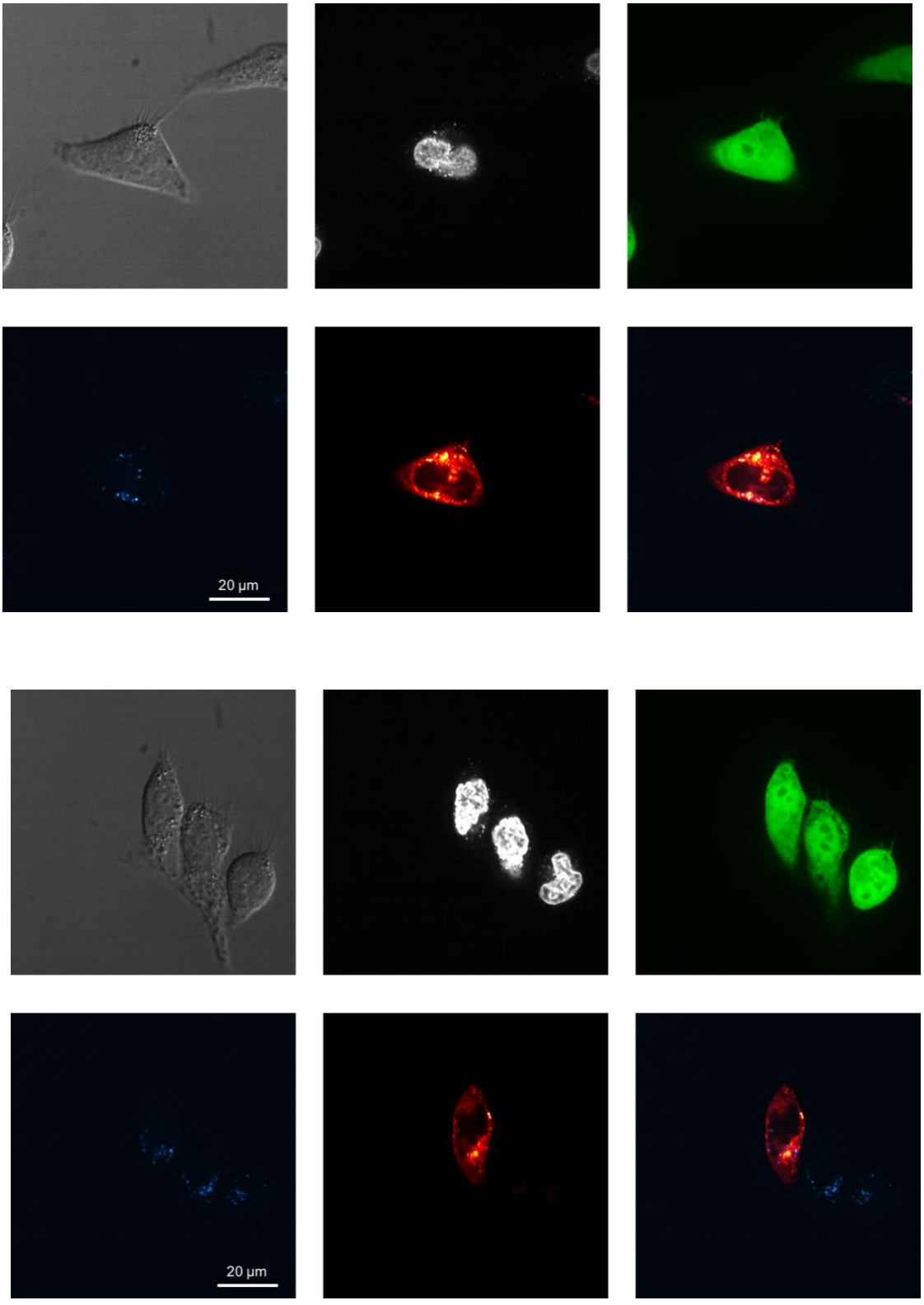

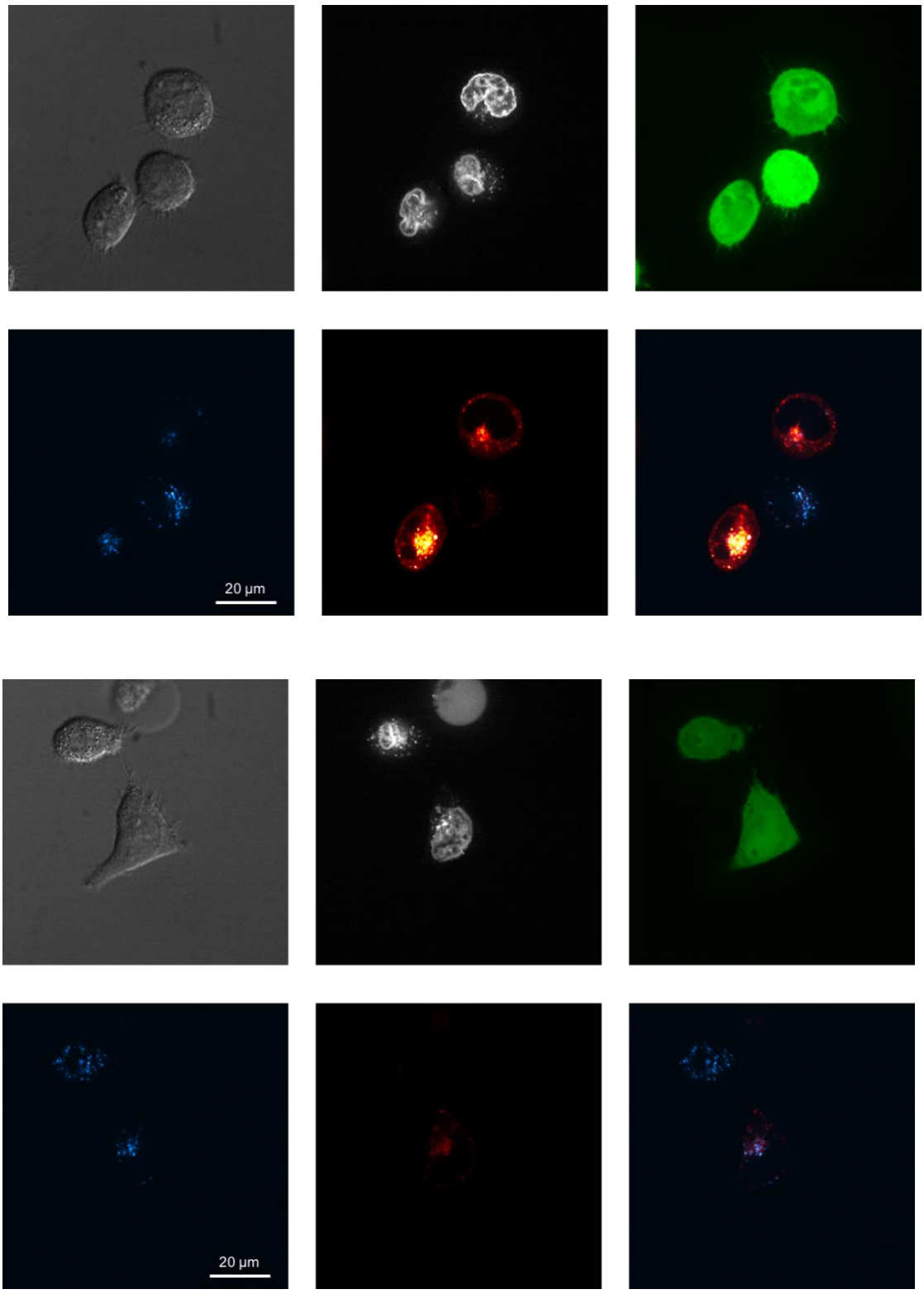
20 µm
20 µm

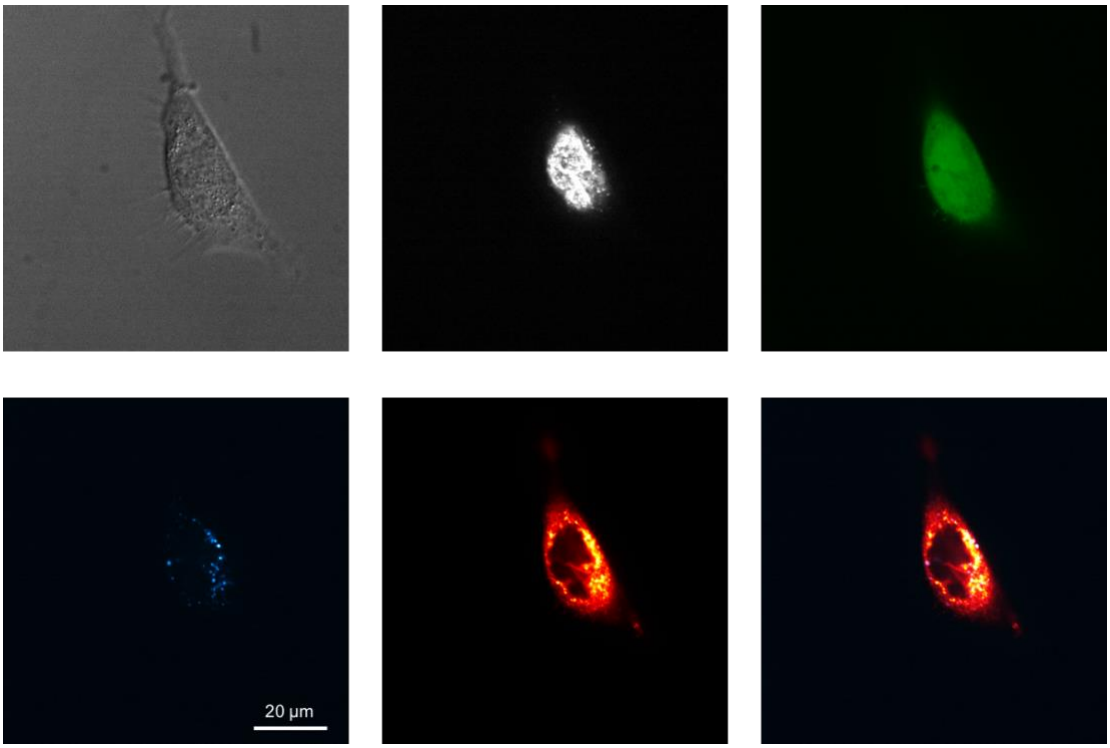

Untreated Cells

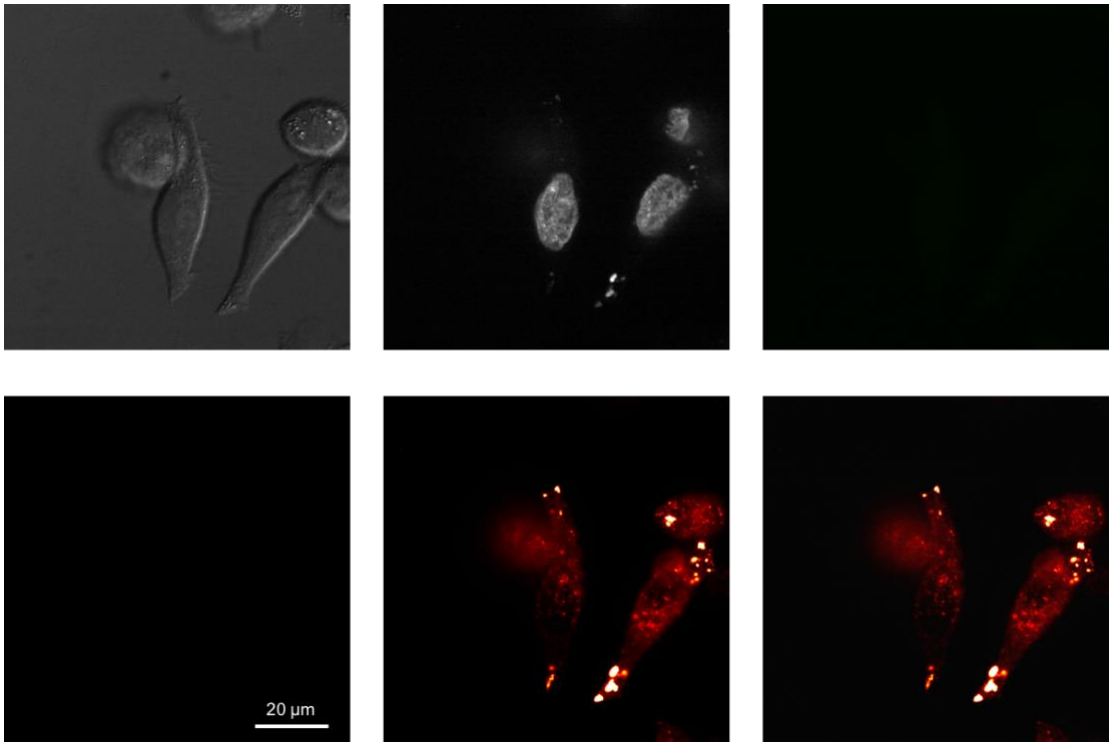

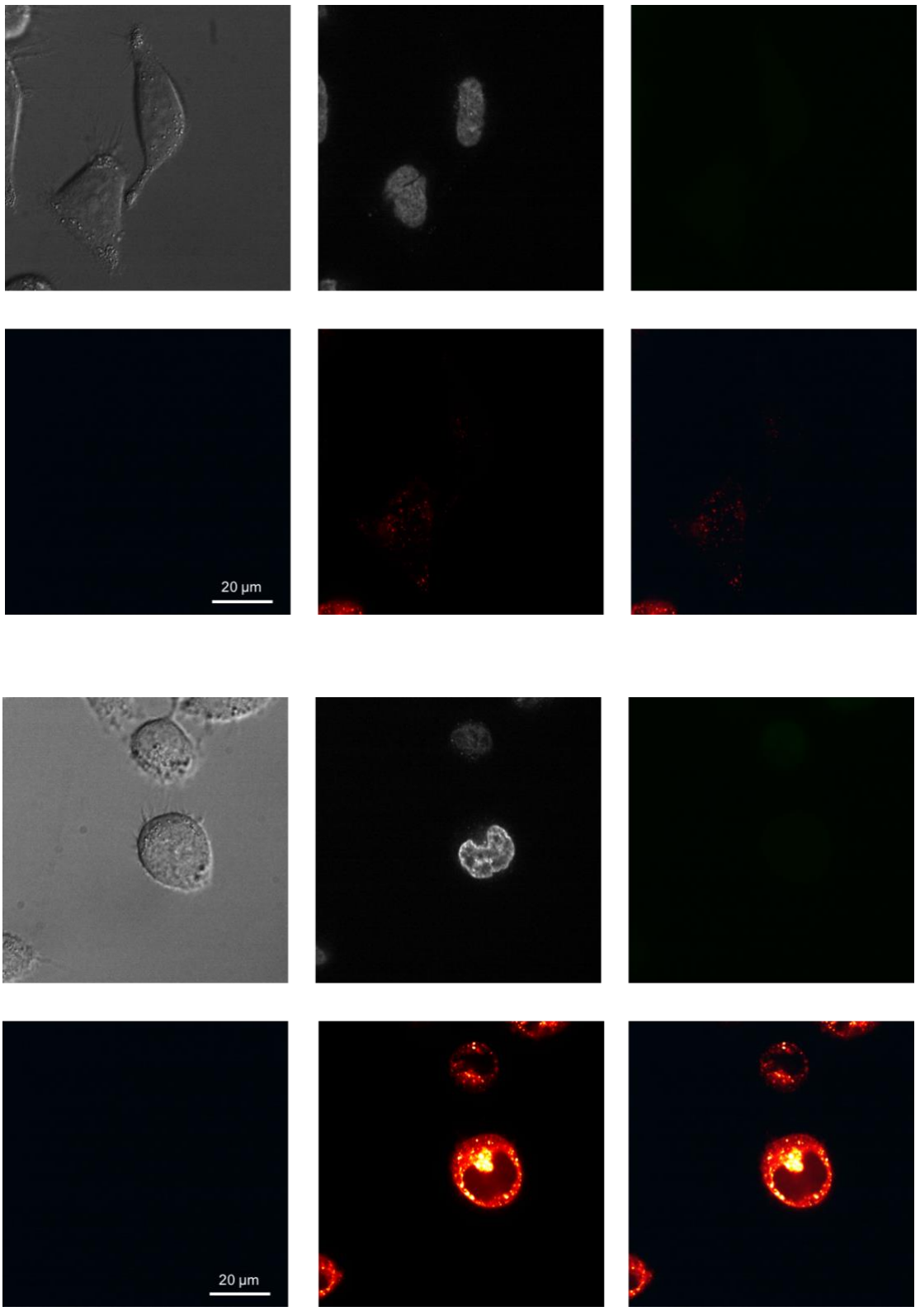
20 µm
20 µm

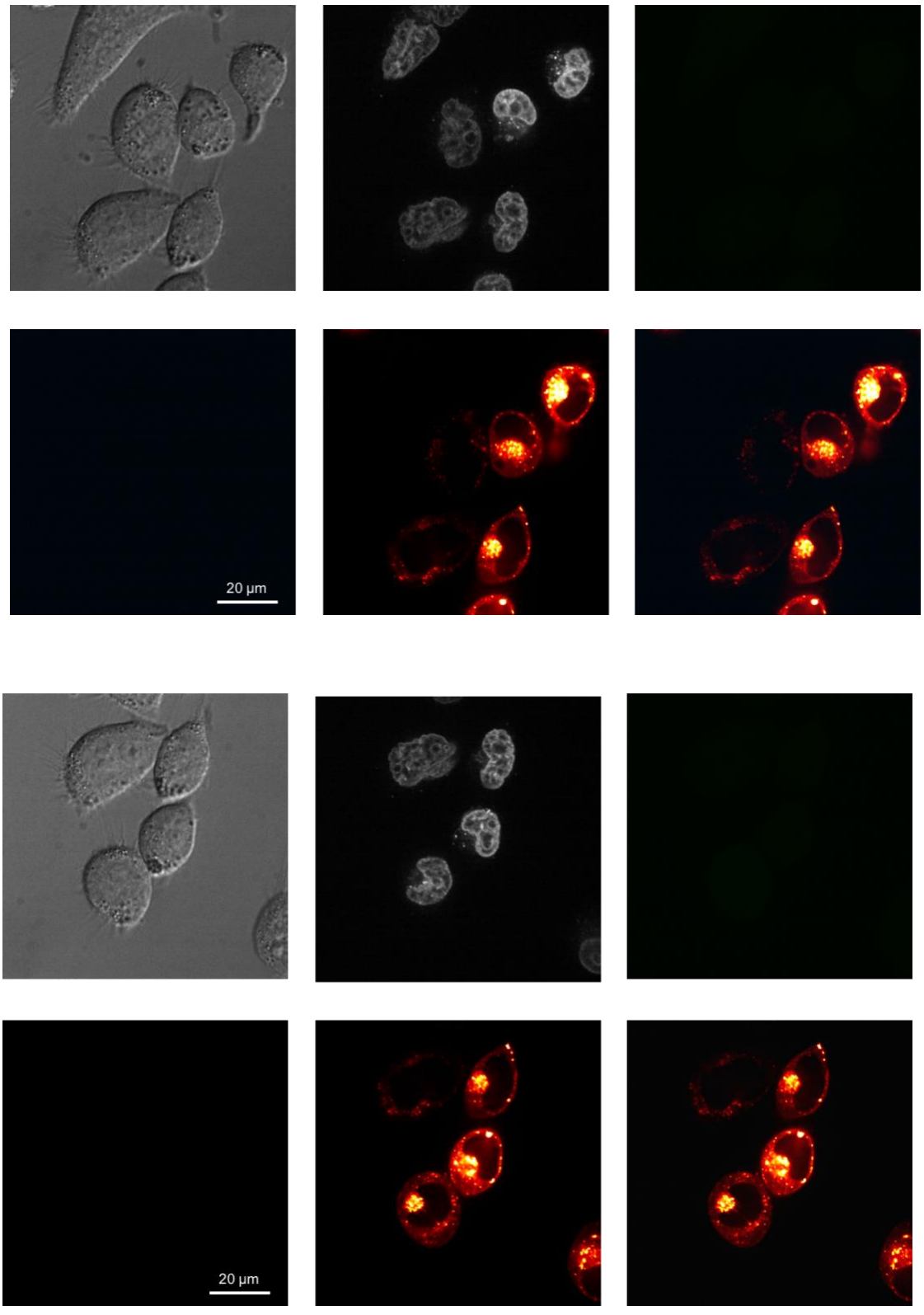
20 µm
20 µm